University of Southampton

Faculty of Engineering and Physical Sciences

School of Mechanical Engineering

Hybrid and Dual Chemistry Battery for Energy Storage Applications

by

Andrei Dascalu

MSc, MIET

ORCID ID 0000-0003-3072-1864

Thesis for the degree of Doctor of Philosophy

June 2025

University of Southampton

Abstract

Faculty of Engineering and Physical Sciences

School of Mechanical Engineering

Doctor of Philosophy

Hybrid and Dual Chemistry Battery for Energy Storage Applications

by

Andrei Dascalu

Energy storage is predicted to play an increasing role in a renewable energy future. There is a wide range of storage technologies available, with different technical characteristics, to assist the renewable transition. Hybrid options are also possible to improve the technical and economic performance of storage systems. The technology proposed in this work is the directly connected hybrid lead-acid and Li-ion battery storage system, which makes use of Li-ion's high-performance characteristics and the low-cost, lower specifications of lead-acid cells.

The work presented in this thesis answers the following key questions, which also summarise the novelty of this research:

- What are the hybrid characteristics of directly coupled, hybrid Li-ion (NMC) and lead-acid (VRLA) systems?
- Can the instantaneous hybrid behaviour be modelled using equivalent circuits?
- How do hybrid battery systems perform over time in real-world applications?
- What storage applications are best suited for hybrid lead-acid and Li-ion systems, and what are the associated techno-economic parameters?

To answer these questions, I have built and tested hybrid systems, developed battery models, and monitored the first commercial hybrid lead-acid and Li-ion system installed in the UK. The lab analysis, done for five domestic-size hybrid systems of 24V and 48V, provides details about the system efficiency and energy flows in a hybrid configuration. The round-trip efficiency drops from a maximum of around 94-95% in the first charge/discharge stages, when only Li-ion strings are active, to 82-90%, depending on the lead-acid strings' depth of discharge. The most important parameters in the round-trip efficiency function are the kWh capacity ratio between the two chemistries, the energy available and the charge/discharge current. The

energy transfer between the strings, caused by the transient currents, is negligible when only Li-ion is active, and increases with the lead-acid depth of discharge.

A hybrid equivalent circuit battery model was built to predict the experimental results. The model approximates the dynamic effects of energy transferred between the strings with an accuracy of 90%, except when the lead-acid strings are discharged to 10-30% depth of discharge. The overall efficiency, the total energy discharged, and the Li-ion energy available for independent cycling can be predicted with above 90% accuracy.

The demonstrator project data shows that the hybrid system is stable over time, the average operating round-trip efficiency in real-world applications is 90%, and the lead-acid degradation in hybrid configurations is around 1.3% per year. The energy transfer between the strings, due to different dynamic time constants of the two chemistries, depends on the charge stopping points, and to a lesser extent, on the discharge interruption depth of discharge. For the analysed system, the average Li-ion to lead-acid energy transfer during the charging process is 13 kWh, 5.5% of the total charged energy. The average lead-acid to Li-ion energy transfer during discharge is 5.2 kWh, 2.47% of the total discharged energy.

The final techno-economic analysis shows that the hybrid battery system can be used for renewable storage applications, dedicated to serving residential, commercial, industrial, and off-grid EV charging load profiles, but it is not suitable for front-of-the-meter applications, which operate in frequency response or balancing markets. The cost-saving potential for using hybrid Li-ion and lead–acid systems varies with the load profile, storage operational strategy, and renewable overgeneration design choices. The total system cost reduction can be up to 26.1% when compared with full Li-ion solutions. However, for the cost-optimised energy solutions, the CAPEX reduction using hybrid storage is between 1.4% and 12.7%, depending on the percentage cost of storage as a share of the total energy system. The minimum cost ratio between Li-ion and lead-acid, beyond which the hybrid storage system is no longer justified, is between 1.1 and 1.5.

Table of Contents

Table of Tables

Table of Tables

Table of Figures

Table of Figures

Table of Figures

Table of Figures

Table of Figures

Table of Figures

Research Thesis: Declaration of Authorship

Print name: Andrei Dascalu

Title of thesis: Hybrid and Dual Chemistry Battery for Energy Storage Applications

I declare that this thesis and the work presented in it are my own and has been generated by me as the result of my own original research.

I confirm that:

1. This work was done wholly or mainly while in candidature for a research degree at this University;
2. Where any part of this thesis has previously been submitted for a degree or any other qualification at this University or any other institution, this has been clearly stated;
3. Where I have consulted the published work of others, this is always clearly attributed;
4. Where I have quoted from the work of others, the source is always given. With the exception of such quotations, this thesis is entirely my own work;
5. I have acknowledged all main sources of help;
6. Where the thesis is based on work done by myself jointly with others, I have made clear exactly what was done by others and what I have contributed myself;
7. None of this work has been published before submission.

Signature: ..... Date:.....

Acknowledgements

The work would not have been possible without the technical help and financial support from the following people and organisations:

- My family.
- My supervisors, Professors Andrew Cruden BEng, MSc, PhD, FIET and Suleiman Sharkh BEng, PhD, CEng, MIET (University of Southampton).
- Andrew Westerman (University of Southampton).
- Peter Stevenson (GS Yuasa).
- UK Engineering and Physical Sciences Research Council (EPSRC).
- GS-Yuasa Corporation (Industrial partner).

Definitions and Abbreviations

AC ..... Alternating Current

ADC ..... Analog To Digital Converter

BESS..... Battery Energy Storage System

BM ..... Balancing Mechanism

CAES ..... Compressed Air Energy Storage

CAPEX ..... Capital Expenditure

CES ..... Chemical Energy Storage

CC/CV ..... Constant Current/Constant Voltage

CSP ..... Concentrating Solar Power

DAC ..... Digital to Analog Converter

DC ..... Direct Current

DoD ..... Depth of Discharge

ESS ..... Electrical Energy Storage

ECM..... Equivalent Circuit Modelling

ES ..... Energy Storage

ESS ..... Electrical Systems Storage

EV..... Electrical Vehicle

EJ..... Exajoules

FES ..... Flywheel Energy Storage

FTM ..... Front of the Meter

GDP ..... Gross Domestic Product

GHG ..... Greenhouse Gas

HBBS ..... Hybrid Battery – Battery System

HE ..... High Energy

HP ..... High Power

HESS ..... Hybrid Energy Storage Systems

IPCC ..... International Panel of Climate Change

Definitions and Abbreviations

LA ..... Lead-acid

LI ..... Li-ion

MES ..... Mechanical Energy Storage

MS-ESS ..... Medium-scale Energy Storage Systems

NMC ..... Nickel Manganese Cobalt Oxide

NiCd ..... Nickel Cadmium

OCV ..... Open Circuit Voltage

OPEX ..... Operating Expenditure

PHES ..... Pumped Hydro Energy Storage

PV ..... Photovoltaics

REPEX ..... Replacement Costs

SC ..... Supercapacitors

SMES ..... Superconducting Magnetic Energy Storage

SoC ..... State of Charge

SS-ESS ..... Small-scale Energy Storage Systems

TES ..... Thermal Energy Storage

VRLA ..... Valve Regulated Lead-acid

Chapter 1 Introduction to the Energy Storage Problem

1.1 Is There a Global Energy Problem?

Energy conversion is one of humanity's greatest stories. Learning to harness additional energy beyond natural capacities is a specific human blueprint. The ages of sail, coal, and oil have dramatically transformed the way people live, rapidly moving societies from subsistence agriculture to highly urbanised, heavily industrialised, and globalised economies [1, 2]. This has also created, with very few exceptions for service-based economies, a worldwide addiction between energy consumption and economic growth. The link is obvious as energy statistics show an ever-increasing total world demand, which reached record levels of around 595 EJ after the COVID-19 pandemic recovery [3, 4]. Remarkably, despite all efforts, 80-82% of the total world energy is still based on fossil fuels, the same ratio as 25 years ago. The remaining 18-20% is covered by biomass, nuclear and renewable energy [4]. The main consequence is an increase in atmospheric greenhouse gas (GHG) emissions. If the problem is not tackled in time, the environmental changes and anthropogenic atmospheric pollution could be catastrophic [5].

Carbon dioxide is by far the most important climate change contributor and accounts for around 78% of the total GHG emissions since 1970 [6]. This has been identified as the main source of global average temperature increase, which is estimated to be around 0.65-1.06 ^{0}C above pre-industrial times. At the current rate of emissions, the 1.5 ^{0}C mark could be hit by the middle of this century. The probability of anthropogenic climate change has been classified by IPCC as *'extremely likely'* (according to IPCC metric, this is between 95-100% probability) [5, 6]. The evidence for this is complex and beyond the scope of this work. However, IPCC includes as evidence the ocean temperature increase (it is estimated that 90% of the energy added due to climate change has been stored in the ocean and only 1% in the atmosphere), the Arctic sea-ice retreat (estimated at around 3.5-4.1% per decade since 1979), the Antarctic sea-ice increase (around 1.2-1.8% growth rate per decade) and loss of biodiversity [5, 7].

A secondary consequence of energy-intensive economies is cost. The long-term average energy cost can be approximated to be 8-10% of a country's gross domestic product (GDP) [8, 9]. Even higher values of around 18% have been recorded in Eastern European countries in the early 1990s or during the 2008 financial crisis. This is significant as prolonged periods of high energy prices have detrimental macroeconomic consequences. Energy cost reductions could increase the economic performance of countries and reduce poverty.

In the last 30 years, environmental issues have slowly reached the top priority list of worldwide governments, but contrary to all efforts, global GHG emissions are rising. In 2023, the global CO_2

emissions per annum reached a historic high of around 37.4 $GtCO_2$ and a growth rate of 1.1%, when compared with 2022. Although CO_2 emissions decreased during the COVID-19 pandemic, in the last decade alone CO_2, emissions grew on average 0.7% per year [6]. Looking at the global trend, this has continuously increased for the last 30 years reaching a value of around 60% higher than 1990 levels [4].

There are three main reasons for this: population and economic growth, failure of international politics and emissions redistribution [9, 10]. The first is obvious when confronted with the staggering fact that the total world economy reached $100 trillion in 2022, from just $33.5 trillion in 2000 [11]. The second shows that reaching global agreements on the climate change problem is very difficult, as countries are in different stages of development. Also, international treaties are notoriously difficult because of the ineffectiveness of enforcement mechanisms. Overall, regarding global climate change policies, there is a long list of treaties banning certain gases or promoting efficiency standards. However, in the last 30 years, there has been just one legally enforceable treaty, the Kyoto Agreement 1997, to deal with the overall emissions of countries signing up to the agreement. The third reason has to do with the fact that in a global economy, manufacturing and energy-intensive industries have slowly been relocated from Western economies to the developing world, where coal is still the most important energy source. In China alone, between 2000 and 2019, the coal power stations sector grew from 200 GW to above 1000 GW. At the same time, the total share of coal in China has decreased in the last years, but in absolute terms is still rising, projected to reach 1300 GW by 2026-2030 [12].

There is a positive story regarding decarbonization progress in the worldwide power sector. Including hydropower, in 2021, around a third of global power generation came from renewables. This is an increase from just 12% in 1990 [13]. The main reason for this is the dramatic fall in renewable power generation costs. Analyses in the REN21 and IRENA [13, 14] report that in the last decade, before the current anomalies in the energy markets, the global average of the levelized cost of electricity produced by utility-scale photovoltaics (PV) dropped by 85%, from 0.381 $/kWh in 2010 to 0.057 $/kWh in 2020. Residential PV electricity cost decreased between 50-80% in the same period, dropping to around 0.055 – 0.236 $/kWh. Onshore and offshore wind also decreased by 56% and 48% to around 0.039 $/kWh and 0.084 $/kWh, respectively. Although dwarfed by PV and wind in terms of global capacity growth, the electricity cost of concentrating solar power (CSP) also decreased by 68% in the last decade reaching an average of 0.108 $/kWh. These figures show a growing share of variable renewable generators connected to power systems worldwide competing successfully with traditional electricity generation plants. This is only going to accelerate in the next decades with the electrification of heat and transport. For example, in the UK, the total electricity consumption could double by 2050 [15].

1.2 Why Energy Storage?

It is clear from the above that urgent action is needed to reduce emissions and promote green economic growth. The United Nations lists clean energy access, under Millennium Development Goals (MDG) – SDG7 and the IPCC reports, and discuss at length the global capacity to achieve these and the rate at which we need to transform the current energy systems [5, 6]. The road to a sustainable energy future is strongly linked with our ability to store energy in the wider power industry.

Power systems will play a crucial role in a sustainable future, especially with the electrification of transport and heat. We've already seen this, between 2013 and 2022, global renewable power generation has expanded from approximately 1567 GW to 3382 GW [16]. Most of the added capacity comes from wind and solar power. For example, at the end of 2022, wind and solar accounted for 29% of renewable power generation worldwide, up from just 17% in 2014. The UK has performed far better than the world average, increasing its renewable power capacity by more than 4.7 times over the same period [16].

Table 1-1. World Renewable Power vs United Kingdom 2010-2022 [16]

World	**Renewable Capacity – 2010**	**Renewable Capacity - 2022**
Total World Renewable Power	1224 GW	3382 GW
Total World Offshore Wind Power	3 GW	63 GW
Total World Onshore Wind Power	178 GW	836 GW
Total World Solar Power Capacity	42 GW	1062 GW
United Kingdom	**Renewable Capacity - 2010**	**Renewable Capacity - 2022**
UK Renewable Power Capacity	9.6 GW	53 GW
Total UK Offshore Wind Power	1.3 GW	13.9 GW
Total UK Onshore Wind Power	4.1 GW	14.2 GW
Total UK Solar Power Capacity	0.9 GW	13.4 GW

Table 1-1 indicates the evolution of renewable power capacity globally and in the UK. Between the PV and wind generation capacities (offshore and onshore), solar PV growth is dominant. However, total PV generation still lags the overall wind capacity in the UK and worldwide.

However, as the share of renewable energy rises, the power grid operation becomes increasingly difficult because of the variable nature of renewable power sources. There are three main challenges associated with this: ***technical***, ***economic*** **and** ***operational*** [10].

The ***technical*** challenges associated with many distributed generators are related to keeping the grid parameters and protection equipment within the grid code specifications. Examples of technical problems to overcome include the distribution and transmission network voltage stabilisation, larger swings in grid frequency, power flow control issues, protection against islanding and power quality issues. For most of the 20th century, the power grids worked as integrated utilities from generation to distribution allowing engineers to design systems to be used as centralised power systems. They assumed well-known patterns of power flow from large generation plants to consumers. The design aspects of the power grids were based on this, like power line protection, transformer monitoring and substation control. Renewables slowly challenge this with large quantities of electricity being produced, transported, and consumed at the distribution level. This raises questions regarding protection, power flows and voltage regulation, especially for old equipment designed for specific network models. Another characteristic of renewable sources is their low inertia, which is directly linked to frequency control. For example, in the UK, the total installed power capacity is around 100 GW, and the renewable power installed capacity is above 50 GW. This already requires new energy storage systems to help the frequency control system.

The second problem is related to the power system ***economics***. The energy plants and utility networks are natural monopolies and typically exhibit a distinct economic profile, characterised by large capital investments and long operational lifespans. Traditionally, electricity could not be stored, and the entire economic model requires complicated regulatory systems to avoid price spikes and offer stable returns for investors. For most of the last century, these challenges were addressed by using vertically integrated utilities, which could plan for the long term and coordinate network expansions alongside investments in associated power generation. To avoid planning uncertainties, competition against utility networks was illegal in most countries, including the UK [10]. Since the early 2000s, the UK has seen a shift with the introduction of independent network operators, who are regulated, technically and economically, as distribution network operators. The centralised model slowly becomes outdated as the electricity market has been liberalised, and generators and network investments are based on competition. Another classical economic problem is the zero-marginal cost of renewable electricity and the challenges

it imposes on revenues for peak generators. As electricity production must match the demand on a second-by-second basis, traditionally, power plants were brought online based on their efficiency and marginal cost – the additional cost of one extra unit of electricity. The marginal cost of electricity is mainly related to fuel, and as renewables have zero 'fuel' cost, this fixes the short-term price of electricity to zero. This simply implies that existing plants, designed for peak operation, struggle to recover their investments as renewables 'cannibalise' their revenue [10].

The third major challenge is ***operational***. The new power consumer types added to the network bring new possibilities for different markets. For example, the utility networks' digitalisation brings new opportunities for time-of-use tariffs, peer-to-peer trading, demand response, smart electric vehicle (EV) charging and many more. All these increase the challenges for the grid operators and even redefine their role. However, due to the complex nature of the proposed new smart grid architectures, the final arrangements are still in the research and development stages.

In conclusion, sustainable energy is linked with the ability to store electricity. Energy storage can help address most of the above problems by storing electricity during low-demand periods and discharging during peak demand. This improves the electricity systems' technical and economic stability and slowly transforms the traditional 'special' electricity market into more like the oil and gas market, where storage plays a much more visible role. The importance of energy storage technologies has been recognised by governments and industry leaders alike and broad national strategies have been developed to tackle the challenge [17, 18].

1.2.1 Energy Storage UK Context

Comprehensive reviews have compiled tens of research studies that estimate the energy storage requirements for grids with a high share of variable renewables. However, the precise electricity storage requirements vary across power grids because each country has unique wind and solar profiles and different hydropower potential. Nevertheless, a general picture emerges, increased variable renewables demand greater storage capacity. A generic power grid with a share of 10-70% variable renewables has relatively low energy storage requirements, below 25% of the maximum power demand (GW), and below 0.1% of the total yearly electricity consumption (GWh). However, studies show that the requirements increase to 75% of the maximum GW grid demand, and around 1% of total yearly electricity consumption for 100% variable renewable grids [19, 20].

For the UK grid, including interconnectors, renewables over-generation, nuclear and demand management, studies estimate that around 46 GW of storage is required for zero-carbon electricity, half of which is long-term storage, above 4-hour duration and up to weeks and months [21]. Currently, the UK has around 5.8 GW of electrical storage installed, around 2.9 GW/26.7

GWh being pumped hydro and 2.8 - 2.9 GW battery storage with 1-2 hours discharge duration [22]. Also, the UK has one of the fastest-growing utility battery storage markets with around 66 GW of new projects in the pipeline [23]. However, most of these are designed for short-duration storage and not all projects will be built due to local planning and network constraints. Aurora estimates that around 24 GW of storage with 1-4 hours duration, generally covered by batteries, will be required for a UK net-zero power grid [21]. The above figures show that energy storage, especially utility battery storage, already plays a significant part in the power sector, and its role will only increase.

1.3 Why Hybrid Storage?

Storage is necessary in any economic system but inevitably adds cost to the overall process. In an ideal world, goods and services are produced, transported, distributed, and consumed steadily, without buffers between supply and demand. However, it's impossible to coordinate thousands of actors to adjust their behaviour to achieve this. Storage adds breaking points in the chain to help the coordination process between supply and demand. In other words, the lack of coordination is measured by the added storage cost in any system.

Electricity markets and power systems are not dramatically different from any other economic system. This is why reducing the energy storage cost and improving the reliability of existing systems is crucial to a renewable future. In addition to technological improvements, economies of scale and production automation, hybrid systems are a quick way to reduce the cost of energy storage. Evidence of this is presented in the literature review chapter, but to illustrate the concept, Figure 1-1 shows a real case study of a daily energy storage demand profile for a full year (this is the daily battery storage profile for a light commercial load with a 1MW PV generation system). It shows that the energy storage must deliver a variable MWh per day across the year with a maximum of 2.3 MWh/day. To supply that, an energy storage system of at least 2.3 MWh, capable of performing at least 144 cycles is needed (there are 144 days in the year when the storage system is cycled). However, technologies which can provide an increased number of cycles are generally more expensive (£/kWh), when compared with lower cycle life options, and any underutilisation or oversizing adds cost. A closer look at Figure 1-1 shows us that around 0.9 MWh of energy storage is underutilised, it performs a maximum of 17 cycles per year. In other words, the system is 'oversized', because we are using a technology which can perform 144 cycles per year but not operate at its potential. An ideally sized energy storage system would be composed of two technologies, one of 1.4 MWh which can deliver around 127 cycles (blue graph, Figure 1-1) and a cheaper, lower specifications storage option, of 0.9 MWh, capable of

performing at least 17 cycles per year (red peaks, Figure 1-1). This potentially saves cost by avoiding over-specification for the 0.9 MWh storage capacity.

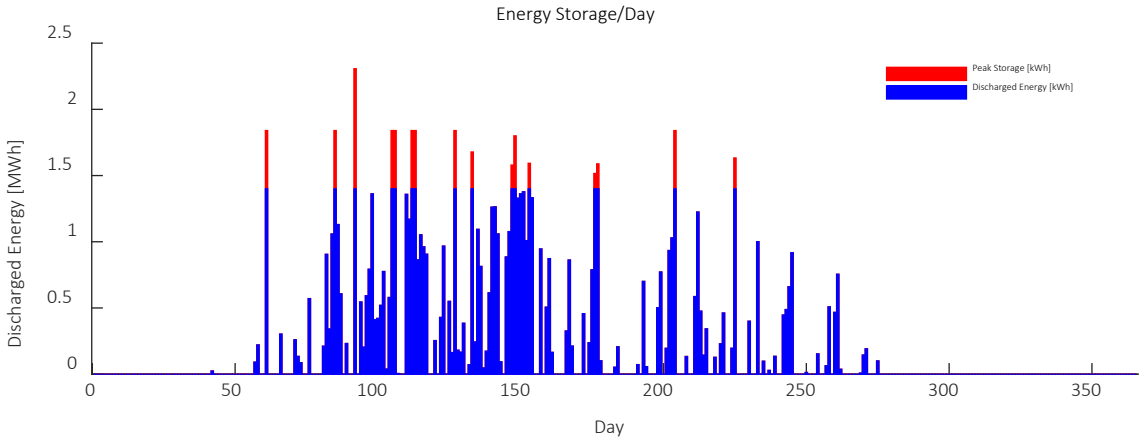

Figure 1-1. Daily Energy Storage Demand

How multiple technologies are linked in hybrid configurations to obtain the 'optimised' system described, and what options are complementary to their operating characteristics, will be discussed in the literature review chapter. However, the main scope of this thesis is the directly connected Li-ion and lead-acid hybrid option, and the reasons why are explained below.

1.4 Research Scope

As explained, energy storage is crucial to the future power systems. This implies that improving the current technologies or using the old options in new ways to reduce cost and improve the recyclability and sustainability issues are desperately needed. The hybrid Li-ion and lead-acid technology achieves that by coupling a cheaper, mature battery with a newer, more expensive option.

The main research objective of this thesis is to investigate one of the simplest hybrid battery storage possible, the directly connected Li-ion (NMC) and lead-acid (VRLA). This is done on three fronts, on-site trials, lab testing and technical and economic modelling. The main reasons for investigating the Li-ion and lead-acid hybrid storage option and the research scope associated are the following:

First, the hybrid NMC and VRLA operating voltage profiles are complementary and, as demonstrated in this work, the hybrid configuration can work effectively, connected directly at the DC level without power converters. In addition to reducing the system cost, this eliminates the additional points of failure in the storage unit. The voltage profiles of the NMC and VRLA cells allow independent use of the Li-ion strings to perform most of the frequent cycling and separate use of the lead-acid strings to address the energy storage discharge peaks, as indicated in Figure

1-1. This can be achieved without control systems, which reduces the cost further. However, the operation of such systems is not well understood, and there is no research on the subject. The results presented in this thesis address, for the first time, the topics of the energy round-trip efficiency in a hybrid configuration, the power and energy sharing between the strings, the general hybrid behaviour, and the system performance over time. This is done by testing a lab-based Li-ion and lead-acid hybrid system and an on-site demonstrator project. A hybrid battery model was built using equivalent circuits populated with the lab data to predict the experimental results obtained.

Second, using a hybrid system, cost savings are possible using a lower specification and lower battery cost technology to capture the energy storage profile peaks. This gives more flexibility to the design process and avoids oversizing the storage system for specific applications. Additionally, compared with a single Li-ion battery storage option, the dual configuration use of Li-ion and lead-acid technologies reduces the environmental footprint. This is because lead-acid battery cells are fully recyclable and have one of the highest recycling rates for battery storage, above 95%. This forms the second major scope of this research, which involves the hybrid sizing issue, and shows that certain load profiles are suited for this type of storage system. The thesis investigates the techno-economic sizing of the solar PV, wind and hybrid storage systems working in on-grid and off-grid configurations, including frequency response and balancing markets.

In summary, the scope of this research project is to investigate the following four main questions mentioned in the beginning:

- What are the hybrid characteristics of directly coupled, hybrid Li-ion (NMC) and lead-acid (VRLA) systems?
- Can the instantaneous hybrid behaviour be modelled using equivalent circuits?
- How do hybrid battery systems perform over time in real-world applications?
- What storage applications are best suited for hybrid lead-acid and Li-ion systems and what are the associated techno-economic parameters?

The following chapters address these questions individually.

Chapter 2 Thesis Structure

2.1 Thesis Structure

This thesis is layered in 8 chapters, including the introductory sections.

Chapter 3 provides a brief review of the energy storage options. It details the traditional energy storage technologies and their operating range, to contextualise the hybrid energy storage options between them. After a review of the general hybrids, the chapter focuses on the possible hybrid battery technologies. The final part of the chapter presents an overview of the equivalent circuit battery modelling options.

Chapter 4 is dedicated to the research methodology, and it presents the main questions addressed in this thesis and how they are investigated. The chapter contains four main sections. The first section describes the experimental lab arrangement used during the project and the testing methodology for the directly connected hybrid battery systems. The battery parameters extraction methodology is presented in the second section, which also includes the main features of the MATLAB model using the parameters obtained. The third section describes the hybrid battery demonstrator project tested for degradation. The final part of the chapter describes the techno-economic model used for the hybrid sizing investigations and the assumptions used to achieve this.

Chapter 5 presents the results of the lab-based investigations addressing the directly coupled hybrid battery system. The results include the lab testing data of 5 different hybrid battery systems and the operating parameters comparison. The main discussion focuses on the round-trip efficiency, power and energy sharing between the strings and the dynamic system behaviour.

Chapter 6 captures the MATLAB hybrid Li-ion and lead-acid modelling results. The chapter ends by comparing the results predicted by the MATLAB tool with the experimental data presented in the previous chapter (Chapter 5).

Chapter 7 shows the experimental data gathered by on-site testing of the ADEPT demonstrator project to address real-world operation research questions, like capacity degradation.

Chapter 8 is dedicated to the techno-economic modelling of the hybrid battery. The section includes the sizing and optimisation for five case studies, residential, off-grid EV charging, industrial, commercial, and front-of-the-meter applications, and investigates the cost comparison between the dual and single chemistry battery systems. The case studies are

analysed under different testing scenarios, on-grid, off-grid and multiple overgeneration scenarios.

Finally, Chapter 9, presents the conclusions of the thesis, the potential future work to improve the hybrid battery system, and the project legacy.

2.2 Publications

Table 2-1. Publications and Presentations

Presentation/Publication	Year	Type
Hybrid Li-ion and lead-acid modelling (planned, based on Chapter 6, the paper was reviewed internally)	Assumed 2025	Energies Journal
Experimental Investigations into a Hybrid Energy Storage System Using Directly Connected Lead-Acid and Li-ion Batteries https://doi.org/10.3390/en17184726	23 September 2024	Energies Journal
A techno-economic analysis of a hybrid energy storage system for EV off-grid charging IEEE Xplore: 13 September 2023 https://doi.org/10.1109/ICCEP57914.2023.10247395	27-29 June 2023	27-29 June 2023 International Conference on Clean Electrical Power (ICCEP), Italy
Experimental DC-coupled Li-ion and lead-acid batteries	October 2022	Conference presentation, World Energy Storage Conference, Birmingham (Best Presentation Award)
Performance of a hybrid battery energy storage system. Energy Reports: https://doi.org/10.1016/j.egyr.2022.05.040	5 May 2022, Accepted 13 May 2022, Available online 28 May 2022	Conference Presentation
Hybrid Battery Storage for Renewable Application	3-4 November 2021	Conference Presentation Northern Industrial Battery Services (NiBS)
Hybrid Battery Modelling	5 November 2021	Conference Presentation 19th Asian Battery Conference

Operational experience and system modelling of dual chemistry ESSs	November 2021	Magazine article, Batteries and Energy Storage Technology Magazine (BEST Magazine)

Chapter 3 Energy Storage Literature Review

This chapter briefly reviews the energy storage technologies currently used in power systems for grid services and energy arbitrage. The first part of the chapter analyses the traditional mechanical, electrical, and chemical energy storage systems and presents their general operating parameters to illustrate potential hybridisation options. The second part is dedicated to general hybrid energy storage, which ends with the specific hybrid battery energy storage family. Within this category, the hybrid Li-ion and lead-acid option is discussed, which is the focus of this thesis. The chapter ends with a battery modelling literature review.

3.1 Introduction

As mentioned, energy storage has gained increased attention in the last few years due to renewable energy playing an increasing role in the energy mix. There is no shortage of technologies to address the current and future energy storage demand, but further development is required regarding these options before global-scale deployments.

It is difficult to estimate the total energy storage capacity worldwide as there is no reliable data on stand-alone systems, like domestic thermal energy storage. However, large data sets exist for grid-connected applications. In 2020, the total world electrical energy storage (EES) capacity was around 4.7 TWh. This is expected to triple by the end of 2030, mainly because of transport electrification [24]. To put things in perspective, the global yearly electricity consumption was around 25,500 TWh in 2022 [4]. EES capacity is less than 0.1% of the current world electricity demand. In terms of size, the global EES market is dominated by pumped hydroelectric (PHES) technologies with around 160 GW installed in 2021 and 96% of the total EES market [25]. However, this is expected to drop to around 51% by 2030 as double-digit growth is expected in the electric vehicles (EV) market and ESS for concentrating solar power (CSP). Overall, the non-pumped hydro storage is predicted to increase to 5500-8500 GWh in 2030 [26].

Depending on their operational role and combined energy and power ratings, energy storage systems can be classed as short, long, and very long-duration energy storage technologies. The short-duration options can discharge at their rated power capacity up to 3-4 hours, long-duration technologies up to hundreds of hours, and very long-duration up to months and years. Alternatively, storage technologies can be categorised based only on their capacity [27]:

- Large-scale energy storage systems (LS-ESS) (1 GW to 100 MW, GWh capacities).
- Medium-scale energy storage systems (MS-ESS) (100 MW to 0.1 MW, MWh capacities).
- Small-scale energy storage systems (SS-ESS) (100 kW to 1 kW, kWh capacities).

For grid-connected systems, each of these categories taps into the power system at different voltage levels, as indicated in Figure 3-1. Large and medium-scale energy storage categories are connected at high voltage, both generation or transmission and at medium voltage for distribution level systems. Small-scale ESS are located close to the demand substations and are connected at the low voltage level [27].

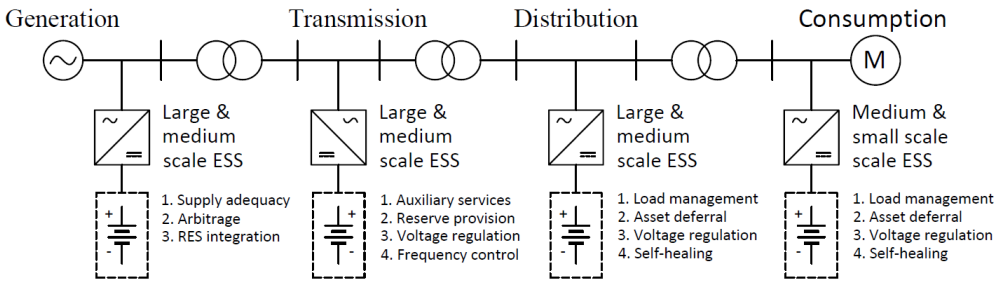

Figure 3-1.ESS at different voltage levels

ESS can provide a wide range of services depending on their power and energy capacity ratings. For each section of the power system (generation, transmission, distribution, and consumption) a non-exhaustive group of energy ES services has been listed in Table 3-1.

Table 3-1. Possible services provided by energy storage.

Generation (LS & MS ESS)	**Transmission (LS & MS ESS)**	**Distribution (LS & MS ESS)**	**Consumption (MS & SS ESS)**
Supply adequacy	Ancillary services	Load management	Load levelling
Energy time shift	Reserve provision	Asset deferral	Peak shaving
RES integration	Voltage regulation	Voltage regulation	Power quality
Electric supply capacity	Frequency control	Self-healing	Power reliability
Frequency control	Congestion relief		

3.1.1 Energy Storage Technologies

There is a wide variety of technologies available to provide the services illustrated in Table 3-1 and there is not a one-size-fits-all solution. Although this report mainly focuses on battery energy storage technologies (BESS), a quick review of the other major options is given to contextualise the BESS market within the overall energy system. Energy storage technologies currently used in power systems are categorised based on the physical transformations used in the process. As illustrated below in Figure 3-2, these can be grouped into three major categories, mechanical, electrical and chemical.

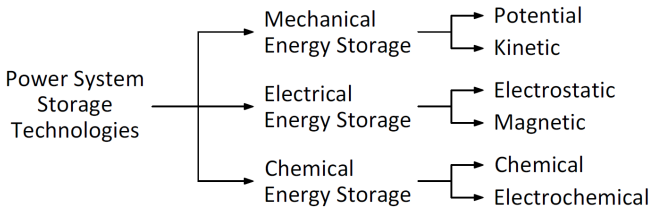

Figure 3-2. Energy Storage Technologies

3.1.2 Mechanical Energy Storage

Mechanical energy storage (MES) technologies are generally divided into two categories, based on how the mechanical energy is stored, potential or kinetic. The most popular potential energy storage technologies are pumped hydro systems (PHES) and compressed air energy storage (CAES). Flywheel energy storage systems (FES) use kinetic energy storage principles.

PHES and CAES provide GWh storage capacities, are usually connected to the power grid at the transmission level and dominate the LS-ESS market. The core working principles of these technologies are well understood. For PHES, during the charging process, water or potentially other mixtures are pumped to the upstream lake, and for discharging, the energy is extracted using standard hydroelectric principles. The round-trip efficiency of PHES technologies is around 70-80%. The technology has a very long lifetime, up to 40-60 years. However, as a mature technology, no major cost reductions are expected in the next decades, but new operational strategies are being investigated. The UK has around 26 GWh of PHES capacity in its currently four operational plants but this could triple in the next decades as several additional plants are in the planning stages [22]. CAES technologies store energy by pumping air into large, sealed reservoirs, usually gas-depleted oil fields or salt caverns. During discharging, the air is expanded through a standard gas turbine. Natural gas can also be used to increase the expansion parameters to improve the system performance. Depending on the heat management of the plant, the round-trip efficiency of the system is between 75-89% [28]. As indicated in Table 3-2, PHES and CAES options are site-specific, require large capital investments, and do not have the potential for drastic cost reduction in the following decades. However, research is being carried out into both these technology categories, especially PHES with variable speed pump turbines or CAES with advanced thermodynamic cycles and thermal storage. Although the response time is of the order of minutes, traditionally, more than 80% of these two technologies have been used for energy arbitrage [26].

Table 3-2. Mechanical energy storage technologies [28, 29]

Metric	Unit	Pumped Hydro Storage	Compressed Air Storage	Flywheels Energy Storage
Specific energy	[Wh/kg]	0.3–1.3	3–60	5–15
Energy density	[kWh/m^3]	0.5–1.3	0.4–20	0.25–420
Specific power	[W/kg]	0.01–0.15	2–24	400–1500
Power density	[kW/m^3]	0.01–0.15	0.04–10	1000–3000
Efficiency	[%]	65–87	57–90	70–96
Lifespan	[years]	20–80	20–40	15–20
Cycle life	[cycles]	Practically unlimited	Practically unlimited	10,000–100,000
Self-discharge rate	[%/day]	Negligible	Negligible	24–100
Advantages		Robustness Fast rump rate Long lifetime Mature technology Most economical	Robustness Long lifetime Possibilities of further improvements	Modular technology High power density High efficiency Fast response time
Disadvantages		Geographical limitations High initial cost Environmental effects	Geographical limitations High initial cost Environmental effects	Advanced controls Low energy density Friction losses
Application		Energy management Reserve provision Frequency response	Energy management Reserve provision	Transient stability Peak shaving Frequency regulation Power quality

Kinetic energy storage is represented by FES, which stores energy using a rotating mass, usually in a vacuum chamber to reduce the self-discharge. The system is charged and discharged using an electric motor-generator system. For low-speed FES, the rotational speed is around 10000 rpm. For high-speed FES, this can reach up to 100000 rpm. The round-trip efficiency of the technology is generally very high, above 95%. There is a wide variety of FES available but, overall, the technology is well understood but improvements are still possible regarding the materials for the spinning mass, bearings, and control methods.

FES fall into MS & SS ESS and can be used in a variety of applications, including frequency support, and power quality, but currently, around 55% of the systems are used for on-site back-up UPS.

3.1.3 Electrical Energy Storage

Electrical Energy Storage (EES) technologies use electromagnetic fields as the storage medium. Examples are capacitors and supercapacitors (SC) for technologies using electric fields and superconducting magnetic energy storage (SMES) for systems based on magnetic field storage. The SC devices use the electrostatic double-layer effect, and electrochemical pseudo capacitance, to increase their total capacity per unit volume or mass up to 100 times the value of standard capacitors. SMES systems consist of large superconductor coils able to sustain high values of magnetic fields by running large currents through practically zero resistance wires. EES cover the high-power market for large and small-scale systems applications. As detailed in Table 3-3, the great advantages of SMES and SC are the high-power densities, up to 100 kW/kg, and the possibility to perform millions of charge/discharge cycles.

Table 3-3. Electrical energy storage technologies [27, 29, 30]

Metric	Unit	Capacitors	Supercapacitors	Superconducting Magnetic Energy Store
Specific energy	[Wh/kg]	0.01-0.05	0.07–86	0.27–75
Energy density	[KWh/m^3]	~0.05	1–35	0.20–14
Specific power	[W/kg]	10,000-1,500,000	5.5–100,000	500–15,000
Power density	[kW/m^3]	~10^6	15–4,500	300–4,000
Efficiency	[%]	90-95	65–95	80–95
Lifespan	[years]	15-20	5–20	20–30
Cycle life	[cycles]	Practically unlimited	10,000–1,000,000	10,000–100,000
Self-discharge rate	[%/day]	10-15	0.5–40	1–15
Advantages		Mature technology Long lifetime & cycle life Robustness High power density	Mature technology Long lifetime & cycle life Robustness High power density	Long lifetime & cycle life High energy efficiency High power density
Disadvantages		Very low energy density and specific energy	High cost Low energy density	Expensive materials Low energy density Complex control systems
Application		Power quality High power applications Power factor correction	Transportation Power tools Power quality Frequency regulation	Power quality Frequency regulation

The SMES technologies can be used in power systems to provide grid services [31]. Typical SMES applications include damping power system oscillations, voltage stability and improving power quality. The energy storage applications using SMES fall into the LS & MS ESS grid-connected system. However, due to high costs, a limited number of projects have been developed worldwide. A typical SMES application is the LTS SMES Hosoo in Japan [32].

SCs have a larger market when compared with SMES, initially used in portable applications and emergency power supplies, they are increasingly used in clean transportation, renewable power conditioning, power tools, solar street lighting and high-power actuators [33].

3.1.4 Chemical Energy Storage

Several comprehensive reviews have been consulted and all these split chemical energy storage (CES) into two major categories, batteries, and power-to-gas systems [27, 30, 34, 35]. From the power system perspective, the battery technologies of interest are lead-acid, Li-ion, nickel-cadmium (NiCd), nickel metal halide, redox flow and high-temperature batteries [30]. The second category, power-to-gas systems, is based on fuel cells to generate electricity from different gases (ex. H_2), produced using renewable power. Batteries dominate the CES, driven by falling prices due to transport electrification and distributed PV systems. It is estimated that the total grid-connected battery capacity could increase to above 400 GWh in 2030 from a baseline of around 170 GWh in 2018 [24, 26]. Currently, the CES technologies cover the MS & SS ESS categories. Fuel cells (or flow batteries) could reach the LS ESS category if large-scale power-to-gas systems become competitive. It is beyond the scope of this report to cover the entire CES category, but the most common technologies used in power systems are mentioned in Table 3-4.

The working principles of batteries & fuel cells are based on redox reactions to store and produce electricity. The main components of a generic electrochemical cell include an anode, an electrolyte, and a cathode. The discharge process is as follows: the active material gets oxidised at the anode, and the electrons are passed through an external circuit to the cathode, where the oxidised ions are reduced. Power is produced due to the potential difference between the positive and negative terminals [36]. During charging the process is reversed.

Table 3-4. Chemical Energy Storage – Batteries [24, 26, 27, 30, 34]

Metric	Unit	Li-ion	Lead-acid	Nickel Cadmium	Nickel MH
Specific energy	[Wh/kg]	30–300	10–50	10–80	30–90
Energy density	[KWh/m^3]	94–500	25–90	15–150	40–300
Specific power	[W/kg]	8–3,000	25–420	50–1,000	6–1,100
Power density	[kW/m^3]	57–800	10–400	38–140	8–590
Efficiency	[%]	70–95	63–90	60–90	50–80
Lifespan	[years]	2–20	3–20	2–20	2–15
Cycle life	[cycles]	250–10,000	100–2,000	300–10,000	300–3,000
Self-discharge rate	[%/day]	0.03–0.3	0.03–1.1	0.07–0.7	0.3–4
Advantages		High energy density High power density	Low cost per kWh and kW Recyclable Simplicity Robustness	Long lifetime Can work in very harsh conditions. Simple control Mature	Long shelf life Good power densities
Disadvantages		High cost Complex control	Hazardous H_2SO_4 Low cycle life	Toxic materials Memory effect	Memory effect High cost
Application		Frequency regulation Peak shaving Transportation Domestic PV applications	Standby power Frequency regulation Load levelling Spinning reserve	Off-grid PV applications LED lighting Backup power Small/medium-scale energy management	UPS, Transportation Small/medium-scale energy management

The first CES technology considered is the lead-acid battery, one of the oldest and most widely used storage options. It has found markets in almost all applications, from utility plants to transportation or other small-scale applications [30]. They usually come in two major categories, Flooded and Valve Regulated (AGM or Gel type). The indicative characteristics of the battery chemistry have been reproduced in Table 3-4, along with the advantages and disadvantages. Compared with other battery technologies, lead-acid systems are robust, simple, cheap and can work in challenging environments giving them an edge in the global market share. Because of their simplicity, almost 98% of lead-acid batteries are recycled in the EU and North America, making it one of the most sustainable battery options. Although new technologies are being researched, lead-acid technology will remain competitive in stationary applications, where weight and volume are not important, even if the cost of Li-ion and other chemistries is falling [24, 37].

Li-ion batteries are relatively new but thanks to their improved performance, they have revolutionised the consumer electronics industry and the EV market in just a few decades. As indicated in Table 3-4, it has one of the largest power and energy densities, which makes it ideal for transportation and consumer electronics, replacing Ni-MH. The detailed chemistry of the battery is complex, but the general arrangement contains the layered anode and cathode with the Lithium ions moving back and forth between the two during charging and discharging [38]. The separators keep the active electrode materials apart to avoid internal short circuits. The entire structure is filled with a liquid or gel electrolyte, usually a lithium salt dissolved in an organic solvent [38]. The overall performance of the battery is highly dependent on the electrode materials. This will be discussed in the following sections, but it is worth mentioning that the anode is usually layered graphite or lithium titanate and the cathode is one of the five major chemistries, LFP, NMC, LCO, NCA and LMO [34]. The Li-ion battery has successfully been used in the UK grid applications to provide grid services, reaching the 2.9 GW mark in 2023. The total capacity is expected to increase rapidly in the following years. For example, in 2020, an addition of 1.3 GW is ready to be built, 5.7 GW are in the planning stages and 6.5 GW have been proposed [39]. The general characteristics of Li-ion batteries have been listed in Table 3-4.

The next battery family is based on nickel, NiCd and NiMH. The technologies have niche energy storage applications, mainly linked with harsh operating environments. The NiMH technology has dominated the hybrid vehicles sector, but the Li-ion option is rapidly replacing it. Both technologies use the same anode electrode, based on nickel hydroxide [30]. NiCd uses cadmium hydroxide as the cathode material, which is reduced to metallic cadmium in the charged state. One of the major disadvantages of this is that cadmium is a toxic material. The NiMH cell uses metal hydride alloys for the negative electrode, which allows the hydrogen ions insertion. A general performance of the technology is listed in Table 3-4. The NiCd and NiMH cells have specific technical characteristics, like low internal resistance, high power capacity and constant voltage discharge. Several examples of energy storage applications for this technology type are LED lighting in off-grid systems, off-grid road signs, backup systems for electrical substations and UPS systems for harsh environments. As an example, one of the largest grid projects using NiCd batteries is the 46 MVA BESS in Fairbanks Alaska, USA, used to provide reserve for the local grid [40].

Table 3-5. High-temperature Sodium Batteries & Fuel Cells. [27, 30]

Metric	Unit	Sodium sulphur (NaS)	Sodium MH ($NaNiCl_2$)	Fuel Cell (PEMFC)
Specific energy	[Wh/kg]	100–240	85–140	100–450
Energy density	[KWh/m^3]	150–345	108–190	112–770
Specific power	[W/kg]	14–260	10–260	4–150
Power density	[kW/m^3]	1.33–50	54–300	4–35
Efficiency	[%]	65–92	21–93	22–85
Lifespan	[years]	5–20	7–14	0.2–10
Cycle life	[cycles]	1,000–4,500	2,000–3,000	Practically unlimited
Self-discharge rate	[%/day]	0.01–20	12–27	Negligible
Advantages		Cheap and common materials Non-toxic components Extreme working environments	Cheap and common materials Extreme working environments	Power is decoupled from energy. High specific energy
Disadvantages		Insulation (makes sense for large applications) Temperature protection	Insulation (makes sense for large applications) Slightly more expensive than NaS	Expensive materials
Application		Utility applications Bulk energy storage Load levelling Peak shaving	Load levelling Frequency regulation Energy management Stationary backup.	Transportation Military equipment Possible large-scale storage in power-to-gas arrangements

Another important group of electrochemical technologies used in power systems is the high-temperature batteries, exemplified in Table 3-5 by sodium sulphur and sodium MH batteries. The working principles are like other batteries, the differences are that the electrodes are liquid, and the electrolyte is solid. The operating cell temperature is also different, around 300-350^{0}C, which is much higher when compared with other technologies. This is required as the electrolyte starts to conduct sodium ions only in this temperature range [30]. The great advantage of these technologies is that the materials used are inexpensive and widely available. The downside is that the high operating temperature of the battery requires thermal insulation and complex thermal management systems. The technology is used for utility-scale applications, especially in Japan and the USA [41]. The total world power capacity has been estimated to be around 400 MW [41]. The general characteristics of high NaS and NaMH are indicated in Table 3-5.

The flow battery technology is another possible CES for large grid-scale applications. These systems differ from traditional electrochemical cells because the active materials are dissolved in liquid electrolytes and stored in separate tanks [42]. The active materials are pumped through a fuel cell, where the redox reaction takes place. The great advantage of this is that increasing the energy capacity of the system does not require an increase in the thickness of a solid material, thus virtually unlimited watt-hours could be achieved, without decreasing the power ratings of the battery. The typical flow battery technologies are the vanadium, bromine, and iron-salt based options but newer solutions include organic-based electrolytes [43, 44]. The flow battery technology can be used in power systems and is a strong candidate for the upper end of the LS ESS. Currently, flow batteries are used in grid-connected applications up to hundreds of MW [44].

3.1.4.1 Temperature Effects on the Li-ion and Lead-acid Batteries

The operational environment impacts the performance of chemical energy storage technologies because chemical reactions depend on temperature. The impact of this on the battery storage performance and degradation has a vast literature and a detailed investigation is beyond the scope of this work. However, this section highlights the main temperature effects on the lead-acid and Li-ion cells from a high-level engineering perspective, as these technologies are investigated later in this thesis. A good place to start is the general assumption that in lower temperatures ion diffusion decreases, which means lower chemical reaction rates. The opposite happens as temperature increases.

The operational temperature of lead-acid cells is linked with the internal resistance variation, capacity available, degradation, charge/discharge time, gassing rate, and self-discharge rate. Typically, manufacturers recommend 20-25^{0}C as the optimal operating temperature for lead-acid storage systems [45]. The internal resistance changes if the battery cells are operated outside this range. Similarly, if the temperature decreases, the ion mobility and the diffusion rates decrease. For example, Bhatt J.M. [25] tests several lead-acid cells and concludes that the internal resistance decreases linearly by 31.5% between 45-10^{0}C. The theoretical resistance, as a function of temperature, can be calculated using the Nernst Equation. The increase in resistance implies lower voltage during discharge and higher during charge [46]. The higher voltage required during charge needs to be implemented in the charger software, otherwise, in lower temperatures, batteries will ‘fool’ the charger to assume it reached 100% SoC. Undercharging the lead-acid battery for long periods will lead to sulfation and degradation. Sulfation happens when the lead sulphate crystallises irreversibly on the plates and no longer participates in the battery reactions leading to capacity loss [47]. To compensate for lower temperatures charging voltage, as a guide, for every degree drop in the battery temperature, 3.5-4 mV per cell should be added to the charger voltage [48]. The Nernst Equation also indicates the

EMF varies with temperature and electrolyte concentration. However, the battery voltage during charge/discharge will mainly be determined by the internal resistance value.

The lead-acid degradation increases if the battery operates above 25^{0}C. The main reasons for this are the plate corrosion due to increased acid reactivity, water evaporation, increased sulfation during discharging and increased risk of thermal runaway due to reduced resistance and increased acceptance rate. As a guide, every 8-10^{0}C temperature increase will shorten the battery lifecycle by 50% [49].

The battery capacity and the charge/discharge time increase with temperature, mainly because of increased reaction rates inside the cells. Bhatt J.M. [50] shows that the battery capacity increases by 98% between 10 and 45^{0}C. Similar results are indicated for the charging time. Gassing is also linked with temperature and can increase up to 5 times between 20 and 45^{0}C operational temperature.

The self-discharge rate for lead-acid batteries also varies with temperature and can rise by 60 to 70% when the temperature is increased from 20 to 45^{0}C.

The broad temperature effects on Li-ion cells are like those mentioned for the lead-acid batteries in terms of degradation and performance loss when storage systems operate outside optimal thermal intervals. However, as the Li-ion chemistry is more complex, the causes of degradation and internal resistance increase are different.

Ma et al. [51] and Leng et al. [52] identify three main effects of low-temperature operation of the Li-ion cells: electrolyte viscosity increase, charge-transfer resistance rise and lithium plating. The increase in electrolyte viscosity is directly linked to the rise of the internal resistance and the charge/discharge performance. Leng et al. [53] demonstrate that the internal resistance can increase to 80% when the Li-ion cells are cooled from 55^{0}C to 25^{0}C. Similarly, the charge transfer resistance increases by 11% in the same temperature range due to a lower charge transfer rate. Similar results are reported by Razi et all [54] concluding that the internal resistance of a Li-ion NMC cell decreases 3.5 times when it is cooled from 80^{0}C to 25^{0}C. If a cell is cooled from 50^{0}C to -20^{0}C, the internal resistance can increase by up to 20 times [55]. Łebkowski [56] reports similar results analysing LFP cells of various sizes, operating at temperatures between 55^{0}C and -30^{0}C and shows that the overall internal resistance can increase up to 15 times when the cells are cooled to -30^{0}C. The first consequence of this is the capacity reduction of the Li-ion battery when is operated at low temperatures. Lv et al. [57] confirm this by comparing three different Li-ion chemistries (LFP, NMC and LCO) at eight temperatures, from -40^{0}C to 60^{0}C. Taking the 25^{0}C temperature tests as a reference, the results show that at -40^{0}C the LFP cells lose 53.4% of their capacity, the NMC technology 63.2% and the LCO 88.3%. Another effect of low-temperature

operation is lithium plating at the anode, which is strongly linked with low ionic diffusion, slower kinetics and higher charge transfer resistance [58]. This impacts capacity, performance and cell safety directly.

At higher operation temperatures the chemical reaction rates at the anode and cathode of a Li-ion cell increase. The first consequence of this is the higher capacity available for cycling [53]. Depending on the Li-ion chemistry, the available capacity can increase as much as 14%, from the optimum operating temperature of 25^0C, if the cells are heated to 55^0C [57]. However, higher temperatures and increased reaction rates introduce unwanted reactions and chemical instabilities. In the long term, this accelerates degradation. Leng et all [52] review the main chemical effects of operating Li-ion cells at higher temperatures and list the following: electrolyte decomposition, structural changes to the electrode, active materials dissolution, phase change in the electrode insertion, active materials dissolution, passive film formation over electrodes and current collector changes. All of these effects are interdependent but the main result is the overall cell degradation, in terms of shelf and cycle life [59]. Spitthoff et all [59] show this by reviewing nine different degradation studies of LFP, NMC and LCO technologies, cycled at 1 and 0.5 C rates and concludes that temperature operation is the most important factor in cell degradation. For example, the LFP cells, cycled at 30^0C, achieve ~3400 cycles before the capacity drops below 80% of the initial value. At the same time, if the LFP cell is cycled at 45^0C, it can deliver only up to 1000 cycles before the capacity decreases to 70% of its initial value. Zülke et all [60] report increased degradation if the Li-ion cells are stored at higher temperatures and high SoC. The study concludes that cells stored at 50^0C, after one year, degraded almost twice as fast as those stored at 25^0C, for the same SoC. Lam et all [61] present a decade-long study on hundreds of Li-ion cells on calendar ageing at different temperatures. The paper indicates variations within the same cell type and temperature storage, but the overall conclusion is that the cells stored at higher temperatures degrade much faster. The study shows that all cells stored at 45^0C or above, reach 80% of their initial capacity within 4 years. All cells that retain more than 80% of their initial capacity were stored at 24^0C. From the engineering perspective, the Li-ion battery degradation under suboptimal temperature conditions directly impacts the range of EVs and the grid operation. For example, Yuksel et all [62] present a dataset of 7000 Nissan Leaf trips across the USA, and because of different climatic conditions, the study concludes that in colder regions the range of EVs decreases by 25 - 35% when compared with warmer climates like the West Coast of the USA (this includes the battery capacity decrease due to lower temperatures and the additional energy consumption). Senol et all [13] present a similar analysis, including the impact of increased EV demand on the grid (peak demand, harmonics increase, voltage drop issues) due to low-temperature charging. In the UK, for example, the grid peak demand difference between winter and summer, for a hypothetical fleet of 11 million EVs, can reach above 600MW.

3.2 Hybrid Energy Storage - Literature Review

3.2.1 High Power vs High Energy Technologies

Analysing the table data presented in the previous section (Table 3-2, Table 3-3, Table 3-4, Table 3-5), it can be seen that some storage technologies perform better in terms of their power and energy characteristics than others. A visual representation of the power and energy characteristics of the different energy storage technologies has also been illustrated in Figure 3-3. There are vast performance differences between the top left of the graph, high-power (HP) technologies and the bottom right, high-energy (HE) technologies. For example, SCs can deliver thousands of times more W/l when compared with lead-acid batteries but have lower specific energy capacity. All the technologies listed in Section 3.1 can be grouped into two main categories, HP and HE sources. There are five major categories of HP and HE sources which have been indicated in Table 3-6 [63]. For grid-connected applications, the fast HP sources are used for instantaneous frequency response and the HE technologies for slower services such as tertiary frequency response or bulk energy management.

Table 3-6. High Power and High Energy Storage Technologies [63]

High Power – Energy Storage	**High Energy – Energy Storage**
Flywheels	Pumped hydro
Supercapacitors	Compressed air storage
Capacitors	Fuel cells
SMES	High energy batteries
High power batteries	Power to gas

Following the information presented in Section 3.1, it can be concluded that most HP devices share a few general characteristics. Firstly, they have the longest cycle life among ES technologies, reaching hundreds of thousands of cycles and lifespans of above 15 years. Secondly, they have very fast response time being able to provide high pulses of power for short periods of time, for example, FES, SMES and SC can respond within one second [64]. Thirdly, they have high energy efficiency and self-discharge rates, and round-trip efficiency values can reach above 90%.

The HE characteristics, however, tend to complement these. As indicated in Section 3.1, they usually have lower cycle lives and lifespans (except PHES and CAES), slower response time, lower efficiencies, and lower discharge rates but higher energy densities. Excluding the economic aspects, some of the technologies presented above can be engineered for both HP and HE. The

most obvious example is batteries which can, to a certain extent, be tailored for both power and energy applications [65].

Several reviews discuss in further detail the differences between the HP and HE sources as well as their current and future applications within the power systems, but essentially, HP are better suited for frequent cycling and HE for energy arbitrage [63, 64, 66, 67].

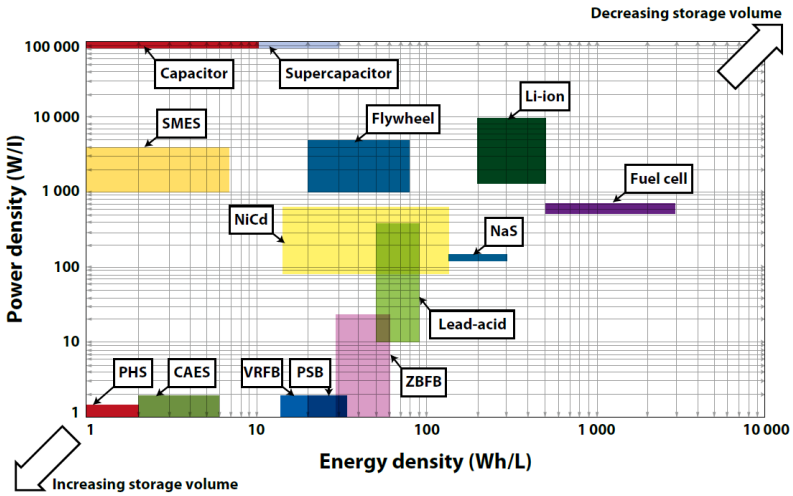

Figure 3-3. Energy and power density for renewable energy storage technologies [26]

The obvious observation is that operating HE systems (excluding PHES or CAES) as HP sources can lead to rapid degradation and performance loss. A hybrid option between HP and HE sources could provide the best of both worlds. This is already the case for the wider power grid, which dispatches different power and energy storage sources as a function of their technical and economic characteristics. Hybridisation of energy storage in the same plant unit can provide further flexibility, including economic benefits.

3.2.2 Hybrid Energy Systems

As explained above, a single storage technology type can't be tailored efficiently (regarding the technical and economic parameters) for both power and energy applications, especially for the extremes. To enhance the performance of individual ESS, hybrid arrangements between HP and HE technologies have been proposed to harvest the benefits of both technology types [63]. Table 3-7 lists the possible options for hybrid storage technologies [63]. Although all options listed are theoretically possible, not all solutions are practical from an economic perspective.

Table 3-7. Possible HESS configurations

HP – Energy Storage	HE – Energy Storage	References
Battery	Supercapacitor	[68-71]
	SMES	[72]
	Flywheel	[73, 74]
	Battery	[75]
CAES	Supercapacitor	[76]
	SMES	-
	Flywheel	[77]
	Battery	-
Fuel Cell	Supercapacitor	[78]
	SMES	[79]
	Flywheel	-
	Battery	[80]
Pumped Hydro	Supercapacitor	-
	SMES	-
	Flywheel	-
	Battery	-
Thermal Storage	Electric energy storage	Future

Detailed solutions for the hybrids are shown in Table 3-7 are discussed, from both practical and theoretical perspectives in literature review works like [63, 66, 67]. Several solutions indicated are more popular than others. One of these is the hybrid option between batteries and SCs. Less known are the battery–battery hybrids which are the focus of this research thesis.

The overall benefits of hybridisation are related to lifespan improvement, cost reduction and power quality improvements. For example, a hybrid arrangement of FES working as an HP source in parallel with a storage unit based on Li-ion technology as the HE element can reduce the stress on the battery cells. This improves the battery life by more than 20% [73]. Similar results can be achieved if different battery types are used in the same battery pack but optimised for HP and HE [75].

The technology surrounding a hybrid energy storage system (HESS) can become very complex (this is one of the main drawbacks of hybrid solutions), but the general structure contains four major elements, the HP, HE storage sources, the hybrid architecture, and the control strategy.

3.2.3 Hybrid System Architectures

Connecting two or more ES technologies in a hybrid arrangement involves a mixture of power converters and control modules. This is usually referred to as the system topology or architecture which defines the system's operation and performance. The literature indicates two broad categories of hybrid architectures, passive and active (semi-active and full active are also

possible) or various combinations of these [81]. An overview is presented below with a focus on the passive hybrid topology as this option is used in the following chapters for the hybrid Li-ion and lead-acid battery system.

The passive architecture is the simplest among the hybrid arrangements because, essentially, it is a direct connection between the HP and HE sources without using any power electronic converters [68-70]. As indicated in Figure 3-4 (a), the HP and HE devices share a common voltage bus with V_{HP} and V_{HE} being the same. An improved version is shown in Figure 3-4 (b) where a DC-DC converter was introduced between the common bus and the inverter input. This allows the voltage bus to work independently of the inverter requirements. In both cases, the voltage window of the two components needs to match, otherwise one of the devices will be underutilised or dangerous conditions could develop. The power-sharing between the HP and HE devices can't be controlled directly, and vary according to the internal resistances of the ES devices, R_{IHP} & $R_{IHE,}$ and their equilibrium voltages [81]. However, the V_{HP}, V_{HE} and R_{IHP}, R_{IHE} also vary with the state of charge, temperature, and degradation of the devices. This can create a variable power distribution behaviour between the units [82]. If the dynamic behaviour of the two energy sources is different, circulation currents between the strings can occur due to the two relaxation voltages being different. The advantages of passive arrangements are that they are simple, require little space, and are cost-effective. An additional advantage over the active systems is efficiency, with no power converters the roundtrip losses are reduced [81]. The disadvantages are the limited power control and voltage matching requirements between the HP and HE sources. The round-trip efficiency can decrease if the circulation currents are significant or difficult to control, but this also depends on the energy storage technologies of the two units.

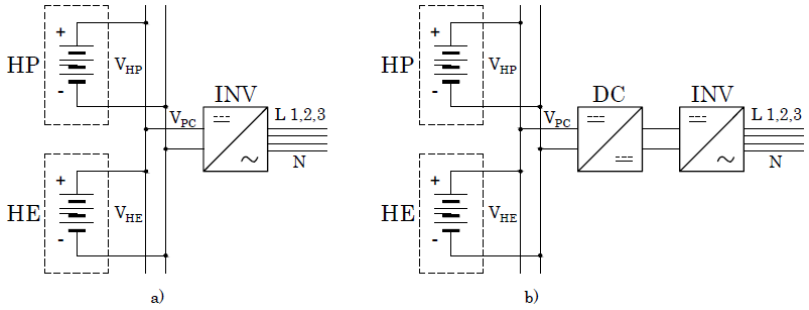

Figure 3-4. Passive Hybrid Arrangements

The literature presents many experimental studies of different technologies using passive architectures, especially for the battery and supercapacitor hybrids. For example, a simple AAA alkaline battery is tested in a passive connection with a SC, and the author concludes that the pulse power of the hybrid arrangement is 40% higher than for the battery alone [83]. This comes at a cost of just 9% weight and 10% volume increase. An example of a 23F supercapacitor bank working in a passive connection with a 7.2V Li-ion battery, and operated under pulse load profiles,

shows that the overall power capacity of the arrangement can be increased by a factor of five [68]. Also, power losses have been reduced by 74%. The results are dependent on the duty cycle of the load. Another passive hybrid between a Li-ion battery and a SC has been investigated under pulse loads, and the author concludes that the optimum capacity utilisation is achieved for a duty cycle of 0.2-0.3 [84]. The impedance of the system is also reduced. Chuan et al. [85] does a comparative analysis between battery-only and hybrid battery-SC systems in terms of power capabilities, discharging time and energy efficiency. The results show improvements of 2.6 times in terms of power ratings, a 30% increase in discharging time and a 10% for energy efficiency.

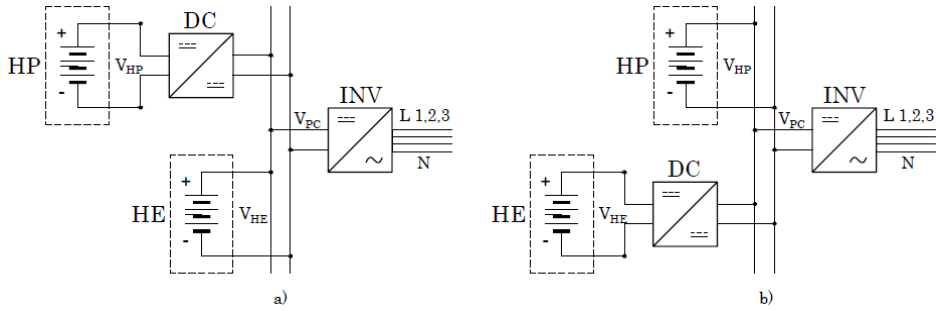

Figure 3-5. Semi-active Hybrid Arrangements, HP semi-active (a) HE semi-active (b)

The next class of hybrid architectures are the HP and HE semi-active topologies which introduce DC-DC converters between the HP and HE storage units and the system bus, Figure 3-5 [81]. Figure 3-5 (a) shows that a DC converter is introduced between the HP and V_{PC} bus voltage, thus creating an HP semi-active system. The advantage of this is that it makes it possible for the HP source to work at an independent voltage from V_{HE}. This allows the full utilisation of the HP device from zero to 100% state of charge. This is especially useful when the HP device is a SC because they have a wider operating voltage range compared with batteries. As the control strategy is independent, it allows for the HP source optimisation for different operating conditions. The disadvantages of the arrangement are that the extra DC converter brings additional losses into the system and must be sized for high power pulses and wide input voltage ranges which adds to the cost of the overall hybrid.

The HE semi-active topology, Figure 3-5 (b), introduces a DC converter between the HE source and the system bus [81]. This allows independent operation of the HE energy source and the DC-DC converters are designed for lower power peak ratings. The disadvantage of the arrangement is that the DC converter and INV must work at the same voltage as the HP source. In this case, the bus voltage needs to operate between wider voltage ranges, especially if the HP source is a SC. Song Z. et al. [86] analyse the performance of different hybrid semi-active topologies.

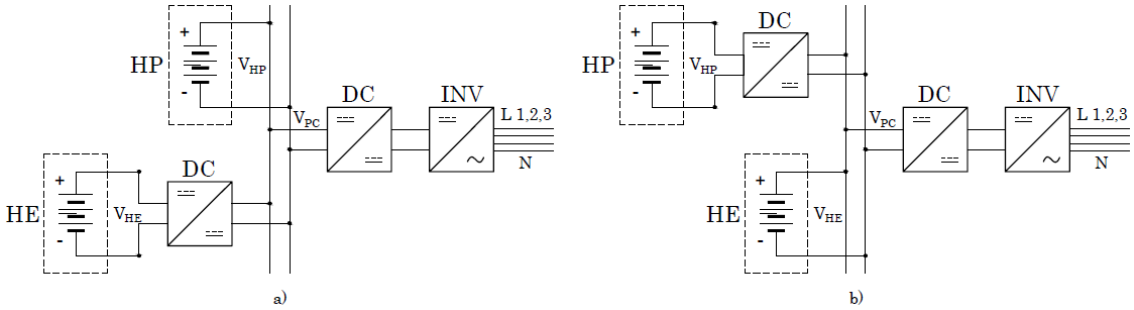

Figure 3-6. HE cascaded full hybrid topology (a), and HP cascaded full hybrid topology (b)

The fully active hybrid architectures have been reproduced in Figure 3-6 (cascaded) and Figure 3-7 (left) (parallel). The full cascaded topologies improve on the semi-active system introducing an extra DC converter between the V_{PC} and the inverter. This allows the HP and HE sources to operate optimally at separate voltages and power ratings. The main disadvantages of a fully active system are complexity, lower efficiency and cost. The cost addition is because the second DC converter must be sized for full load. The lower efficiency, when compared with other architectures, is due to the two conversion stages across the DC converters, which is also cited as a disadvantage [81]. The full active topology, Figure 3-7 (left), includes separate DC converters for each HP and HE storage unit. This allows true independent control of the HP and HE sources. Compared with the cascaded systems, the DC converters are cheaper because the HP-DC are sized for peak power and HE-DC for the average demand.

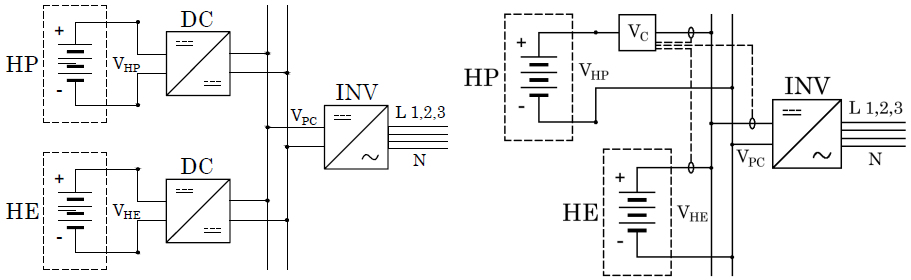

Figure 3-7. Parallel full-active hybrid topology (left) & Semi-active topology (right)

A special case of semi-active hybrid topology is indicated in Figure 3-7 (right). The additional element added to the system is a power electronic component inserted in series with the HP or HE sources (or both) to balance the voltage difference between the strings during the system rest period. The power electronics component measures the currents on all strings and the total system output, to determine if the system is discharging or resting, and based on this, it actively adjusts the V_c voltage introduced to minimise the circulation currents. The advantage of this system is that the converter could be cheaper when compared with the full-active topology, as it can be sized for a much lower power rating (tens to hundreds of watts). The disadvantages are that there is limited string control, which relies on the voltage profiles of the individual HP and HE sources, and the additional losses introduced into the system.

3.2.4 The Case for Battery Hybrid Energy Systems

Every hybrid solution presented in Section 3.2 has its advantages and disadvantages. This section, however, will make the case for one of the most attractive hybrid options, hybrid battery–battery systems (HBBS). Currently, battery storage packs use just one cell chemistry carefully optimised between power and energy performance but a hybrid solution does this separately and has the potential of cost reduction without performance losses [75]. The arguments are centred on three main points, the possibility of simple hybrid architecture, different chemical properties, and cell specialisations.

Firstly, when compared with battery-SC hybrids, HBBS have the potential to work effectively using just passive architectures. As discussed in Sections 3.2.1, 3.2.2 and 3.2.3, developing a HESS brings additional power electronics equipment and complicated control systems. This adds extra cost because the power electronics associated with battery storage systems can be as high as 30% of the total system cost [26] (around 40% is the cell cost and 30% the peripherals, which include cables, connectors, switches and transformers). The use of passive architectures limits the extra power electronics equipment needed but as discussed, it requires that HP and HE sources have similar operating profiles. Because of this, HBBS becomes an attractive option, as batteries like Li-ion or lead-acid can be connected in series to achieve the same operating voltage window. The Li-ion technologies can be hybridised between themselves or with other battery families.

Table 3-8. Li-ion chemiseries vs Lead-acid [26, 34].

	Unit	Lithium Iron Phosphate	Lithium Manganese oxide	Lithium Titanate	Lithium Cobalt Oxide	Lithium Nickel Cobalt Aluminium	Lithium Nickel Manganese Cobalt	Lead-acid
Cathode Chemistry	-	LFP	LMO	LTO	LCO	NCA	NMC	PbO_2
Specific Energy	[Wh/kg]	80-130	105-120	70	120-150	80-220	140-180	10-50
Energy Density	[Wh/l]	220-250	250-265	130	250-450	210-600	325	25-90
Specific Power	[W/kg]	1400-2400	1000	750	600	1500-1900	500-3000	25-415
Power Density	[W/l]	4500	2000	1400	1200-3000	4000-5000	6500	10-400
Voltage	[V]	3.2-3.3	3.8	2.2-2.3	3.6-3.8	3.6	3.6-3.7	2.1
Cycle life	-	5000-6000	300-2000	5000-20000	300-1500	1000-3500	3000-4000	300-1500
Installation Cost	[$/kWh]	400-500	400-900	600-2000	500-600	600-1000	500-900	65-120

Secondly, different battery chemistries are more suitable for power or energy performance. As it can be seen in Table 3-8 and Figure 3-8, the Li-ion battery family has multiple chemistries with different characteristics. Some can provide cheaper high-power properties but not energy capacity and vice versa. This has to do with the fundamental nature of the active materials, the cathode in particular. Christian Julien et al. [87] explains that the Li-ion battery cathode can have

a layered, spinel or olivine structure. Generally, a 2D layered structure (ex. LCO) makes it harder for Li^+ ions to move in and out of the active material and this limits its power capabilities. The olivine or spinel structures (ex. LFP) have multiple dimensions for ion mobility, facilitating faster and ultimately safer charge and discharge cycles. This is also reflected in the cell cost, Table 3-8. The same is valid between battery chemistries, especially lead-acid batteries which have a very low cost per kWh but can't provide the same power density as most Li-ion technologies. This concludes that hybrid options between the various Li-ion chemistries mentioned or as discussed in this thesis, between Li-ion and lead-acid can provide cost-reduction opportunities.

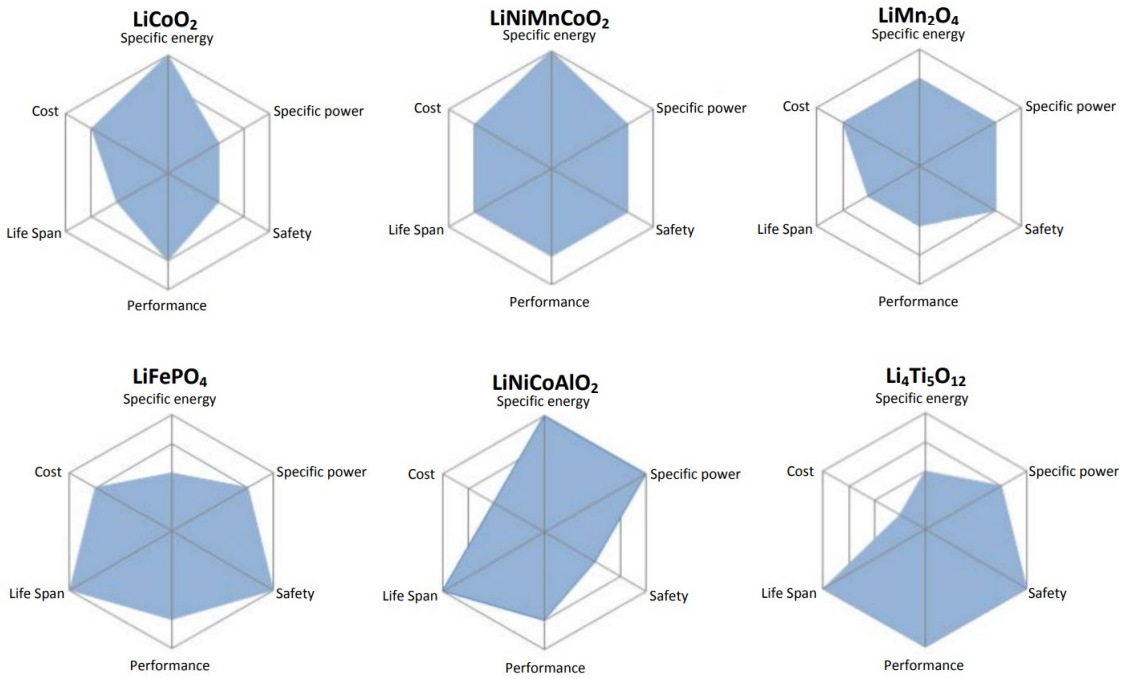

Figure 3-8. Li-ion chemistries characteristics

Thirdly, another advantage of HBBS is cell specialisation. The power and energy characteristics of battery cells are not solely determined by the chemistry used but also by the cell engineering. Generally, the power and energy capacity of batteries are linked. Modifying one changes the other which inevitably results in oversizing. Lain M.J. et al, Becker J. et al, Chuan Y. et al, Quinn J.B. et al, Burke A. et al [65, 75, 85, 88, 89] discuss in detail the engineering parameters of high-power and high-energy battery cells. The studies mentioned include detailed discussions about how this determines their overall performances.

For example, Lain M.J. et al [65], employ a teardown approach of nine Li-ion cells from well-known manufacturers like Samsung, LG and Sony to determine the cell engineering properties. They conclude that all cell components, especially the electrodes, are different from HE cells to HP cells,

Table 3-9. The most important differences, however, are the active materials used for the electrodes. For example, small particle sizes are important for HP cells to improve the time necessary for Li ions to move in and out of the cathode. Coating porosity is also a determining factor, as high porosity improves ion mobility. All these characteristics are significant for the manufacturing cost and that is why, depending on the application, a balance between power and energy is usually employed.

Table 3-9. Cell Components for HE and HP batteries

Component	**High Energy Cells**	**High Power Cells**
Electrodes	High coat weights Low coating porosity Medium to large particle sizes Low conductive carbon content Minimum possible binder content	Low coat weights High coating porosity Small to medium particle sizes High conductive carbon content
Current Collectors	Thinner Coated to improve adhesion	Thicker Coated to reduce resistance
Separator	Thin	Thin
Electrolyte	High conductivity	High conductivity
Connection tags	Thin/narrow tags Single tag on each electrode	Thick/wide tags Multiple tags

A HBBS can take advantage of this, and ‘specialise’ the storage cells just for power or energy. Later, in the design stage of energy storage units, the necessary power and energy characteristics can be achieved through combinations of the two battery cells. This has the potential for cost reduction and improved design flexibility. This is graphically shown in Figure 3-9, the power and energy cell parameters are represented by vectors. The X and Y vector components are the energy and power of the cell, the ratio between the two is fixed.

In Figure 3-9 (a), a generic battery pack needs to be sized to the indicated ‘System Requirements’ of power and energy. Designing the system using just one battery type, HP or HE with fixed power-to-energy ratios, results in oversizing. This is because manufacturers do not provide battery cells with any power-to-energy ratios. In Figure 3-9 (b), the same battery pack is sized using both HP and HE which have different power-to-energy ratios. This gives much greater flexibility in design, achieving the ‘System Requirements’ without oversizing the system in either power or energy. Visually, the two vectors can cover any point on the X-Y plane thus, in theory, two batteries, with two fixed power-to-energy ratios, can provide any optimised solution.

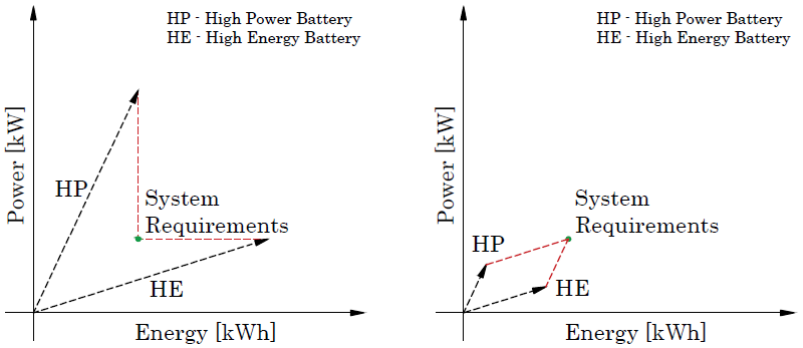

Figure 3-9.Sizing HBBS, Single battery type (a), Hybrid arrangement (b) [90]

Finally, as explained in the introduction, the variable nature of renewable generation means that when coupled to energy storage, the energy stores are subjected to many partial cycles, which do not make full use of battery systems, and this results in oversized storage systems. To illustrate this, Figure 3-10, shows a simple daily energy profile delivered by an energy storage system for one year. The load profile is a real case study of a light commercial site (Lidl supermarket) which has a 1 MW roof-mounted PV system and a 1 MW/2.5 MWh battery storage system. For this profile, the storage capacity and cycle life specifications required are around 2.5 MWh/day, capable of doing at least 144 cycles/year. This is however an 'oversized' system as around 0.9 MWh of storage capacity is only used for 13% of the time when the storage is active (red peak Figure 3-10). This means that 0.9 MWh of capacity can be a cheaper battery with a lower cycle life. The result of this would be a lower overall storage system cost.

One promising hybrid energy store for use with renewable generation is Li-ion cells directly coupled with lead-acid [91]. In this design, the Li-ion deals with frequent, partial charge/discharge cycles, and the lead-acid is reserved for the less frequent cycles when a greater depth of discharge is required. The Li-ion would cover the frequent, blue portions of the storage profile and the lead-acid would do the occasional read peaks indicated in Figure 3-10. This allows for a comparatively smaller Li-ion battery coupled with a much lower cost lead-acid to be used for the remaining required capacity. As the lead-acid is only cycled infrequently, the shorter cycle life is not a major issue.

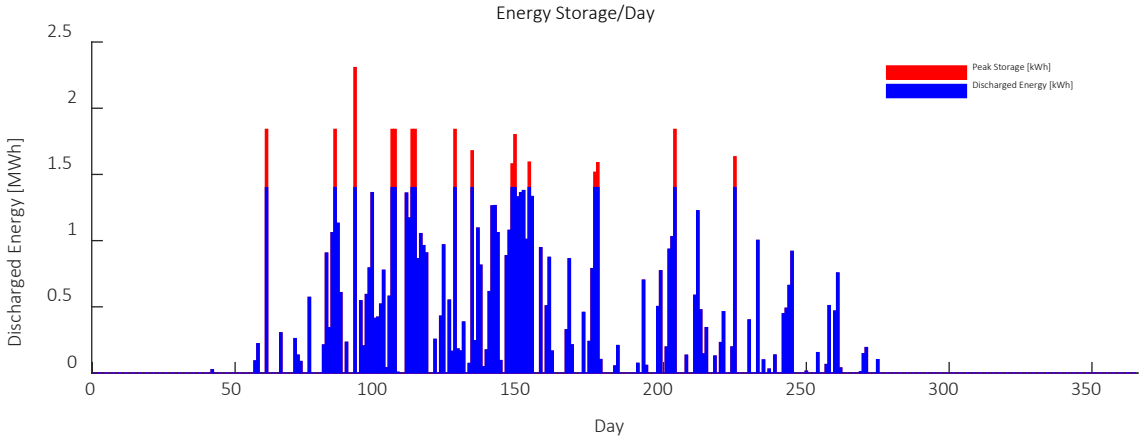

Figure 3-10. Example of an energy storage profile with a baseline storage requirement and short periods requiring additional capacity.

In conclusion, following the arguments presented above, hybrid battery systems have the potential for lower costs, more flexibility and can maintain the same performance as single-cell battery packs.

3.2.5 Examples of Hybrid Battery – Battery Systems

As mentioned, most of the battery storage systems use just one type of battery chemistry, however, there are several studies and commercial projects regarding HBBS. Most of these have been developed for electric transportation applications or grid services. This section will briefly discuss the current HBBS developments and include the relevant experimental conclusions.

Becker J. et al. [75], analyse the best-suited battery pack in terms of battery mass, volume and cost for five types of electric vehicles as illustrated in Figure 3-11. The study compares the single-cell pack performance versus a hybrid solution. For the analysis, the authors use five Li-ion battery types from different manufacturers, SB LIMotive, Kokam, Panasonic, A123 Systems and Toshiba. As indicated in Table 3-10, the battery cells have different characteristics in terms of their energy or power capabilities. Their physical shape is also different, prismatic, pouch bag or cylindrical. The energy densities of the chosen cells vary from the lowest of 46 Wh/kg to the highest 241 Wh/kg for the Toshiba and Panasonic cells. Similarly, the power densities vary from 362 W/kg to 3200 W/kg for the Panasonic and Toshiba cells.

Table 3-10. Cell Characteristics [75]

Cell Characteristics	SB LiMotive 60 Ah	Kokam 46 Ah	Panasonic NCR185650B	A123 Systems 26650 M1B	Toshiba 2.9 Ah
Cell Type HP or HE	Prismatic HE	Pouch Bag HE	Cylindrical HE	Cylindrical HP	Prismatic HP
Cathode/Anode	NMC/Graphite	NMC/Graphite	NCA/Graphite	LFP/Graphite	LMO/LTO
Energy Density	123 Wh/kg	144 Wh/kg	241 Wh/kg	109 Wh/kg	46 Wh/kg
Power Density	860 W/kg	433 W/kg	362 W/kg	2170 W/kg	3200 W/kg
Relative Cost	304 $/kWh	264 $/kWh	153 $/kWh	360 $/kWh	899 $/kWh

The paper does an in-depth Matlab – Simulink optimisation analysis to find the best cell type for single-cell and hybrid arrangements for the five types of vehicles indicated in Figure 3-11. The first row of Figure 3-11 shows the results for the single-cell battery pack using one of the cell types shown in Table 3-10. The clear winners are the SB LiMotive and Kokam cells. The second line shows the optimised hybrid arrangements using two battery cells, and the third, shows the relative difference between the reference battery pack (single cell) and the hybrid arrangements.

The results indicated in Figure 3-11 conclude that using a combination of HP and HE cells, significant savings on all three fronts, mass, volume, and cost are possible. The potential reductions vary for each vehicle and are up to 20% for the battery mass, 30% for the volume and 21% for the cost. The cost approximations include the DC/DC converters for fully hybrid architectures but not for the extra cost of the control system. In conclusion, Becker J. et al. [75] show that, depending on the vehicle specifications, HBBS could achieve reductions in terms of battery pack mass, volume and cost.

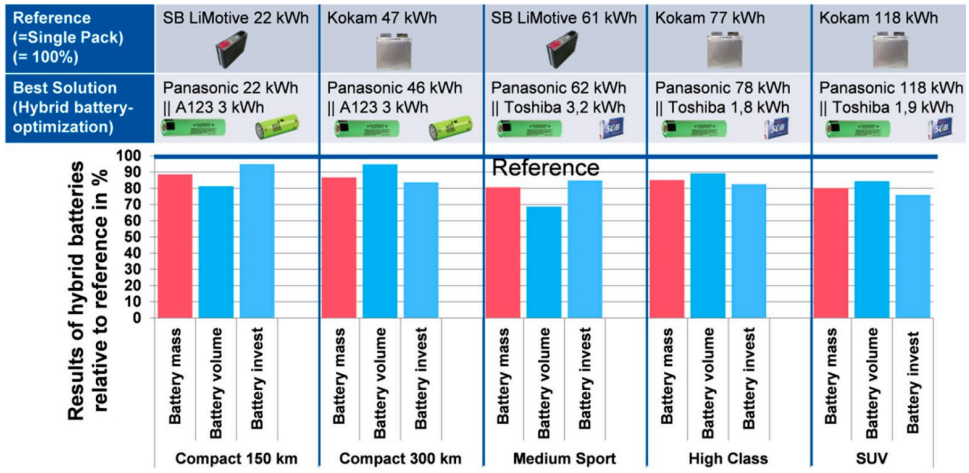

Figure 3-11. Single Cell vs Hybrid Battery Pack Comparison [75]

Another set of studies into HBBS is by Chung S. et al. [92, 93] in which they analyse and develop a hybrid configuration of Li-ion and lead-acid battery packs for the Polaris Ranger EV. Regarding the battery pack, the commercial Ranger EV vehicle comes in two options, the first option is eight 12V lead-acid batteries with a total capacity of 8.85 kWh and the second, is three 44V Li-ion

batteries with 9.34 kWh. The battery details have been reproduced in Table 3-11. When compared with the lead-acid, the Li-ion option is lighter and has much greater specific energy and energy density. This is also reflected in the price as the authors approximate that the lead-acid system is around 160 $/kWh and the Li-ion pack around 500 $/kWh. The goal of the papers was to develop a hybrid system with a price per kWh between the single lead-acid and Li-ion options and an improved range when compared with the simple lead-acid battery pack option.

Table 3-11. Ranger EV Commercial Battery Options

Characteristics	**Unit**	**Lead-acid Battery Pack Ranger EV**	**Li-ion Battery Pack Ranger EV**	**HBBS Pack Ranger EV**
Total vehicle mass	kg	777.9	547	655.9
Energy available 1C	kWh	8.85	9.3	8.42
Specific energy	Wh/kg	28.4	148	44.2
Energy density	Wh/l	10.1	179.7	85.2
Cost/kWh	$/kWh	160	500	322

The design strategy presented, centres around the hybrid architecture and the power algorithms. The topology used is a full hybrid system, with modular DC/DC converters, which allows independent control of each battery module. The power mix algorithm is a major part of the work and was designed to minimise the capacity reduction of the lead-acid battery due to the Peukert effect (capacity available is a function of the discharge current, higher discharge currents decrease the available capacity). The papers also do an in-depth optimisation analysis to determine the optimised ratio between the lead-acid and Li-ion as well as the configuration of the hybrid architecture. The final optimised hybrid solution is a battery pack consisting of two Li-ion battery modules and one lead-acid. The HBBS characteristics have been reproduced alongside the single chemistry options in Table 3-11.

After building and testing the system, Chung S. et al. [92, 93] results show that the HBBS is competitive with the simple lead-acid system but retains most of the performances of the full Li-ion option. Also, when compared with the simple lead-acid benchmark, the authors conclude that with just a 5% reduction in available energy, the HBBS achieved a 17% range improvement and a 23% efficiency increase for a full vehicle range cycle.

Takeda K. et al. [90] presents a dual chemistry Li-ion hybrid battery system for renewable applications developed and tested by Hitachi Research Laboratory and Shin-kobe Electric Machinery co. Ltd. The system uses a full hybrid architecture, with each battery chemistry bank being connected separately to the grid via a 200 kVA power converter. The battery characteristics have been reproduced in Table 3-12. The research is centred on two power-sharing algorithms,

First Order Filtering and Amplitude Sharing and demonstrates the advantages of Amplitude Sharing. The paper concludes that the HBBS cost is estimated to be 36% lower than the single chemistry pack.

Table 3-12. HBBS characteristics

Battery modules	**Unit**	**Power type Li-ion Battery**	**Energy type Li-ion Battery**
Nominal Voltage	V	173	25.9
Nominal Capacity	Ah	5.5	10
Total System	no.	26	414
System Voltage	V	346	414
System Capacity	Ah	71.5	80.0
Rated Power	kW	520	66

Another HBBS project is the M5BAT described by Thien T. et al. [94, 95]. M5BAT is a unique multi-battery system adding up to 5 MW and 5.4 MWh HBBS developed in Aachen, Germany by E.ON, RWTH Aachen University, SMA Solar Technologies (and others) to provide frequency services to the grid. It uses multiple types of lead-acid, Li-ion and Sodium Nickel Chloride chemistries, as indicated in

Table 3-13. The final arrangement can provide storage capacities for seconds, minutes and hours. The batteries are connected using ten 630 kVA inverters and the entire plant is controlled by a SCADA system. Currently, the system is being used for multiple research projects.

Table 3-13. M5BAT HBBS characteristics

Battery	**AC Rating Power [kW]**	**AC Rating Energy [kWh]**
Lead-acid 1 OCSM	1.260	1.325
Lead-acid 2 OPZV	761	761
Sodium Nickel Chloride	179	537
Lithium-Ion 1 (no LFP/LTO)	2.263	2.263
Lithium-Ion 2 (LFP or LTO)	537	537
Total	**5.000**	**5.423**

Schweer D. et al. [96], presents another HBBS using two battery technologies. The project was developed in Varel, Germany by Hitachi and NGK Insulators. Figure 3-12 shows the final arrangement of the plant. The hybrid system uses two battery chemistries, Li-ion and high-

temperature Sodium Sulphur. The project aimed to demonstrate the possibility of using the HP properties of Li-ion alongside the HE capacity of NaS to improve the overall plant performance.

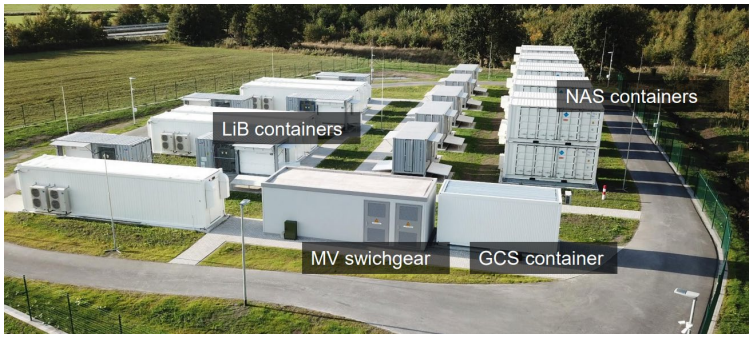

Figure 3-12. HBBS, Varel, Germany

The ratio between the two chemistries is 7.5 MW / 2.5 MWh for Li-ion and 4 MW / 20 MHh for NaS. These use a full hybrid topology provided by Hitachi Power Solutions. Currently, the system can provide Primary and Secondary Control Reserve, Supply Balancing and Reactive Power Generation. The system is integrated into a virtual power plant to participate in various power markets.

Another example is the hybrid battery solution for the Energy Superhub (Oxford, UK) which uses 2MW of vanadium flow batteries for heavy cycling, and 50MW of Li-ion system for longer duration loads [97]. A similar solution can be found in Braderup, Germany, where 2MW/2MWh of Li-ion batteries are linked with 325kW/1MWh vanadium flow batteries to support a local wind farm [98, 99]. The largest hybrid battery in Poland, Gdansk uses 1MW of lead-acid and 1MW of Li-ion to provide a total of 27MWh capacity to smooth the output of the Bystra wind farm [100]. Hoppecke has also installed hybrid lead-acid and Li-ion solutions at all scales [101]. Takeda K. et al [90] (Hitachi) present a lead-acid and Li-ion hybrid system for grid applications and discuss its sizing principles. GS Yuasa has also developed Li-ion and lead-acid hybrid systems for R&D purposes and EV charging station applications [102, 103]. The German company BOSS has developed a small-scale DC-linked lead-acid and Li-ion and hybrid system (LE300 – Smart Battery System) [104]. The BOSS storage system has successfully been used in academic studies for microgrid optimisation [105-107]. Similar studies discuss the sizing and control strategies of hybrid systems [75, 90, 93, 96]. Recently, GS Yuasa has installed two more Li-ion and lead-acid hybrid battery systems in Portsmouth and for a microgrid application for the UK Royal Mint site [103, 108].

In the commercial automotive sector, the Chinese car manufacturer NIO has introduced hybrid battery packs of 75 kWh combining NMC and LFP cells. The design ratio between the two cell types is not public but the company claims that the synergy of the NMC high energy density and the LFP power density improves the overall space utilisation and energy density. The company

states that the new hybrid system of 75 kWh has roughly the same price as the previous 70 kWh pack option. At the same time, with the 7% increase in the storage capacity, the space utilisation is also improved by 5% and the energy pack density by 14%. Also, the combination offsets the LFP's poor cold-weather performance [109-111].

The luxury SUV, BMW iX, uses the Gemini Dual-Chemistry Battery technology which mixes the LFP and anode-free cells (for the anode-free cells, lithium is deposited on a current collector, usually copper, not intercalated into the active material). The LFP technology provides 99% of the daily trips and the anode-free cells are used for longer trips. The system achieves one of the longest EV ranges available on the market, 600 miles on a single charge (WLTP test). The hybrid system reduces the use of lithium by 20% and graphite by 60% [112-115].

3.3 Battery Modelling

Mathematical models are of fundamental importance to any physical system. Battery storage systems are not an exception. From small electronic applications to grid storage, all battery systems use some type of modelling to describe the processes involved. Without this, system measurements and parameter predictions are impossible. This section reviews the background theory necessary for developing an empirical battery cell model, used later in the thesis, for battery cells and battery pack simulations.

There are multitudes of possible approaches to modelling an electrochemical system, but almost all of them fall into one of the following major categories:

- **Physics-based models (PBM)** – PBM models are based on modelling the fundamental physical processes inside the electrochemical systems and are built bottom-up. The internal chemical reactions, ion diffusion processes and the complex interactions between the electrolytes and electrodes are inherently difficult to model and that is why PBMs tend to be more difficult to implement, and not widely outside research activities.
- **Equivalent-circuit models (ECM)** – ECM models are based on equivalent electrical circuit elements as ‘models’ for the various processes taking place inside the battery. Complex phenomena like ion diffusion, for example, are lumped into just one or two electrical elements. This is a top-down approach where the battery's external voltage and current variations are assumed to follow models of simple electrical circuits, although the electrochemical processes can behave very differently from standard circuit theory. The solutions to the mathematical equations associated with these equivalent circuits are easier to compute. This is why almost all battery management systems (BMS) implement one version of these. Although ECMs do not offer the same in-depth information as PBMs, they are robust, computationally simpler, and adequate for most applications.

The electrochemical processes within Li-ion and lead-acid batteries are different, but both can be modelled using equivalent circuits. The differences appear in the magnitude of the various equivalent circuit elements.

In a typical Li-ion cell, the discharge process begins in the negative electrode, which is usually made of graphite. The lithium atoms intercalated in the graphite layers are released and travel through the material layers up to the particle surface. At the surface of the material particle, the lithium atom releases an electron, becomes positively charged and enters the electrolyte. The released electron travels through the material and the external circuit to the positive electrode. The lithium ions diffuse through the electrolyte and separator and reach the electrode-electrolyte interface of the positive active material where they reconnect with the electrons. The next process is the positive material diffusion, when the lithium atom diffuses through the material particle and gets stored between the material layers. During charging, the processes reverse.

For a traditional lead-acid cell, the reactions are different, but the overall idea is the same. During discharge, at the negative electrode, usually sponge lead, the surface Pb atoms get ionised and enter the electrolyte, where they react with SO_4 ions to create PbSO4. The released electron travels through the electrode and the external circuit to the positive terminal, usually a lead frame covered with PbO_2, where it reacts with hydrogen ions to produce Pb ions, which later react with the electrolyte SO_4 ions to create $PbSO_4$. The electrolyte is thus consumed during discharging. During charging, the process is reversed, and the $PbSO_4$ deposited at both electrodes is reversed to the original electrode materials, Pb and PbO_2.

In all the simple reactions explained above for both Li-ion and lead-acid, the electrochemical transformations are accompanied by ion and atom diffusion phenomena and various conduction processes. These can be summarised as follows:

- Diffusion in the solid phase
- Charge transfer reaction
- Electronic conduction in active materials and current collectors
- Diffusion in the electrolyte phase

Each of these can be modelled by one or more equivalent circuit elements.

3.3.1 Electrical Equivalent Circuit Elements

At no load, the battery chemical reactions are at equilibrium, which means they are balanced by the electric field formed at the electrode-electrolyte interphase. If current is being drawn from the battery, the electrodes are said to be polarised and move away from their open-circuit voltage. This is due to the batteries' internal impedance, which includes the *electrolyte resistance, charge transfer resistance, double-layer capacitance* and *diffusion impedances (Warburg)* in the electrolyte and active material. This has been indicated in Figure 3-13. When under load, all these elements contribute to the battery voltage dynamics. A mathematical relationship between these

and the battery voltage can be established using equivalent circuits. However, before considering the actual circuits, I will briefly provide a short description of each element [116].

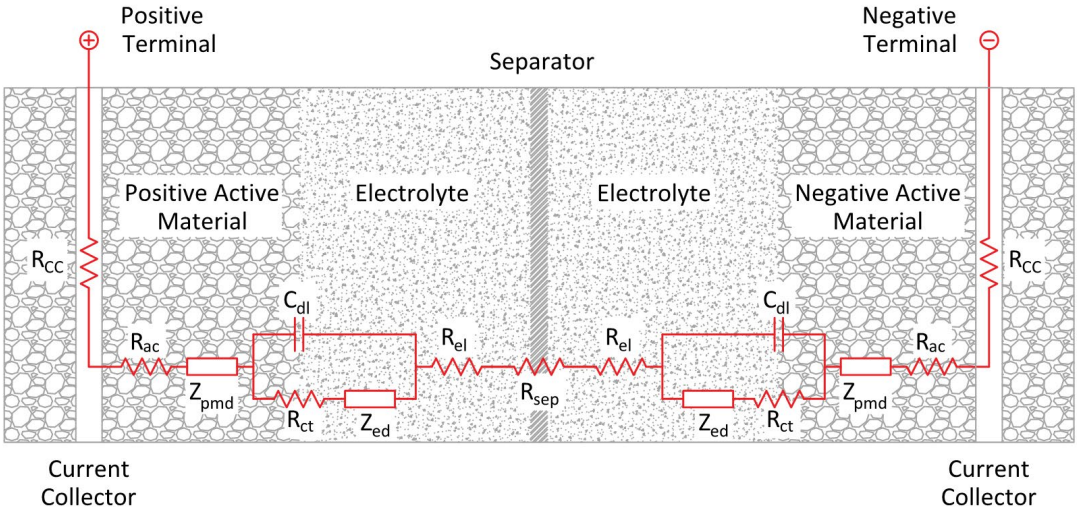

Figure 3-13. Typical electrochemical cell and the equivalent circuit elements

3.3.1.1 Active electrolyte resistance (R_{el})

An electrolyte is a mixture of positive and negative ions in a polar solvent. Typically, the electrolyte resistance depends on several factors like the ionic concentration, type of ions presents in the solution, ionic mobility, temperature, and geometry of the cell. The simple formula shown below can be used to calculate the total resistance for simple geometries at fixed concentrations. Unfortunately, the current distribution through the electrolyte cannot be easily determined in real-life applications. That is why the resistance is usually determined experimentally [117].

The electrolyte resistivity plays an important role in the total internal battery impedance. Depending on the battery type and the electrolyte used, the resistivity can vary significantly with the battery state of charge and temperature. As an example, the lead-acid batteries use H_2SO_4 for the electrolyte, with a varying specific density between 1.1 and 1.4 (density relative to water) and concentration between 1.133 and 6.246 [mol/kg] [118]. This is the optimum active region for the lowest H_2SO_4 electrolyte resistivity. Above and below this window, the ion concentration has a profound effect on the electrolyte resistivity. In the case of lead-acid batteries, a decrease in temperature also affects the electrolyte resistance, especially for temperatures below 0^0C [118]. The electrolyte resistance is indicated in Figure 3-13 as R_{el}.

3.3.1.2 Charge transfer resistance (R_{ct})

The chemical reactions occurring at the battery electrodes generate electrical charge transfers (ions or electrons) across the electrode-electrolyte interface layers. The electrode reaction kinetics associated with this depends on many factors, like the electrode potential, temperature,

type of reaction, electrolyte concentration and so on. [30]. The charge-transfer kinetics can be ultimately modelled as a resistance R_{ct}, as indicated in Figure 3-13. The Butler–Volmer equation, which links the reaction rate (battery current) with the electrode potential, can be used to derive the R_{ct} resistance as shown below:

$$I = I_0 \left(e^{\frac{\alpha Z_e F (E-E_0)}{RT}} - e^{\frac{(1-\alpha) Z_e F (E-E_0)}{RT}} \right); \quad (3.1)$$

$I_0 -$ exchange current, under equilibrium I_0 is zero;
$Z_e -$ number of electrons involved in the reaction;
$\alpha -$ charge transfer coefficient between 0 and 1;
$(E - E_0) -$ electrode overpotential;
$R -$ gas constant;
$T -$ absolute temperature;
$F -$ faraday constant;

The charge-transfer resistance R_{ct} is obtained by computing the derivative of the Butler–Volmer equation:

$$R_{ct} = \left(\frac{dE}{dI}\right) \approx \frac{RT}{nFI_0}; \quad (3.2)$$

3.3.1.3 Double layer capacitance (C_{dl})

Mortimer R.G. et al. [119] and Peter Atkins et al. [36], explain that any metal inserted in its electrolyte solution has a chemical potential, which, at equilibrium, is balanced by the electrical field formed at the boundary between the active material and the electrolyte solution. Many models are used to build an understanding of the electrode-electrolyte interface phenomenon like the Helmholtz layer model, Gouy-Chapman model, or the Stern model. All of these use the same fundamental idea, that the electrolyte ion arrangements near the electrode material, and their interaction with the electrode electrons, create a capacitor-like behaviour. The insulating space between the electrolyte ions and the electrode material electrons is usually minimal, of the order of angstroms. Later in this thesis, the double layer capacitance has been modelled as a traditional C_{dl} capacitance as indicated in Figure 3-13.

3.3.1.4 Constant phase elements (Z_{pmd}, Z_{ed})

Simple electrical components cannot describe the nonlinear nature of real electrochemical processes. Described by Peter Atkins et al. [120], the constant phase elements has been used to map processes like electrode ion diffusion (Z_{pmd} in Figure 3-13), electrolyte convection and diffusion (Z_{ed} in Figure 3-13), ion transport and so on. In its simplest form, a constant phase element is a 'modified' impedance, generally capacitive, whose phase angle is independent of the test signal frequency. A generalized formula of a constant phase element is shown below:

$$Z_{CPE} = \frac{1}{Z_0\,(j\omega)^n}\,; \tag{3.3}$$

$\omega -$ angular frequency $\left[\frac{rad}{s}\right]$;
$n -$ number between $[-1, 1]$, for a pure capacitor $n = 1$;
$j -$ imaginary unit.;
$Z_0 -$ constant phase elepment (CPE) coeficient $[s * s^n]$(siemens $-$ seconds);

The impedance phase angle for a constant phase element has numerical values of (-π/2*n) degrees and it is frequency-independent. For special cases, n=1, the constant phase element relationship resembles the impedance of a capacitor, $1/j\omega C$, where Z_0 is identical to the capacitance C. As described by Lasia A. and Rodgers D.B. [121, 122], there are multiple factors which explain the peculiar behaviour of the phase elements, but the main ones are related to the electrode roughness, uneven distribution of the reaction rates and the non-uniform current distribution over the electrode surface.

In electrochemical cell modelling, one of the most important constant phase elements is the Warburg impedance, which models the ion diffusion processes in the electrode and electrolyte. The Warburg impedance is a special case of a constant phase element. This is because the phase angle is constant at -45^0 and, as mentioned, is frequency independent. The absolute value of the impedance is proportional to $1/\omega^{0.5}$ (n=0.5). In other words, for a Warburg impedance, the real and imaginary part are equal, as indicated below.

$$Z_W = A_W\left(\omega^{-\frac{1}{2}} + j\sigma\omega^{-\frac{1}{2}}\right); \tag{3.4}$$

The diffusion impedance can be measured using electrochemical impedance spectroscopy (EIS) techniques, which allows for the separation of ohmic, charge transfer, capacitance and diffusion components. Figure 3-14 illustrates the frequency response of a typical Warburg impedance and a typical EIS spectrum with the associated regions for each resistive component. The magnitude and phase response of Z_w are similar to that of a capacitor, Plett G.L. [123], the differences are that for a capacitor, the magnitude drops with 20 dB/decade and the phase is constant at -90^0. For the Warburg impedance, the magnitude slope is 10 dB/decade, and the phase angle value is constant at -45, as shown below.

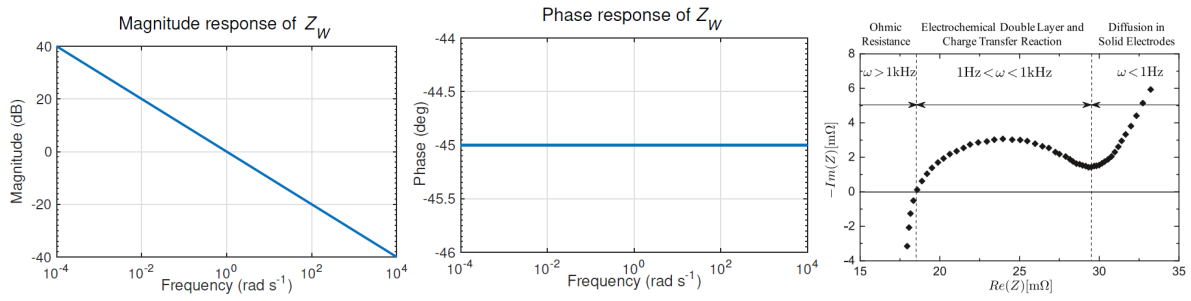

Figure 3-14. Warburg (diffusion) impedance – frequency/phase response and

EIS spectrum indicating the ohmic, charge transfer and diffusion components [123].

However, the Warburg impedance cannot be expressed using ordinary differential equations [123]. As described by Plett G.L. [124], Z_W is modelled as an equivalent circuit using a series combination of resistors and capacitors (RC groups). Figure 3-15 illustrates the magnitude and phase response of a real Warburg component versus the approximated values using multiple RC circuit elements. The response converges to the actual diffusion impedance behaviour as the number of RC groups increases. In this report, due to computational limitations, the number of RC groups has been limited to three.

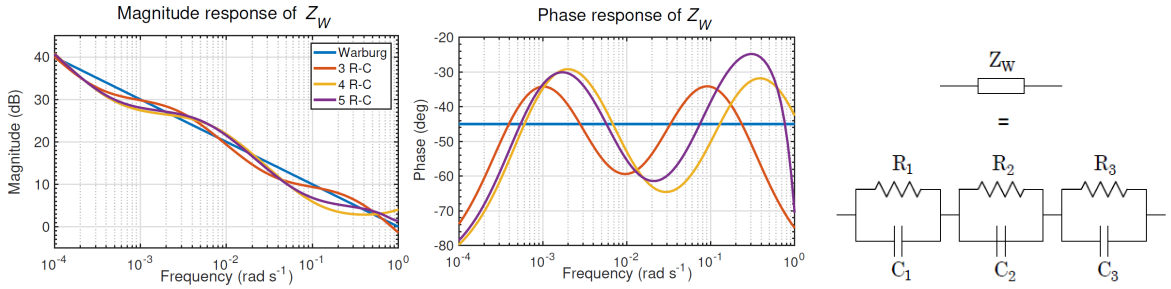

Figure 3-15. Warburg impedance modelled as equivalent RC groups [124].

3.3.1.5 Conduction elements (R_{CC}, R_{ac})

The other components of the internal impedance of a typical electrochemical cell are the electronic resistance of the active material and current collectors, which have been indicated in Figure 3-13 as R_{CC} and R_{ac}.

3.3.2 Equivalent Circuit Model (ECM)

As explained in the previous sections, the major elements in the battery ECMs are the electrolyte resistance, charge transfer resistances, double layer capacitances and diffusion impedances. The task of each software model is to capture the information provided by these and use it in detecting other external parameters, like the state of charge (SoC), state of health (SoH), and cell's voltage and current. However, depending on the model accuracy requirements, some of these elements can be ignored when constructing the actual battery equivalent circuits. The literature indicates a wide range of ECMs [125-130] and it is common to find different variations of the same circuit for specific applications. Zhang L. et al. [131] and Li S. et al. [132] compare different circuit models and their simulated voltage errors. Later in this thesis, I will use the Double Polarisation model to model the hybrid behaviour. Below, there is a quick derivation of the circuit starting with the simplest model, R_{int}, and working through the Thevenin model and Randles circuit. Most of the derivations in the following sections are based on the works presented by Plett G.L. et Al. [123, 124].

3.3.3 R_{int} & Thevenin ECMs

One of the simplest ECM is the R_{int} circuit, which models the battery cell as a voltage source and its associated internal resistance $R_{0,}$ as indicated in Figure 3-16 (a). For this model, the value of the open-circuit voltage source (OCV) it is a function only of the state of charge $\mathrm{soc(t)}$. The OCV also depends on temperature, dynamic parameters and the previous charge/discharge states of the battery, but this is ignored in this simple analysis.

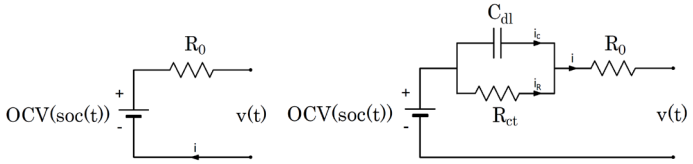

Figure 3-16. R_{int} circuit model (a) and Thevenin circuit model (b)

The starting point to derive the differential equations for the state of charge and the output voltage begins with the self-evident equation (3.5). Integrating the equation, we can obtain the $\mathrm{soc(t)}$ as a function of time. The output voltage of the cell can be obtained by subtracting the voltage drop across the polarisation resistor from the OCV.

$$\frac{\mathrm{dsoc(t)}}{\mathrm{dt}} = -\frac{\eta(\mathrm{t})\mathrm{i(t)}}{\mathrm{Q}}; \tag{3.5}$$

$$\mathrm{soc(t)} = \mathrm{soc(t_0)} - \frac{1}{\mathrm{Q}}\int_{\mathrm{t_0}}^{\mathrm{t}} \eta(\tau)\mathrm{i}(\tau)\,\mathrm{d}\tau;$$

$$\mathrm{v(t)} = \mathrm{OCV\big(soc(t)\big)} - \mathrm{i(t)R_0}; \tag{3.6}$$

where:

$\mathrm{v(t)} -$ output voltage (V);

$\eta(\mathrm{t}) -$ culombic efficiency (unitless);

$\mathrm{Q} -$ battery capacity (Ah)

$\mathrm{i(t)} -$ cell current (A)

$\mathrm{soc(t)} -$ state of charge (unitless)

The definitions of the cell capacity, state of charge and coulombic efficiency have been reproduced below:

Capacity Q	The total charge capacity of a cell Q is defined as the maximum charge that can be extracted from an electrochemical cell, at 1C rate, until the voltage level reaches the minimum voltage level acceptable without damaging the cell
State of Charge soc(t)	The state of charge of a battery $soc(t)$ is defined as the ratio between the cell's charge status at a certain time and the total charge capacity Q. The state of charge values vary between zero and one.
Columbic efficiency η(t)	Some of the charge is lost during the charging process of an electrochemical cell because of unwanted side reactions. The ratio between charge in and charge out of a battery cell is the coulombic efficiency.

It can be noted that for a more accurate R_{int} model, R_0 can also be modelled as a function of the state of charge and temperature. In addition, the resistor R_0, accounts for the fact that the charging and discharging voltages are different. Although simple, this ECM is used in low-power electronic applications, but for multi-cell battery power packs, more sophisticated models are required, such as the Thevenin model.

The Thevenin model is an improved version of the R_{int} circuit to account for the dynamic behaviour of a battery cell. Apart from the voltage source OCV and the internal resistance R_0, it contains an additional RC component as shown in Figure 3-16 (b).

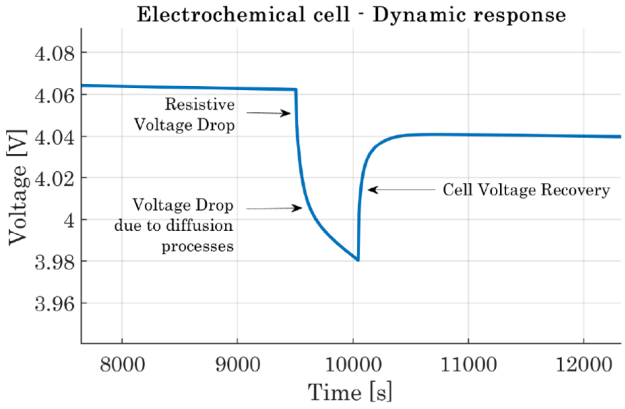

Figure 3-17. Dynamic response of an electrochemical cell

It is known that when current is drawn from the cell, the output voltage drops because of the internal resistance. However, the transition doesn't happen instantaneously because of the various diffusion processes. In addition, after the battery load is removed, its voltage slowly recovers. The output voltage of a typical electrochemical cell has been illustrated in Figure 3-17,

where a pulse current was applied to a 4V Li-ion battery. The sharp voltage drop is due to the resistive components $\mathrm{Ri(t)}$ of the cell. The capacitor-like behaviour during discharge and the recovery period is due to the additional polarisation processes. Up to a certain degree, this can be modelled using a resistor and a capacitor group connected in series with resistor R_0. The capacitor C_{dl} models for the electrochemical double layers and the effect of charges building up in the electrolyte at the electrode surface. The R_{ct} accounts for the charge transfer resistances as indicated in Figure 3-13. R_0 models the rest of the cell resistances.

To derive the equations of the Thevenin circuit, one can start by applying the Kirchhoff current law to the RC node as indicated. Following the manipulations indicated below, we get to the first state equation (3.7). The second state equation, (3.8), is the same as in the R_{int} model and describes the state of charge equation. The output equation for the system is the (3.9) and is simply the value of the voltage source minus the voltage drop across the RC and R_0 components.

Kirchhoff's current law to the RC node:
$$\mathrm{i_R(t) + i_C(t) = i(t)}$$

But also, $\mathrm{i_C(t)}$ is equal to:
$$\mathrm{i_C(t) = C\frac{dv_{RC}(t)}{dt}}$$

The voltage $\mathrm{v_{RC}(t)}$ is also equal to the voltage drop across the resistor:
$$\mathrm{Ri_R(t) = v_{RC}(t)}$$
and taking the derivative,
$$\mathrm{R\frac{di_R(t)}{dt} = \frac{dv_{RC}(t)}{dt}}$$

After substitution, the current through the capacitor, $\mathrm{i_C(t)}$, becomes:
$$\mathrm{i_C(t) = CR\frac{di_R(t)}{dt}}$$

Replacing this in the initial Kirchhoff equation we obtain:
$$\mathrm{i_R(t) + RC\frac{di_R(t)}{dt} = i(t)}$$

Rearranging terms we obtain the first state equation:
$$\mathrm{\frac{di_R(t)}{dt} = -\frac{1}{RC}i_R(t) + \frac{1}{RC}i(t);} \quad (3.7)$$

The second state equation has been derived earlier and is:
$$\mathrm{\frac{dsoc(t)}{dt} = -\frac{\eta(t)i(t)}{Q};} \quad (3.8)$$

The output voltage equation is OCV minus the voltage drops:
$$\mathrm{v(t) = OCV\big(soc(t)\big) - Ri_R(t) - R_0i(t);} \quad (3.9)$$

The three equations indicated above (3.7), (3.8) and (3.9) form the state representation of the Thevenin circuit. These equations are not a complete description of an electrochemical cell, but the circuit holds for less rigorous dynamic modelling. A more accurate model will involve additional elements to account for diffusion processes which will be modelled using constant phase elements.

3.3.4 Randles & Double Polarisation ECMs

The Randles circuit is obtained by adding a constant phase element to the Thevenin circuit explained above. As explained in the previous sections, simple electrical elements cannot accurately describe the complicated voltage behaviour generated by the diffusion processes within a cell. One option is to use constant phase elements. The Randles circuit introduces such a phase element, a Warburg impedance. Figure 3-18 (a) indicates the standard form of the Randles model. It contains a voltage source OCV, the resistance R_0 and a modified RC group. The RC group contains the double layer capacitance C_{dl}, the charge transfer resistance R_{ct} and the Warburg impedance Z_w.

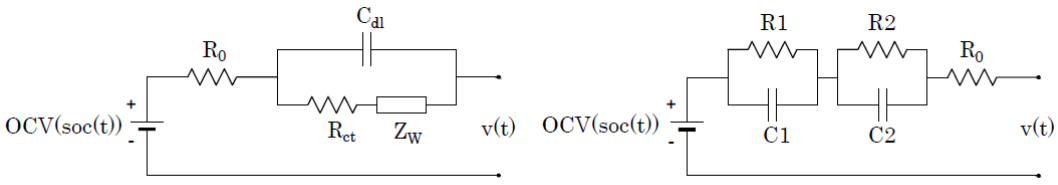

Figure 3-18. Randles (a) and Double Polarisation (b) ECMs

An important point worth mentioning is that the Warburg element cannot be described using simple differential equations. In practice, the Warburg effect can be approximated using multiple RC branches connected in series, as explained in the Section 3.3.1.4. The dual-polarisation model makes use of this and replaces Z_w with two RC groups connected in series. For simplicity, the double layer capacitance C_{dl} is ignored, and the charge transfer resistance R_{ct} is integrated into R_0 resistance. The result is shown in Figure 3-18 (b) which is the standard form of the double polarisation ECM. The equations for this circuit can be derived using the same results obtained for the Thevenin model, the only difference is that there will be another state equation accounting for the extra RC component. The complete set of equations have been indicated below, (3.10), (3.11), (3.12) and (3.13).

State equation 1:
$$\frac{di_{R_1}(t)}{dt} = -\frac{1}{RC} i_{R_1}(t) + \frac{1}{RC} i(t); \tag{3.10}$$

State equation 2:
$$\frac{di_{R_2}(t)}{dt} = -\frac{1}{RC} i_{R_2}(t) + \frac{1}{RC} i(t); \tag{3.11}$$

State equation 3:
$$\frac{dsoc(t)}{dt} = -\frac{\eta(t) i(t)}{Q}; \tag{3.12}$$

Output equation:
$$v(t) = OCV\big(soc(t)\big) - R_1 i_{R_1}(t) - R_2 i_{R_1}(t) - R_0 i(t); \tag{3.13}$$

3.4 Literature Review – Conclusions

This chapter does a brief literature review of the energy storage technologies to determine where the hybrid Li-ion and lead-acid systems sit within the wide energy storage technology group. The first section describes the energy storage categories and their technical characteristics. Within these, there is the hybrid storage family, which includes multiple hybrid possibilities between mechanical, chemical and electrical energy storage, using active, passive, or semi-active topologies. Further down, within the hybrid family, we find HBBS, which includes the combination of HP with HE batteries to minimise the cost and improve the system's performance. In this category, we find the hybrid Li-ion and lead-acid system.

The chapter concludes that there are several hybrid battery systems at all scales, from EVs to MW-scale, grid-connected applications. The advantages of hybrid systems are mentioned, and the findings show that, depending on the application, hybrid Li-ion and lead-acid systems can reduce the cost by up to 36% (using active architectures and based on the Li-ion battery prices at that time). The literature shows that, if different Li-ion battery technologies are optimised for power and energy, the cost reduction could be as high as 20%.

The chapter ends with the equivalent circuit battery modelling literature review and concludes that using RC circuits is an established technique to model batteries, and this will be used later in this thesis, because of implementation simplicity compared with physics-based models.

Chapter 4 Research Methodology

This chapter presents the research methodology followed to achieve the proposed objectives of this work. The overall strategy has three main fronts, hybrid storage systems lab testing, on-situ performance analysis of a demonstrator, and techno-economic system modelling. As mentioned in the introduction section, the key questions addressed in this thesis are the following:

The first question is, ***what are the hybrid characteristics of directly coupled, hybrid Li-ion and lead-acid systems?***

To achieve this, I have tested in the lab five different hybrid storage systems. Specifically, I have determined the energy flows in a hybrid configuration, the hybrid energy round-trip efficiency, the energy charged/discharged independently from the Li-ion chemistry as a function of the SoC, the lead-acid behaviour, when only Li-ion is active, and the dynamics during charge/discharge.

The detailed steps to determine these are indicated below.

The findings of the first objective lead to the second question, ***can the instantaneous hybrid behaviour be modelled using equivalent circuits?***

To answer this, I have built a MATLAB hybrid battery model using equivalent circuit cell models and studied different hybrid systems. The battery model is populated with experimental results used in answering the first question, like the coulombic efficiency (CE) and the voltage profiles. I have used pulsed discharge testing methods for both chemistries to determine the additional dynamic parameters. All tests have been performed using the same lab experimental arrangement prepared to determine the hybrid characteristics. For system parameter extraction, I have also used MATLAB's internal tools.

The detailed methodology addressing the question is indicated in the following sections.

The third question asked is, **how do hybrid battery systems perform over time in real-world applications?**

To determine this, I have monitored the first-of-its-kind demonstrator project for a directly coupled hybrid storage system. I analysed the data for the first four years of operation and determined the energy system flows, the round-trip efficiency, the capacity degradation of both chemistries and the general stability of the system over time. The details of the hybrid system demonstrator, as well as the specific steps set to answer the question, are also indicated below.

The last question addressed is, ***what storage applications are best suited for hybrid lead-acid and Li-ion systems, and what are the associated techno-economic parameters?***

The results from the first three questions lead to the fourth research target, which is to determine how the hybrid system would perform in different applications with different load profiles. To achieve the set objective, I have built an additional MATLAB tool that receives economic and technical parameters for generation, storage, and grid import connection data and returns parameters like the total energy system cost, Li-ion, and lead-acid utilisation rates, as well as the periods when each chemistry is active. Finally, I have tested the model using real case studies for residential, EV charging stations, industrial, front-of-the-meter applications and commercial load profiles. The detailed steps and assumptions are indicated below.

4.1 Experimental Arrangement Description

The first step in answering the questions addressed above was to prepare a hybrid battery experimental testing arrangement. The experimental setup allows for both individual and hybrid parameters calculations. This section describes the batteries, equipment and arrangement used.

GS Yuasa has provided a Li-ion battery pack and several lead-acid batteries along with a general-use UPS battery charger. The work also made use of the Southampton University Energy Technology Group equipment, like the programmable electronic load and power supply necessary for the discharge testing and data logging. The necessary auxiliary equipment like cables, connectors, switches, test equipment, and connection tools, have been provided by the mechatronics lab.

The main technical characteristics of the GS Yuasa batteries tested, lead-acid (SWL3300) and Li-ion (LEV50), have been indicated in Table 4-1 and Figure 4-2.

Table 4-1. GS Yuasa Battery Data

Battery / Cell type	Voltage Range [V]	Capacity [Ah]	Total Energy [Wh]	Mass [kg]	Specific energy [Wh/kg]	Specific Power [W/kg]	Internal Resistance [mΩ]
Lead-acid SWL3300	10.8-13.6V (Nominal 12V)	100 (At C/10 rate)	1200 (At C/10 rate)	37 kg	32	32	5.64
Li-ion Pack 7 x LEV50	2.75 / 4.1V (Nominal 4.1V)	50 (At 1 C rate)	167.5 / cell	1.56 / cell	110 / cell	110 / cell	3.2/cell

The testing equipment provided by the university lab are the EA ELEKTRO-AUTOMATIK products, the EA-PSI 9080-510 power supply, and the EA-EL 9080A electronic load. The programmable load and the power supply are equipped with internal data logging options and load profile customisation possibilities. The discharge profile can be loaded onto the machines using Microsoft Excel spreadsheets and the recorded data can be stored on a standard PC in Excel format. The data transfer between the electronic load/power supply and the data logging laptop is done via a USB connection using a specialised interface card. The equipment can also be

controlled remotely using a laptop via different software platforms like the 'Easy-load', provided by the EA ELEKTRO-AUTOMATIK or other customised Lab-View applications. The voltage and current accuracy of both machines does not exceed 100 mV/mA and the maximum data logging resolution is 0.5 seconds. The equipment can be used in various modes but for this project, only the 'battery mode' has been used. The overview of the testing arrangement is indicated in Figure 4-1 and Figure 4-2.

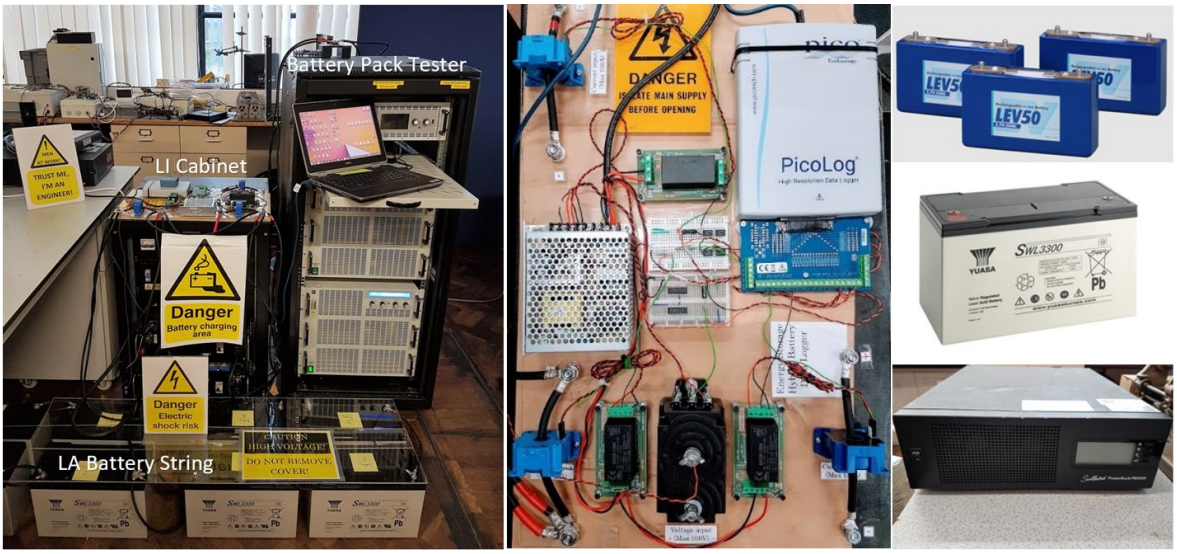

Figure 4-1. Lab Battery Testing Arrangement (a) indicating the Li-ion and Lead-acid battery banks and Batteries Tested (b)

The testing schematic is indicated in Figure 4-2. On top of the internal data logging capabilities of the load and power supply, an additional data acquisition system has been installed to be able to collect data over the internet as indicated.

The switching system allows the configuration of different hybrid arrangements in terms of the number of strings of each chemistry.

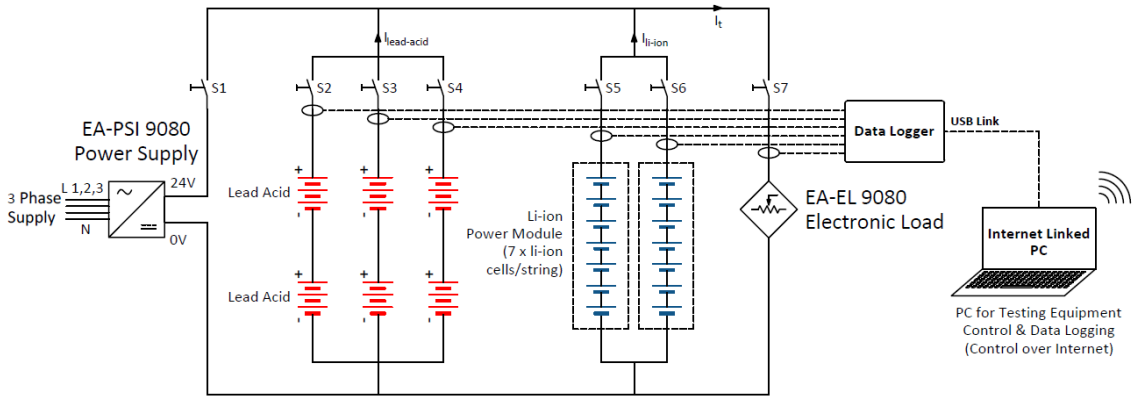

Figure 4-2. Experimental testing – Schematic

4.1.1 Data Acquisition System

As explained in the previous section, the EA ELEKTRO-AUTOMATIK equipment used during this project has various built-in data-gathering features. These, however, are not ideal for directly connected hybrid battery systems testing as they can't record the circulation currents between the battery strings. To be able to accurately record the necessary battery data, a complete data acquisition system has been specifically developed for this project.

4.1.1.1 General description

The data acquisition system (DAQ) has four main channels that can measure one voltage and three current values simultaneously. The general arrangement of one DAQ channel contains three main components:

- Three current and one voltage sensor with the corresponding power supplies.
- Signal conditioning unit (op-amps and resistors).
- Data logger (PicoLog Technology).

The current sensors used for this project are the LEM LF205-S/SP3 and LEM LF210-S/SP5. Each is separately powered by a 15V differential RAC20-15K power supply. The current sensor outputs are +/-100mA for the LF205-S and +/-210mA for the LF210-S. The voltage sensor used is the LEM DVL 125 which is powered by a +/-15V differential RT-65C power supply. The voltage sensor output has a range of +/-75.2mA. The most important technical details for each component have been listed in Table 4-2.

All sensor outputs are passed through current to voltage converters, which can be simple resistors or op-amp current to voltage converters, as indicated below, Figure 4-3. The resistors R_1, R_2, R_3 and R_4 have been selected to provide a maximum range of +/-2.5V, not to exceed the maximum input voltage allowed by the analogue-to-digital converter (ADC) of the PicoLog data logger. The resistance values have been listed in Table 4-2. The power ratings of the resistors have been selected to be above the power generated by the secondary currents. The maximum power dissipation, 525mW, is due to the secondary current of the LF210-S sensor.

All the op-amp voltage outputs are connected to the PicoLog data logger input channels. The connections between these are made using the dedicated PicoLog Terminal Board. The maximum data logger voltage inputs are between +/-2.5V. Each channel contains 24 bits digital to analogue converter (DAC) and can read a maximum of ten measurements per second.

To avoid galvanic interference between signals, all sensors and the op-amp current to voltage converters are powered from separate power sources as indicated in the DAQ schematic, Figure 4-3.

The incoming data can be visualised in real-time and is stored on a laptop or PC. The final connection between the data logger and the data storing device is made via a USB connection. The PC/laptop user interface is provided by the PicoLog 6 data logging software, provided for free by the manufacturer.

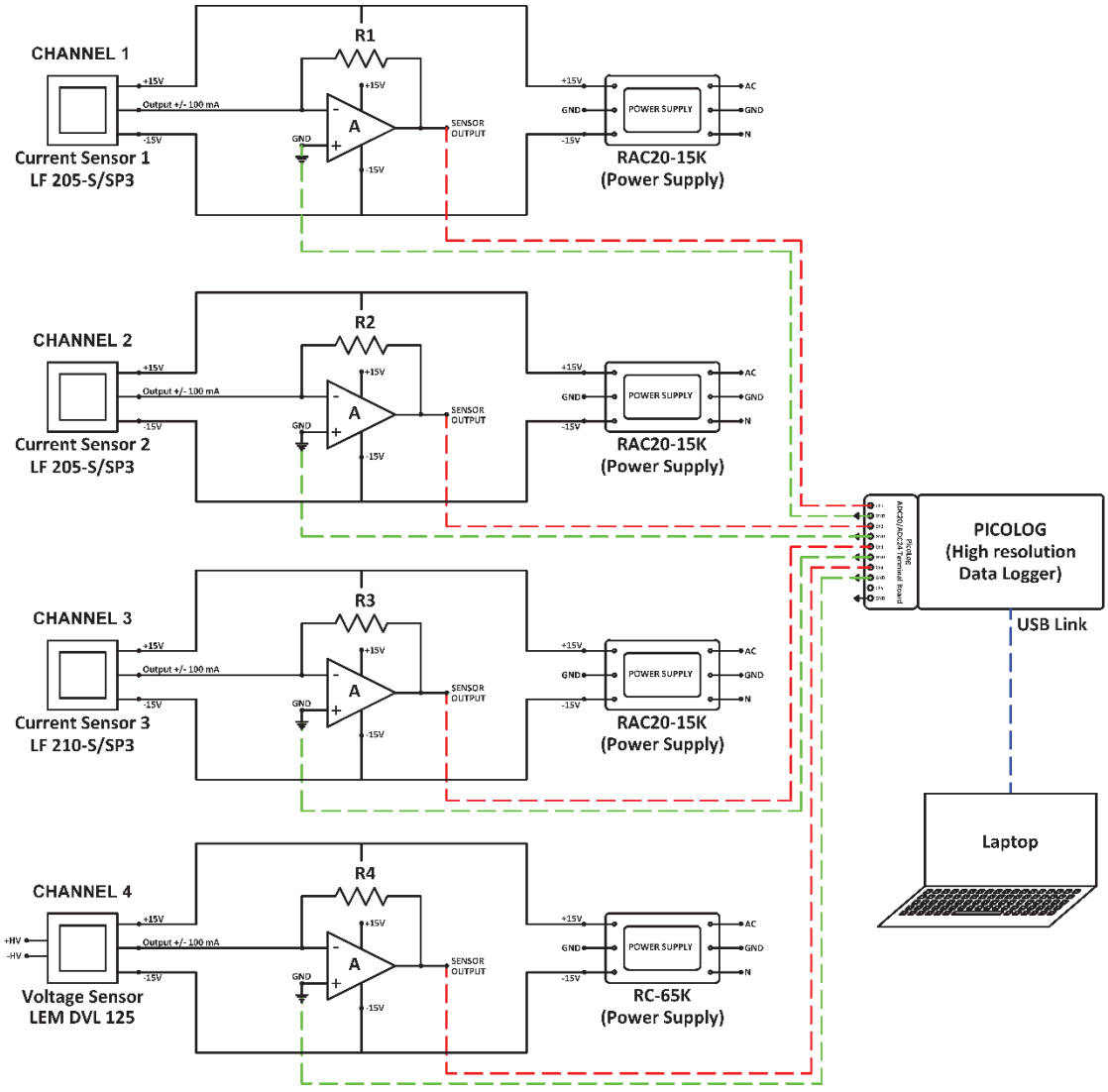

Figure 4-3. Data Acquisition System Schematic (DAQ)

4.1.1.2 Main DAQ components

The main DAQ components used during the project have been listed in Table 4-2.

Table 4-2. Data Acquisition System – Project components

 Current sensor 1: LF 205-S/SP3 I_{PN}=+/-100A (Primary current) I_{SN}=+/-100mA (Secondary Current) Error at I_{PN}=+/-0.5% Voltage Supply: +/-15V	 Current sensor 2: LF 210-S I_{PN}=200A (Primary current) I_{SN}=+/-210mA (Secondary Current) Error at I_{PN}=+/-0.2% Voltage Supply: +/-15V
 Voltage Sensor: LEM DVL 125 V_{PN}=+/-188V (Primary voltage) I_{SN}=+/-75.2mA (Secondary Current) Error % V_{PN}:+/-0.5% Voltage Supply: +/-15V	 Data logger: Pico Log ADC-24 8 differential & 16 single-ended channels Max Voltage Input: +/-2.5V 24 bits ADC
 Resistor 3: ER7415RJT 15Ω Wire Wound Resistor, 3W	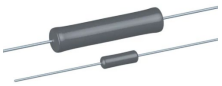 Resistor 2: RS02B20R00FE12 20Ω Wire Wound Resistor, 3W
 Resistor 1: ER7439RJT 39Ω Wire Wound Resistor, Power: 3W	 Resistor 4: RWM041062R0JR15E1 62Ω Wire Wound Resistor, Power: 3W
 Sensor power supply: RAC20-15K Input: 85-265 VAC Output: +/-15V Output Current: 1.3A	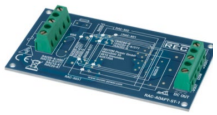 Power supply board: RAC-ADAPT-ST-1 Adapter board.
 Power supply: RT-65C CH1: 5V, 5A CH2: 15V, 2.2A CH3: -15V, 0.5A	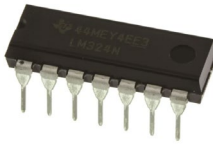 Op Amp: General Propose LM124-LM224-LM324

The DAQ system's final arrangement is indicated in Figure 4-4 and Figure 4-5. All the system components have been bolted onto a support structure. As can be seen in Figure 4-5, the current sensors have connection points that allow easy connection to the battery strings.

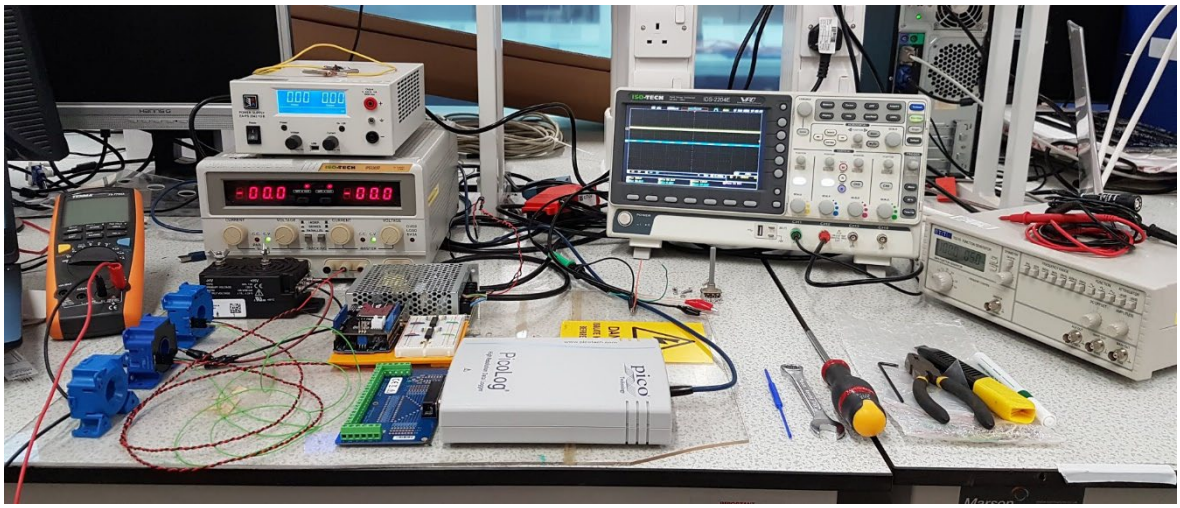

Figure 4-4. Data Acquisition System Setting

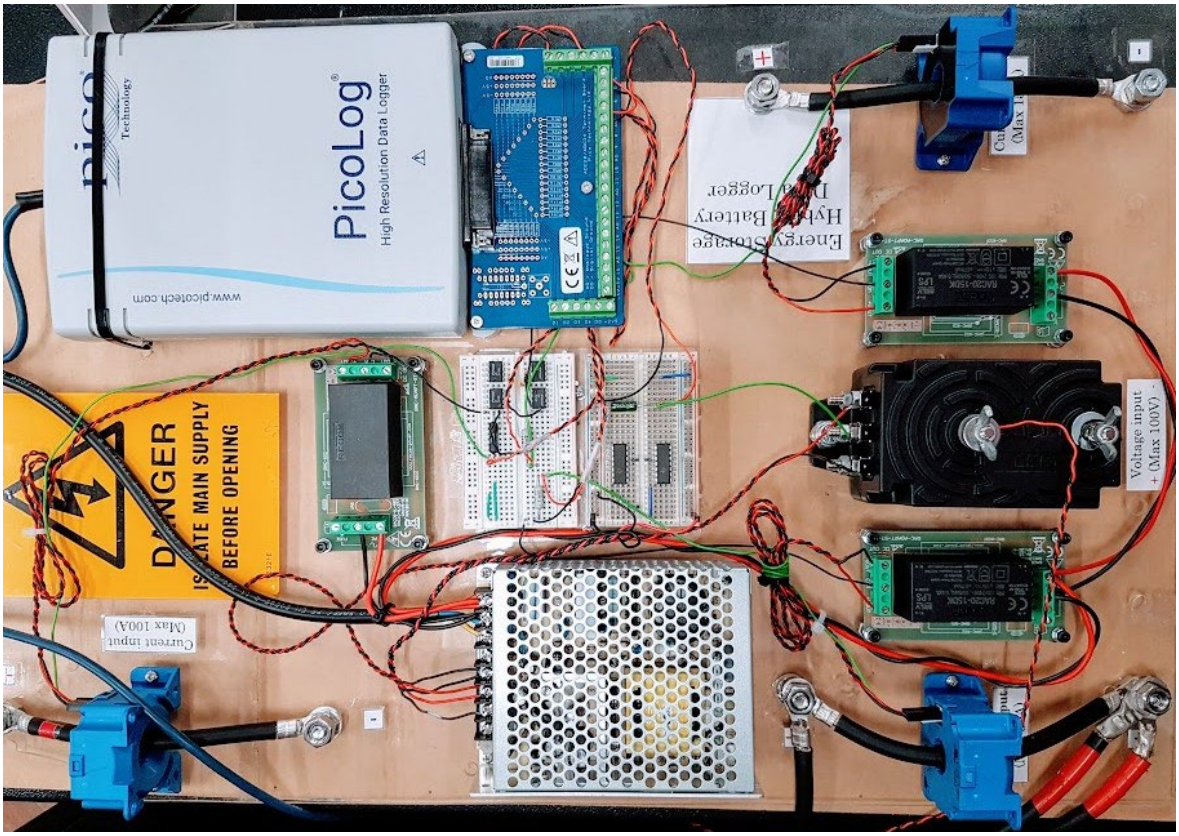

Figure 4-5. Data Acquisition System - Final Arrangement

Figure 4-6 show the input-output characteristics for all measurement channels. The calibration was done against a standard TENMA 72-7730A Digital Multimeter. The input-output is linear for all channels with 0.8-3 mV offsets. Current Sensor 1 has been set to measure a maximum of 50A, Current Sensor 2 a maximum of 100A and Current Sensor 3 a maximum of 150A. All offsets are considered during data processing.

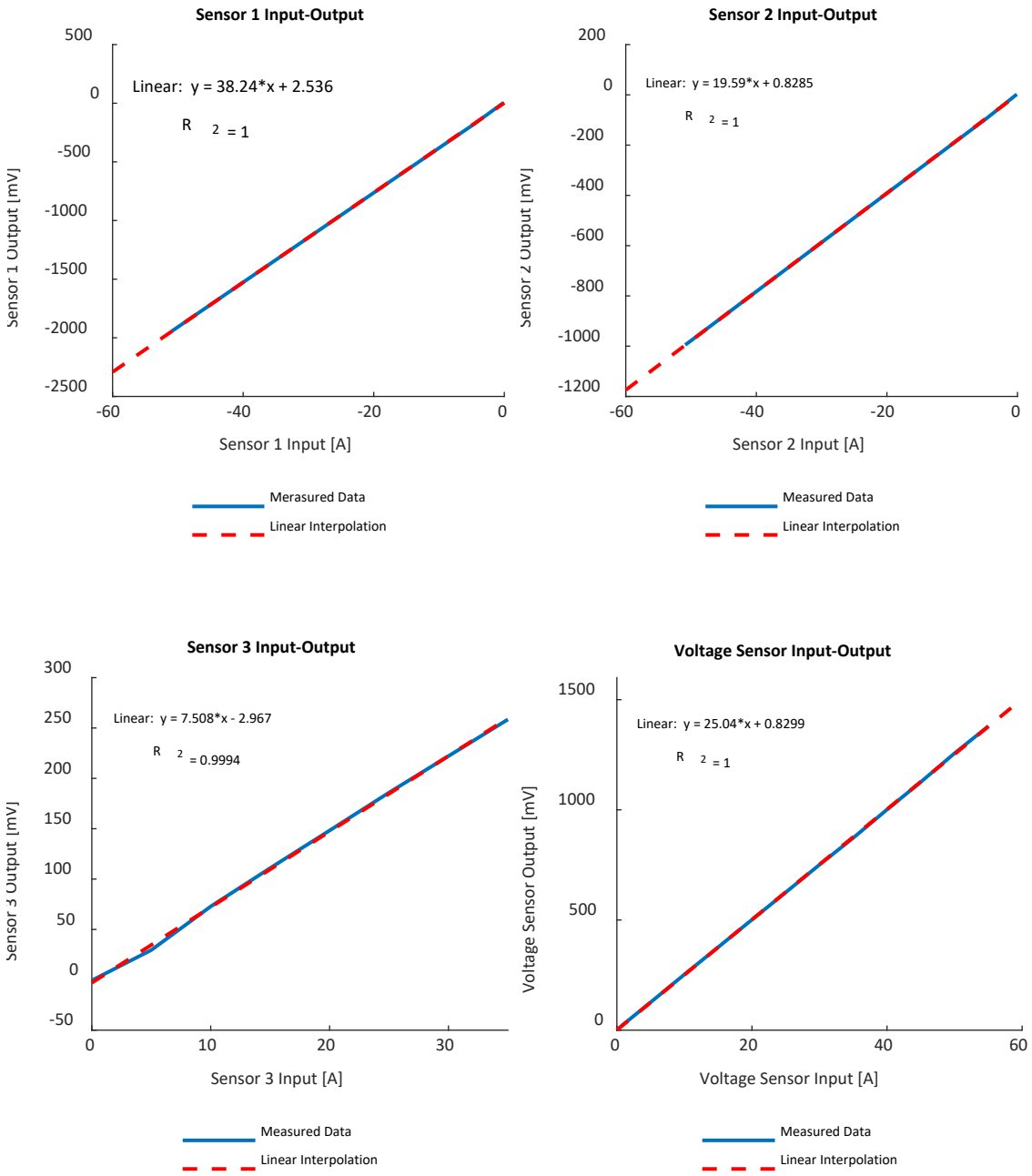

Figure 4-6. Current and Voltage Sensors Input-Output Characteristic

4.2 Testing Methodology for Directly Coupled Battery Systems.

4.2.1 Research Objectives

As mentioned, to achieve the first objective of this work, I have tested five hybrid systems, 24V (1 Li-ion & 1 lead-acid strings, 1 Li-ion & 2 lead-acid strings, 1 Li-ion & 3 lead-acid strings and 2 Li-ion & 1 lead-acid strings) and one 48V (1 Li-ion & 1 lead-acid) to experimentally determine the performance of directly connected hybrid Li-ion and lead-acid systems in various parallel configurations. Figure 4-7 shows the typical charge/discharge voltage and current profiles of a

24V system with only two strings, one for Li-ion and one for lead-acid, when the system is discharged and charged (CC/CV) at 10A.

This has been done by analysing the following parameters:

1. The energy (kWh) and charge (Ah) charged/discharged as a function of the charge/discharge rate, depth of discharge, and the number of strings of each chemistry.
2. The hybrid systems' round-trip efficiency as a function of the depth of discharge (DoD), charge/discharge rate, and the number of lead-acid and Li-ion strings operating in parallel.
3. The Li-ion DoD, before the currents delivered by both chemistry strings become equal, between points A-B and A-X, Figure 4-7, as a function of discharge rate and the hybrid configuration.
4. The lead-acid behaviour, during the first part of the discharge process when only Li-ion strings are active, between points A-B, Figure 4-7, as a function of the discharge rate and Li-ion, lead-acid mixture, and the hybrid system voltage.
5. The energy and charge transfer between the strings, between points D-E, as a function of lead-acid depth of discharge, discharge current, and system configuration.
6. Analyse the intermittent charging/discharging behaviour and the impact on the overall round-trip efficiency of the system.

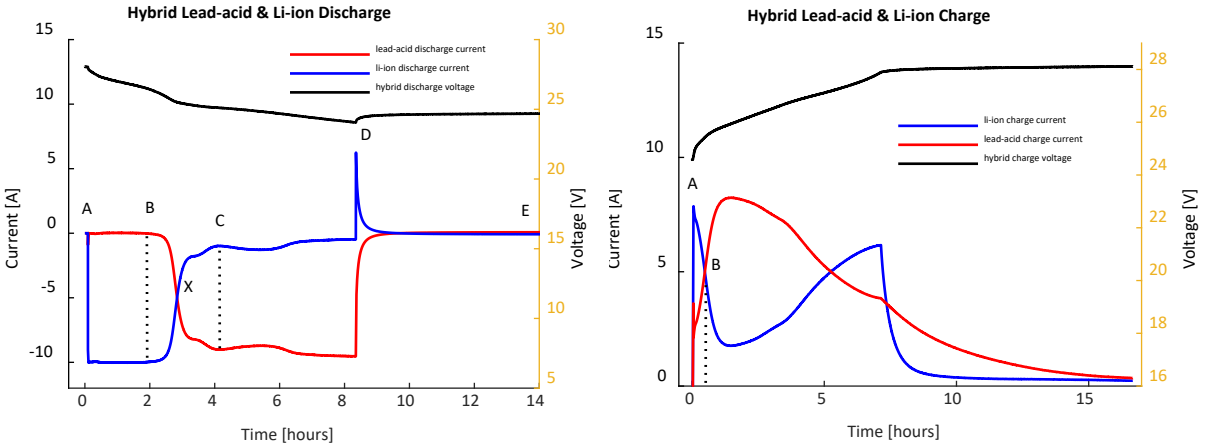

Figure 4-7. Hybrid Li-ion and Lead-acid Charge/Discharge Profile

The following systems have been tested using the experimental arrangement indicated in Figure 4-1 and Figure 4-2:

- Hybrid System 1: 2LI&1LA (24V) – Two strings of Li-ion and one of lead-acid at 24V. Using the experimental schematic indicated in Figure 4-2, switches S_5, S_6 and S_4 are closed, S_2 and S_3 opened. The power supply and electronic load switches are kept closed all the time.

- Hybrid System 2: 1LI&1LA (24V) – One string of Li-ion and one of lead-acid. Switches S_5 and S_2 closed along with the power supply and electronic load and S_3, S_4, and S_6 opened.
- Hybrid System 3: 1LI&2LA (24V) – One string of Li-ion and two lead-acid strings at 24V. Switches S_5, S_2, and S_3 closed and S_4 open.
- Hybrid System 4: 1LI&3LA (24V) – One string of Li-ion and three strings of lead-acid at 24V. Switches S_2, S_3, S_4 and S5 closed and S_6 open.
- Hybrid System 5: 1LI&1LA (48V) – Hybrid system at 48V using one Li-ion and one lead-acid strings.

4.2.2 Research Methodology

To achieve the objectives indicated above, I compared the parameters of five hybrid Li-ion/lead-acid battery systems tested under different charge/discharge C rates and hybrid configurations. All tests were performed at room temperature (20^0C). Due to the low charge/discharge rates, and because the battery testing system was sufficiently ventilated to keep the temperature constant, no environmental chamber was used.

The testing methodology steps are the following:

- Link the Li-ion and lead-acid strings and let the system rest for 3-5 hours at room temperature or until the system reaches equilibrium (no circulation currents between the strings and no further voltage variations).
- Cycle the system between 100% SoC, for both strings, to various SoC for the lead-acid. The SoC was measured using the coulombic counting method. As the Li-ion string discharges first, the disconnection point is set by the minimum voltage allowed by the lead-acid strings. To avoid rapid degradation, the lead-acid strings were kept above 50% SoC. The cycling intervals are indicated in Figure 4-8 and described below.

1. Cycling Range 1: charge/discharge the hybrid system from 100% SoC (both Li-ion and lead-acid strings at 100% SoC and a system voltage of 28.1V or 56.2V) and discharge to 2.25V/cell for the lead-acid cells, corresponding to 100% lead-acid SoC.
2. Cycling Range 2: charge/discharge the hybrid system from 100% SoC (both Li-ion and lead-acid strings at 100% SoC and a system voltage of 28.1V or 56.2V) and discharge to 2.091V/cell lead-acid corresponding to 90% lead-acid SoC.
3. Cycling Range 3: charge/discharge the hybrid system from 100% SoC (both Li-ion and lead-acid strings at 100% SoC and a system voltage of 28.1V or 56.2V) and discharge to 2.067V/cell lead-acid corresponding to 80% lead-acid SoC.

4. Cycling Range 4: charge/discharge the hybrid system from 100% SoC (both Li-ion and lead-acid strings at 100% SoC and a system voltage of 28.1V or 56.2V) and discharge to 2.047V/cell lead-acid corresponding to 70% lead-acid SoC.
5. Cycling Range 5: charge/discharge the hybrid system from 100% SoC (both Li-ion and lead-acid strings at 100% SoC and a system voltage of 28.1V or 56.2V) and discharge to 2.027V/cell lead-acid corresponding to 60% lead-acid SoC.
6. Cycling Range 6: charge/discharge the hybrid system from 100% SoC (both Li-ion and lead-acid strings at 100% SoC and a system voltage of 28.1V or 56.2V) and discharge to 2V/cell lead-acid corresponding to 50% lead-acid SoC.
7. Let the system rest for 3-6 hours until the circulation currents between the strings become negligible.
8. Record the currents $I_{li\text{-}ion}$ and $I_{lead\text{-}acid}$ indicated in Figure 4-2, as well as the system voltage every second.

Repeat the steps above for different C rates, 0.2-1C, and for the Li-ion and lead-acid configurations indicated.

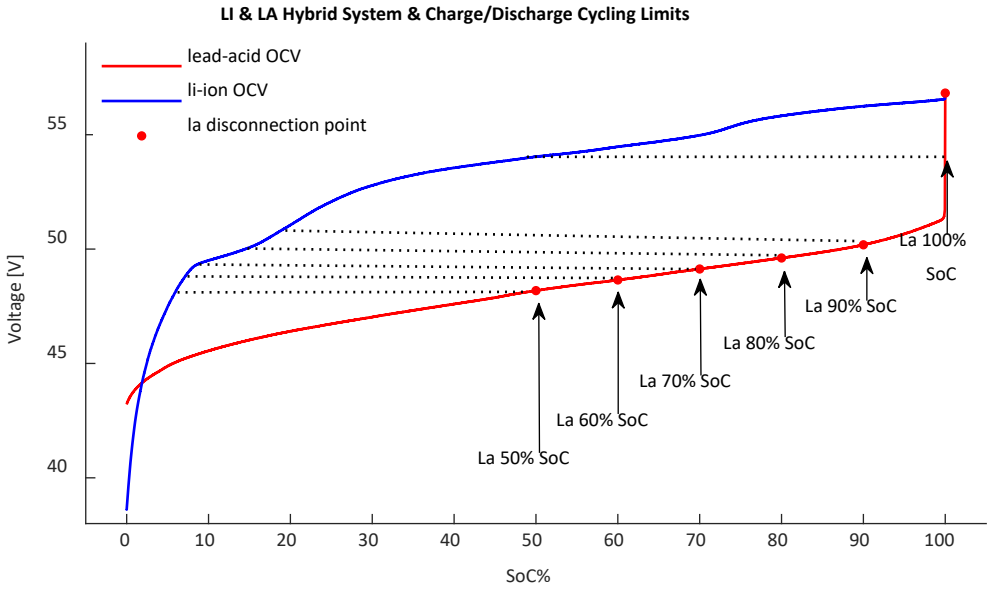

Figure 4-8. Hybrid lead-acid and Li-ion voltage profile

To manipulate the data, obtained during the above tests, I have built bespoke MATLAB scripts to calculate the parameters indicated. Finally, I have compared the results from the different systems tested.

The ratio between the number of Li-ion and lead-acid cells connected in series was chosen to maximise the Li-ion discharge voltage window between A-X points, Figure 4-7. To calculate this ratio, the starting point is the maximum system voltage which is dictated by the lead-acid float voltage. Although the hybrid systems tested had nominal voltages of 24 and 48V, the maximum

system voltages are 28.1V and 56.2V (between 2.27-2.35V per lead-acid cell). It is worth mentioning that the boost voltage for the lead-acid cells used is 2.42V per cell. When the lead-acid cell is at 100% SoC, the rest voltage is 2.13V per cell or 25.56V for the 24V systems and 51.12V for the 48V system. This implies that between the maximum 28.1V and 25.56V or between 56.2V and 51.12V, the Li-ion strings have a voltage window to discharge before the lead-acid cells. Ideally, to maximise the Li-ion discharge potential in this voltage window, the number of Li-ion cells connected in series would add up to 28.1V or 56.2V. Dividing 28.1V or 56.2V by 4.1V (nominal Li-ion cell voltage) we obtain 6.85 and 13.7 cells (rounding this to 7 and 14 results in the Li-ion cells being able to charge just below the 4.1V per Li-ion cell, or 100% SoC). This concludes that 7 Li-ion cells are to be connected in parallel with the 24V lead-acid system and 14 for the 48V. The ratio between the number of Li-ion and lead-acid cells is 0.58.

4.3 Hybrid Modelling – Methodology

To achieve the second objective of this thesis and determine if the hybrid dynamic behaviour can be modelled using equivalent circuits, I have built equivalent circuit models for both Li-ion and lead-acid cells. I have followed the steps below to achieve this:

- Test the batteries described in Table 4-1 using standard pulsed and constant current tests. The testing methodology is indicated below.
- Extract the equivalent circuit parameters for a 3RC circuit using the MATLAB internal optimisation tools.
- Build a MATLAB model for the directly connected Li-ion and lead-acid storage system.
- Use the MATLAB tool to compare the modelled results with the hybrid behaviour experimental data gathered for Chapter 5 (the first question addressed in this thesis).

As explained in the literature review chapter, battery models have been developed in the literature to cover the whole range from atomistic and physical models to mathematical approximations for battery pack-level simulations. This study uses equivalent circuits for cell modelling as they are easier to implement and less computationally demanding. The literature indicates multiple equivalent circuit models [124, 125, 127]. However, this work uses standard Randles equivalent circuits for both Li-ion and lead-acid cells. A typical Randles circuit is indicated in Figure 4-9.

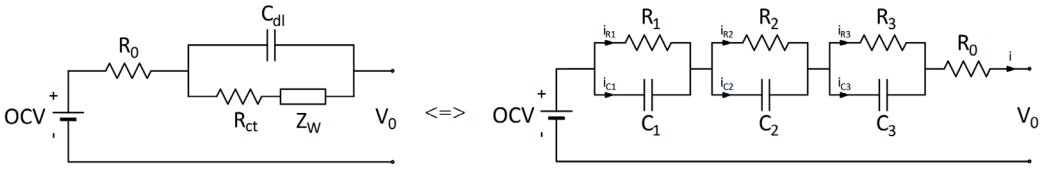

Figure 4-9. Randles Equivalent Circuit (left), Randles Circuit 3RC (right)

A Randles circuit contains a voltage source OCV, the resistance R_0 and a modified RC group. The RC group contains the double layer capacitance Cdl, the charge transfer resistance Rct and the Warburg impedance Zw, which models for the diffusion processes within the cells. The Warburg element (Zw) cannot be describe using simple differential equations and in practice, is approximated using multiple RC branches connected in series, as explained in [123]. The 3RC-polarization model makes use of this and replaces Zw with three RC groups connected in series. For simplicity, the double layer capacitance Cdl is ignored and the charge transfer resistance Rct is integrated into R_0 resistance. The result is shown in Figure 4-9 (right) which is the standard form of the 3RC polarization equivalent circuit model and can be implemented in any computational software. The equations for the 3RC polarisation circuit can be derived using well-known circuit theory. The complete set of equations has been indicated below, (3.10), (3.11), (3.12) and (3.13).

State equation 1: $$\frac{di_{R_1}(t)}{dt} = -\frac{1}{RC} i_{R_1}(t) + \frac{1}{RC} i(t); \quad (4\text{-}1)$$

State equation 2: $$\frac{di_{R_2}(t)}{dt} = -\frac{1}{RC} i_{R_2}(t) + \frac{1}{RC} i(t); \quad (4\text{-}2)$$

State equation 3: $$\frac{di_{R_3}(t)}{dt} = -\frac{1}{RC} i_{R_3}(t) + \frac{1}{RC} i(t); \quad (4\text{-}3)$$

State equation 4: $$\frac{dsoc(t)}{dt} = -\frac{\eta(t) i(t)}{Q}; \quad (4\text{-}4)$$

Output equation: $$v(t) = OCV\big(soc(t)\big) - R_1 i_{R_1}(t) - R_2 i_{R_1}(t) - R_2 i_{R_1}(t) - R_0 i(t); \quad (4\text{-}5)$$

The final discrete system equations for the 3RC polarization model can be derived from the analytic solutions and the results are the equations (4-6) – (4-10). The full derivations are detailed in [123].

State equation 1: $$i_{R_1}[k+1] = e^{-\frac{1}{R_1 C_1}\Delta t} i_{R_1}[k] + (1 - e^{-\frac{1}{R_1 C_1}\Delta t}) i[k] \quad (4\text{-}6)$$

State equation 2: $$i_{R_2}[k+1] = e^{-\frac{1}{R_2 C_2}\Delta t} i_{R_2}[k] + (1 - e^{-\frac{1}{R_2 C_2}\Delta t}) i[k] \quad (4\text{-}7)$$

State equation 3: $$i_{R_3}[k+1] = e^{-\frac{1}{R_3 C_3}\Delta t} i_{R_3}[k] + (1 - e^{-\frac{1}{R_3 C_3}\Delta t}) i[k] \quad (4\text{-}8)$$

State equation 4: $$soc[k+1] = soc[k] - \frac{\eta[k] i[k] \Delta t}{Q} i[k] \quad (4\text{-}9)$$

Output equation: $$v[k] = OCV[soc[k]] - R_1 i_{R_1}[k] - R_2 i_{R_2}[k] - R_3 i_{R_3}[k] - R_0 i[k] \quad (4\text{-}10)$$

Additional components like the hysteresis and self-discharge elements have been ignored in this thesis.

4.3.1 Constant Current Tests – Methodology & Results

In this thesis, two types of battery tests, constant current and pulse charge / discharge, have been performed to determine the current and voltage ($\mathrm{i}[\mathrm{k}]$,$\mathrm{v}[\mathrm{k}]$) profiles for each Li-ion and lead-acid cell of the overall hybrid arrangement. The index k is the time in seconds, i.e., the data sample for the current and cell/battery voltage taken at second number k since the start of the test. The current and voltage data vectors are the only direct battery measurements, all the other parameters, like the state of charge ($\mathrm{soc}[\mathrm{k}]$), open circuit voltage ($\mathrm{OCV}[\mathrm{k}]$) or cell capacity have been calculated using the equations described below.

The aim of the constant current tests is to determine the open-circuit voltage $\mathrm{OCV}[\mathrm{k}]$, the energy and coulombic efficiencies as a function of $\mathrm{soc}[\mathrm{k}]$ for each second. This can be done by slowly charging and discharging the cells between the minimum and maximum voltages specified by the manufacturer. The low current ensures that the temperature remains constant during the test (room temperature), and the dynamic parameters of the cell have a minimum effect on the output voltage measurement, so they can be ignored. Because the test requires low currents, one test can take up to 60 hours.

The constant current test methodology contains the following steps:

1. Identify the maximum and minimum cell voltages, $\mathrm{v}_{\mathrm{max}}$ and $\mathrm{v}_{\mathrm{min}}$, specified by the cell/battery manufacturer and indicated in Table 4-1.
2. Soak the battery at room temperature for at least two hours to ensure uniform temperature distribution.
3. Calibrate the battery by slowly discharging it to the specified voltage level.
4. Start the test by slowly charging the cell/battery and record the voltage and current samples $\mathrm{v}[\mathrm{k}]$, $\mathrm{i}[\mathrm{k}]$ every second. In this work, C/60 to 1C current rates have been used for the lead-acid battery and Li-ion cell, respectively.
5. When the cell/battery is completely charged, repeat the above tasks for the discharge curve using the same C rates mentioned in step 4.

The result of these five steps is a set of data containing the voltage and current vectors $\mathrm{v}[\mathrm{k}]$, $\mathrm{i}[\mathrm{k}]$ for charge and discharge curves with a sample resolution of 1 second. The data obtained can be used to calculate the parameters indicated below.

4.3.1.1 Coulombic Efficiency Calculation

To calculate the columbic efficiency (η) we use the equation (4-11). If we discharge and charge the cell, the final states of charge terms are identical, $soc[0]$ is equal to $soc[k]$. The equation $soc[k] = soc[0] - \frac{1}{Q}\sum_{j=0}^{k-1}\eta[j]i[j]$ becomes $0 = -\frac{1}{Q}\sum_{j=0}^{k-1}\eta[j]i[j]$ which further multiplied by $-Q$ becomes $0 = -\sum_{j=0}^{k-1}\eta[j]i[j]$. This can further be split into discharge and charge terms, and the final form becomes $0 = \sum_{j=0}^{k-1} i[j] - \sum_{j=0}^{k-1}\eta[j]i[j]$. Approximating $\eta[j]$ to be constant across the $soc[k]$ range, the relation used to calculate the columbic efficiency becomes $0 = \sum_{j=0}^{k-1} i[j] - \eta[25^0]\sum_{j=0}^{k-1} i[j]$. The final solution for the η can be calculated by dividing Ah discharged by Ah charged, equation (4-12).

$$soc[k+1] = soc[k] - \frac{\eta[k]i[k]\Delta t}{Q} i[k] \tag{4-11}$$

$$\eta = \frac{\sum_{j=0}^{k-1} i[j] \text{ (discharged Ah)}}{\sum_{j=0}^{k-1} i[j] \text{ (charged Ah)}} \tag{4-12}$$

4.3.1.2 Cell Capacity – Calculation

The cell capacity Q is defined by the manufacturer at room temperature. To find its value from the constant current discharge tests, we use the same equation as before (4-11). Starting from $soc[k] = 0$ and $soc[0] = 1$, the equation, $soc[k] = soc[0] - \frac{1}{Q}\sum_{j=0}^{k-1}\eta[j]i[j]$ becomes $-1 = -\frac{1}{Q}\sum_{j=0}^{k-1}\eta[j]i[j]$. The final solution to find Q becomes:

$$Q = \sum_{j=0}^{k-1}\eta[j]i[j];$$

4.3.1.3 Open Circuit Voltage – Calculation

As mentioned, the constant current charge/discharge tests generate two $v[k]$, $i[k]$ data vectors. This implies that for each state of charge $soc[k]$ there are two voltage values $v[k]$, one for charge and one for discharge, due to the hysteresis effect, but also because of the small $Ri(t)$, during charge/discharge processes (R being the internal resistance). This creates a challenge in trying to find the $OCV(soc[k])$ function. The following steps describe the approximations made to find the best fit for the open circuit curve.

1. Approximate the internal resistance of the battery at $soc[1]$ by measuring the instantaneous voltage drop between the battery voltage before discharge begins at $v[0]$ and the immediate $v[1]$ when the constant current test begins. Knowing the discharge

current, the approximate value of the internal resistance can be calculated using Ohm's law $(\mathrm{v}[0]-\mathrm{v}[1])/\mathrm{i}[1]$.

2. Approximate the internal resistance of the battery at $\mathrm{soc}[0]$. This can be done in the same way by measuring the instantaneous voltage rise between the last data point $\mathrm{v}[\mathrm{k}]$ and the following rest data point $\mathrm{v}[\mathrm{k}+1]$.
3. Assume that the internal resistance varies linearly between $\mathrm{soc}[1]$ and $\mathrm{soc}[0]$.
4. Read just the $\mathrm{v}[\mathrm{k}]$ voltage points by removing the $\mathrm{Ri}(\mathrm{t})$ component.

Once the $\mathrm{Ri}(\mathrm{t})$ component for both curves is removed, the only remaining difference between the charge and discharge curves is the hysteresis component and the edges of the curves where the data points do not complete the $\mathrm{v}[\mathrm{k}]$, $\mathrm{i}[\mathrm{k}]$ data set. The following steps must be followed to obtain the single value $\mathrm{OCV}(\mathrm{soc}[\mathrm{k}])$ function:

1. Approximate the OCV at 50% state of charge, $\mathrm{soc}[0.5]$ as the midpoint between the charge and discharge voltage.
2. At low state of charge, the OCV follows the charge voltage curve.
3. At high state of charge, the OCV follows the discharge voltage curve.
4. Between $\mathrm{soc}[0.5]$ and $\mathrm{soc}[0]$ or $\mathrm{soc}[1]$ the final OCV vary from the midpoint between the two voltage curves to either charge or discharge voltage values.

The final OCV voltage curve is not the perfect approximation of the open voltage curve of the cell, but it is good enough for the current calculations.

4.3.2 Pulse Discharge Tests – Methodology

The pulse discharge or dynamic tests have been used to determine the other cell parameters, the RC components and R_0. These involve discharging the Li-ion and lead-acid battery cells with a certain dynamic profile and recording the voltage behaviour of the system. Using optimisation tools, the Randles circuit parameters can be tuned to match the measured system output. These types of tests are usually more complicated and computationally demanding than the constant current tests. In this thesis, simple pulse voltage profiles have been used because of their simplicity and programmability in the EA-PSI 9080 power supply and load. The general steps of the testing methodology are the following:

1. Identify the battery cell $\mathrm{v}_{\max}$ and $\mathrm{v}_{\min}$ specified by the manufacturer.
2. Ensure uniform room temperature distribution for the battery as for the constant current tests.
3. Calibrate the cell by charging or discharging the cell until $\mathrm{v}_{\max}$ or $\mathrm{v}_{\min}$ is reached.

4. Apply a discharge square wave with a specific duty cycle. This report uses three sets of waveforms, 2.5min, 5min and 10min discharge pulse widths with the corresponding rest periods of 1-hour, 1.5-hours and 2-hours rest. Each of these tests has been done at five different C-rates, 0.2, 0.4, 0.6, 0.8, 1C-rate.
5. Assuming that the constant current tests have been performed, calculate the $\mathrm{OCV}(\mathrm{soc}[\mathrm{k}])$, capacity and columbic efficiency.
6. Extract the RC components using optimisation tools.

The results of the pulse discharge test give a complete set of information regarding the 3RC polarisation model components as a function of the state of charge, $\mathrm{R}_0(\mathrm{soc}[\mathrm{k}])$, $\mathrm{R}_1(\mathrm{soc}[\mathrm{k}]), \mathrm{C}_1(\mathrm{soc}[\mathrm{k}]), \mathrm{R}_2(\mathrm{soc}[\mathrm{k}]), \mathrm{C}_2(\mathrm{soc}[\mathrm{k}]), \mathrm{R}_3(\mathrm{soc}[\mathrm{k}]), \mathrm{C}_3(\mathrm{soc}[\mathrm{k}])$. More complex effects, like the hysteresis components, have been ignored in this analysis.

4.3.2.1 Parameter Extraction

The battery parameters, open circuit voltage, RC resistance and capacitor groups as well as the internal resistance R_0 can be calculated using some form of system optimisation. The system parameters extraction can be done using optimisation algorithms, which vary the 3RC Randles circuit parameters presented above to minimize the difference between the voltage experimental data curves and the simulation results. In this thesis, I have used the open-source MathWorks code - BatteryEstim3RC_PTBS which brings together a few MATLAB functions like the Curve Fitting Toolbox, Optimisation Toolbox and Simulink Design Optimisation.

This tool is open source and offers the possibility of parameter extraction for 1 to 5 RC battery equivalent circuit models. Various other tools have been investigated but the great advantage of the BatteryEstim3RC_PTBS is that it splits the optimisation problem into multiple sections, one for each current pulse thus speeding up the process and avoiding local minimum problems. The detailed workings of the tool are described in MathWorks documentation, but the general steps of the code are the following:

1. **Load battery data.** This section of the code loads the battery v[k] and i[k] data vectors.
2. **Determine the number of RC pairs.** In this step, the script determines the indicative number of RC pairs required to match the input data. To do this, the code uses the MATLAB Curve Fitting Tool.
3. **Estimate parameters.** This section performs most of the optimisation work in tuning the parameters to calculate the Randle circuit R_0 and R_XC_X time constants. This is done using the Simulink Optimisation Toolbox and the general MATLAB optimisation functions.
4. **Set equivalent circuit block parameters.** The last part of the code saves the extracted parameter data in look-up tables.

Figure 4-10 and Figure 4-11 show typical 0.4C pulsed discharged profiles for the Li-ion and lead-acid cells as well as the discrepancies between the output of the tuned system and the measured data. For the 3RC Randles circuit, the absolute errors between the experimental and simulated values are within 100 mV for the Li-ion cells and 200 mV for the lead-acid cells. This is valid across all pulsed discharged tests performed.

The dynamic tests have been performed at 0.2-1C discharge rate, 2.5, 5-min and 10-min pulse widths and 1, 1.5-hour and 2-hour rest periods. The reason for this was to capture the dynamic behaviour under different conditions and to notice discrepancies between each corresponding parameter data set. The extracted parameter data, as well as the comparisons between different test results, are indicated in the Appendix section of the thesis. Generally, the 3RC circuit matches the experimental Li-ion and lead-acid data within a 1% error for each data point, as indicated by the residuals plots, Figure 4-10 and Figure 4-11.

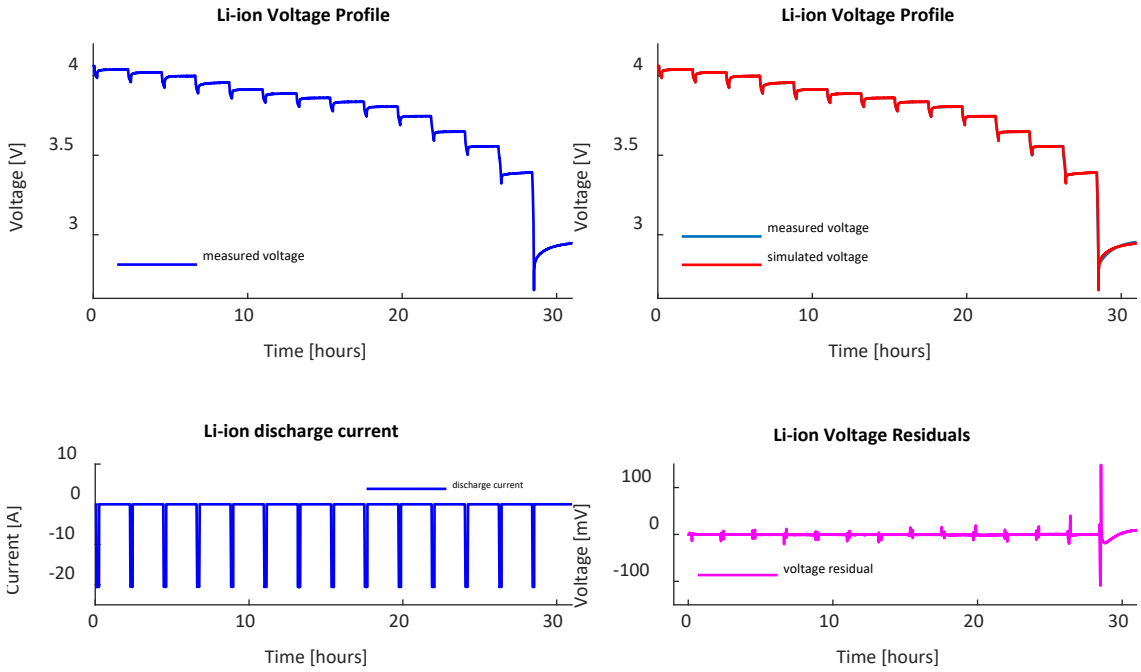

Figure 4-10. Typical pulsed discharge test Li-ion, experimental vs tunned system output & errors

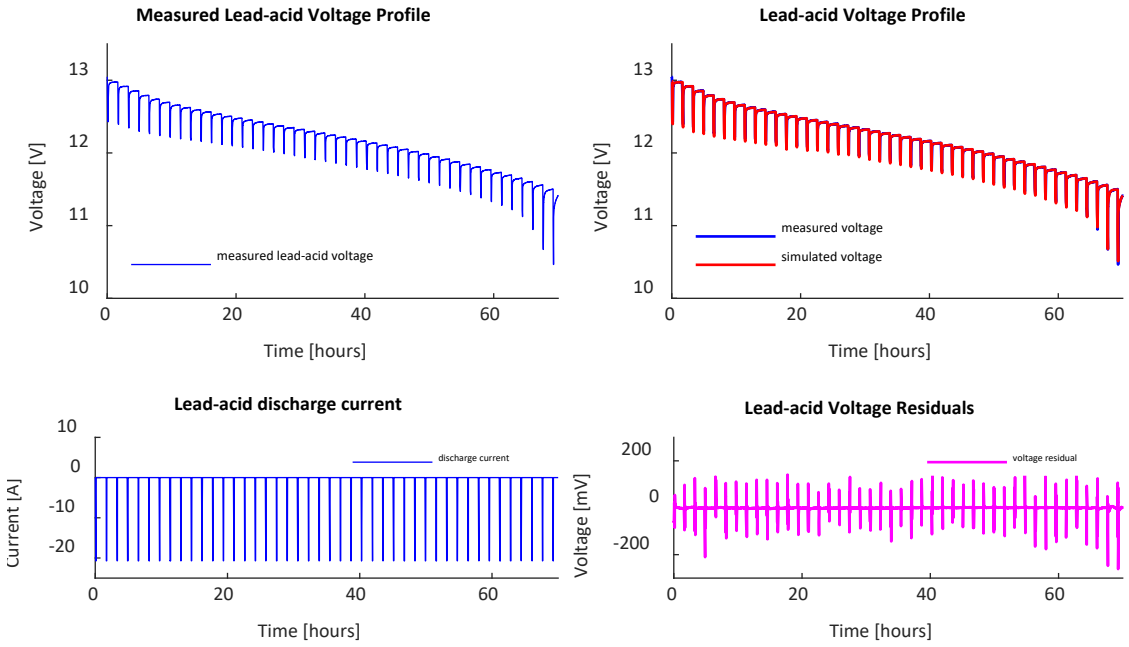

Figure 4-11. Typical pulsed discharge test lead-acid, experimental vs tunned system output & errors

4.3.3 MATLAB model description

The MATLAB modelling philosophy behind all simulations done in this project is based on the principles described in [123]. Each battery cell, Li-ion, or lead-acid, has been modelled using a 3RC polarisation circuit, presented in Figure 4-12 and explained in the previous sections. Figure 4-12 illustrates the MATLAB implementation of the 3RC circuit where the electrical elements, $OCV, R_0, R_1, R_2, R_3, C_1, C_2, C_3$, have been implemented as a Simscape subsystem block.

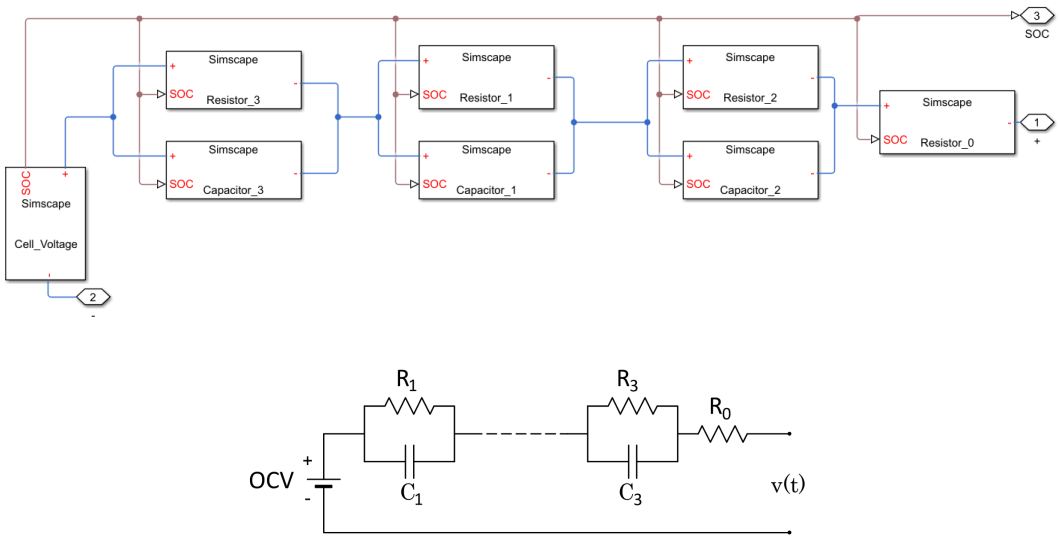

Figure 4-12. 3RC Polarisation ECM and its MATLAB/Simulink implementation

Each Simscape block shown in Figure 4-12, is a lookup table, which returns data from a MATLAB matrix as a function of the state of charge. There are 9 data matrices in total, one for each component of the dual polarisation ECM and each block contains 100 values of OCV, $\mathrm{R_x}$ or $\mathrm{C_x}$, at different states of charge from 0 to 1 at 0.1 intervals.

For a typical resistance R block, the system has two input variables, SOC and cell current. Its output is the voltage drop across the resistor. When values, are not recorded in the data input file, for example, the value of R when the state of charge is 0.35, the code does a linear interpolation of the existing R-values. Once the value of R has been calculated, the block exports the voltage drop across the resistor depending on the input current. This is calculated using the simple Ohm's law relation.

Similarly, the capacitor blocks $\mathrm{C_x}$ have 2 input variables, SOC and the input current. The output is the voltage drop across the capacitor. The block reads the values of the capacitances stored in the data matrix, the initial charge of the capacitor and the SOC vector. The only difference is the output equation which is specific to a capacitor $\mathrm{i(t) = C_x dv(t)/dt}$.

A cell's voltage source (open circuit voltage), $\mathrm{E_m}$, has two inputs, the current through the cell and the cell's Ah capacity and two output variables, the state of charge and the voltage across the source. The system calculates the state of charge by integrating the input current and outputs its value along with the interpolated value of the voltage.

4.3.3.1 Hybrid Lead-acid & Li-ion Model Description

Once the equivalent circuit parameters were extracted, the final directly connected hybrid lead-acid and Li-ion was implemented in MATLAB – Simulink using the equivalent circuits described in the previous sections. The model implements the battery equivalent circuits and a bidirectional CC/CV charger. The general workings of the hybrid model are the following:

- **Set the initial conditions.** To set the initial conditions, the first step is to insert the number of strings for each chemistry and the system voltage, which will also dictate the number of cells in series. The second step is finding an equilibrium point between the two lead-acid and Li-ion battery strings. If the voltage between the storage banks is different or if the two OCVs do not intersect, the system will generate a large circulation current between the two chemistries. Once an equilibrium point is found, and based on the SoC point, the system will set the charge and discharge voltage limits. Usually, the upper voltage limit is dictated by the lead-acid or Li-ion strings and the minimum discharge voltage by the lead-acid. The final step is setting the charge/discharge current.

- **Read the corresponding parameters**. For the starting SoC, the model reads the linearly interpolated parameters for all components of the system. The internal voltage source reads the Ah capacity, the OCV at each SoC point and the CE at each SoC point. For the Li-ion, the CE is practically constant, but that is not the case for the lead-acid. The internal resistance R_0 and the RC groups read their corresponding values.
- **Solve the System.** For each step, the system calculates the currents, voltages, discharged energies and SoC points at 1-second resolution as indicated by the literature.
- **Export data.** The data is exported from the Simulink model and fed into additional calculation tools to compute the overall system behaviour.

Figure 4-13 indicates the MATLAB-Simulink hybrid battery model with the additional graphical interface.

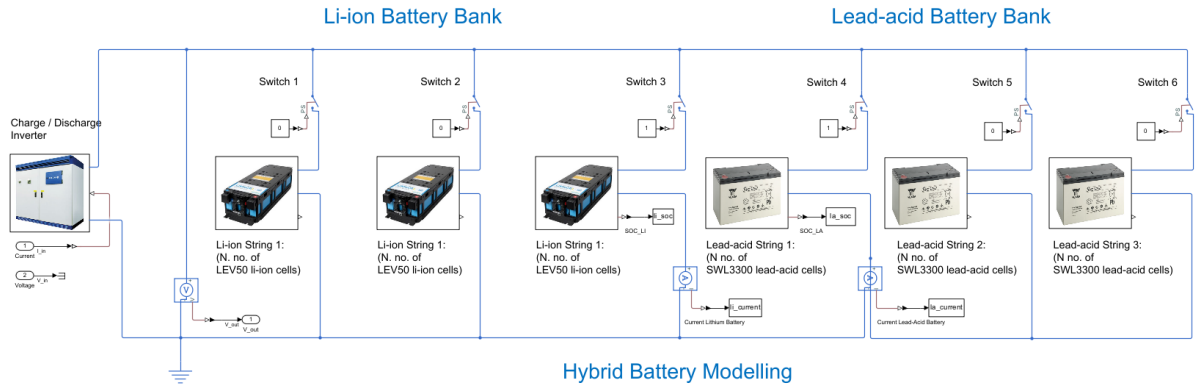

Figure 4-13. Hybrid Battery System - MATLAB - Simulink Model

4.4 Hybrid Battery System Demonstrator – Methodology

To answer the fourth question addressed in this thesis and to determine the performance over time, in real-world conditions of a hybrid Li-ion and lead-acid system, I have monitored a demonstrator project for the hybrid Li-ion and lead-acid system. The project is the first of its kind in the UK. The lead-acid and Li-ion strings are directly connected at the DC level as described below. The data collected was cleaned and fed into various bespoke MATLAB scripts to calculate the round-trip efficiency, the transient behaviour, the energy transferred between the strings, the total energy discharged by each string in a hybrid configuration, as well as the degradation of the system.

4.4.1 GS Yuasa – Hybrid Battery System

The hybrid battery storage demonstrator project used in this work is part of a wider UK micro-grid system developed in partnership with Innovate UK, the University of Sheffield, GS Yuasa, and

Infinite Renewables. The project is in Ebbw Vale, Wales, next to the GS Yuasa manufacturing facilities. The high-level schematic for the entire system is shown in Figure 4-14. The microgrid brings together a wind turbine, a small solar array, and a battery storage unit. Additionally, the system monitors the factory's low voltage electrical loads and based on this information the storage system is charged or discharged.

The technology used for the energy storage system is a hybrid combination of two different battery chemistries lead-acid and Li-ion provided by GS Yuasa. There are two main reasons why these chemistries are being used. First, they have complementary strengths, Li-ion – (high cycle life, high discharge rate, partial SoC operation, high efficiency, and high energy density) and lead-acid – (sustainable and abundant materials, simple control, abuse tolerant, economical, low embodied energy). Second, the voltage profiles of the two chemistries allow the Li-ion strings to be cycled before lead-acid thus providing some control over the strings even when using a direct DC bus connection.

The project was commissioned in December 2018 and the data collection started in January 2019. As mentioned, at that time, it was the first of its kind in the UK. The entire system is controlled remotely via the internet using the ADEPT software platform.

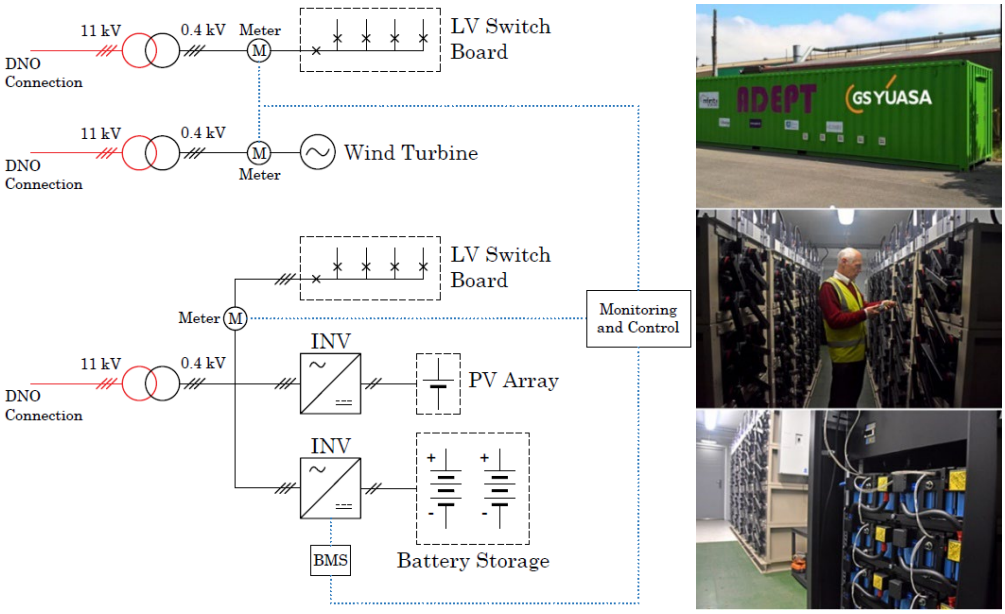

Figure 4-14. GS-Yuasa ADEPT, Dual Chemistry Battery System

The total storage capacity of the system is 270 kWh with the energy split between three strings of Li-ion and one string of lead-acid. The cells are grouped in battery modules, LIM50Ah and SLR500Ah. The Li-ion chemistry used is manganese oxide and the lead-acid is of VRLA type. The system is connected to the grid using a HiT POWER, PS100, 100 kW bidirectional converter. The overall schematic of the dual chemistry system is indicated in

Figure 4-15.

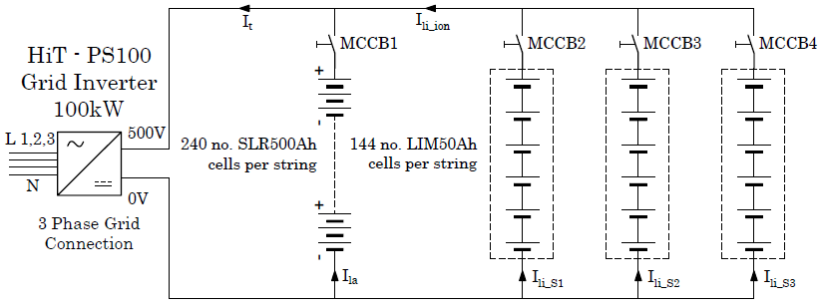

I_{la} – lead-acid string current

I_{li_S1} – Li-ion string 1 current

I_{li_S2} – Li-ion string 2 current

I_{li_S2} – Li-ion string 3 current

$I_{li\text{-}ion}$ – total Li-ion current

I_t – total system current

MCCB – Molded Case Circuit Breaker

Figure 4-15. Dual Chemistry System - Schematic

Table 4-3 presents the battery module's technical data taken from the GS Yuasa manufacturing catalogues.

Table 4-3. GS Yuasa Battery - Data

Battery / Cell type	Nominal Voltage [V]	Capacity [Ah]	Internal Resistance [mΩ]
Lead-acid SWL3300	12 (max 13.6)	100 (C/10 rate)	5.64
Li-ion Pack 6 x LEV50	3.75 / cell (max 4.1)	50 (at 1C rate)	0.5 / cell

4.5 Research Methodology – Sizing Hybrid Battery Systems

To achieve the last research objective and determine which applications are best suited for the hybrid system, the following methodology has been developed:

First, build a MATLAB energy balance model (techno-economic model) that can take as inputs hourly demand profiles of different categories, a generation profile mix of solar, wind, and hydro, the hybrid storage characteristics as well as the economic data for each technology. The outputs of the model will calculate the storage interaction between generation and demand. The results will include a list of technical operation parameters as well as the economic performance of the generation and storage system. The full model description is detailed below.

Secondly, set a range of load profiles to be analysed. This was done based on typical ELEXON category types such as residential, commercial, and light industrial as well as EV loads. Based on these load characteristics, such as the capacity factor, the performance of the hybrid system was tested to determine the economic solution when the system works in self-consumption and peak shaving modes.

Thirdly, I performed simulations of the hybrid Li-ion and lead-acid battery system operating in front of the meter (FTM) applications. To achieve this, a typical 10 MW medium-size FTM battery storage system was studied in the context of the UK energy storage market. Two main types of

battery applications were analysed, stand-alone FTM battery systems and co-located with solar systems. The storage capacity was varied between 1 and 4-hour durations (10 MWh to 40 MWh). For all options, the grid constraint was 10MW. Because the FTM storage optimisation is a complex process and beyond the scope of this project the battery operation profile was determined using Gridcog, a widely used industry software for FTM modelling. The Gridcog models calculate the battery storage operation profile based on maximising the revenue from both balancing (BM) and frequency markets services (BM and dynamic containment high and low). The battery operation profiles generated were compared against the single Li-ion option using the model described below.

4.5.1 Financial and Technical Assumptions

The financial inputs for the analysis done in this thesis are based on current UK industry prices. In 2023, the commercial PV and Wind systems prices stand at £750/kW and £1250/kW. The overall cost of the renewable generation systems also includes the O&M (operational and maintenance) and REPEX (inverter replacements) costs. The O&M costs stand at £6.7/kW/year for PV systems and £24/kW/year for wind. The REPEX costs are £34/kW/year for PV and £37/kW/year for wind. The hybrid battery system costs have been indicated in the Appendix.

All price data indicated have kindly been provided by Hydrock Consultants Ltd and used with its permission. Hydrock has signed various non-disclosure agreements (NDAs) with installers and manufacturers to feed market information and update its price database regularly.

For the technical data, the model uses a variable round-trip efficiency profile as a function of the SoC for the Li-ion and lead-acid profiles as experimentally determined in Chapter 5. The Li-ion batteries used in the model can perform 5000 cycles and the lead-acid only 2000 cycles.

The micro hydro CAPEX used in this work is based on the 2023 market prices and stands at £10.800/kW. The OPEX is £50/kW/year and the REPEX is £56/kW/year.

4.5.2 Hybrid Battery Model Description

The techno-economic model was built in MATLAB to calculate the interaction between generation, storage, and electrical demand. The model uses three main types of data sets, technical, economical, and operational information (on or off-grid, assessment periods, peak shaving, or self-consumption prioritisation). The input data sets include the technical characteristics (like the round-trip efficiency of each string) for Li-ion and lead-acid determined in Chapters 5, 6, and 7 as well as demand data from the research trials studied. The number of data points depends on the demand and generation of data resolution. The data resolution for the

input model can vary between seconds and hours. Most of the data resolution used in the thesis is half-hourly.

The overall flow of the model is indicated in Figure 4-16. As indicated, the MATLAB block components are the 'Main Script' file, the 'Storage Calc script', and the results generation function. The Main Script calls the three data sets and compiles data structures for each assessment year which is passed to the 'Storage Calc script' where the main calculations take place. Each structure passed for calculations contains the modified input data based on the operational scenario information. The 'Storage Calc script' returns a data structure with the main results.

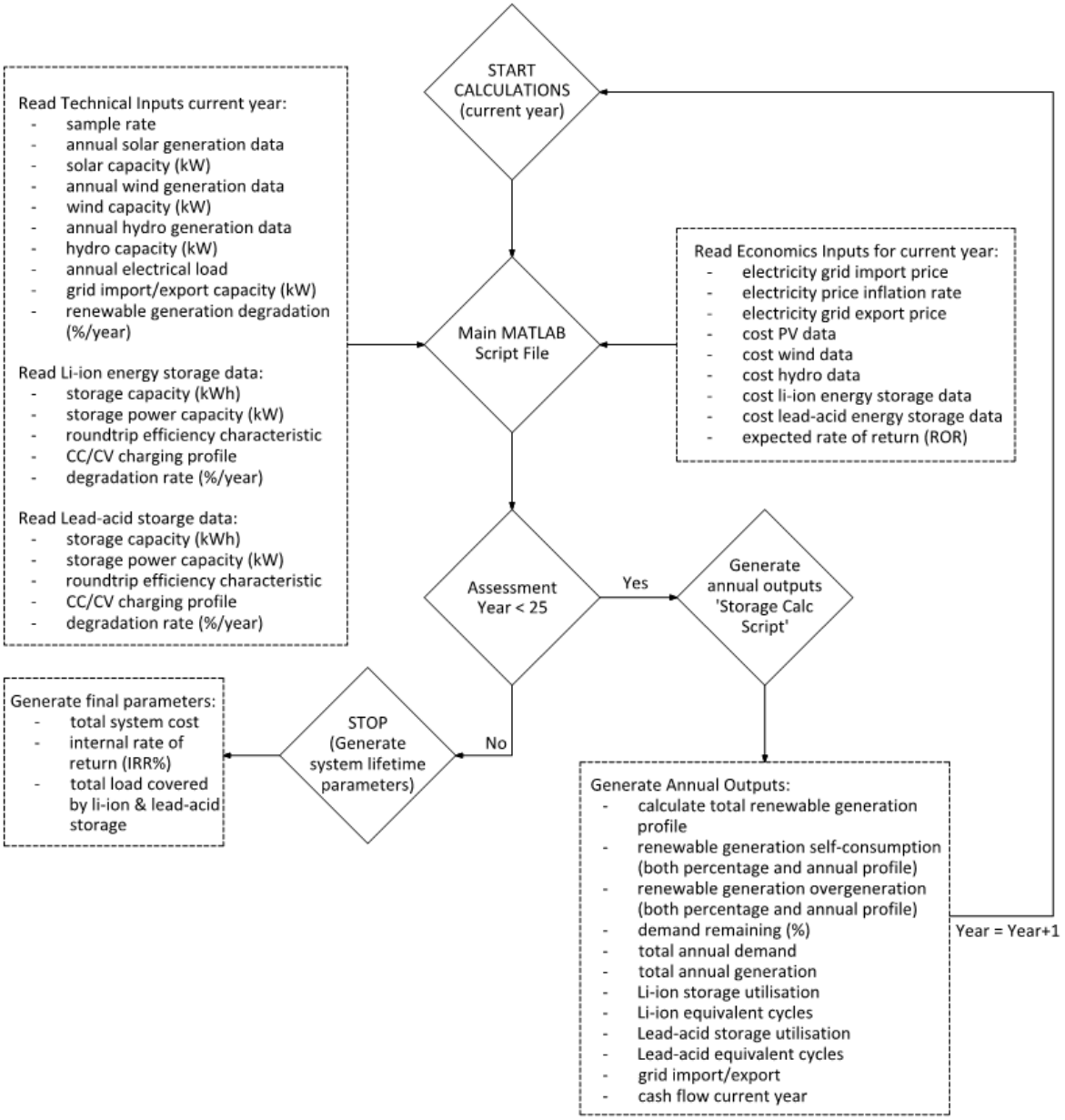

Figure 4-16. Energy Balance Model – Overview

The technical data input contains the following information:

- **Assessment sample rate**. The sample rate sets the time interval granularity of the overall calculations. The default option is half-hourly assessments, but it can be set to any resolution if the data available for generation and electrical load have been recorded at specific rates. Interpolations can be made to make the generation and load data match. It is worth mentioning that the sampling rate is the most important factor in terms of the computational time required to run a specific scenario.
- **Solar generation data.** The solar generation data contains the annual generation for a particular application as well as the inverter power for the system. This can be scaled based on a proportionality factor set in the Main Script file.
- **Wind generation data.** The wind generation data for a specific geographical area.
- **Hydro generation data.** Hydro generation data for a specific location.
- **Grid import capacity.** The grid import capacity is the maximum kW that can be imported from the local grid. If set to zero this implies a G100 (UK standard for zero export generation), zero export solution.
- **Electrical load.** The electrical load is the annual experimental data recorded for a particular application. All generation and the electrical load vectors must have the same sampling rate.
- **Li-ion technical data.** The Li-ion data contains the power rating of the energy storage system, the inverter efficiency curve as a function of the power loading, the cells efficiency curve as a function of the SOC, the CC/CV charging profile, and the capacity degradation rate.
- **Lead-acid technical data.** Like the Li-ion data, the lead-acid information contains the battery cell efficiency curve as a function of the SOC, the CC/CV charging profile, and the capacity degradation rate. As the lead-acid cells work directly connected in parallel with the Li-ion, the inverter efficiency curve is the same in both data sets.

The only fixed technical parameters used for the model input are the electrical load profile for the application and battery data parameters (except the battery power, capacity and the kWh ratio between Li-ion and lead-acid).

The economic input data contains the following information:

- **Electricity grid import/export price.** The model allows for any grid import/export prices input but for simplicity, across all scenarios, these were set at 30p/kWh and 5.5p/kWh. This was done as per 2022 and 2023 electricity market rates.
- **Import electricity inflation rate.** Throughout the scenarios analysed in this report, the inflation rate for the grid electricity price is constant and set to 2%. The model can adapt variable inflation rates but to avoid adding complexity a constant value was used.

- **Cost PV generation data set.** The PV cost generation data contains a matrix with the CAPEX, OPEX, REPEX per kW and the maximum lifetime of the system as a function of the power capacity installed. Each time the Main Script requests a cost calculation, a linear interpolation function is used to extract the cost information for a particular PV capacity within the data set range.
- **Cost Wind generation data set.** Like with the PV, the wind cost data contains the CAPEX, OPEX, REPEX per kW and the lifetime of the system as a function of the power capacity. The cost calculations are done as in the PV case.
- **Cost storage Li-ion data.** The Li-ion cost data contains the CAPEX, OPEX, and REPEX per kWh as a function of the total kWh capacity installed. Additional information is provided about the cycle lifetime of the cells. The information is extracted using linear interpolation functions.
- **Cost storage lead-acid data.** Identical to the Li-ion case.

In terms of the results, the most important technical parameters are the following:

- **Self-consumption (S_C).** The self-consumption is the total renewable generation in kWh that is directly consumed by the site load. In the Store Calc script, I have calculated it with Equation 4-13.

$$S_C[k](kW) = \min(\text{Demand}[k], \text{Gen}[k]) \quad \text{Equation 4-13}$$

k – time sample.

Demand – electrical demand at time k

- **Self-consumption percentage (S_C%).** The self-consumption percentage is the annual generation directly consumed by the site load as a percentage of the site load or the total annual renewable generation. This can be calculated either for demand or generation using Equation 4-14.

$$S_C\% = 100 * \sum_{k=1}^{n} (S_C[k] * k) / \sum_{k=1}^{n} (\text{Demand}[k] * k) \quad \text{Equation 4-14}$$

k – time sample (seconds or hours).

n – total time sample number in a year.

S_C – self – consumption.

Demand – electrical demand at time k.

- **Demand remaining (D_r).** Is the total energy remaining to be covered by the hybrid energy storage system.
- **Demand remaining percentage D_r%.** Is the total demand remaining as a percentage of the total electrical load analysed. It was calculated with Equation 4-15.

$$D_r\% = 100 * \sum_{k=1}^{n} (D_r[k] * k) / \sum_{k=1}^{n} (\text{Demand}[k] * k)$$ Equation 4-15

k – time sample.

n – total sample number in a year.

D_r – demand remaining.

Demand – electrical demand at time k.

- **Overgeneration (O_g).** The total overgeneration is the annual renewable generation in kWh which was not directly consumed on-site and needs to be either stored in the hybrid storage system or exported to the grid. It is also expressed as a percentage of the total annual renewable generation.
- **Li-ion storage usage (Li_{use}%).** The Li-ion energy storage usage is the total annual kWh discharged by the Li-ion cells as a percentage of the total annual energy demand. This was calculated using Equation 4-16. It is also expressed as a percentage of the total annual demand.

$$Li_{use}\% = 100 * \sum_{k=1}^{n} \left(Li_{dp}[k] * k\right) / \sum_{k=1}^{n} (\text{Demand}[k] * k)$$ Equation 4-16

k – time sample.

Li_{dp} – Li-ion discharge power at time k

n – total sample number in a year.

Demand – electrical demand at time k.

Li-ion storage usage at each time sample k, the power discharged from the Li-ion cells at time k, was calculated using the following:

$$S_C = \min(\text{Demand}[k], \text{Gen}[k])$$ Equation 4-17

k – time sample.

n – total sample number in a year.

4.5.3 FTM Optimisation

For the FTM optimisation, I have built two models in Gridcog for a 10MW DC-coupled (15MW PV system) and a 10MW standalone battery storage system. Gridcog is an industry standard for calculating PV and battery revenues working in frequency and balancing markets. All modelling was done for the UK markets, and I have used the latest 2023 market data.

The optimised battery charge/discharge profiles generated in Gridcog were used as inputs to the MATLAB model developed to calculate the impact of the hybrid ratio on the overall system operation.

4.5.4 Renewable & Hybrid Storage and Scenarios

For each application, the techno-economic and Gridcog models have been run for different scenarios. This will be discussed in the results chapter, specific to each application. I have compared the results and made observations based on the total storage requirements, the hybrid operation, and the total system cost.

Chapter 5 Experimental Investigations – Hybrid Systems

This chapter presents the results which answer the first question addressed in this work:

What are the hybrid characteristics of directly coupled, hybrid Li-ion (NMC) and lead-acid (VRLA) systems?

To answer this question, according to the steps indicated in the methodology chapter, five domestic-size battery storage systems are being examined to understand how the behaviour changes with the number of strings and system voltage. This is done by charge and discharge cycling of 24V (1 Li-ion & 1 lead-acid strings, 1 Li-ion & 2 lead-acid strings, 1 Li-ion & 3 lead-acid strings and 2 Li-ion & 1 lead-acid strings) and one 48V (1 Li-ion & 1 lead-acid) hybrid systems at 0.2-1C rates and 10-50% DoD. The results include discussions about the overall round-trip efficiency, transient currents, energy transfers between the strings, and the amount of energy discharged by each string across all systems. The general observation is that the round-trip efficiency drops from a maximum of around 94-95%, in the first stages of the charge/discharge process, when only Li-ion strings are active, to around 82-90% for lead-acid DoD up to 50%. The most important parameters in the round-trip efficiency function are the ratio between the Li-ion & lead-acid energy available and the charge/discharge current. The energy transfer between the strings, caused by the transient currents, is negligible in the first stages of the discharge and grows with the DoD peaking at around 60% DoD. Finally, in the first stage of discharge, only the Li-ion strings are active, and the amount of energy discharged decreases to almost half between 0.2-1C.

5.1 Research Objectives

This chapter aims to experimentally determine the performance of directly connected hybrid Li-ion and lead-acid systems in various parallel configurations. As described in the methodology chapter, this has been done by analysing the following parameters:

7. The energy (kWh) and charge (Ah) charged/discharged as a function of the charge/discharge rate, depth of discharge, and the number of strings of each chemistry.
8. The hybrid systems' round-trip efficiency as a function of the depth of discharge (DoC), charge/discharge rate, and the number of lead-acid and Li-ion strings operating in parallel.

9. The Li-ion DoD, before the currents delivered by both chemistry strings become equal, between points, A-B and A-X, Figure 5-2, as a function of discharge rate and the hybrid configuration.
10. The lead-acid behaviour, during the first part of the discharge process when only Li-ion strings are active, between points A-B Figure 5-2, as a function of the discharge rate and Li-ion, lead-acid mixture, and the hybrid system voltage.
11. The energy and charge transfer between the strings, between points D-E Figure 5-2, as a function of lead-acid depth of discharge, discharge current, and system configuration.
12. Analyse the intermittent charging/discharging behaviour and the impact on the overall round-trip efficiency of the system.

The technical characteristics of the cells analysed as well as the experimental test arrangement are described in the research methodology chapter.

5.2 Lead-acid and Li-ion hybrid behaviour - Results

Li-ion and lead-acid electrochemical cells operate at different voltages. Figure 5-1 (a) shows the OCV of a Li-ion, NMC cell, and a lead-acid cell. The OCV curves do not intersect as, depending on the chemistry, the Li-ion cells generally operate above 2.5V and lead-acid cells below 2.5V. The voltage range between 100% SoC and 0% SoC is also different between Li-ion and lead-acid.

For the case shown in Figure 5-1 (a), the Li-ion NMC cell operates between 2.7-4.2V and lead-acid between 1.8-2.25V. This means that both cells can't be connected directly in parallel, and some type of power electronic converters are required between the two cells/strings and the DC bus. However, for larger battery packs and multiple strings, the discharge curves of both chemistries can overlap as indicated in Figure 5-1(b). Figure 5-1(b) also shows that for the 0.58 ratio (see the Methodology Chapter) of the number of Li-ion to lead-acid cells connected in series, the two discharge voltage curves can intersect at 100% SoC and just above 0% SOC for both strings. This means that hybrid systems made up of directly connected (DC-linked/DC-coupled) Li-ion and lead-acid strings are possible without power converters between the two chemistry strings. Additionally, this allows the system to charge/discharge both strings from 0% SoC to 100% SoC without individual battery string control. This is advantageous as it eliminates the extra cost associated with hybrid systems and brings the possibility of simple and cheap integration of Li-ion and lead-acid chemistries.

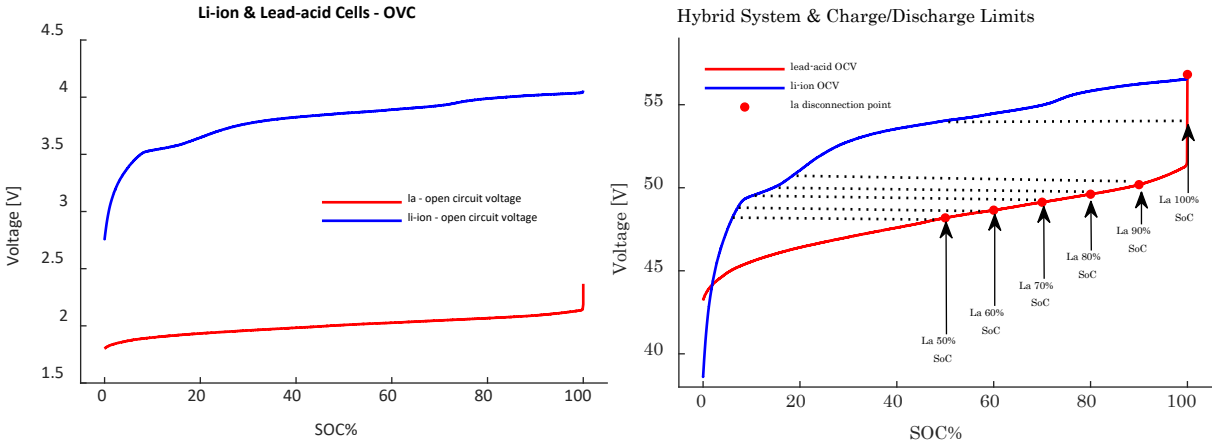

Figure 5-1. Li-ion (NMC) and lead-acid – cell open circuit voltages (a), Hybrid lead-acid and Li-ion voltage profile (b)

Figure 5-2 shows an example of the charge/discharge current dynamics of a two-sting, directly connected hybrid battery along with the corresponding charge/discharge voltage profiles. Figure 5-2 (a) indicates the discharge current strings, between points A and B, the Li-ion string discharges first, providing most of the current, and only when it reaches levels below 40% SoC, the lead-acid string is activated. After the transition point, between points B and C the lead-acid string takes over providing most of the discharge current. This can simultaneously be followed in Figure 5-1 (b) where the horizontal dotted lines indicate the steady state equilibrium voltage points between the two strings. At point D, Figure 5-2 (a), the discharge is stopped, and between points D and E the system rests. In the rest period, because of the different chemistry dynamics, the lead-acid string charges the Li-ion one. The current spike between the strings falls to zero as the system naturally reaches equilibrium (the circulation currents reach negligible values, and the system voltage stabilises).

Figure 5-2 (b) shows the CC/CV charging current dynamics of a hybrid system. In the first instance, between points A and B, the Li-ion string briefly absorbs most of the charging current but after point B, the lead-acid string current takes over. After charging the bulk of the lead-acid string, the Li-ion string current starts to increase, and eventually, as the charger switches to CV, both strings reach 100% SoC.

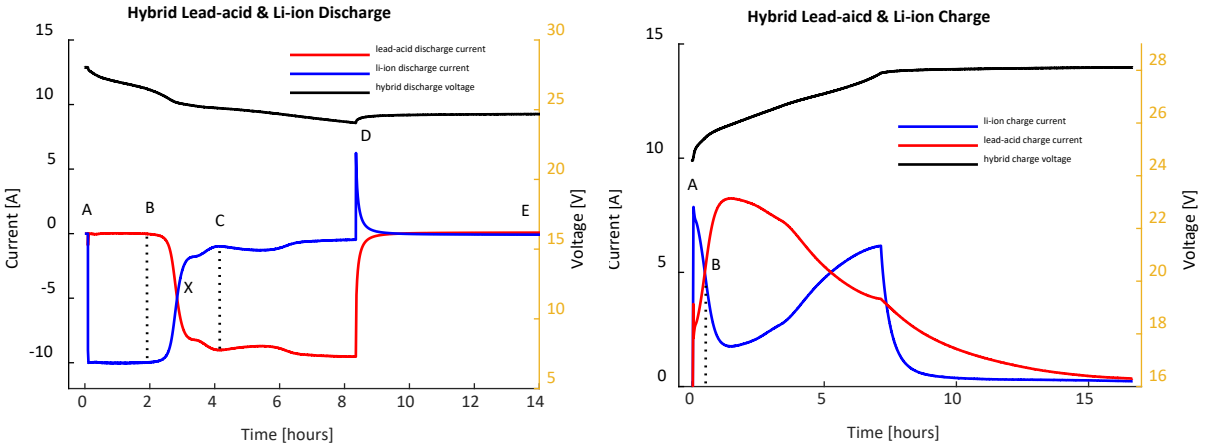

Figure 5-2. Hybrid Li-ion and Lead-acid Discharge Profile (a), Charge Profile (b)

The charge/discharge dynamics described above vary with factors like the number of strings of each chemistry connected in parallel, the charge/discharge C rates, and the cycling DoD. For example, the energy and Ah discharged between points A and B, Figure 5-2 (a), is crucial to hybrid applications because it shows the capacity available for frequent cycling and how much of the Li-ion string is available for independent control. Similarly, the energy transferred between the strings during the rest period, between points D and E, Figure 5-2 (b), depends on the discharge current, DoD for the lead-acid strings, and the number of strings connected in parallel. These parameters will be investigated in the following sections.

The hybrid behaviour indicated in Figure 5-2, and detailed in the following sections, was obtained by cycling the system at room temperature (20^0C). Additional experimental investigations are required for a detailed system characterisation at different temperatures. However, the overall philosophy of the system operation will not change substantially. The voltage range for the independent Li-ion string operation (A-B region) will be identical, as this is determined by the float and boost voltage of the lead-acid cells. This will continue to allow independent charge/discharge of a portion of the Li-ion capacity. The differences will appear in the Li-ion energy available for cycling between A and B points, as higher/lower temperature implies higher/lower capacity and lower/higher internal resistances for both chemistries. At low temperatures, the internal resistance of the Li-ion strings will increase, and even if the A-X voltage range is identical, less energy will be available for independent cycling, on top of the natural Li-ion capacity decrease due to temperature. The opposite will happen if tests are performed at higher temperatures. Point X will also shift depending on the relative rate of change of internal resistances, between the two chemistries. The circulation currents (Point D) will modify with the relative rate of change of ionic diffusion. An accurate description of these temperature effects can provide further research directions. The results presented in the following sections describe the hybrid system operation at constant temperature (20^0C) and under different strings and voltage configurations.

5.3 Hybrid system analysis – Results

5.3.1 Hybrid System 24V, 1 Li-ion string, and 1 lead-acid (1LI&1LA)

The first arrangement analysed is the 24V hybrid system with only two strings, one for each chemistry. The system was cycled between the state of charge intervals indicated in the methodology section. In normal operation conditions, the hybrid system will never be fully discharged, because of this, the lead-acid strings were kept above 50% DoD, and this is used as a reference across the analysis.

Figure 5-3, shows the total energy and amp-hours discharged by each system string as a function of discharge rate and lead-acid depth of discharge. The energy and Ah were calculated using Equation 5-1. The figure shows that the total energy and charge, available within any operating voltage range of the hybrid system, depend on the charge/discharge C rate. This is mainly because the charge and energy available from the lead-acid string are dictated by Peukert's law (the capacity available decreases with the discharge current). When only the Li-ion is cycled, the total available charge and energy are dictated by the internal resistance of the Li-ion strings. For example, during cycling range 1, when only the Li-ion string is cycled, and the lead-acid is kept at 0% DoD, the total available energy ranges from 0.418 to 0.689 kWh for 1 to 0.2C rates, respectively in Figure 5-3 (b). The corresponding amp-hours range from 15.765 Ah to 24.6 Ah. For the following five cycling ranges, when the lead-acid string is discharged to 10% - 50% DoD (cycling range 2 to 6, methodology section), the Li-ion discharged energy slowly rises to a maximum of 0.91 kWh, which corresponds to 34.9 Ah, when the hybrid strings are discharged to 50% DoD.

$$\mathrm{E} = \frac{1}{3.6 * 10^{6}} * \sum_{\mathrm{k}=1}^{\mathrm{SoC_x}} (\mathrm{I[k]} * \mathrm{V[k]} * \mathrm{k}) \qquad \text{Equation 5-1}$$

$$\mathrm{AH} = \frac{1}{3.6 * 10^{3}} \sum_{\mathrm{k}=1}^{\mathrm{SoC_x}} (\mathrm{I[k]} * \mathrm{k})$$

k – time sample (seconds).

SoC_x – total number of sample tests between 100% SoC and the SoC_x

E – total energy in kWh between the SoC interval analysed.

AH – total Ah charge in the SoC interval analysed.

This shows that in normal operating conditions of the hybrid system, most of the Li-ion energy capacity is available for cycling independently of the lead-acid string cycling. For the 1LI&1LA system, charged/discharged at 0.2C, a maximum of 75-76% of the available Li-ion energy (kWh)

or charge (Ah) can be cycled independently for frequent charge/discharge cycles, keeping the lead-acid strings at 100% SoC. This drops to 45-46% if the system is charged/discharged at 1C.

A total energy capacity of 2.201 kWh is available from the 1LI&1LA hybrid system when the arrangement is discharged at low C rates (0.2C for the analysed case). This includes 0.91 kWh delivered by the Li-ion strings and 1.291 kWh by the lead-acid. The same figure drops to a total of 1.695 kWh for 1C charge/discharge rates, 0.91 kWh from the Li-ion string and 0.785 kWh from the lead-acid chemistry. As explained, this is due to less energy and charge being available from the lead-acid string according to Peukert's law.

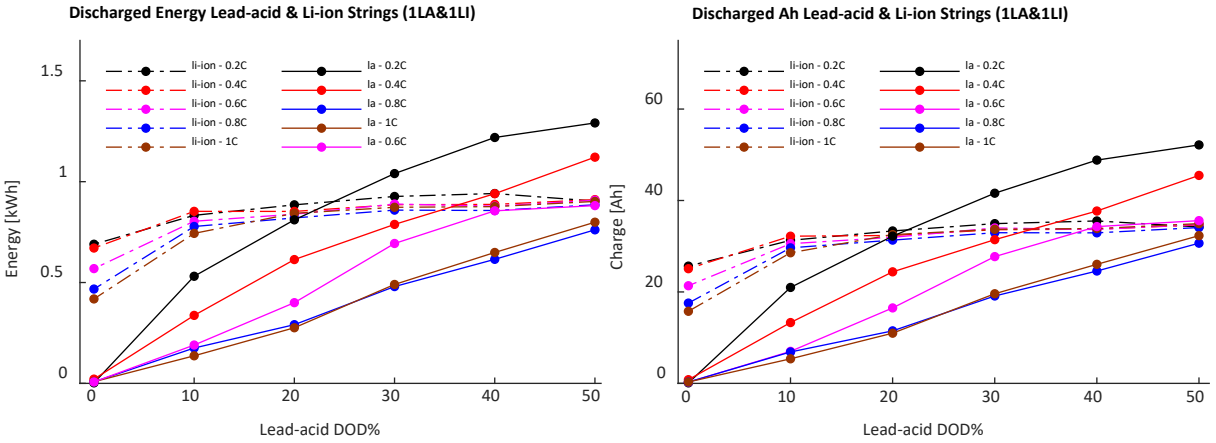

Figure 5-3. The energy (kWh) (a) and amp-hours (Ah) (b) discharged by the 24V (1LI&1LA) system.

Figure 5-4 shows the energy (kWh) and charge (Ah) discharged from the Li-ion string, for each cycling range, as a function of the charged/discharged C rate (0.2-1C). The figures also indicate the energy and charge available from the Li-ion chemistry before any significant activity is noticed on the lead-acid string (i.e., the energy discharged between points A-B and A-X, Figure 5-2), as a function of charge/discharge rate. Like in the previous indications, the system follows the normal hybrid discharge sequence, first the Li-ion discharges to around 25% SoC, when the power delivered by both chemistries equalises, and after that lead-acid slowly takes over. If the lead-acid string is discharged below 10% DoD, the energy and charge available from the Li-ion chemistry is independent of the discharge rate, Figure 5-4. For the 1LA&1LI system, this is around 0.75-0.77 kWh and 28-28.5 Ah. This means that in normal operation conditions, most of the Li-ion strings will be discharged before the lead-acid battery strings drop below 90% SoC.

If the lead-acid string is not discharged at all, i.e., the system is cycled only within 'cycling range 1 (see research methodology)', or points A-B (Figure 5-2) indicated above, the energy and charge available from the Li-ion string drops as the C rate increases, black line Figure 5-4. This is due to the voltage drop of the Li-ion internal resistance and diffusion processes. A higher discharge current will produce a higher voltage drop, and the system reaches the lead-acid discharge voltage faster. This limits the Li-ion energy available for independent cycling. For the 1LI&1LA

system and the tested batteries, this ranges from 0.69 kWh (25.6Ah) for the 0.2C rate to 0.42 kWh(15.76Ah) for the 1C rate. In other words, a fivefold increase in the charge/discharge current decreases the Li-ion energy and charge available for independent cycling by around 38.4%.

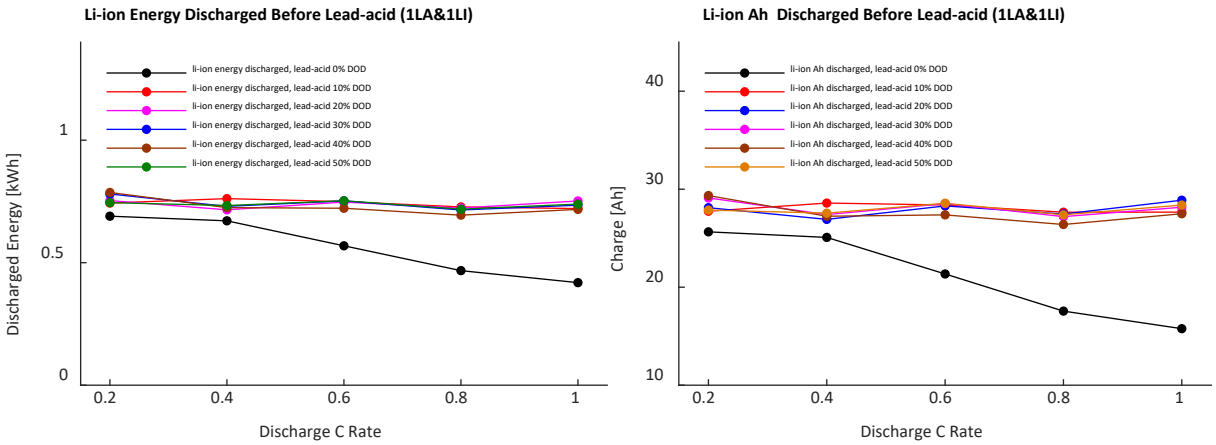

Figure 5-4 Li-ion energy and charge available during discharge from 1LI&1LA, before the Lead-acid string becomes fully active (energy & charge available only between points A-X)

Figure 5-5 shows the energy round-trip efficiency for the individual chemistry strings and the overall hybrid system. As expected, the energy round-trip efficiency of the Li-ion string is almost independent of the discharge rate, or the DoD, and its average is around 0.95 (0.94 for 1C and 0.97 for 0.2C rate). However, this is not the case for the lead-acid string, where the round-trip efficiency depends on the DoD and the charge/discharge C rate. The lead-acid round-trip efficiency is heavily dependent on the coulombic efficiency (which is much lower when compared with Li-ion) and the internal resistance, which is also higher when compared with the Li-ion cells. If the lead-acid string is cycled within 'cycle range 1 (see research methodology)', 0-10% DoD, the average round-trip efficiency is 0.59. The higher the discharge rate, the lower the round-trip efficiency, as indicated in Figure 5-5 (a). For 'cycle range 1' this rises from 0.55 at 1C rate to 0.75 at 0.2C. Across all DoD, the average energy round-trip efficiencies for the lead-acid string were measured to be, 0.81, 0.76, 0.68, 0.64, and 0.66 for the 0.2, 0.4, 0.6, and 1C rates.

The total hybrid system round-trip efficiency, however, is a much more complex function of parameters like the ratio between the Li-ion and lead-acid charged/discharged energy, the DoD for the entire system, the charge/energy transfer between the strings during the transient period, the charge/discharge rate, and so on. Experimentally, the measured values for the round-trip efficiency as a function of the lead-acid DoD are indicated in Figure 5-5 (b).

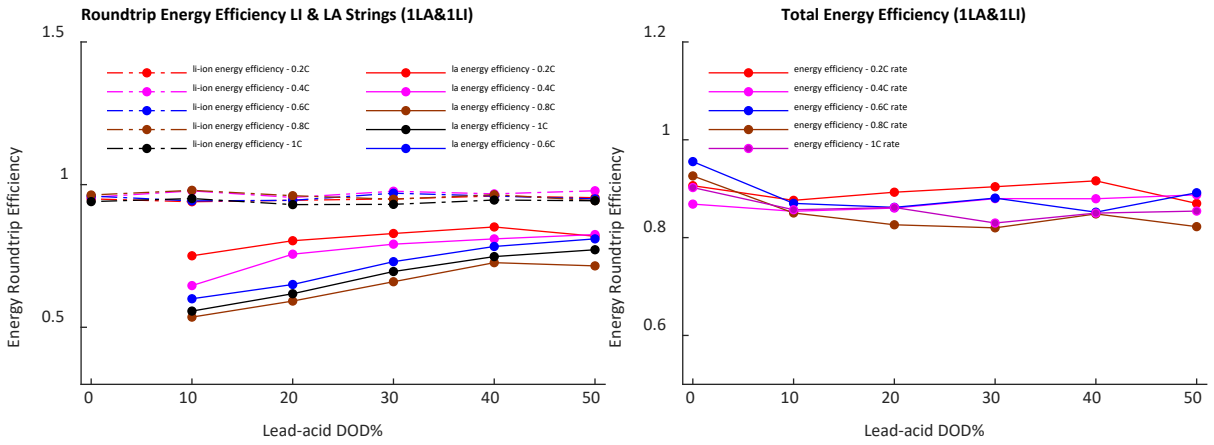

Figure 5-5. Round-trip energy efficiency of the individual strings (a) and total system energy round-trip efficiency (b)

If the Li-ion dominates the total charged/discharged energy, the round-trip efficiency is going to be close to the stand-alone Li-ion round-trip efficiency. However, this is not constant as the activity on the lead-acid string, although insignificant, is not zero. For the 1LA&1LI system, during discharge, the average lead-acid current between points A-B Figure 5-2, is around 500mA for the 0.2C and this slowly rises to 700mA for the 1C rate. This small activity on the lead-acid string decreases the overall energy round-trip efficiency of the hybrid system in the A-B region - Figure 5-2. Ideally, in this region, only the Li-ion string would be active. The average values for the energy round-trip efficiencies of the hybrid system, in the A-B region Figure 5-2, are indicated in Figure 5-5 (b).

The opposite happens when the lead-acid charged/discharged energy dominates. When the ratio between the charged/discharged lead-acid and Li-ion energy increases, the overall round-trip efficiency is closer to the standalone lead-acid value as indicated in Figure 5-5.

The effects of a higher discharge rate for the hybrid system are threefold. First, it has a direct impact on the lead-acid and Li-ion charged/discharged energy ratio, because of Peukert's law, and subsequently on the overall round-trip energy efficiency. A higher discharge rate results in lower lead-acid energy available between the cycle ranges examined and a lower charge/discharge energy ratio between the lead-acid and Li-ion. Secondly, a higher C rate results in higher ohmic losses due to the internal resistances of both battery strings. Finally, as illustrated below, a higher C rate implies higher energy transfers between the strings during the transient period.

As explained above, during the rest period, between D-E points Figure 5-2, energy is transferred between the strings due to the different dynamic responses of the two chemistries. The amount of energy transferred from the lead-acid to the Li-ion string varies with the discharge current and the lead-acid DoD point when the discharge process is stopped. Figure 5-6 (a)shows the energy

transfer curves for different C rates and lead-acid DoD points. Generally, for the 1LA&1LI system, a higher discharge rate implies a higher energy transferred during the transient period but only if the lead-acid string is discharged below 30% DoD.

Taking all of this into account, the overall results, indicated in Figure 5-5, show a relatively flat round-trip efficiency as a function of the lead-acid DoD, with higher values when only the Li-ion is cycled.

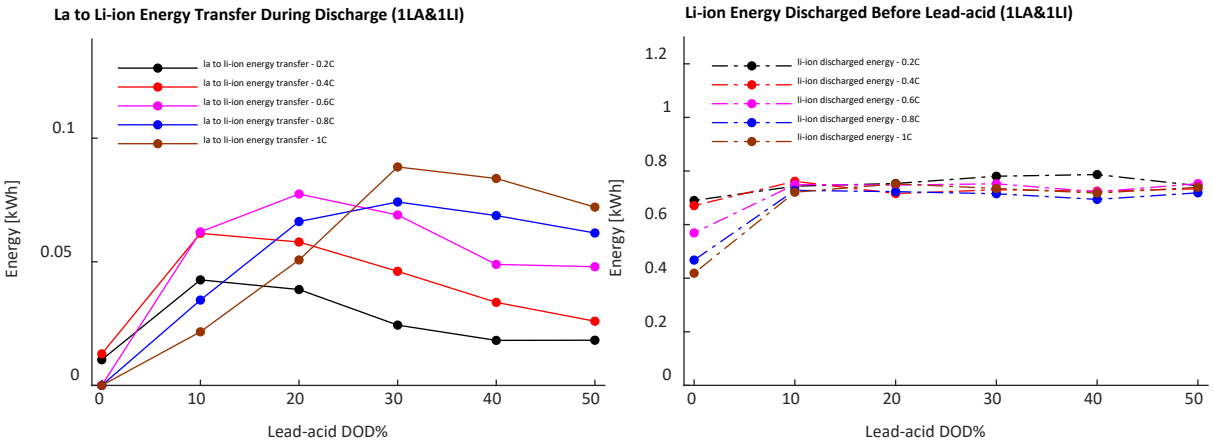

Figure 5-6. Energy transfer between the strings during the discharge rest period (a)

Figure 5-7 indicates the total lead-acid energy and charge which is charged/discharged when the hybrid system is operated in the A-X region - Figure 5-2, for each charge/discharge region. As mentioned, even when the hybrid system is only operated in the A-B region the activity on the lead-acid system is not zero, black line Figure 5-7. When the lead-acid string is discharged below 0% DoD, the amount of energy charged/discharged within the A-X region varies linearly with the discharged rate. The maximum lead-acid activity in the A-X region measured is around 4.5Ah or 0.12 kWh. This implies that a directly connected hybrid system does not operate as an ideal actively controlled hybrid energy storage system. The activity on the lead-acid string, before the main bulk of the lead-acid discharge starts, is not zero and can't be ignored in the overall system round-trip efficiency calculations. Because the lead-acid cells operate at low, below 50% round-trip efficiency in the A-X region, the small amount of lead-acid activity does have an impact on the overall system round-trip efficiency, especially for shallow discharges when only the Li-ion string is active. This is discussed below.

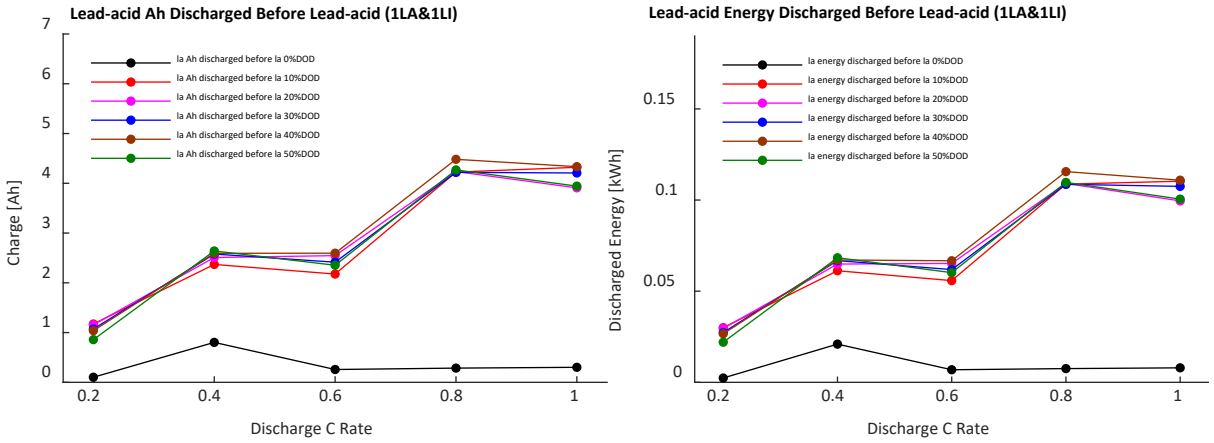

Figure 5-7. Lead-acid energy and charge discharged/charged during A-X interval.

5.3.2 Hybrid System Data

Like the analysis presented in the previous section, I have calculated the parameters for the 2LI&1LA, 1LI&2LA, and 1LI&3LA hybrid systems. Without detailing the values for each individual option, the following data sets are presented below, capturing the following:

- Total energy and charge discharged by each string.
- Total energy discharged from the Li-ion strings before the power delivered by the two chemistries equalise (A-X region Figure 5-2).
- Total energy transferred between the strings during the rest period (D-E region, Figure 5-2).
- The total lead-acid energy and charge recorded when only the Li-ion is active and between the A-B points, and before the power delivered by both chemistries equalises A-X region.
- Round-trip energy efficiencies for each string and for the overall hybrid system.

5.3.2.1 2LI & 1LA - Hybrid System Data

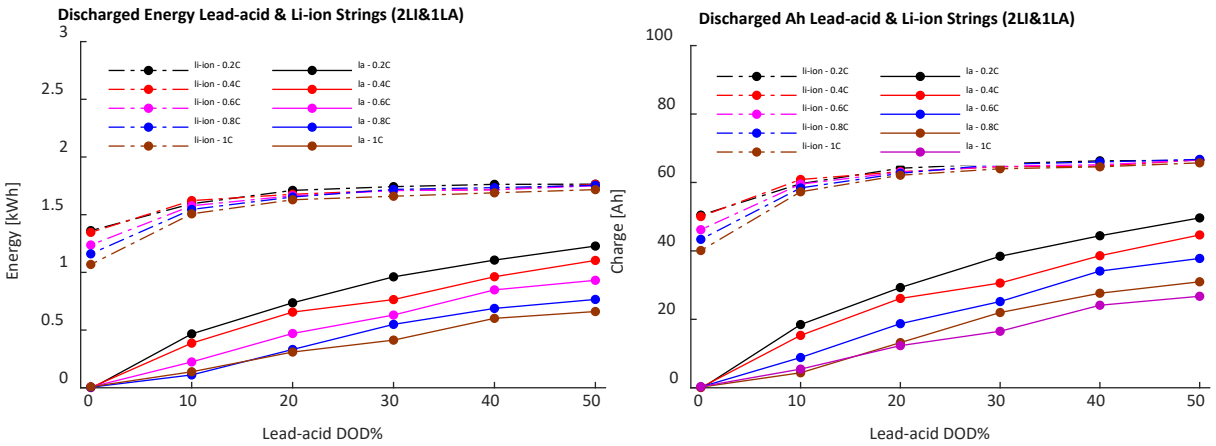

Figure 5-8. The energy (kWh) and amp-hours (Ah) discharged by the 24V (2LI&1LA) system.

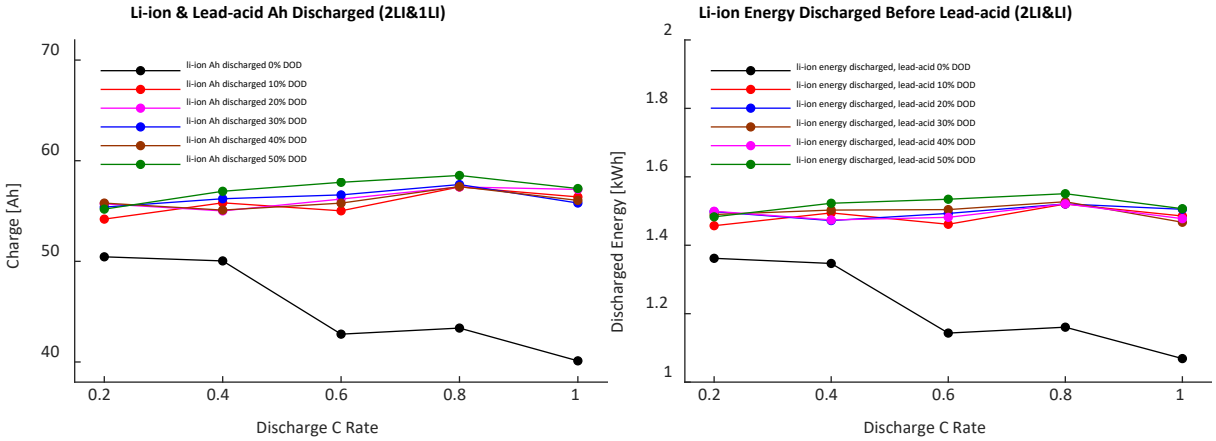

Figure 5-9. Li-ion energy & charge available during discharge before the Lead-acid string becomes fully active (energy & charge available between A-B and A-X points)

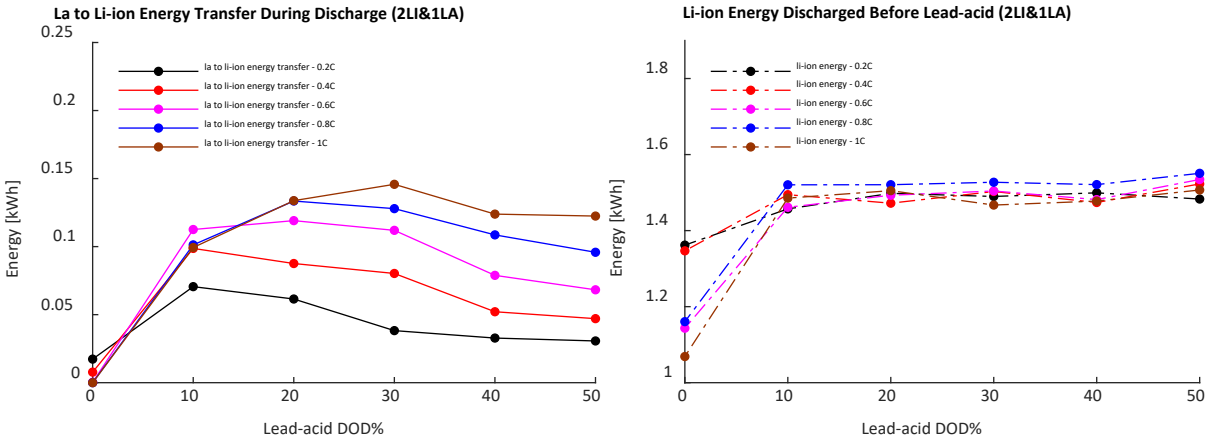

Figure 5-10. Energy transfer between the strings during discharge (left)

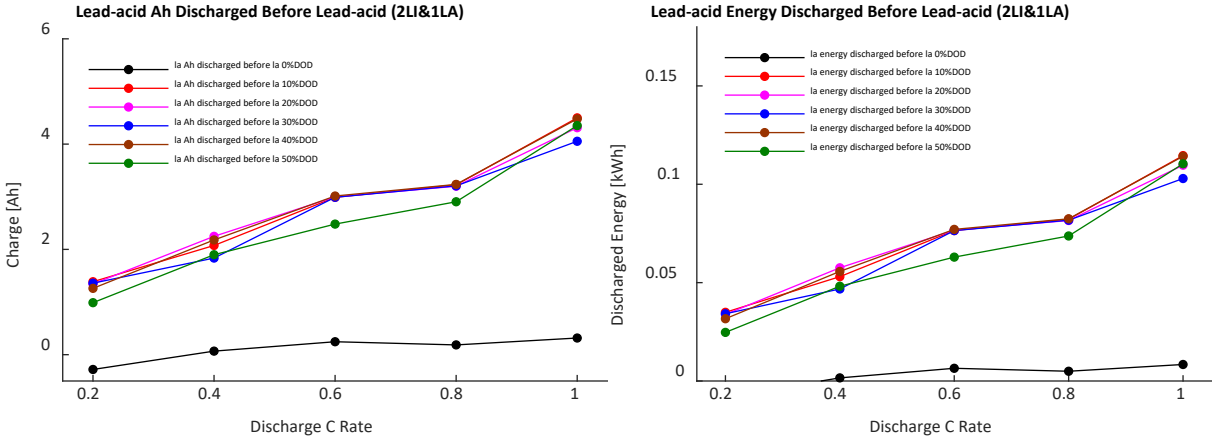

Figure 5-11. Lead-acid energy and charge discharged during A-B and A-X intervals

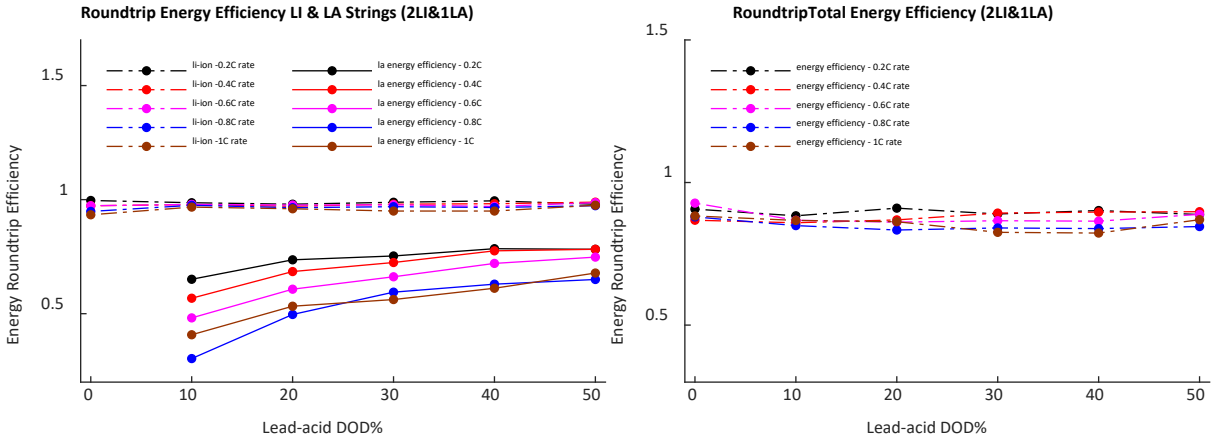

Figure 5-12. Round-trip energy efficiency of the individual strings (left) and total system energy round-trip efficiency (right)

5.3.2.2 1LI & 2LA - Hybrid System Data

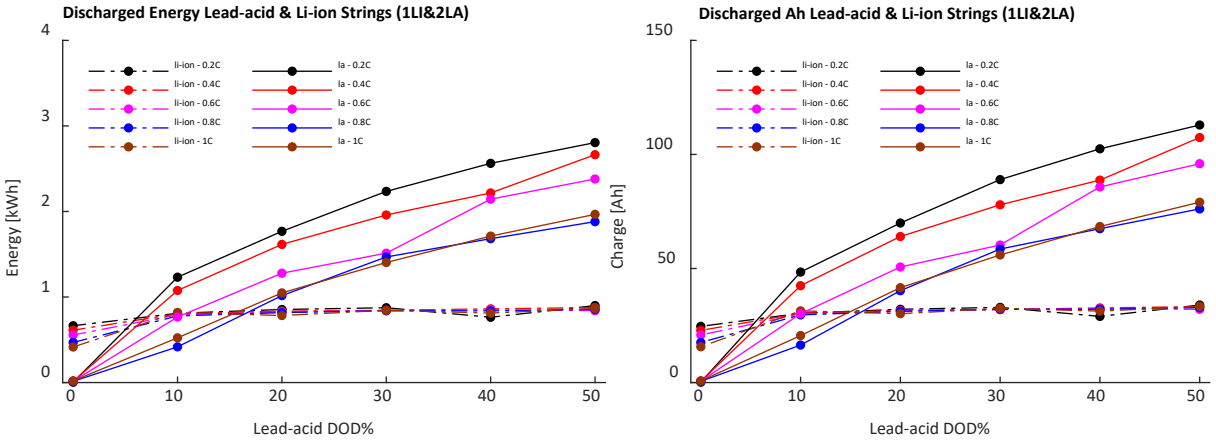

Figure 5-13. The energy (kWh) and amp-hours (Ah) discharged by the 24V (1LI&2LA) system.

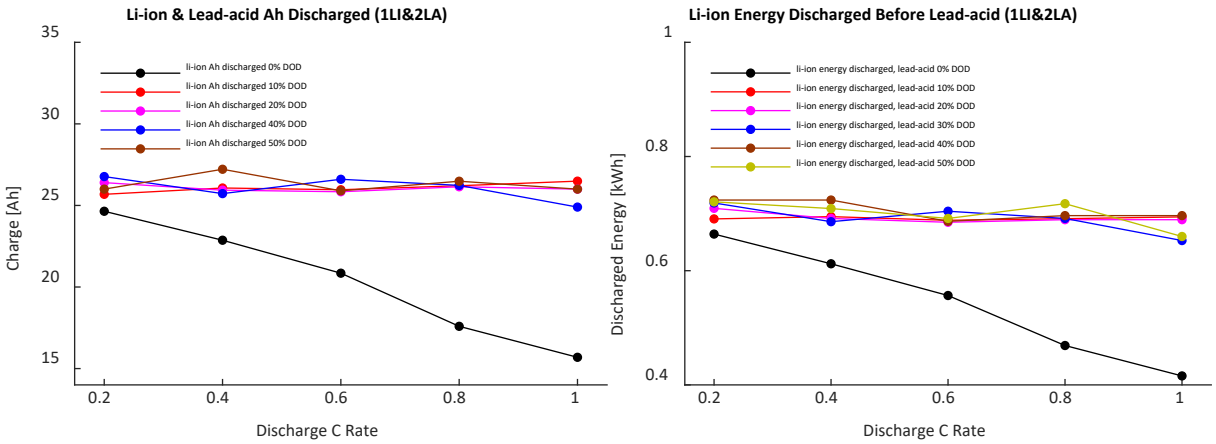

Figure 5-14. Li-ion energy & charge available during discharge before the Lead-acid string becomes fully active (energy & charge available between A-B and A-X points)

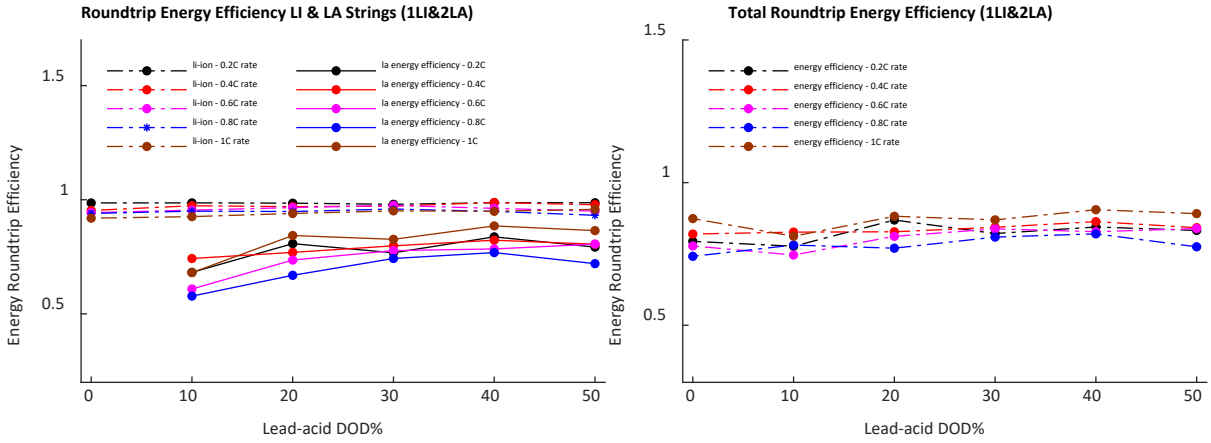

Figure 5-15. Round-trip energy efficiency of the individual strings (left) and total system energy round-trip efficiency (right)

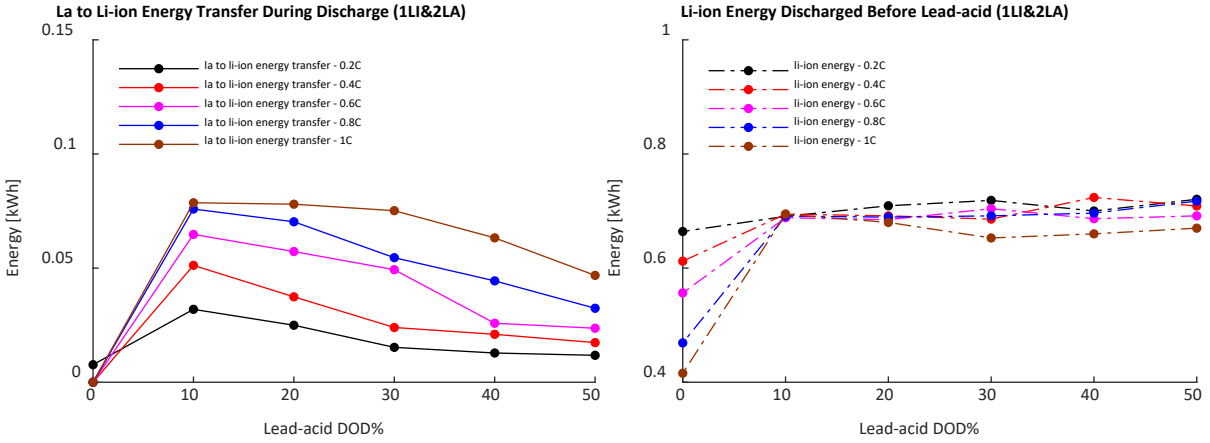

Figure 5-16. Energy transfer between the strings during discharge (left)

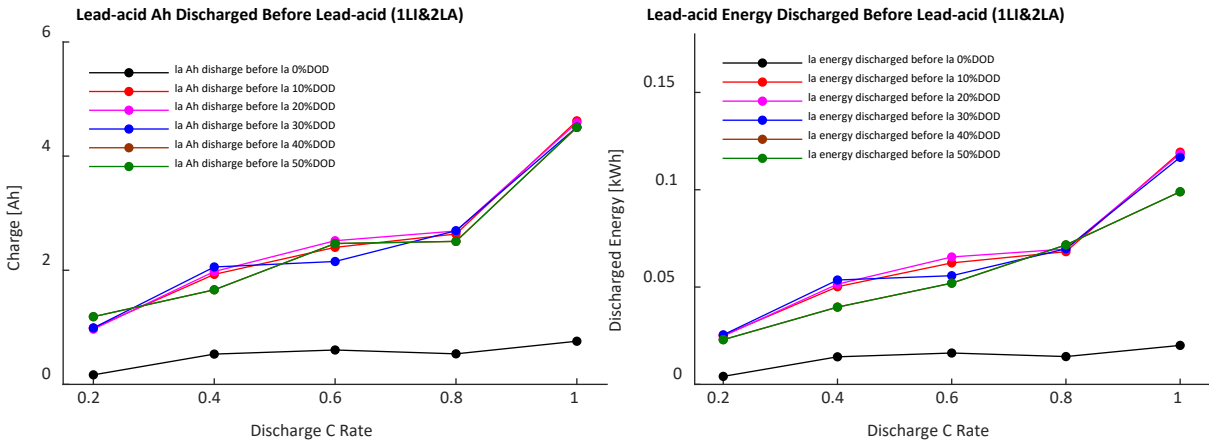

Figure 5-17. Lead-acid energy and charge discharged during A-B and A-X intervals.

5.3.2.3 1LI & 3LA - Hybrid System Data

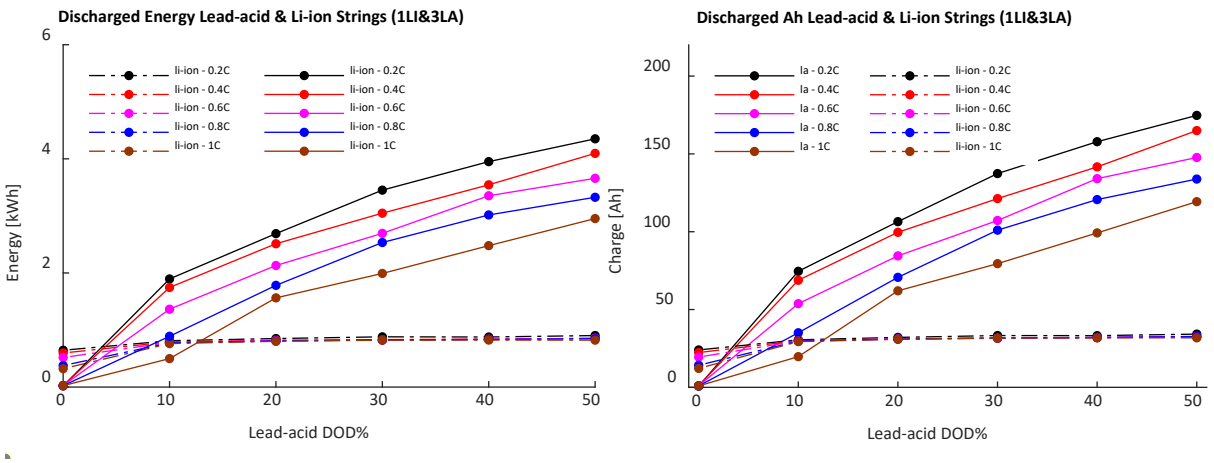

Figure 5-18. The energy (kWh) and amp-hours (Ah) discharged by the 24V (1LI&3LA) system.

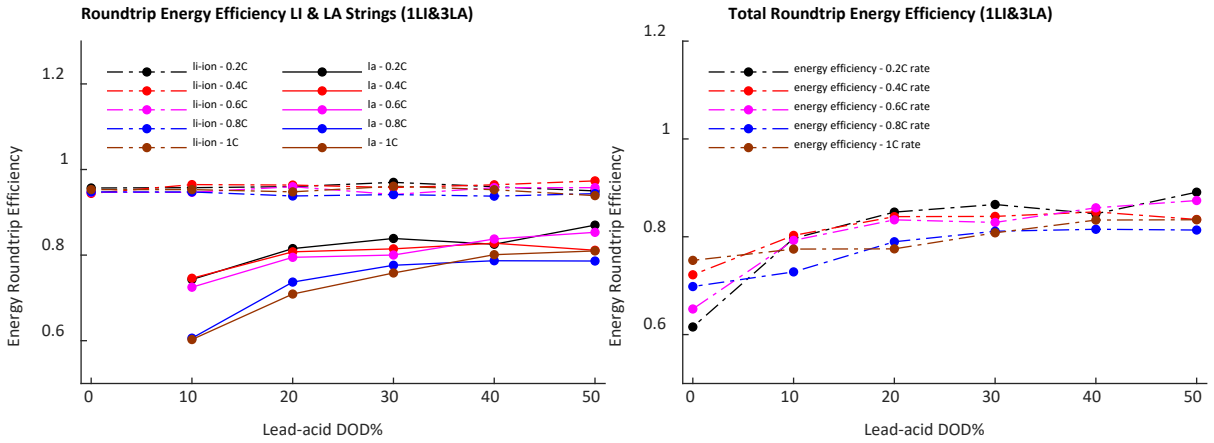

Figure 5-19. Round-trip energy efficiency of the individual strings (left) and total system energy round-trip efficiency (right)

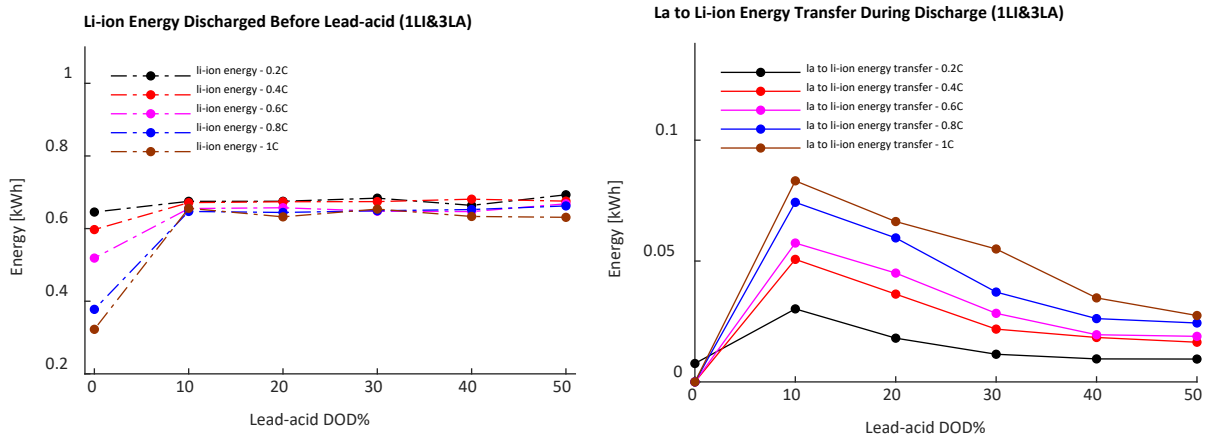

Figure 5-20. Energy transfer between the strings during discharge (right)

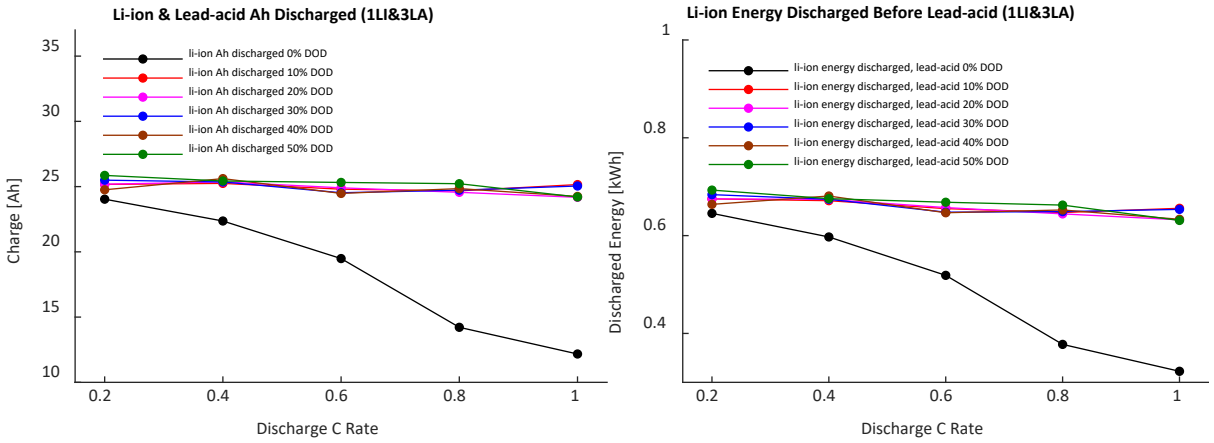

Figure 5-21. Li-ion energy & charge available during discharge before the Lead-acid string becomes fully active (energy & charge available between A-B and A-X points)

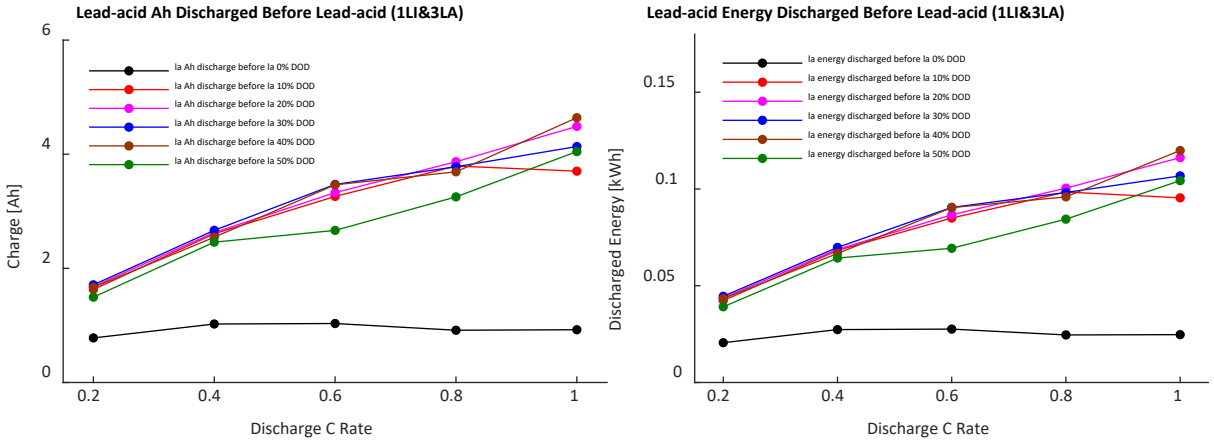

Figure 5-22. Lead-acid energy and charge discharged during A-B and A-X intervals.

5.3.3 Hybrid Systems – Comparison between hybrid systems configurations

Similar testing and analysis done for the 24V 1LA&1LI system, and detailed in the previous section, have been performed for each hybrid system configuration mentioned, 1LA&2LI, 2LA&1LI and 3LA&1LI. By modifying the number of Li-ion & lead-acid strings, the overall charge/discharge characteristics of the system change. This section presents the comparison between all 24V systems by analysing the Li-ion energy independently available, sections A-B (Figure 5-2) before lead-acid strings start to discharge, the lead-acid activity between A-X (Figure 5-2), the round-trip efficiencies and the transient energy transferred between the strings during the rest period.

The comparison presents the average values recorded for different parameters but the detailed data for each system is presented in the previous section.

Without detailing the exact energy discharged values for each hybrid system, Figure 5-23 shows the overall energy discharged by each hybrid system as a function of the lead-acid DoD. The first obvious similarity is that the energy discharged by the Li-ion is less dependent on the discharge

C rate when compared with lead-acid and this is the case across all hybrid configurations. This is not surprising as even when the overall internal resistance of the hybrid system is modified by increasing the number of strings, the fundamental charge/discharge characteristics of each chemistry do not change. The second general observation is that doubling the number of strings of one chemistry roughly doubles the energy available for a particular discharge rate. For example, for the 1LA&1LI case, 1C charge/discharge rate, 50% lead-acid DoD, the total lead-acid available energy is 0.79 kWh. For the same charge/discharge SoC interval and C range, the value doubles to 1.96 kWh for the 1LI&2LA system and reaches 2.95 kWh for the 1LI&3LA. Similar observations are valid when increasing the number of Li-ion strings. The differences between the systems appear when only the Li-ion strings are cycled.

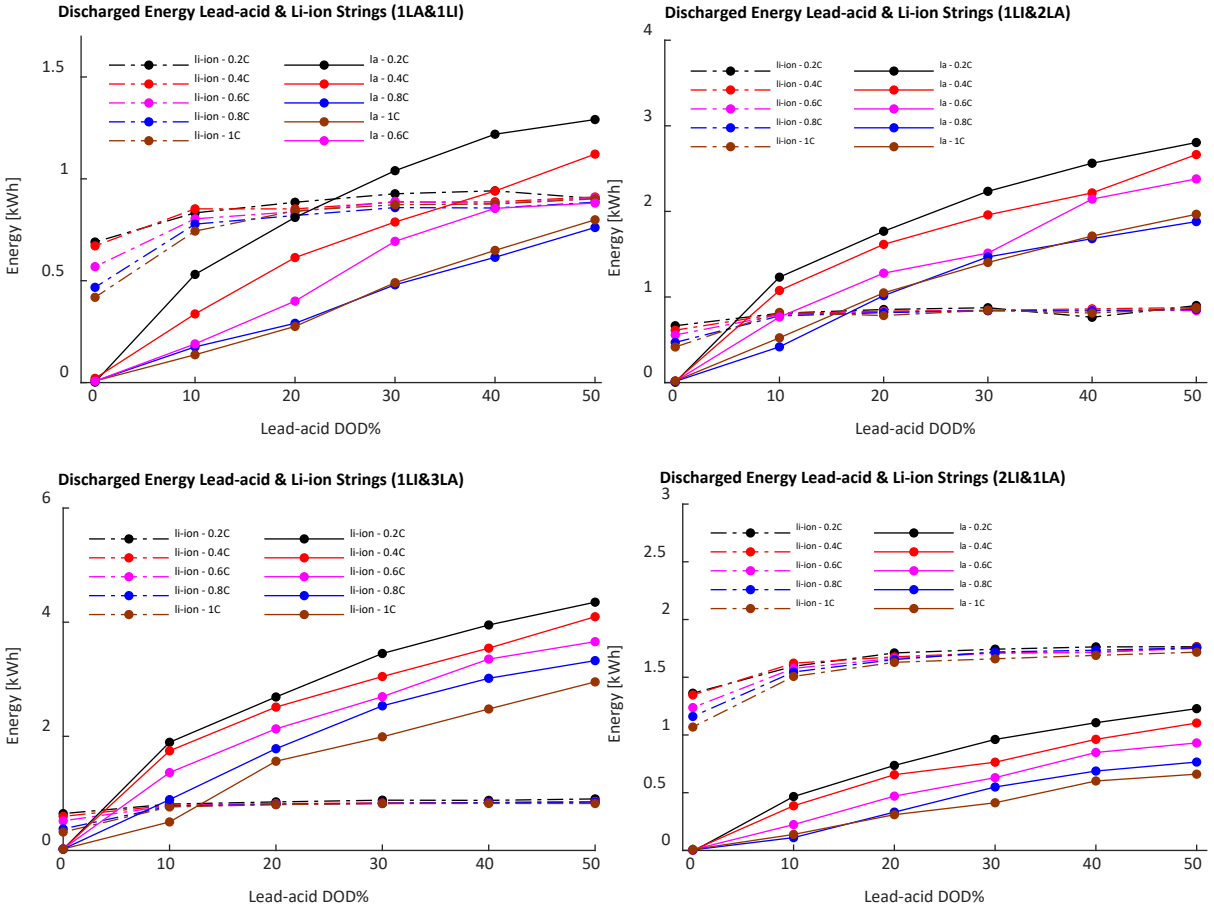

Figure 5-23. Li-ion and lead-acid discharged energy for different hybrid systems.

Figure 5-24 shows the comparison between the hybrid systems analysed from the average energy discharged perspective. The energy discharged by each chemistry for every hybrid system, in each cycling interval, is averaged across all 0.2-1C rates. This helps to illustrate three main properties of these arrangements:

First, increasing the number of lead-acid strings reduces, on average, the Li-ion energy available for independent cycling, A-B region - Figure 5-2 (or cycling range 1) across the tested 0.2-1C rates. Increasing the number of Li-ion strings, the opposite happens. Figure 5-24 (a) shows that in the A-

B region, where most of the Li-ion activity takes place, the lowest Li-ion energy available for independent cycling was recorded for the 1L1&3LA system. This is 58% (0.5 kWh) of the total available 0.85 kWh Li-ion energy which is available for cycling for the 1LI&3LA. On the opposite end, for the 2LI&1LA hybrid option, for each Li-ion string, the average Li-ion energy available for independent cycling is 70% (0.62 kWh) of the total available energy of 0.89 kWh. This shows an increase of 24% between the two extremes. From the practical perspective, this shows that by increasing the lead-acid number of strings, which implies reducing the overall lead-acid energy bank internal resistance, less Li-ion energy is available for independent cycling. The opposite happens when the Li-ion strings are increased or the lead-acid decreased, more Li-ion is available for independent cycling. On average, increasing a hybrid system by one Li-ion string or decreasing one lead-acid string will increase the Li-ion energy available within A-B limits (Figure 5-2) to 8%.

Secondly, it's worth noting that even the maximum Li-ion energy available in hybrid configurations is reduced by increasing the number of lead-acid strings. For example, for the 1LI&1LA, the total Li-ion energy available is 0.91 kWh, when the hybrid system is discharged to 50% DoD for the lead-acid battery bank. This is 7% above the total Li-ion energy, 0.85 kWh, available in the 1LI&3LA hybrid configuration. This accounts for a 3.5% decrease per lead-acid string added. This shows that increasing the number of lead-acid strings has a lower impact on the total Li-ion energy available in hybrid systems when compared with the Li-ion energy available for independent cycling.

Third, there is a linear relationship between the number of Li-ion strings and the total Li-ion available energy. This is not the case for the lead-acid delivered energy because of Peukert's law, doubling the lead-acid number of strings will more than double the total lead-acid energy available for cycling. The C rate of the hybrid system is dictated by the lowest C rate sum between the two chemistries. Increasing the lead-acid strings does not automatically mean increasing the maximum discharge current for the whole system, as this might be limited by the Li-ion bank. This means that when more lead-acid strings are added and the discharge current is kept constant, less current will flow through each string, thus increasing the total lead-acid energy available according to Peukert's law and indicated in Figure 5-24 (b).

The overall differences between hybrid systems presented above are related to the total Li-ion energy available and the energy available for independent cycling. However, the conclusions are only for the analysed number of strings, which captures the medium to small battery storage system.

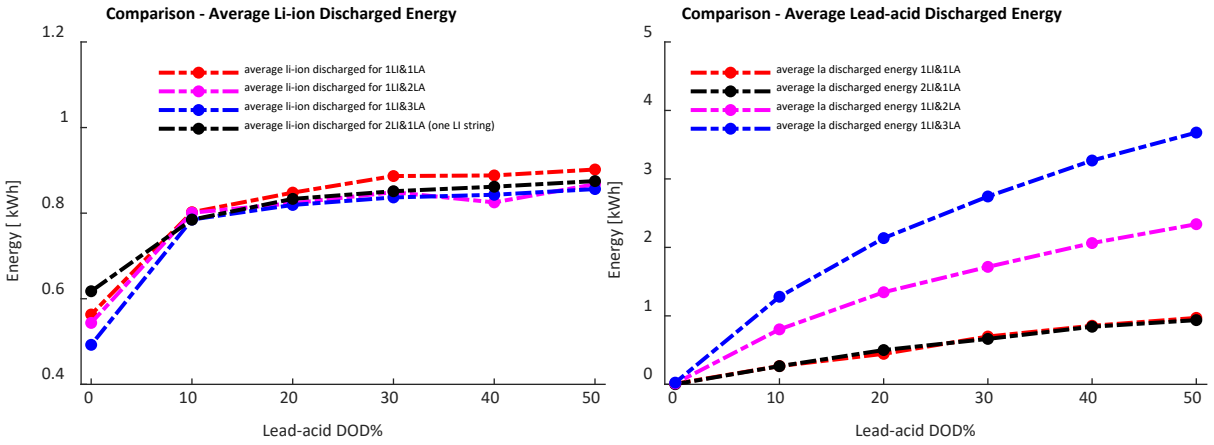

Figure 5-24. Li-ion (a) and lead-acid (b) discharged energy, averaged across 0.2-1C rates, for different hybrid systems.

Figure 5-25 details the discharge characteristics as a function of the discharge C rate for the A-B region. As mentioned in Figure 5-24, the average Li-ion energy to be cycled independently varies with the number of Li-ion and lead-acid strings in parallel. Here, I plotted the discharge characteristics for each hybrid system as a function of the C rate. As expected, as the charge/discharge C rate increases, less Li-ion energy is available between A-B interval. For example, at the extreme, at 1C rate, there is 24% more Li-ion energy available to be cycled independently for the 2LI&1LA when compared with the 1LI&3LA hybrid system. This shows that as the C rate increases, the larger the difference between the Li-ion energy available between A-B points, Figure 5-2.

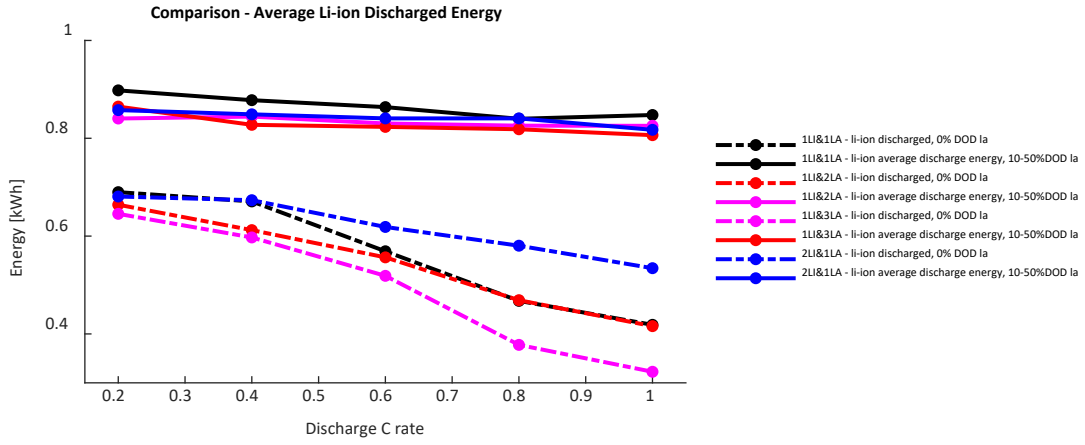

Figure 5-25. Li-ion discharged energy, as a function of the discharged C rates (0.2-1C rates), for different hybrid systems

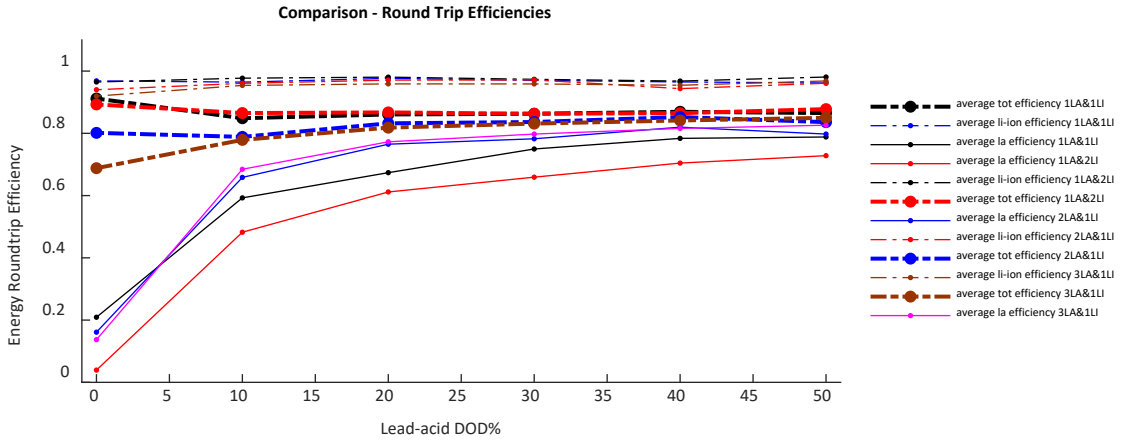

Figure 5-26. Energy Round-trip Efficiency for different hybrid systems for different DOD

Figure 5-26 shows the most important aspect of the hybrid system, the energy round-trip efficiency, calculated as the average across all 0.2-1C charge/discharge rates for the analysed options.

The first major observation is that the energy round-trip efficiency depends on the overall DoD interval of the hybrid system. If the system is cycled only in the A-B region, operating only the Li-ion strings, the energy round-trip efficiency should be close to the Li-ion round-trip efficiency. This is the case for the 1LI&1LA hybrid system when the measured average round-trip efficiency is 91% if only the Li-ion part is active. However, as we add more lead-acid strings, the activity of the lead-acid string in the A-B interval increases, which has a detrimental effect on the overall round-trip efficiency. Figure 5-27 (b) and Figure 5-28 indicate the lead-acid activity for the A-B region. The lowest recorded lead-acid average discharge energy values are for the 2LI&1LA & 1LI&1LA systems, 0.005 kWh and, on the opposite end, for the 1LI&3LA case, the value triples to 0.015 kWh. As mentioned above, this insignificant energy charged/discharged from the lead-acid strings during A-B region decreases the overall efficiency. The main reason for this is that the coulombic efficiency for the lead-acid cells in this region is low as indicated in the previous sections and the thesis Appendix.

In the A-B region, the average recorded values for the energy round-trip efficiency are 90-91% for the 2LI&1LA, 80% for the 1LI&2LA and 68% for the 1LI&3LA. This accounts for an efficiency drop of 10-11% for each lead-acid string added. This decrease is only visible if the Li-ion battery bank is cycled in the A-B cycling range. If the hybrid system discharges to lower SoC for the lead-acid strings, the average energy round-trip efficiency approaches 86-87%. This is expected, as more lead-acid energy is being discharged, the efficiency of the system should slowly approach the stand-alone lead-acid parameters. This insight into the working parameters of the hybrid system is important in sizing the battery system for various applications. Keeping the ratio between the internal resistances of Li-ion and lead-acid strings as low as it is practically feasible would help

in delivering a directly connected hybrid battery system as close as possible to fully active control of the battery strings.

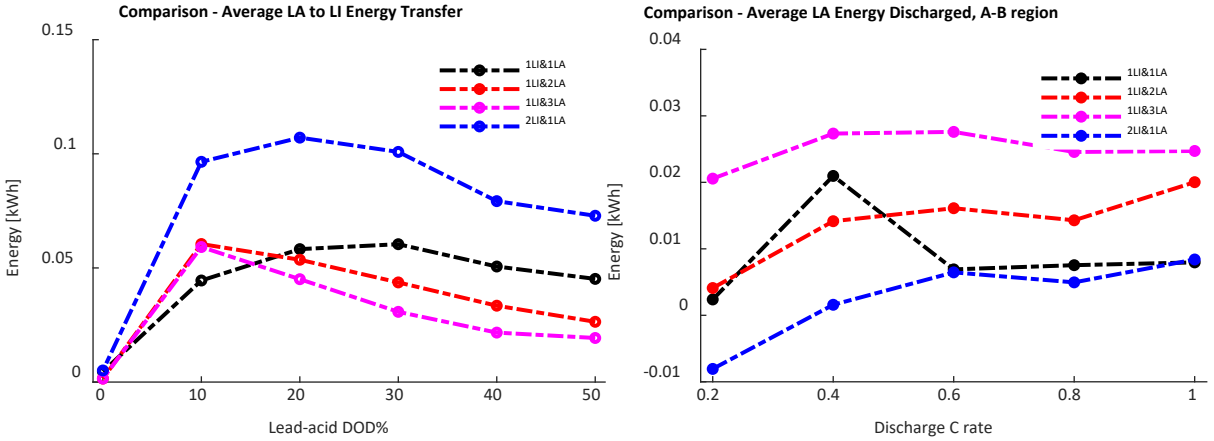

Figure 5-27. Average LA to LI energy transfer (a) and Average LA energy discharged (b)

The last comparison between the hybrid systems is regarding the energy transferred between the lead-acid strings to the Li-ion, during the rest periods. As detailed in the previous sections, for 1LI&1LA specific hybrid example, the energy transferred between the strings depends on the discharge current, the SoC of the lead-acid when the discharge process is stopped and the ratio between the two chemistries. For a clearer overall picture, Figure 5-27 (a), shows the average energy transferred during the transient period, across all C rates as a function of the lead-acid DoD, for all hybrid systems analysed.

The obvious observation is that as we increase the Li-ion string number, the energy transferred during the rest period increases. For the analysed cases, the largest values were recorded for the 2LI&LA hybrid system, Figure 5-27 (a). The energy transferred rises from zero when the lead-acid strings are kept at 100% SoC and only the Li-ion strings are cycled, to a peak of 0.1 kWh when the lead-acid strings are discharged to 80% SoC. If the lead-acid is discharged further the value falls to 0.07 kWh when the discharge is stopped at 50% SoC for the lead-acid strings.

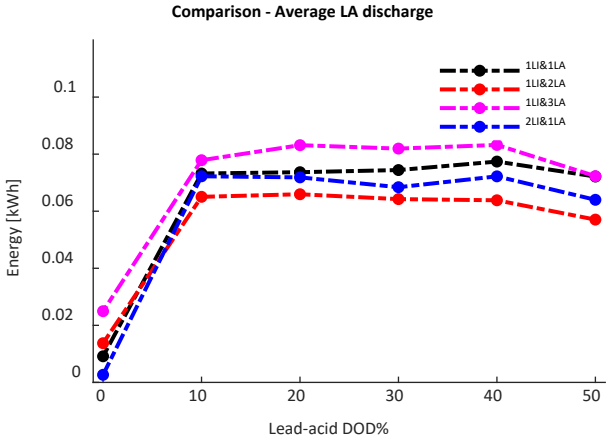

Figure 5-28. Average lead-acid energy discharged between A-X points.

If we increase the lead-acid number of strings, the peak of the energy transferred profile shifts to the left as indicated in Figure 5-27 (a). The measured peak value recorded for the 1LI&1LA, 1LI&2LA and 1LI&3LA is 0.06 kWh, the only difference is that the peak value is shifted to the left. The maximum transferred energy between the system strings accounts for 6-7% of the total Li-ion energy available for discharge. If we compare it with the total energy discharged the percentage of energy transferred drops to 1% for the 1LI&3LA (total energy discharged by the 1LI&3LA is 5.26 kWh).

It is worth mentioning that the energy transferred between the strings only happens when the total discharge current drops to zero. This is rarely the case in practice because, depending on the load profile, the battery storage systems are continuously charging/discharging. However, analysis of complete annual electrical load profiles for specific applications is needed to determine the true impact of the transient transfers during rest periods.

5.3.4 Hybrid Systems with Different Voltage Levels – 24V vs 48V

Similar testing and analysis detailed above were done for the 48V, 1LA&1LI hybrid system to understand how the hybrid behaviour changes when the system voltage is increased. For the 1LI&1LA – 48V system, parameters like the energy round-trip efficiency, coulombic efficiency, and total charge available remain the same as for the 24V system. The total energy available, the Li-ion energy discharged in the A-X region doubles as this varies linearly with the system voltage.

Figure 5-29 shows the lead-acid energy transfer between the strings for the 1LI&1LA – 48V system in comparison with the 1LI&1LA – 24V. The data indicated is for 1C rate and the rest period recorded is for when the discharge process was stopped at 100 to 50% lead-acid string SoC. The total energy transferred follows the same shape as for the 24V system but the peak energy value doubles. The charge transferred between the strings is identical in both systems as well as the peak transient currents during rest as indicated in Figure 5-29 (b). This shows that increasing the system voltage does not have an immediate impact on the hybrid system operation.

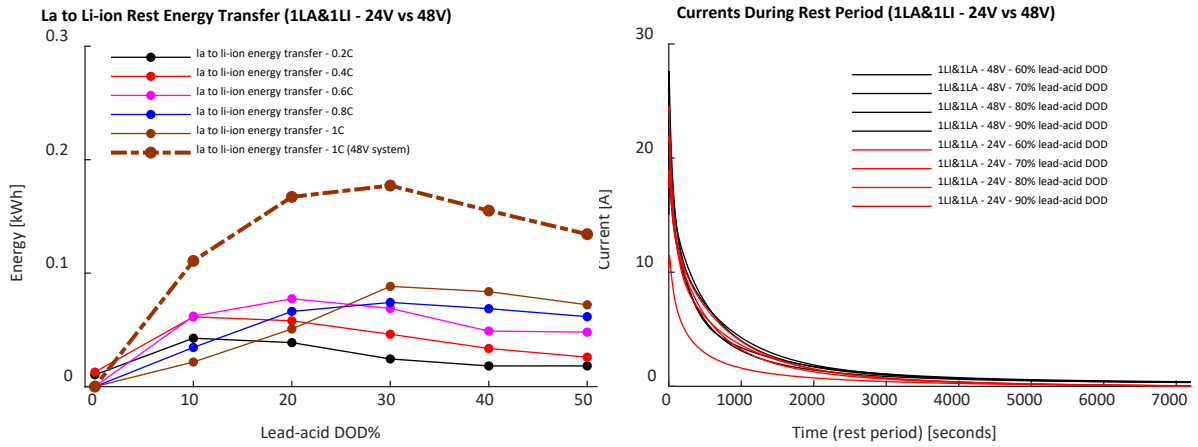

Figure 5-29. Energy Transfer During the Transient Period, 1LI&1LA, 24V vs 48V Hybrid Systems

5.3.5 Hybrid Systems – Intermittent Charging

This section presents the intermittent charging behaviour for the hybrid systems analysed above. Figure 5-2 (b) indicates the continuous charging process of any of the hybrid systems analysed, and Figure 5-30 (a) indicates the general intermittent charging. If the charging process is stopped before the storage system reaches 100% SoC for both strings, energy is transferred between the Li-ion strings to the lead-acid as indicated. This is the opposite of what happens during discharge in the rest period. As explained above for the discharge case, this happens because of the different dynamic behaviour of both chemistries, which is linked with the diffusion and electrochemical processes within the cells.

Generally, any energy and charge transfer between the strings is undesirable as this impacts the system's round-trip efficiency values and other possible degradation effects. The long-term effects have been investigated in Chapter 7, but this section aimed to measure the charge transfer between the strings during charging and calculate the high-level impact of this on the round-trip efficiency.

To illustrate the intermittent charging effects, in point C - Figure 5-30, the CC/CV charging process is stopped, and the system is left to rest for 8.2 hours between points C-D. During this time, the Li-ion strings charge the lead-acid cells with the final top-up charge required to reach 100% SoC. In point D, the lead-acid reaches full charge, and the battery charger turns on to add the final charge to the Li-ion between points D-E. Depending on the total charging current at the time of charging interruption in point C (C rate interruption), the full charging process can take up to 1.5-2 times the normal continuous CC/CV charging. The transfer between C-D is massively reduced if the charger continues to inject even a small current into the system. This is important because in practical applications, like solar energy systems, it is unlikely that the charging or discharging

current will be abruptly cut off which implies little to no energy transfer between the strings. This can be analysed in a separate study.

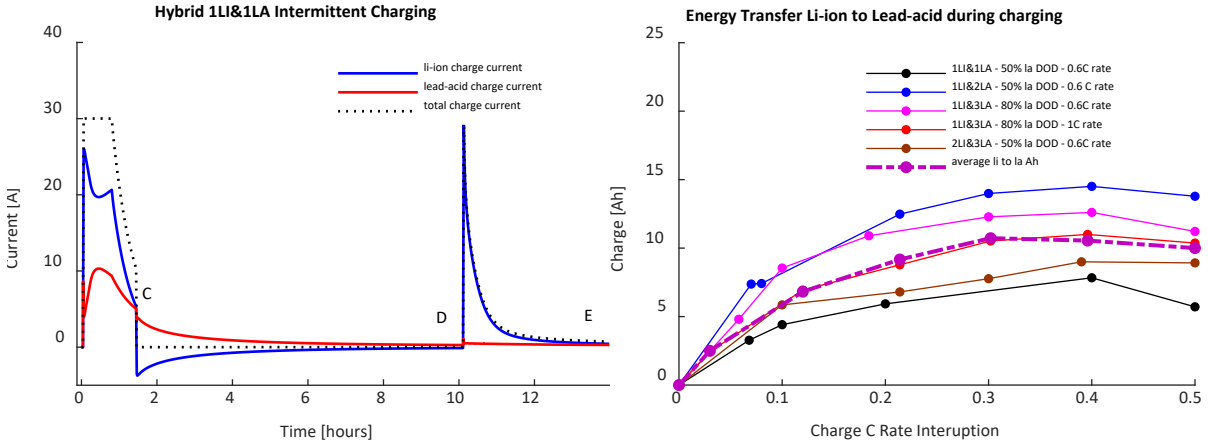

Figure 5-30. Intermittent Charging for hybrid systems (a), Ah transfer Li-ion to lead-acid strings (b).

The energy transferred between the strings has three main effects. The first is the slight efficiency loss because energy is moved from one string to the other. Depending on the current between C-D points - Figure 5-30, the eventual efficiency loss is a function of the Li-ion string round-trip efficiency. The second phenomenon is linked with the ohmic losses. Because the internal resistance of lead-acid is higher when compared with Li-ion, depending on the charging current, it can be beneficial to charge or discharge the Li-ion strings at a higher rate and in the rest periods, to slowly transfer the energy to lead-acid strings, thus minimising the thermal losses. The third effect is linked with the overall battery storage system efficiency which includes the inverter/charger operating efficiency. Figure 5-31 (a) indicates a typical efficiency curve for a battery storage inverter/charger as a function of its loading factor. The data indicated in Figure 5-31 is based on the SMA – Sunny Boy Storage inverter/charger. To fully charge a lead-acid cell, it takes anywhere between 10-15 hours and bringing the lead-acid cells to 100% SoC implies that a typical CC/CV charger will work for hours in the low-efficiency operating points of the curve, below 5-10% loading factor. If the CC/CV process is stopped as it enters the CV mode, or when the current falls below a certain threshold, the Li-ion cells will take the role of the CV charger and continue the process. This way, we avoid drawing power from the grid at an efficiency below 90%.

To analyse the above, the 1LI&1LA, 1LI&2LA, 1LI&3LA and 2LI&1LA have been charged intermittently by cutting off the CV charging phase when the current reached 0.5-0.1 C rate. Each time the hybrid systems were left to rest until the circulation currents were negligible C-D points - Figure 5-30. The charging process is restarted immediately afterwards - D-E points. The precise maximum charge & energy transferred between the strings are difficult to calculate as they depend on a multitude of factors like the CC charging current, the number of strings of the hybrid system, the CV current at the time of interruption, the rest time, and less obvious factors like the

hysteresis of the system. The purpose of this analysis is to find the indicative charge transfers as a function of the current interruption because, from a practical perspective, this is the most important factor in approximating the overall operation. Figure 5-30 (b) indicates typical values for the charge transfers as a function of the current interruption value. The maximum values recorded do not rise above 15Ah. The peak transfer occurs when the CV process is stopped between 0.3-0.5C rate.

A model was built to calculate the overall hybrid system efficiency using the inverter/charger data indicated in Figure 5-31 (a). For illustration, typical results for the 1LI&2LA system are indicated in Figure 5-31 (b). For this example, the charge/discharge was done at 0.6C rate and the charging current interruption was done at points 0.1-0.5C. The stand-alone battery energy round-trip efficiency measured varies very little with the charging current interruption. However, when the inverter/charger efficiency is considered, the overall efficiency drops below the initial values. As it can be seen, if the system is charged continuously, the overall round-trip efficiency decrease is around 4.5% when compared with the stand-alone values. Initially, the system efficiency rises when the system is intermittently charged with the interruption currents between 0.05-0.1C. After the initial efficiency increase, the overall efficiency drops by 6-7% when the charging current is interrupted at 0.5C. The results for the overall energy round-trip efficiency are not complete, as more testing is required at different DoDs. However, this shows that the energy transfers between the strings can help improve the overall storage system round-trip efficiency by controlling the charge current interruption.

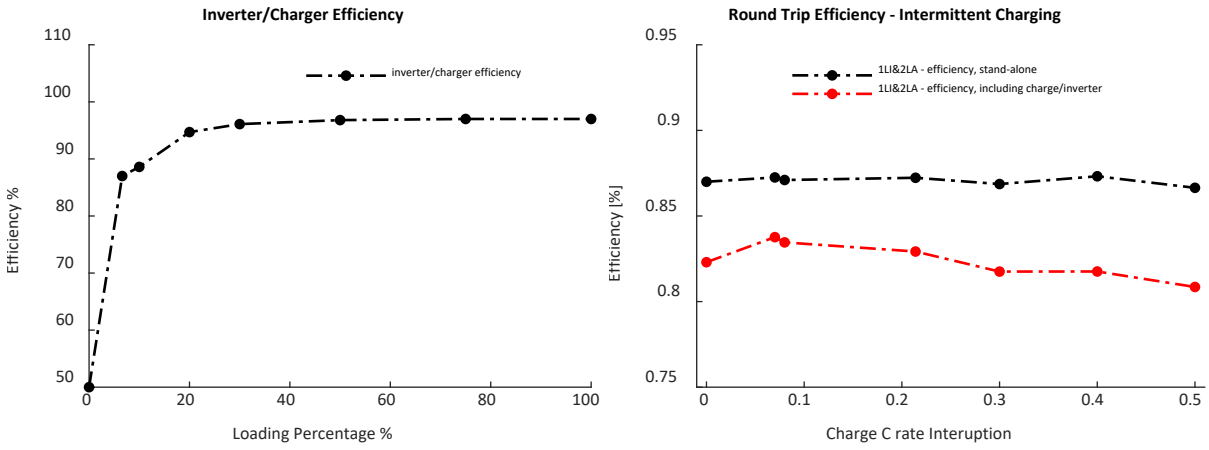

Figure 5-31. Inverter/Charger Efficiency (a) & Intermittent Charging Efficiency (b)

5.4 Conclusions

This chapter analyses the performance of five hybrid Li-ion and lead-acid battery energy storage systems to understand the directly connected hybrid behaviour and the benefits of such systems.

This was done by comparing various charging and discharging parameters across different hybrid systems with different numbers of strings and voltage levels.

The overarching conclusion is that directly connected Li-ion (NMC), and lead-acid (VRLA) battery storage systems are possible as the arrangement is stable, and the voltage profiles of the two chemistries allow for semi-active string control without power converters. This implies that part of the Li-ion energy capacity can be cycled independently of the lead-acid thus offering the advantage of limiting the additional cost generally associated with hybrid systems.

The first major conclusion of this study is that both, the total energy available from a hybrid system as well as the energy available independently for frequent cycling are mainly driven by the number of lead-acid strings and the charge/discharge C rates. The number of strings modifies the total energy available by changing the equivalent electrical resistance and the subsequent dynamics of each battery string. The Li-ion energy available for independent cycling can reach around 75-80% of the total Li-ion capacity available when coupled in hybrid configurations, but this happens for C rates below 0.2C. On average, across 0.2-1C rates, each extra lead-acid string reduces the independent Li-ion capacity by around 8%. The total Li-ion energy available per string does not change on average with the number of strings, if the system is discharged below 10% DoD for the lead-acid, the Li-ion energy available is practically the same across all different configurations analysed. However, the total energy available from the hybrid system depends on the lead-acid capacity, more strings imply less current per string for the same discharge current, and this means more energy available for cycling.

The second set of conclusions is related to the round-trip efficiency of the entire system. Again, the number of lead-acid strings relative to the Li-ion ones plays a crucial role. If we increase the number of Li-ion strings, the round-trip efficiency of the hybrid system, when only the Li-ion is cycled, is close to the standalone Li-ion efficiency values of 90-91% for the analysed cells. However, as the number of lead-acid strings is increased, the round-trip efficiency of the system drops by 10-11% per lead-acid string added. The measured round-trip efficiency value for the 1LI&3LA system, when only the Li-ion is cycled, drops to 68%. This happens because the lead-acid activity increases in the A-X region (Figure 5-2), with each added string. If the system is discharged below 10% DoD for the lead-acid string, the system comes close to the overall 86-87%, which is relatively the same across the analysed system.

The third observation is that the charge and energy transfers between the strings are mainly driven by the number of Li-ion strings. The measured peak energy transferred between the strings is less than 7% of the total Li-ion energy independently available and less than 1-2.5% of the total energy available. Also, increasing the number of lead-acid stings, or the voltage of the whole system, does not modify peak transient currents and the peak energy transferred between the strings.

Finally, this analysis briefly discusses intermittent charging and its effects on the overall performance of the system. The analysis indicates that energy & charge can be transferred between the strings during charging. This changes the round-trip efficiency of the complete (inverter & battery cells) hybrid storage system.

Chapter 6 Hybrid System Modelling

The work undertaken in this chapter aims to answer the second question addressed at the beginning of this thesis:

Can the instantaneous hybrid Li-ion and lead-acid behaviour be modelled using equivalent circuits?

To answer the question, this chapter presents the modelling of such a system intending to understand the high-level hybrid system behaviour. The hybrid modelling uses equivalent circuit theory for both chemistries. The system parameters have been extracted using experimental data, collected and optimised using MATLAB/Simulink tools as indicated in the methodology chapter.

The modelling results are compared with the experimental data presented in Chapter 5 and the conclusions indicate that reasonable modelling accuracy can be achieved using simple equivalent circuit modelling (ECM). The model approximates the dynamic effects between the strings with an accuracy of 90%, except when the lead-acid strings are discharged to 10-30% DoD. Also, the overall efficiency, total energy discharged, and the Li-ion energy available for independent cycling can be predicted with above 90% accuracy.

The model fails to predict the energy round-trip efficiency for a multi-string system when the lead-acid dominates. The chapter looks at different hybrid systems, with different voltage levels and number of strings, to approximate the dynamic effects and the system round-trip efficiency.

The modelling results show that, for the tested batteries, increasing the lead-acid strings reduces the peak energy transferred during the transient period by 29% (on average with each string added). The efficiency of the system depends on the energy capacity ratio between the lead-acid and Li-ion strings, and it varies between 85%-95%.

6.1 Research Objectives

To arrive at a satisfactory answer to the question stated above, the following research objectives have been set for this chapter:

- Using the MATLAB tool developed in the methodology chapter, model a directly coupled lead-acid and Li-ion system using simple equivalent circuits.
- Calculate the circulation currents, energy round-trip efficiency and energy transferred between the strings and compare the results with the experimental data presented in Chapter 5.

- Using the MATLAB model, investigate the effects of increasing the number of strings and cells, on the overall hybrid behaviour.

6.2 Battery Modelling – Parameters Results

The equivalent theory, the parameter extraction and the methodology steps are described in Chapter 4.

6.2.1 Results - Constant Current Charge/Discharge Tests

The constant current test results, determined experimentally as detailed in the methodology chapter, are indicated in Figure 6-1 and Figure 6-2.

- Figure 6-1 (a), shows the open circuit voltage for the lead-acid and Li-ion cells as a function of the SoC.
- Figure 6-1 (b) and (c) indicate the Ah capacity for both lead-acid and Li-ion cells at different discharge rates. The lead-acid Ah available drops with the discharge current and because of this, all the tests have been done at below 0.5C, assuming that in practice the lead-acid strings will not be discharged at 1C rates. The maximum lead-acid capacity recorded was above 80% (of the datasheet parameters) at 0.1C, indicating that the lead-acid batteries were in the first half of their lifetime. As indicated, the Li-ion Ah capacity is practically constant with the discharge C-rate.
- Figure 6-2 indicates the coulombic efficiencies (CE) at different C-rates for both chemistry types. For a full discharge, the average CE for the lead-acid cells stands at 0.94 and 0.99 for the Li-ion.

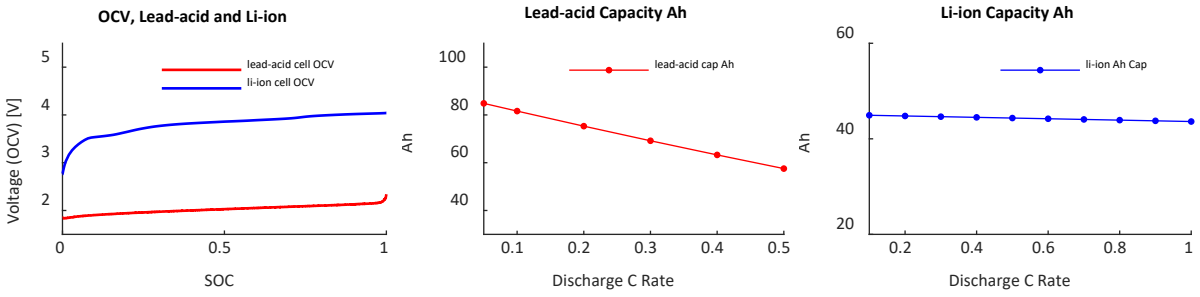

Figure 6-1. OCV (a), Ah Capacities for the lead-acid (b) and Li-ion (c) cell/battery

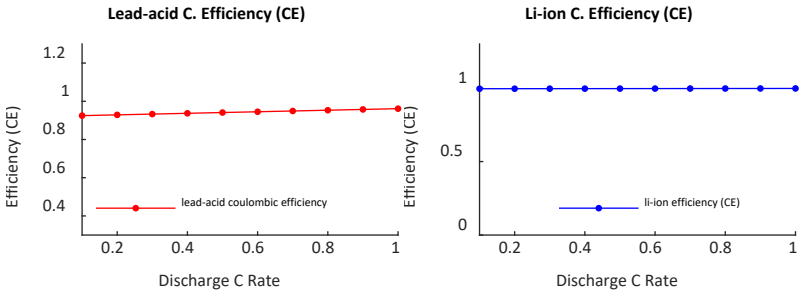

Figure 6-2. OCV, Ah Capacities, CE for the lead-acid and Li-ion cell/battery

6.2.2 Results - Pulse Discharge, Li-ion

The parameter datasets presented in the Appendix don't show meaningful differences between each test type, at least for the battery storage modelling type attempted in this chapter. To capture the results of all tests, the data was averaged for each RC component at every SoC point. The average Li-ion results are indicated in Figure 6-3. The total Li-ion cell internal resistance increases dramatically between 90-100% DoD. The capacitor behaviour, however, follows more irregular variation with the SoC.

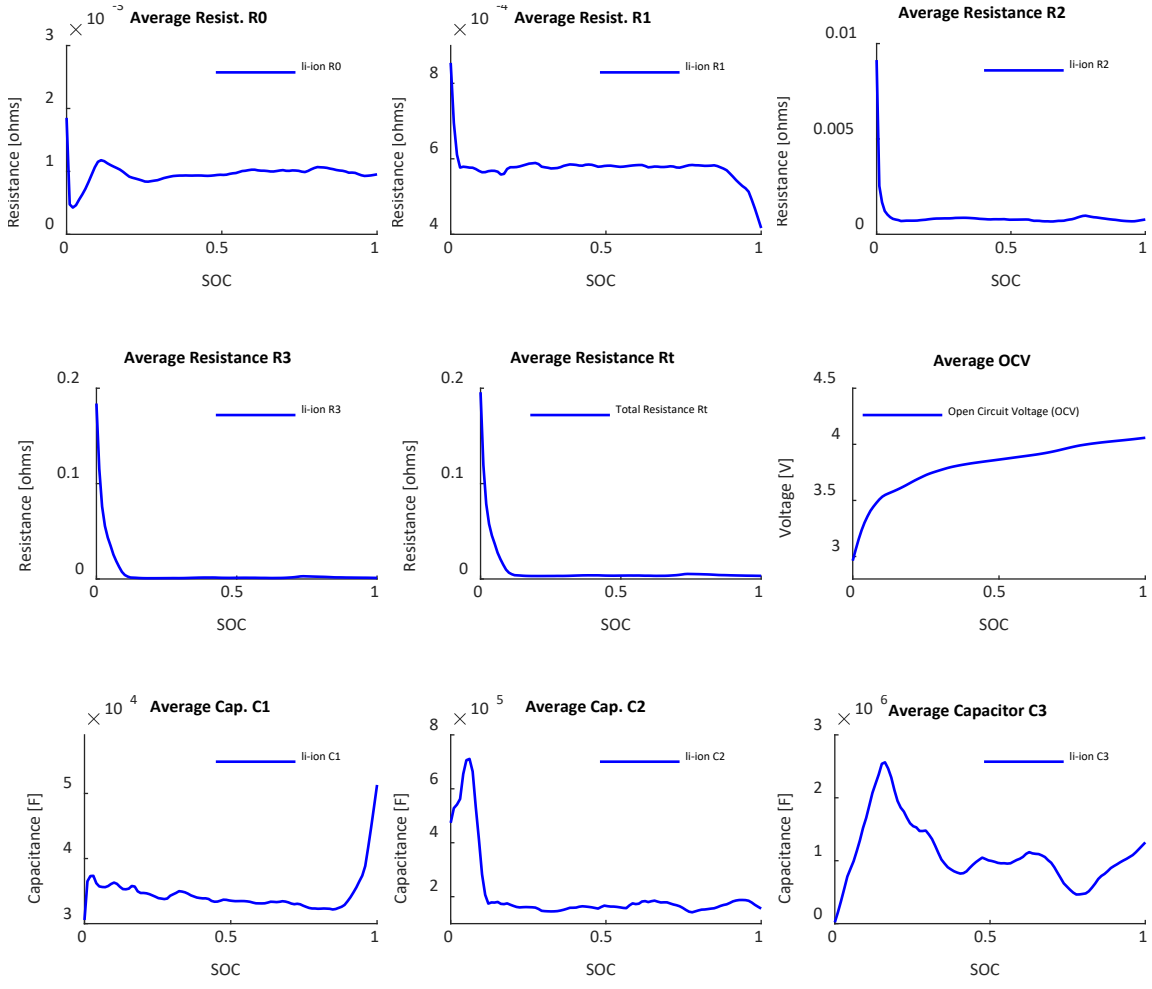

Figure 6-3. Li-ion equivalent circuit parameters.

6.2.3 Results - Pulse Discharge Lead-acid

As for the Li-ion case, Figure 6-4 indicates the average lead-acid parameters across all tests conducted, at each SoC point. The total internal resistance of one 12V battery increases from below 20 milliohms to around 80 milliohms between 10 - 0% SoC. Like the Li-ion cells case, the dynamic components vary more irregularly with the SoC.

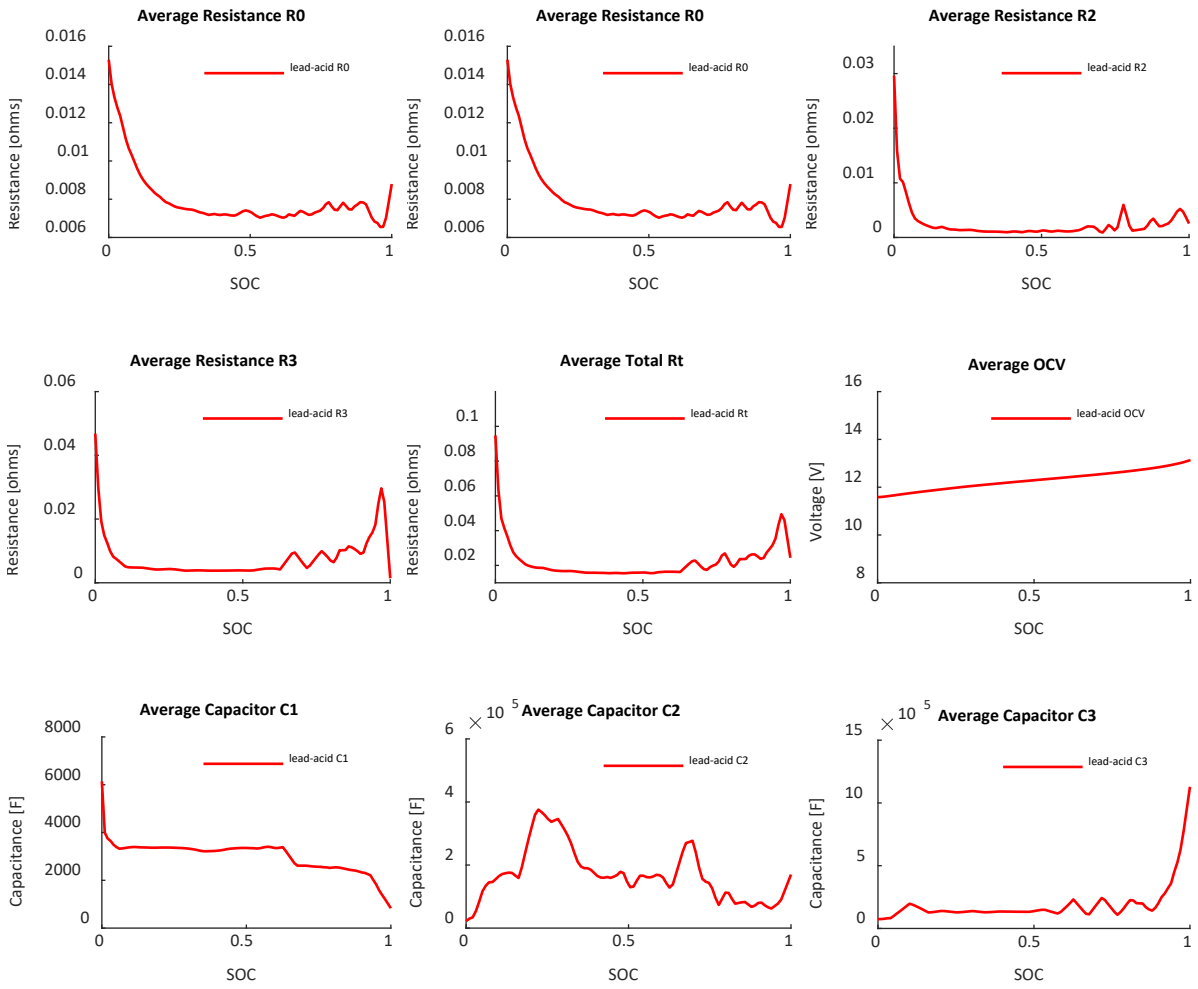

Figure 6-4. Lead-acid equivalent circuit parameters

6.3 Hybrid Systems - Modelling Results

The overarching objective discussed in this chapter is to model the directly coupled hybrid lead-acid and Li-ion. The results presented in the section capture the hybrid behaviour for different system configurations. Also, during the study, several hybrid systems have been tested using the system described in Section 6.1. The modelling results will be compared with the experimental data presented in Chapter 5.

To exemplify the typical hybrid discharge behaviour, Figure 6-5 shows the modelling results of a 48V hybrid system, 1LI&1LA (one string of Li-ion and one string of lead-acid) discharged at a 0.6C

rate. As for the experimental data results, the following sections can be identified on a typical discharge curve:

- **A-B region.** In this section of the discharge process, only the Li-ion batteries are active and provide most of the total charge/discharge current. From the practical perspective, in this region, part of the total Li-ion energy capacity can be cycled independently of lead-acid cells. This is of crucial importance as it provides a measure of string control over the hybrid system. In normal operation, this region will be used for frequent cycling and the lead-acid will only cover the peaks of the energy storage profile.
- **B-X region**. In this section, the Li-ion current/power starts to decrease and the lead-acid increases. In point X, both chemistries provide the same power to the discharge load.
- **X-C section.** Between points X and C, most of the discharge load is supplied by the lead-acid strings and the Li-ion current slowly decreases.
- **C-D region.** In this section, from the practical perspective, only the lead-acid is active and provides most of the discharge current.

In point D, the discharge process is interrupted, and the system relaxes until the circulation currents between the strings are negligible. Because Li-ion and lead-acid cells have different internal electrochemical processes, the relaxation voltages are different, and this creates circulation currents between the strings as indicated. Depending on the discharge current and when the discharge process is interrupted, the transient behaviour and the subsequent energy transferred between the two chemistries vary with the SoC.

Figure 6-5 (b) shows the modelled Li-ion currents when the discharge is interrupted at different lead-acid SoC. Points F to K correspond to 100%-50% lead-acid SoC. Point F is the same as point B and corresponds to when the lead-acid cells just begin to slowly discharge. If the system is cycled between A-B (or left of point F), the circulation currents are insignificant – although in practice, the Li-ion string charges the lead-acid for a very short period.

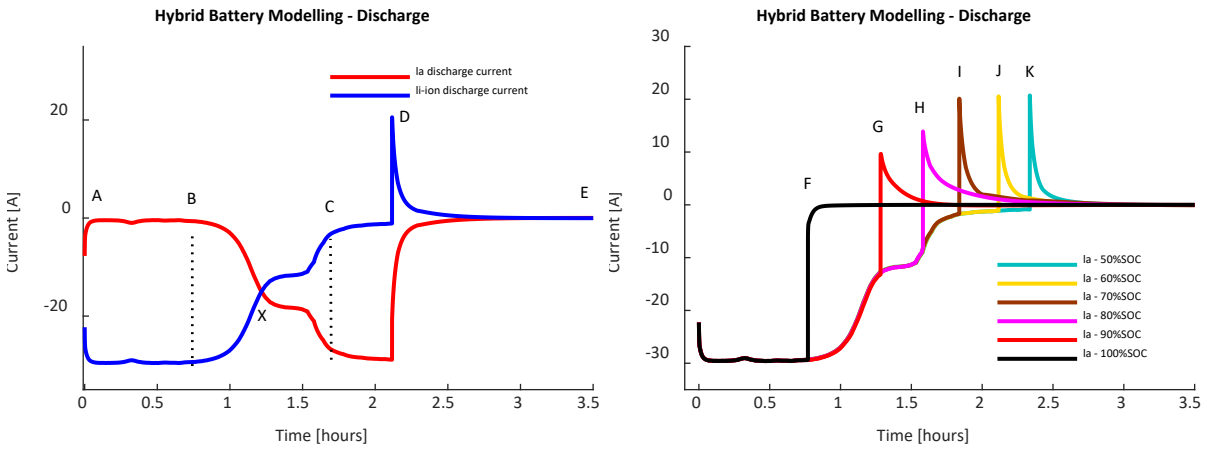

Figure 6-5. Hybrid Battery Modelling – Typical Discharge (a), Discharged interrupted at different lead-acid SoC points (b)

6.4 Experimental vs Modelled Data Comparison

This section presents the comparison between the modelling results and the experimental data for the hybrid battery model. This is done by analysing the simulation and experimental data of a 24V-1LI&1LA hybrid battery system cycled between 0.2- 1C rate. Similar results have been obtained for the other tested and modelled systems. The experiments and the simulations consist of cycling the hybrid storage system between 100% SoC, both Li-on and lead-acid at 100% SoC, and the F-K points (Figure 6-5) corresponding to 0-50% DoD for the lead-acid strings.

The following four parameters are compared with the experimental data, as these are the most important in system sizing for various applications:

- The Li-ion to lead-acid energy transferred during the rest period, points D-E Figure 6-5 (a).
- Total round-trip efficiency of the system as a function of the system DoD.
- Total discharged energy as a function of the system DoD.
- Li-ion energy available for cycling independently of the lead-acid strings, between A-B and A-X regions, Figure 6-5 (a).

The first parameter analysed is the energy transferred between the Li-ion and the lead-acid strings during the rest period, points D-E - Figure 6-5. Figure 6-6 (a), shows the experimental data for the energy transfer for a 24V - 1LI&1LA system at 0.2-1 C rates for each F to K point. The energy transferred follows a skewed bell curve. As indicated, the energy transferred is almost insignificant if the lead-acid strings are kept at 100% SoC, it rises to a peak between 10-30% lead-acid DoD and slowly drops when the system is discharged to 50% lead-acid SoC. The measured

peak is around 0.1 kWh which occurs at 30% lead-acid DoD, at 1C rate. The modelling results of the same system are indicated in Figure 6-6 (b). As indicated, the simulation results follow the same general pattern as the experimental results, but the match between the experimental and predicted data is not perfect.

To compare the results, Figure 6-7 (a), shows energy transferred between the strings averaged across all 0.2-1C rates for both measured and modelled results. The average modelled data matches the experimental information on almost all intervals, between 0-10% DoD and 40-50% DoD of the lead-acid strings. The simulation overestimates the energy transferred if the system is discharged to 20-30% DoD lead-acid. Figure 6-7 and Figure 6-6 (b) indicates the percentage error between the measurements and the simulation results. Although the largest error overestimates the transferred by 65%, the model is satisfactory for general hybrid storage systems sizing and gives indicative information about the transient currents during the rest period. Outside the 20-30% DoD interval, the model is 90% accurate in calculating the average energy transferred between the strings.

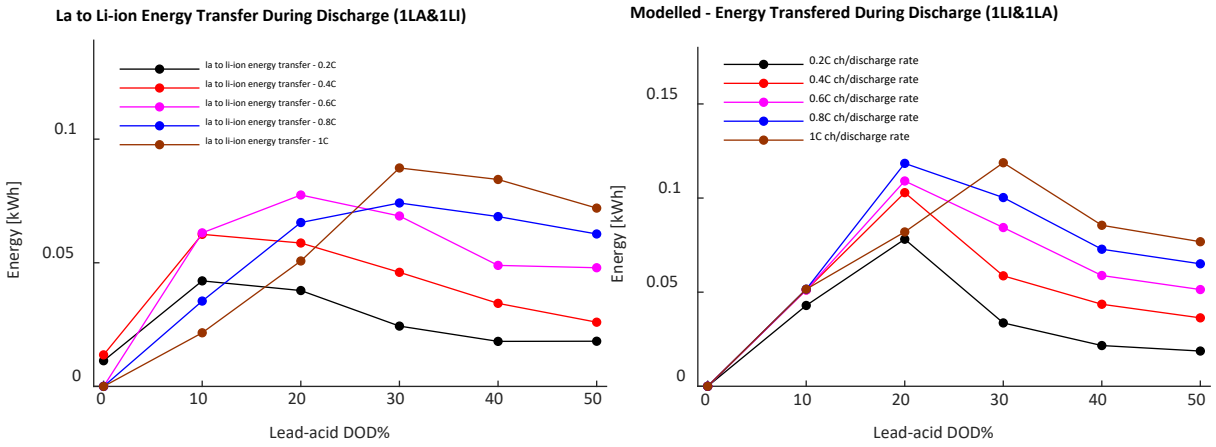

Figure 6-6. La to Li-ion Energy Transfer During Discharge – Experimental (a) vs Modelled (b)

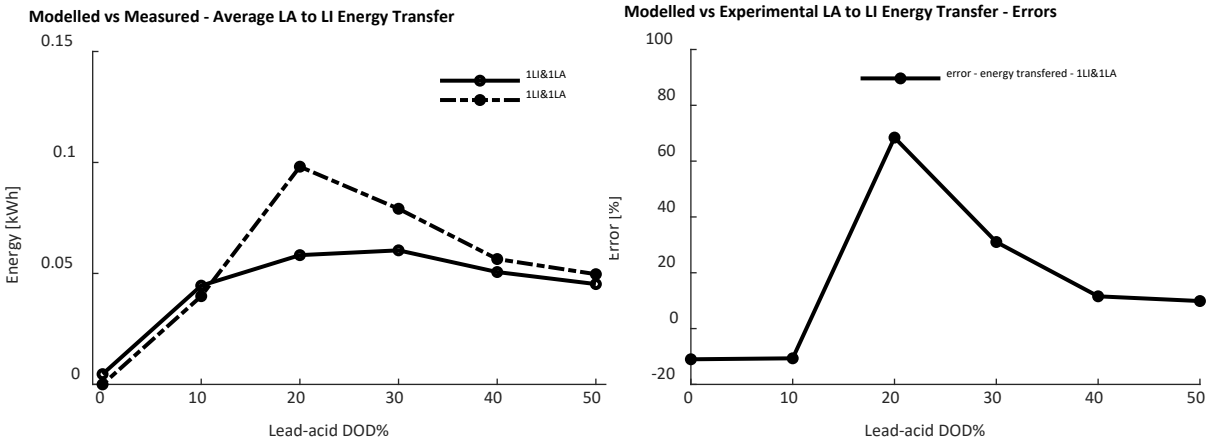

Figure 6-7. Average Lead-acid to Li-ion Energy Transfer (a), Errors between measured and simulation results (b)

The second parameter compared with the experimental data is the energy round-trip efficiency of the hybrid storage system. Like in the previous case, a 24V–1LI&1LA system was cycled both experimentally and using the MATLAB model between 100% SoC of the hybrid systems and points F-K, Figure 6-5. Figure 6-8 (a) shows the experimental data vs the simulation results for the energy round-trip efficiency of the system. The model slightly overestimates the efficiency if the lead-acid is not discharged below 90% SoC. Figure 6-8 (b) shows the percentage errors between the experimental and modelled results, the error values are within 9%. The largest errors were recorded when the system was cycled between 100% system SoC and 10% lead-acid DoD.

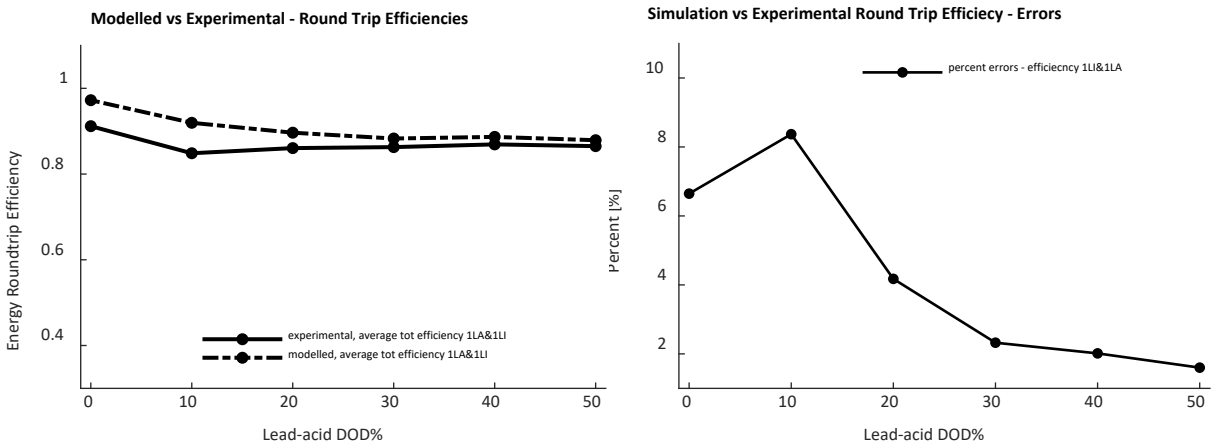

Figure 6-8. Modelled vs Experimental Average Round-trip efficiency (a), Round-trip efficiency percentage error (b)

The third set of comparisons is between the measured total charged/discharged energy and the simulation results. Figure 6-9 (a), shows the total Li-ion and lead-acid discharged energy, averaged across 0.2-1C charge/discharge rate, between 100% SoC and 0-50% lead-acid DoD. Figure 6-9 (b), shows the percentage errors between the experimental and modelled results. The recorded errors are within 10%.

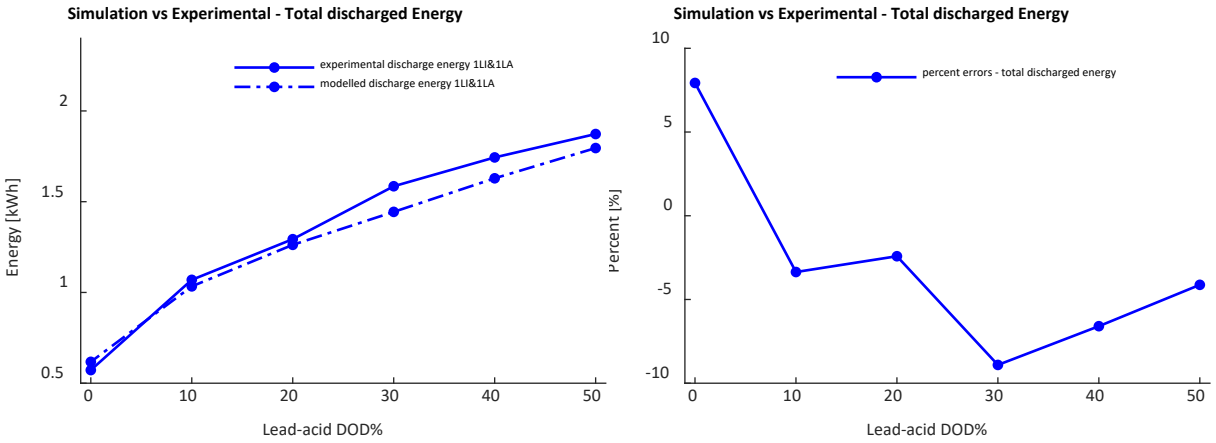

Figure 6-9. Total average measured & modelled discharged energy (a), Percentage errors total average discharge energy (b).

The last parameter to be compared between the experimental tests and the simulation results is the Li-ion energy discharged between A-B and A-X points. This is important in sizing hybrid storage systems as it captures the total energy available for independent cycling. Figure 6-10 (a), shows the measured and the simulation results. Like in the previous cases, both experimental and simulation cycling were done between 100% SoC and 0-50% DoD for the lead-acid string for 0.2-1C rates. The simulation results overestimate the experimental data by around 10-11%. This is because the X point, Figure 6-5 (a), it is very difficult to predict using simple equivalent circuit modelling. When the hybrid system changes from the Li-ion discharge to the lead-acid, A-B points Figure 6-5, the lead-acid works at high SoC and within a very narrow voltage range, the Li-ion can vary between 60% SoC and 20% while the lead-acid only varies a few SoC percentages. This discrepancy in SoC ranges is difficult to model, simply because of the different measurement resolutions required for each chemistry. Hundreds of measurements would be required to determine the system parameters within the 0.1V lead-acid range, from 2.25V/cell to 2.1V/cell which, if possible, would require specialised equipment. Also, the lead-acid chemical reactions between the float voltage, 2.25V/cell, and the charge rest voltage, 2.13V/cell, are too complicated to be accurately modelled using simple electrical components and more complex electrochemical battery models are required for both chemistries.

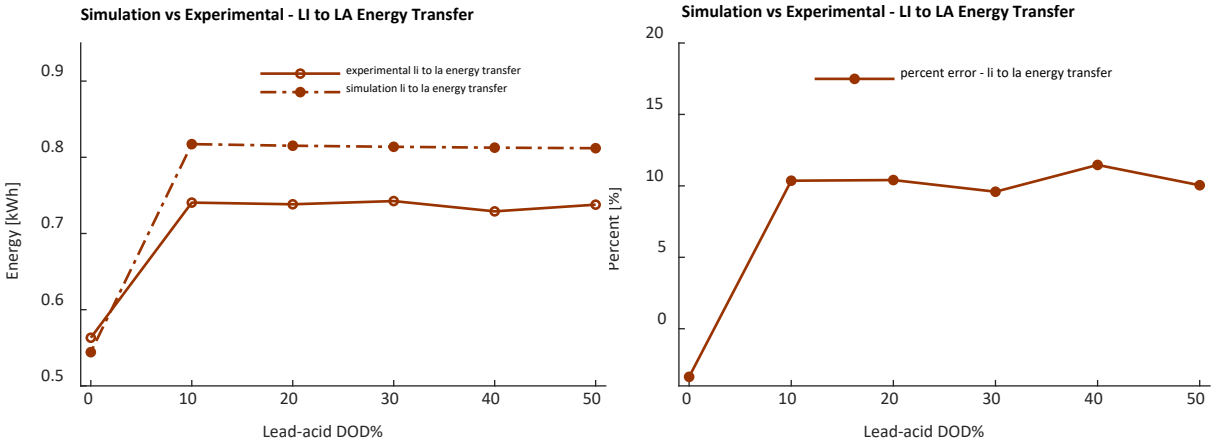

Figure 6-10. Average Li-ion energy discharged before Lead-acid (a), Percentage errors between the modelled & experimental results (b).

The hybrid model presented in this section can only be used to size hybrid Li-ion and lead-acid storage systems in terms of calculating the Li-ion energy available for independent cycling (as a function of the number of cells connected in series or the number of strings connected in parallel), circulation currents calculation, and energy transferred between the strings. This is the case as it can only predict the high-level parameters required for high-power storage systems. However, it needs to be used carefully if detailed electrochemical results are required. More complex physical models of both cell types are recommended if the system is to be used in electrochemical cell design to optimise the hybrid system operation.

6.5 Hybrid Systems – High Voltage Systems

Having established the accuracy of the model, this section explores the general behaviour of the hybrid system when the number of lead-acid and Li-ion strings and cells is increased. The main purpose of this is to understand the sizing principle for large hybrid storage systems. To achieve this, the following 9 hybrid systems have been modelled:

- 1LI&1LA (1 Li-ion and 1 lead-acid string) hybrid system at 48, 240 and 480V.
- 2LI &1LA (2 Li-ion and 1 lead-acid string) hybrid system at 480V.
- 3LI&1LA (3 Li-ion and 1 lead-acid string) hybrid system at 480V.
- 1LI&2LA (1 Li-ion and 2 lead-acid strings) hybrid system at 480V.
- 1LI&3LA (1 Li-ion and 3 lead-acid strings) hybrid system at 480V.

For the 480V hybrid systems, each lead-acid string consists of 40 SWL3300 batteries connected in series, and each Li-ion string has 140 LEV50 Li-ion cells linked in series. Both chemistry strings are connected directly in parallel and cycled between maximum 4.05V/Li-ion cell, 14.1V/lead-acid battery (or 2.35V per lead-acid cell) and minimum 3.5V/li-on cell, 12.24V/lead-acid battery (or 2.045V per lead-acid cell). The cycling ranges are the same as those indicated in Figure 6-5, between 100% SoC for both strings and disconnection points F-K, corresponding to 100%-50% SoC for the lead-acid strings. The first point of interest is the modelled dynamic behaviour between the cell strings. Figure 6-11 shows the charge and energy transfers between the lead-acid and Li-ion strings during the discharge rest period (points D-E Figure 6-5), for the 48V, 240V and 480V hybrid systems. For simplicity, the modelling was done at a 0.6C rate, but similar scaled variations can be observed for higher or lower charge/discharge rates. The charge transfer between the strings and the peak transient current is the same across all three systems, Figure 6-11 (b). The simulation results show that increasing the system voltage does not have an immediate, practical effect on the transient current behaviour. The maximum charge transfer expected depends on the discharge current and, for the 0.6C rate, this stands at a peak value of 2.4 – 2.5Ah. This happens when the systems are discharged to around 20% DoD for the lead-acid strings. For higher C rates, the peak of the curve shifts to the right. As expected, the energy transferred is not identical across all systems, it increases linearly with the system voltage. For the 0.6 C rate modelled, the energy transferred reaches 0.11 kWh, 0.56 kWh and 1.1 kWh for the 1LI&1LA, 48V, 240V and 480V.

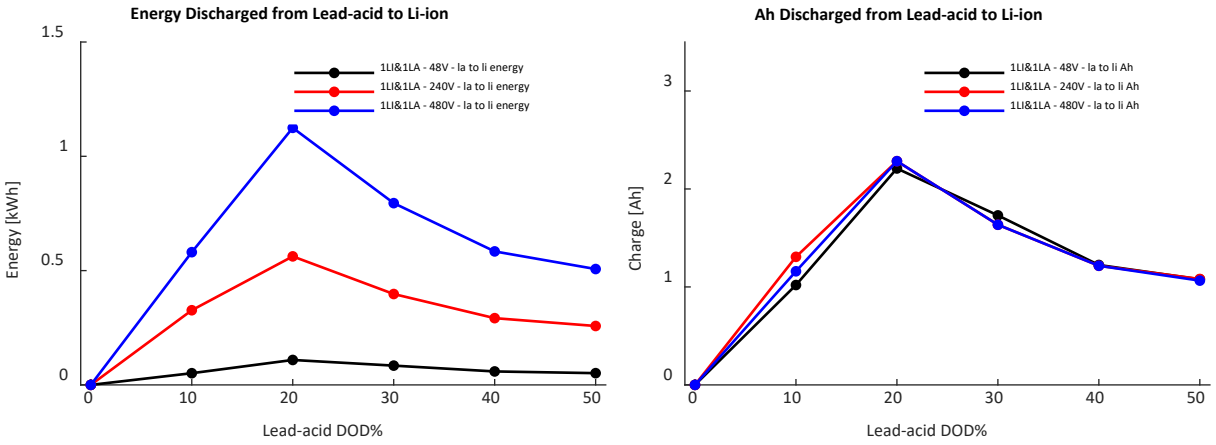

Figure 6-11. Energy (a) & Charge (b) transferred between the one lead-acid & one Li-ion string during the discharge rest period.

The second point of interest is the energy transferred and its variation with the number of Li-ion and lead-acid strings connected in parallel. Figure 6-12 shows the energy transferred for five 480V hybrid systems when they are charged/discharged at 0.6C rate, as a function of the lead-acid DoD. Across all systems, the maximum energy transferred occurs when the discharged systems are stopped between 20-30% DoD for the lead-acid strings. The charge transferred follows the same pattern as indicated in Figure 6-12 (b). The lowest energy transferred occurs for the 1LI&3LA system with a peak of 0.84 kWh. For the 3LI&1LA case, this rises to 1.85 kWh. The conclusion is that increasing the number of Li-ion strings in a hybrid system or decreasing the number of lead-acid strings, increases the circulation currents and the maximum energy transfer. For the 0.6C rate, this adds on average, around a 29% increase per Li-ion string added or lead-acid removed.

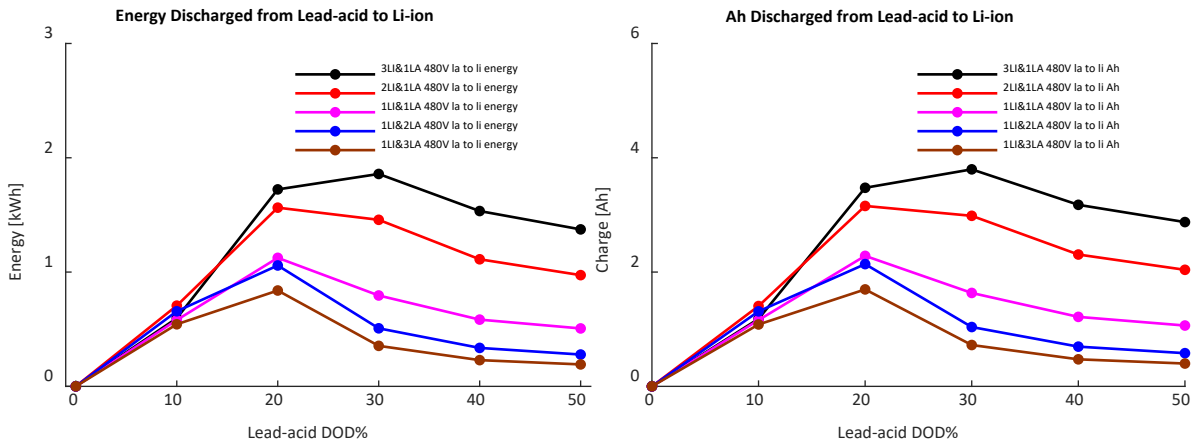

Figure 6-12. Energy (a) & Charge (b) transferred between multiple lead-acid & Li-ion strings during the discharge rest period.

The third point of interest is the hybrid energy round-trip efficiency variation with the number of Li-ion and lead-acid strings connected in parallel. Figure 6-13 shows the energy efficiency of the systems analysed as a function of the lead-acid DoD. The obvious observation is that as more Li-

ion strings are added to the system, the efficiency approaches the standalone Li-ion values. Similarly, when the lead-acid dominates the efficiency of the system approaches the lead-acid values. Also, the efficiency values vary with the system DoD. For the analysed cases presented in Figure 6-13, at the 0.6C charge/discharge rate and if the system is discharged below 10% DoD for the lead-acid string, the average modelled efficiency values are 87%, 87%, 90%, 92% and 94.5% for the 1LA&3LA, 1LI&2LA, 1LI&1LA, 2LI&1LA and 3LI&1LA. This is largely in accordance with the experimental data and within the error margins indicated in Figure 6-8. However, the system fails to predict the efficiency when only the Li-ion strings are cycled and the lead-acid strings are kept at 100% SoC (region A-B, Figure 6-5 (a)). The experimental data indicates that the efficiency drops by around 10% per lead-acid string added and the modelled only by around 2.5%. This discrepancy is attributed to the difficulty in modelling the complicated lead-acid chemistry at very high SoC. More complex models are required to predict this and to accurately predict the hybrid behaviour at the transition between Li-ion and lead-acid, B-C points - Figure 6-5.

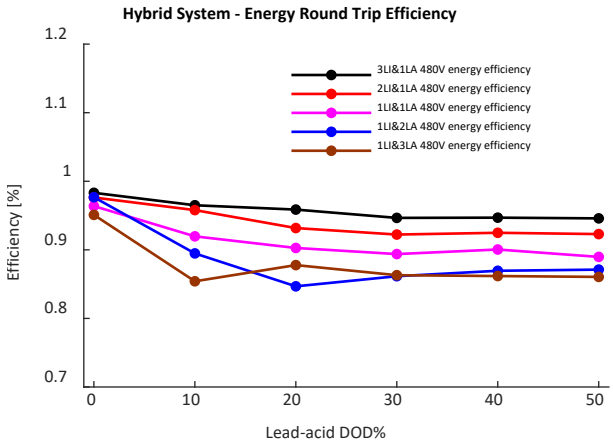

Figure 6-13. Energy round-trip efficiency

6.6 Conclusions

In this chapter, I've discussed the modelling of a hybrid, directly connected lead-acid and Li-ion energy storage system. The study uses equivalent circuit theory to model the hybrid behaviour and presents the complete process of battery testing, parameters extractions and model building of hybrid Li-ion and lead-acid directly DC-connected systems. The overall operation of the hybrid system allows for the Li-ion strings to be operated independently of the lead-acid, and this offers passive control over the discharge process. The final MATLAB model describes the hybrid behaviour and how it performs when compared with the experimental data.

The analysis is done between the simulation and the experimental data of a 48V 1LI&1LA system. The modelled results indicate that the dynamic average circulation currents between the strings can be modelled with 90% accuracy, except when the system is discharged to 20-30% lead-acid

DoD range. The comparison is made based on the total energy transferred during the rest period. The discrepancies between the experimental and the simulated values, in the 20-30% lead-acid DoD, are due to the difficulty in modelling the lead-acid cells at high SoC. More advanced models are required to capture the complex lead-acid chemistry in this SoC interval.

The round-trip efficiency and the total charge / discharged energy, as a function of the DoD, can also be predicted with 91% accuracy.

The simulated values for the Li-ion energy available for independent cycling overestimate the experimental values by 10% if the lead-acid strings are discharged between 10-50%. If the system is operated only in the A-B region, the lead-acid is kept at 100% SoC, the Li-ion energy cycled independently can be predicted with 95% accuracy.

To understand the behaviour at different voltage levels and for systems with different numbers of strings, I compared 9 hybrid systems at 48V, 240V and 480V in terms of the circulation currents and energy efficiency. The modelled results suggest that the circulation currents vary with the lead-acid DoD but do not increase with the system voltage. The energy transferred, however, varies linearly with the DC bus voltage increase. For hybrid systems with multiple strings, the simulation shows that increasing the number of lead-acid strings reduces the transient currents and the energy transferred between the strings. The peak energy transferred decreases on average by 29% for each lead-acid string added. If the Li-ion strings are increased, the opposite happens.

The energy efficiency of the systems depends on the ratio between the Li-ion and the lead-acid charged/discharged energy and the system DoD. If the system is discharged between 10-50% DoD for the lead-acid strings, the average modelled efficiency varies between 85% and 95% for different Li-ion and lead-acid energy storage ratios. The model fails to predict the efficiency drop when the lead-acid strings dominate and only the Li-ion is cycled, A-B region.

Overall, the work undertaken in this chapter shows that the hybrid Li-ion and lead-acid directly connected system can be modelled using simple equivalent circuit theory for general system sizing, however advanced battery models are required to improve the accuracy of the power and current sharing between the strings, especially in the transition region.

Chapter 7 Experimental Investigations – Demonstrator Project, ADEPT System

This chapter aims to answer the fourth question addressed in this research project:

How do hybrid battery systems perform over time in real-world applications?

The lab experiments detailed in Chapter 5 show promising results. However, they do not show how the hybrid system performs in real-world applications. This chapter presents the performance overview of a 100kW/270 kWh, grid-connected, hybrid battery energy storage system. The hybrid system uses two types of battery chemistries, Li-ion and lead-acid directly connected at the DC bus - without power electronic converters. The chapter presents a three-year, 2019 to 2021, operational data set. The battery data is later split into individual charge/discharge cycles and analysed in terms of power and string current sharing, energy, round-trip efficiency, and energy transfer between the strings. The analysis shows that the average round-trip energy efficiency of the system is 90% and depends on the depth of discharge. The energy transfer between the strings takes place during charge or discharge, and the average values are 5.5% (during charge) and 2.47% (during discharge) of the total discharged energy. A minimum capacity loss of 3.9% (1.3% per year) was recorded for the lead-acid cells, and practically no capacity degradation for the Li-ion cells.

7.1 Performance Analysis and Results

The GS – Yuasa Hybrid ESS has been in operation since December 2018, with interruptions between October 2019 – January 2020 and March – April 2020. During this time, the system was monitored using multiple BMS modules, one for each battery cabinet. The Li-ion BMS systems provide comprehensive information up to the individual cell level, but the lead-acid monitoring system records data only at the pack level. The information was stored on SD cards and later transferred in stages to a laptop. The Li-ion data was generally recorded at 30-second resolution, and the lead-acid at 15-30-second resolution. The final data time step resolution was set to 30 seconds, as it is the most common among all data files.

The overall data set is shown in Figure 7-2 and Figure 7-3. Figure 7-2 shows the information about the system voltage, total lead-acid current (I_{la} indicated in Figure 7-1), and total Li-ion current ($I_{li\text{-}ion}$ indicated in Figure 7-1). The gaps in the dataset are due to the interruptions of the system for inverter technical interventions.

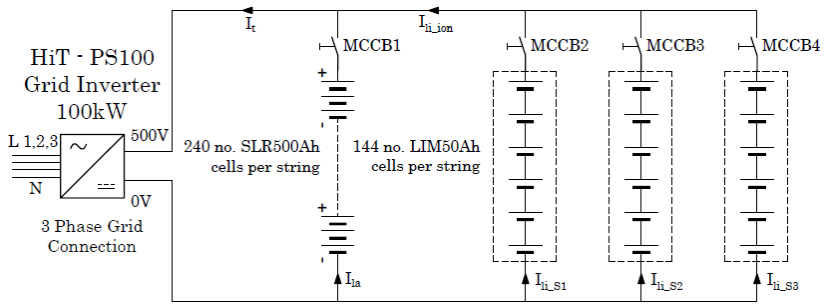

I_{la} – lead-acid string current

I_{li_S1} – Li-ion string 1 current

I_{li_S2} – Li-ion string 2 current

I_{li_S2} – Li-ion string 3 current

$I_{li\text{-}ion}$ – total Li-ion current

I_t – total system current

MCCB – Molded Case Circuit Breaker

Figure 7-1. Dual Chemistry System - Schematic

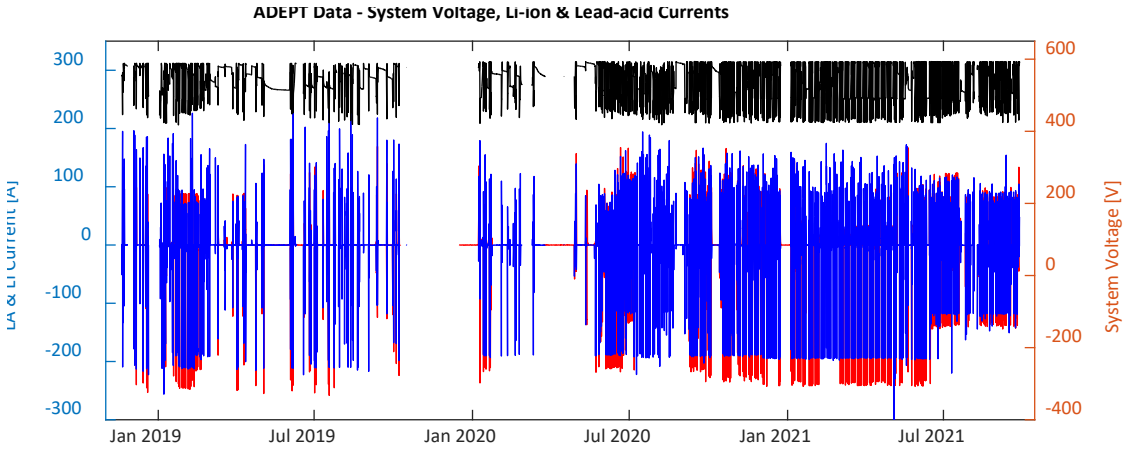

Figure 7-2. Total ADEPT Data, System Voltage, Li-ion & Lead-acid Currents

Figure 7-2 shows the state of charge (SoC) for the overall Li-ion and lead-acid strings as well as the temperatures of the battery modules. As indicated, for most of the cycles, the Li-ion strings have been charged/discharged from 100% to low SoC but the lead-acid strings have generally been cycled between 100% and 50% SoC.

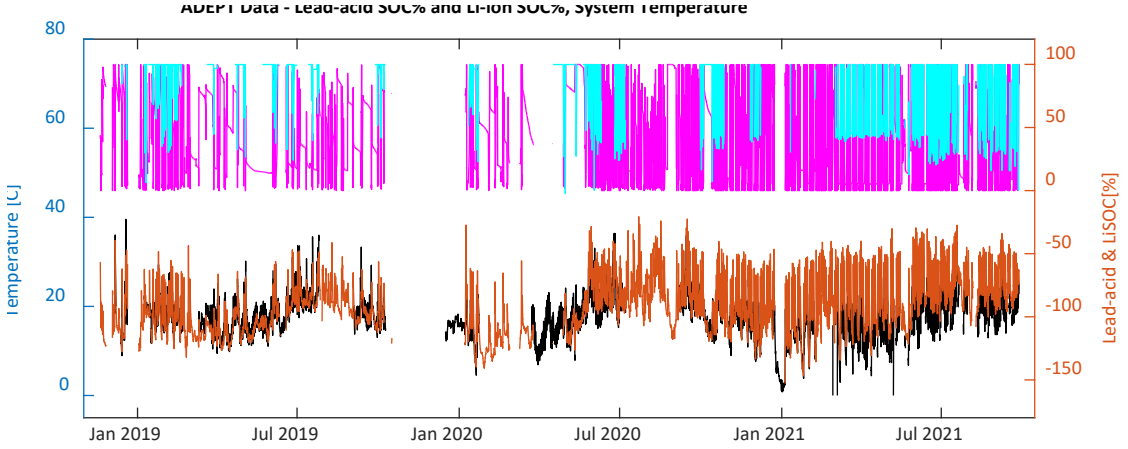

Figure 7-3. Total ADEPT Data, Li-ion & Lead-acid SoC, Li-ion & Lead-acid temperatures

The data shown in Figure 7-2 and Figure 7-3 contains around 500 complete charge/discharge cycles of the entire system. Typical daily charge/discharge cycle waveforms are shown in Figure 7-4, the Li-ion and lead-acid currents are the $I_{li\text{-}ion}$ and I_{la} shown in Figure 7-4.

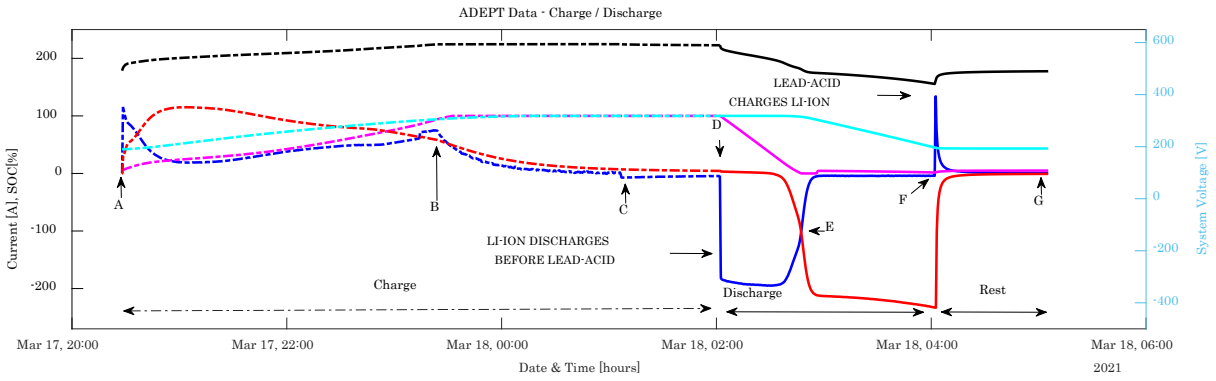

Figure 7-4. Typical Daily Charge / Discharge Cycle

The general points of interest indicated in Figure 7-4 are the following:

- **A-B:** Between points A and B, the system charges at constant power. There is an initial current & power spike on the Li-ion strings as these react faster but after a brief period, the lead-acid starts to charge.
- **B-C:** At point B, the system reaches nominal voltage and the charger changes to constant-voltage (CV) mode.
- **C-D:** At point C, the CV charge is stopped. If the system is not charged completely, the Li-ion strings slowly transfer the final top-up charge to the lead-acid string.
- **D-E:** The system starts to discharge at constant power at point D. Between points D and E, the Li-ion strings discharge, and there is no lead-acid activity in the first 3/4 of this period. At point E, the current and power provided by the lead-acid and Li-ion strings equalise.
- **E-F:** Between points E and F, the lead-acid string discharges at constant power. As it can be seen the Li-ion activity is almost insignificant.
- **F-G:** At point F, the system stops the discharge process and rests between F and G. During this time (F-G), because of the different dynamic responses of the two strings, the lead-acid string charges the Li-ion ones until the system reaches final equilibrium.

A total number of 140 such charge/discharge cycles have been analysed (around 30% of the total performed so far) to obtain a general picture of how the system performs under real working conditions. The cycles have been randomly picked across the data timespan and no two charge/discharge cycles are identical.

Figure 7-5 shows the lead-acid and Li-ion cell voltage intervals for each cycle: the starting cell voltage, the final charged voltage, and the final discharged cell voltage. As indicated, the lead-acid cells have generally been cycled between 2 – 2.41V and Li-ion between 3.4-4.1V. This corresponds to the SoC charge/discharge intervals indicated in Figure 7-6. Figure 7-6 shows that the lead-acid cells have generally not been discharged below 40% SoC. On the contrary, Li-ion cells have been discharged to around 5.5% SoC.

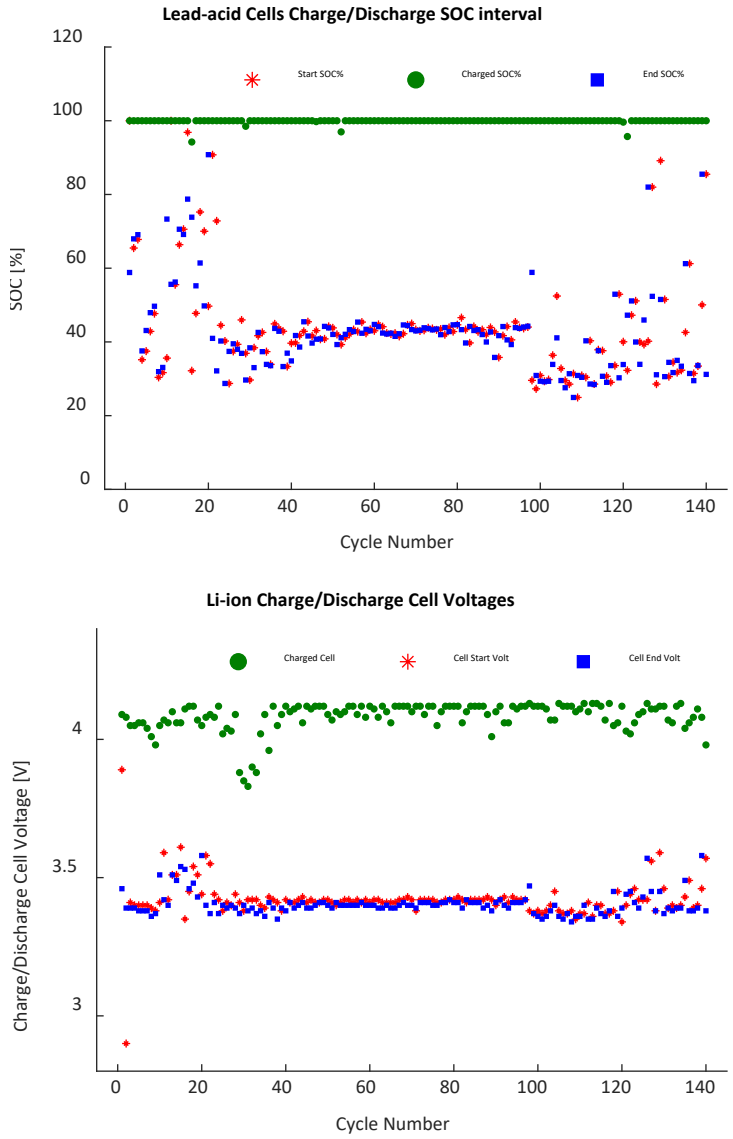

Figure 7-5. Lead-acid & Li-ion Charge/Discharge Cell Voltage Interval

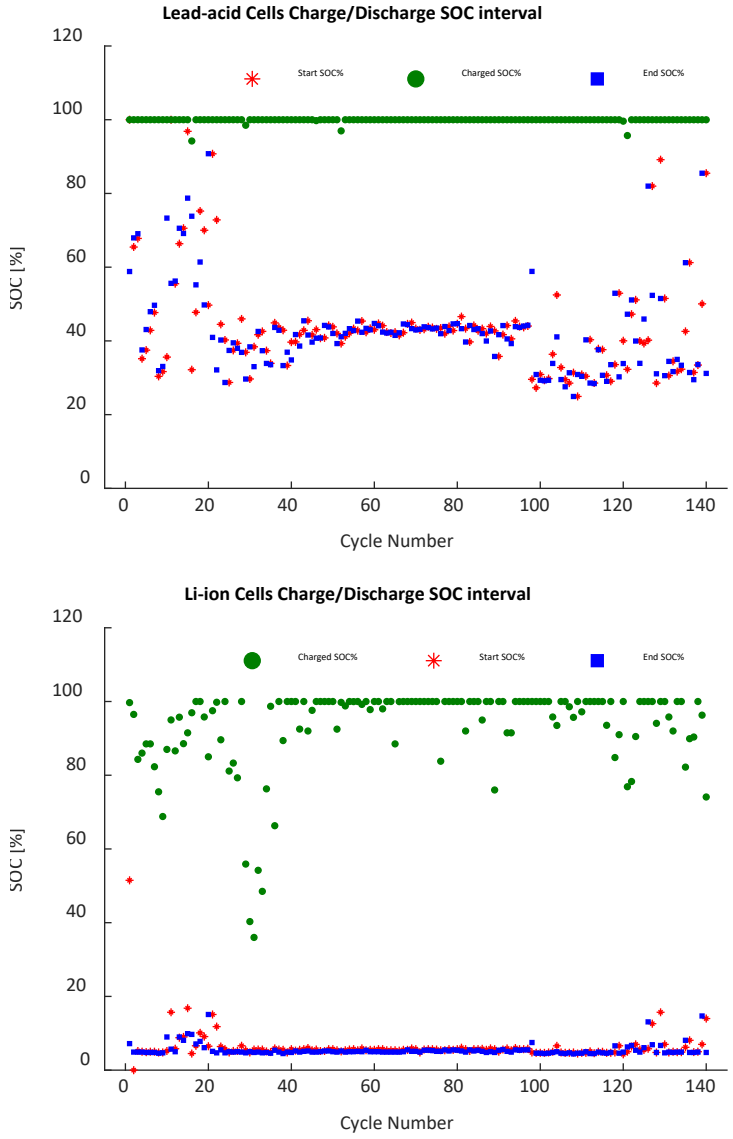

Figure 7-6. Lead-acid & Li-ion strings Charge/Discharge SoC Interval

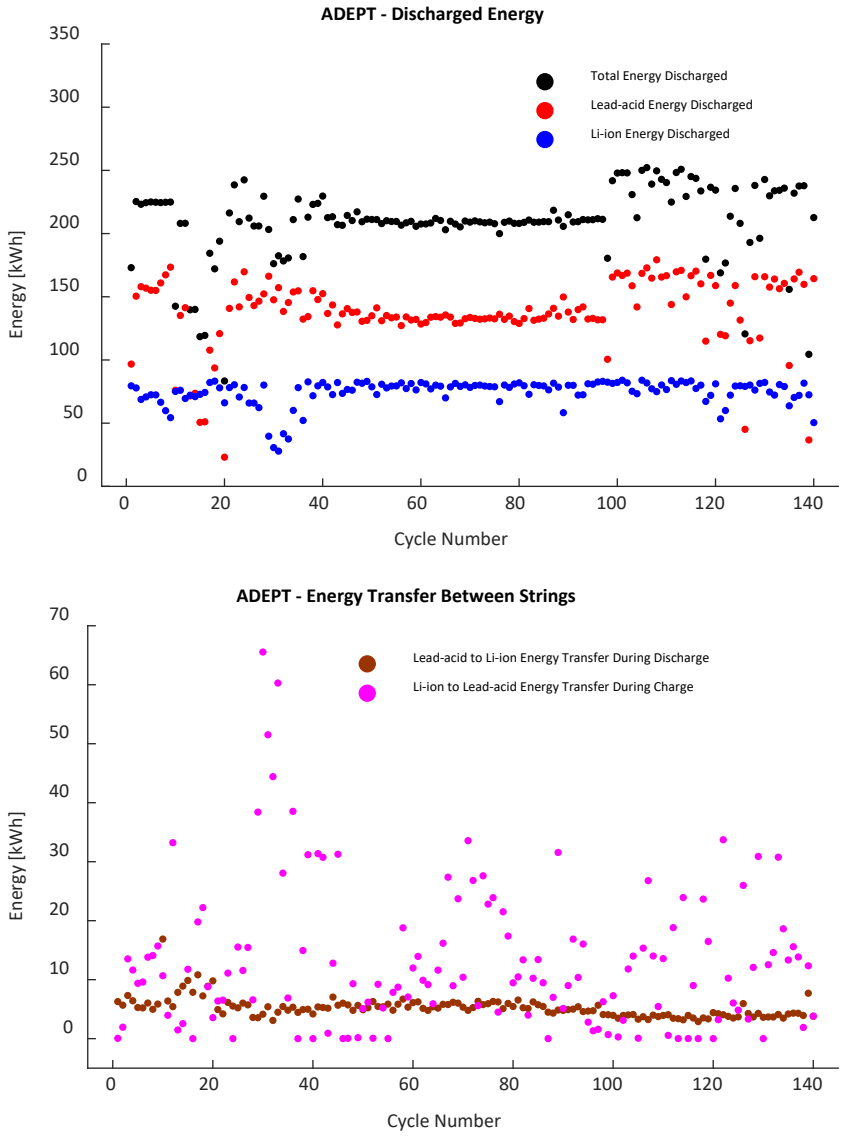

Figure 7-7. ADEPT System Energy Flows, Total Energy (a) and Energy Transfer (b)

Figure 7-7 (a) shows the total system discharged energy for each cycle, as well as the energy discharged by each chemistry. The total average discharged energy is 210 kWh, 138 kWh by lead-acid and 75 kWh by Li-ion. The total available lead-acid energy depends on the discharge current. Between cycles 100 and 140, the discharge power was set to 60 kW, and this is reflected in the total available lead-acid discharged energy.

Figure 7-7 (b) shows the total energy transfer between the strings due to the different dynamic responses of the two chemistries. The energy transfer from Li-ion to lead-acid strings happens during charge, between points C-D indicated in Figure 7-4. This only takes place if the charging process is stopped before both strings reach 100% SoC. As shown, the total energy transfer varies significantly, from 0 kWh to 50 kWh, depending on the charge stopping point (point C, Figure 7-4). For the analysed cases, the average energy transferred from Li-ion to lead-acid strings is 13 kWh. On the other hand, the energy transfer between lead-acid to Li-ion stings happens during

discharge, points F-G indicated in Figure 7-4. This is relatively constant across all discharge cycles and varies little with the discharged power or when the discharge process is stopped (point F, Figure 7-4). The average energy transferred from lead-acid to Li-ion is 5.2 kWh or 3.7% of the total lead-acid discharged energy.

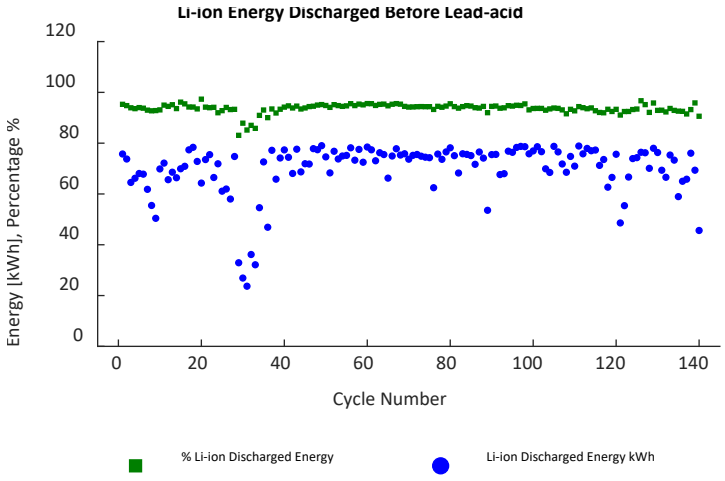

Figure 7-8. ADEPT System Energy Discharged Between Points D-E

Figure 7-8 shows the total energy discharged by the Li-ion strings between D-E points, indicated in Figure 7-4. This is crucial as it indicates the total energy the Li-ion strings can discharge independently of the lead-acid string. The average of these values, across all 140 cycles is 70 kWh, which corresponds to 93% of the total lead-acid discharged energy. This means that the Li-ion strings reach around 7% SoC when the power share between the lead-acid and Li-ion strings equalises.

The average round-trip energy efficiency of the hybrid system was calculated to be around 90% over the analysed cycles. This includes only the battery cells and does not consider the overall system efficiency, which includes losses in the inverter and cabling.

Three on-situ capacity tests were performed to determine the system's degradation over its operational history. This was done in January 2019 (10/01/2019), April 2020 (29/04/202) and October 2021 (25/09/2021). Although the measurements are not done in a lab testing environment, the results show good insights into the hybrid system capacity evolution. The capacity testing procedure was as follows:

- Set the charge/discharge power to 20 kW (the first discharged test was done at 23 kW).
- Discharge the system to 0% SoC and rest the system for 2 hours.
- Charge the hybrid system to 100% SoC for both strings and rest the system for 2 hours.
- Fully discharge the system until it reaches 1.8V/lead-acid cell.

Figure 7-9 and Table 7-1 show the capacity test results. The initial test was done at 23 kW charge/discharge power, and the following two at 20 kW. As indicated, no Li-ion capacity degradation was recorded, it remained at 79-80 kWh. The differences are attributed to the slightly different operating conditions between the tests. Although this is not a controlled lab environment, the capacity test data is satisfactory to indicate that the Li-ion degradation is minimal. The lead-acid battery capacity degraded from the initial recorded capacity of 251 kWh, measured in January 2019 to 241 kWh at the end of 2021. This implies a total capacity degradation of 3.9%, around 1.3%/year. This is as per the manufacturer's technical information, and it shows that no unexpected degradation was recorded due to the arrangement of the hybrid system. This means the system degradation is as if the cells were operated independently in single chemistry storage systems.

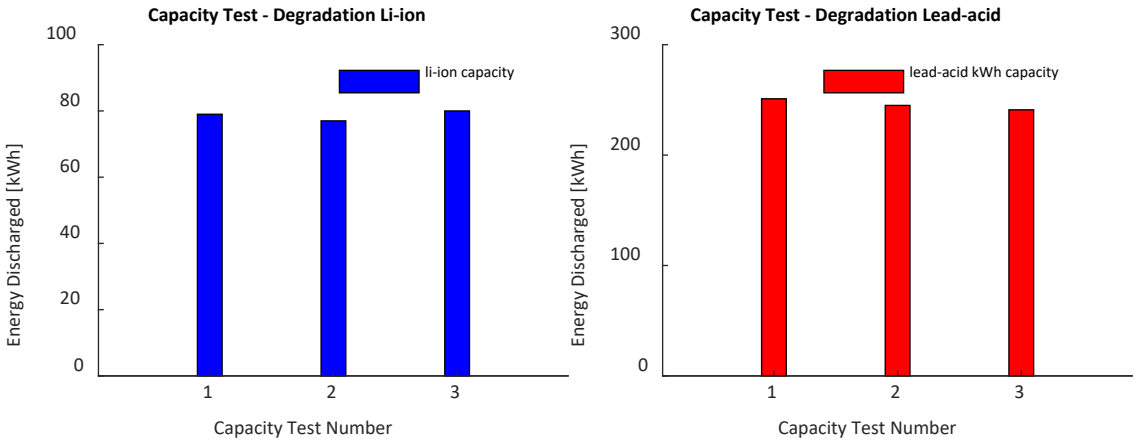

Figure 7-9. Capacity Degradation for Li-ion and Lead-acid strings.

For the lead-acid cells, the total Ah charged/discharged between the capacity testing dates are 131772 Ah and 125920 Ah, showing 95% coulombic roundtrip efficiency over the analysed time interval. For the Li-ion, as the coulombic efficiency is practically 100%, the charged and discharged Ah are identical.

Table 7-1. Hybrid Battery System Capacity Degradation

Capacity Test Number	Date	Test Ch/Dis Power kW	Li-ion Capacity [kWh]	Lead-acid Capacity [kWh]
1	10/01/2019	23	79	251
2	29/04/2020	20	77	245
3	25/09/2021	20	80	241

7.2 Conclusions

The general data presented above shows that the dual chemistry Li-ion and lead-acid hybrid storage system is stable and can work successfully connected directly at the DC bus, without power converters. The interaction between the two chemistries shows that I can discharge the Li-ion strings independently of the lead-acid ones, thus providing semi-control of the strings.

The overall system round-trip efficiency depends on the ratio of Li-ion and lead-acid capacity and the depth of discharge of the overall system. The calculated average round-trip efficiency across the analysed tests is 90%, and the average energy discharged by the system is 210 kWh, 138 kWh being delivered by the lead-acid and 75 kWh by the Li-ion strings.

The energy transfer between the strings due to different dynamic time constants of the two chemistries depends on the charge stopping point C and, to a lesser extent, on the discharge point F. For the analysed system, the average Li-ion to lead-acid energy transfer during the charging process is 13 kWh, 5.5% of the total charged energy. The average lead-acid to li-in energy transfer during discharge is 5.2 kWh, 2.47% of the total discharged energy.

During discharge, the Li-ion strings provide most of the power between points D-E. The data shows that around 93% of the total Li-ion discharged energy takes place before the lead-acid and Li-ion power share equalises (point E). This is important as it allows the Li-ion strings can take most of the short charge/discharge cycles, thus protecting the lead-acid ones.

Three in-situ capacity tests have been performed at the beginning of the study, on the 10th of January 2019, on the 29th of April 2020 and on the 25th of September 2021. The results do not show abnormal degradation. The Li-ion did not record any measurable degradation as the capacity decreased by 3.9%, around 1.3%/year.

This shows that the system is stable over time and the directly connected strings do not contribute, at least within the measured timeframe, to additional battery degradation.

Chapter 8 Dual Chemistry Hybrid Energy Storage Sizing

This chapter aims to answer the final question addressed in this research project:

What storage applications are best suited for hybrid lead-acid and Li-ion systems and what are the associated techno-economic parameters?

8.1 Introduction and General Research Objectives

This chapter investigates potential applications for the hybrid and dual chemistry battery storage systems described in the previous sections.

Any technology has specific applications and if the suitable market for that product is not identified, the commercialisation opportunity can be lost, and the R&D efforts and investments wasted. The energy storage systems are no different. As explained, there is a wide range of technologies with vastly different technical characteristics suitable for multiple applications. The 'right' application of a hybrid storage system depends on several factors, among which are the renewable energy mix, the load factor, and the seasonality of the load profile supplied.

This chapter proposes a set of load profile types to investigate if they can be supplied using renewables and hybrid Li-ion and lead-acid storage systems. Depending on the interaction between the generation, grid connection, and storage system, the potential use of the dual chemistry system may or may not bring economic advantages.

This aims to be achieved by setting the following research objectives:

1. Calculate the cost comparison between simple Li-ion battery storage systems and the hybrid system described and developed in this project for typical renewable energy applications. This is done by comparing the cost of a simple Li-ion storage solution and a hybrid option with different hybrid ratios. This will be investigated under various grid connection capacities to determine how local network constraints change the economics between the two chemistries.
2. Determine the impact of the generation capacity factor, load factor, and the smoothness of the load profile on the ratio between the two chemistries for each application. This will also be calculated for different grid scenarios, on-grid systems, off-grid, and grid-constrained options.
3. Calculate the technical parameters, the cycles performed, and the power profile for each chemistry of the hybrid system and how these change with each application type

proposed. Depending on the depth of discharge, the ratio between the two chemistries, and the number of cycles performed by the lead-acid component, the efficiency, and the overall performance of the system change.

4. Calculate the renewable technology ratios of solar, wind, and hydro to work in tandem with the hybrid system. The complementary nature of these renewable technologies will be investigated as a potential hybridisation option and how these improve the application options for the dual chemistry storage system.
5. Analyse the dual chemistry hybrid system in front of the meter application offering grid services and operating in different UK markets, like the dynamic containment and balancing markets. The investigation examines both standalone front-of-the-meter battery storage applications and PV colocation systems in both unconstrained and constrained grid options.

8.2 Hybrid Battery System - Residential Applications

8.2.1 Introduction

The first case study for the Li-ion and lead-acid hybrid battery system considered in this thesis is the communal energy systems for residential applications. The new and existing residential developments are undergoing, along with all other economic sectors, a rapid renewable transition by replacing gas heating, domestic hot water production, and general domestic electricity consumption with cleaner, renewable energy solutions. In the UK, the two most popular technologies advocated for heating are heat pumps, solar (PV) and wind for local electricity generation. Not only do these technologies reduce CO_2 emissions, but they are also more efficient in terms of primary energy consumption when compared with direct gas or electric heating. Also, they are relatively simple to integrate into the existing housing stock compared with other technology options like centralised district heating.

This study proposes the analysis of a residential development of 125 homes in South Wales. The location is Coedely – Ynysmaerdy area, Rhondda Cynon Taff, UK. The reason for choosing this geographical area is twofold. First, the site is a perfect case study for onshore wind and solar PV colocation, as excellent wind resources are available on the Taff-ElyTaff Ely Ridgeway, UK, marked by the presence of the Mynydd Portref Wind Farm and more recently, Graig Fatha community wind project [133, 134]. Secondly, the hybrid battery system discussed throughout this study was installed by GS Yuasa as part of a microgrid in the same location (Royal Mint site), and I'm familiar with the wider region and its renewable energy potential [108, 135].

Figure 8-1. Wind Turbines on Taff Ely Ridgeway

As mentioned, the residential development has 125 homes with off-site solar, a community wind farm, and ASHP for heating and hot water. The wind turbines are located on the Taff Ely Ridgeway, which offers an annual capacity factor of 22-24%, depending on the turbine size. The annual wind generation data was compiled using the Global Wind Atlas datasets [136]. The current study bases the renewable generators on Vestas V100-2.0 turbines and standard PV technology based on Q.PEAK DUO ML-G11S panel series. The annual solar generation load factor for the Coedely – Ynysmaerdy area is around 10.1%, and the annual generation profile was extracted using the SolarEdge designer [137]. The electrical power schematic for the site is indicated in Figure 8-2. The development is supplied at 11kV and there is a private network distributing power around the site. The renewables, wind, and solar generators, as well as the storage assets, are connected behind the meter on the private 11kV network. The renewable power is generated and stored at low voltage, and the inverters are connected to a 0.4/11kV substation which steps up the voltage to supply the residential development. The distribution network operator (DNO) grid supply point is at 11kV as indicated in Figure 8-2. In the UK, a connection of this type needs to comply with G99/G100 standards, which set the power network framework for any generators connected at the distribution level.

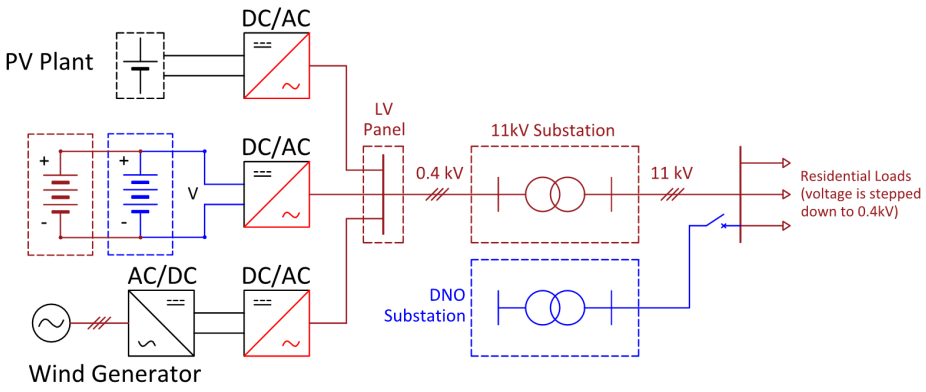

Figure 8-2. Wind, PV & Hybrid Storage for the Residential Microgrid

The total residential demand profile was approximated using the Electrification of Heat UK demonstration project data [138, 139]. This contains one of the most recent and largest heat pump domestic data sets in the UK. The participants included in the analysis were picked to achieve a good diversity of property types and to avoid data gaps across the year. The data was cleaned and set into the format required for the techno-economic model described in the methodology chapter. The final half-hourly annual site demand profile is indicated in Figure 8-3. This shows a seasonal demand profile, as electricity consumption increases during the winter, and it does not match the annual solar generation profile. The maximum peak demand for the site is 263 kW, the diversified load is 2.104 kW/home during the winter and 0.32 kW/home during the summer. The variation in the peak demand over the year is due to the heat pump's increased operation during the winter. The total annual electricity demand for the site is 498,070 kWh which translates into 3,984 kWh/home/annum. The total domestic electrical demand capacity factor when heating is provided via heat pumps is 21%.

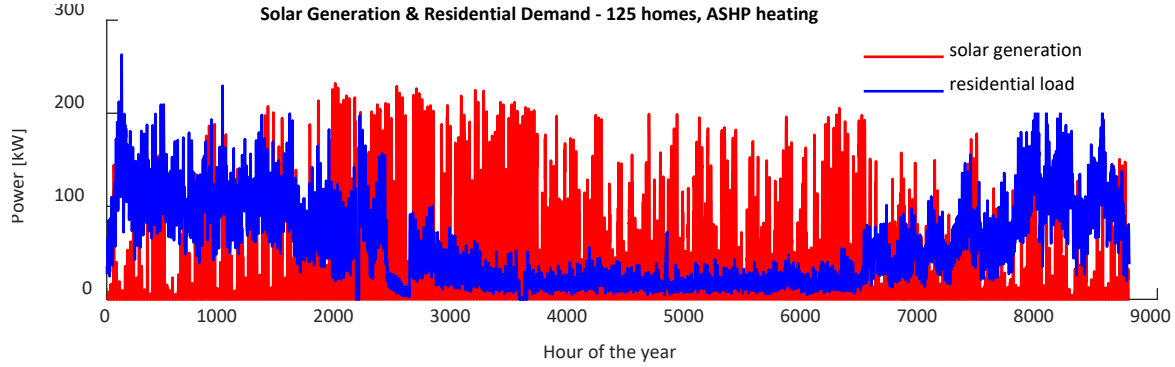

Figure 8-3. Residential Demand (Seasonal Generation & Demand).

For illustrative purposes, Figure 8-4 indicates a typical solar and wind generation profiles necessary to cover 100% of the site's electrical demand indicated in Figure 8-3.

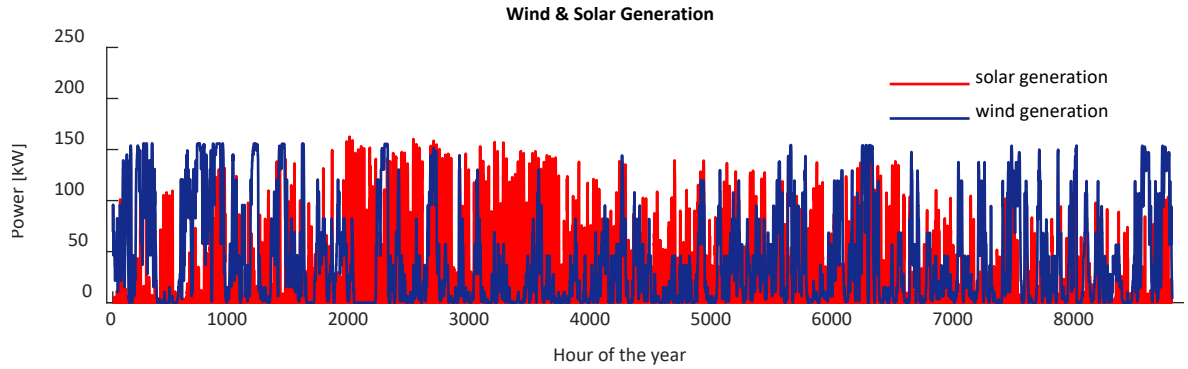

Figure 8-4. Wind and Solar generation profiles

8.2.2 Off-grid Residential - Methodology

In an off-grid residential scenario, the energy system would have to source and store its entire energy requirements from renewable generation throughout the year. Inevitably, the demand discrepancy between summer and winter will lead to impractical battery storage sizes to address the seasonal demand mismatch.

One common way to reduce the storage requirements is by installing oversized generation capacity, and even if a large part of the PV and wind will have to be curtailed over the year, the overall system cost can be reduced substantially. To understand the storage requirements, the hybrid battery operation, and the total system cost, I have modelled six excess generation scenarios, when the renewable system generates 100%, 200%, 300%, 500%, 800%, and 1300% of the load requirements.

Each scenario was tested against the hybrid battery storage options as follows:

- Set the renewable generation for each scenario as a percentage of the demand.
- Calculate the total energy storage required for the entire demand to be covered.
- Set the hybrid lead-acid to Li-ion ratio range between 0 and 4 and generate 60 linearly spaced ratio values within the interval.

A larger ratio would be impractical as the number of lead-acid strings would be greater than the Li-ion one, thus reducing the efficiency of the whole system as indicated in Chapter 5. For each scenario, I have calculated the total storage required, the hybrid battery operation, as well as the system cost for simple Li-ion and hybrid storage solutions.

Scenario 1. In this scenario, the total annual electricity generation of wind and solar was set to 100% of the annual residential demand. This accounts for 320 kW of renewable generation capacity with 110 kW of solar PV and 210 kW of wind capacity. The ratio between the wind and solar capacities is 2 and was chosen as the starting point as a practical consideration of the fact that the residential load is highly seasonal (a higher wind capacity implies more overall generation in the winter months when the electrical demand is higher.). In this scenario, to cover the entire annual demand only from wind and solar renewable power, a total of 82.4 MWh of energy storage capacity is required, assuming a max 90% depth of discharge. To test the economic performance of the different hybrid options, 60 hybrid battery storage systems have been investigated with different hybrid ratios, (lead-acid kWh / Li-ion kWh) ranging from 0 (a full Li-ion option) to 4.

Scenario 2. In this option, the annual generation of wind and solar was set to 200% of the total demand. This adds up to 640 kW of renewable generation with a ratio of 2 between wind and solar as in Scenario 1. The calculated storage required to cover 100% of the residential load is 36.2

MWh. Like in all other scenarios, 60 hybrid battery storage options have been investigated with the lead-acid/Li-ion capacity ratios from 0 to 4.

Scenario 3. The annual generation of wind and solar was set to 300% of the total demand. This adds up to 960 kW of renewable generation with a ratio of 2 between wind and solar as in Scenario 1. The storage required to cover 100% of the residential load is 18.5 MWh. Like in all other scenarios, 60 hybrid battery storage options have been investigated with lead-acid/Li-ion capacity ratios ranging from 0 to 4.

Scenario 4. The annual generation of wind and solar was set to 500% of the total demand. This adds up to 1600 kW of renewable generation with a ratio of 2 between wind and solar capacity. The storage required to cover 100% of the residential load is 14.5 MWh. Sixty hybrid battery storage options have been investigated with lead-acid/Li-ion capacity ratios from 0 to 4.

Scenario 5. The annual generation of wind and solar was set to 800% of the total demand. This adds up to 2560 kW of renewable generation with a ratio of 2 between wind and solar generating capacities. The storage required to cover 100% of the residential load is 8.75 MWh. Sixty hybrid battery storage options have been investigated with lead-acid/Li-ion capacity ratios from 0 to 4.

Scenario 6. The last scenario has 1300% generation of the total site demand which implies 4160 kW of renewable generation with the same ratio between wind and solar capacities. The storage required to cover the demand is 5 MWh and a similar number of hybrid storage was tested to determine the variations.

8.2.3 Modelling Results Off-grid Scenario.

Figure 8-5 (a) summarises the percentage demand remaining which is covered by the storage system across the year for each renewable generation scenario. Without energy storage, for Scenarios 1 to 6, the calculations indicate that 45.9%, 33%, 27.2%, 21.5%, 17.8% and 14.7% of the annual demand is not directly supplied by the on-site generation system.

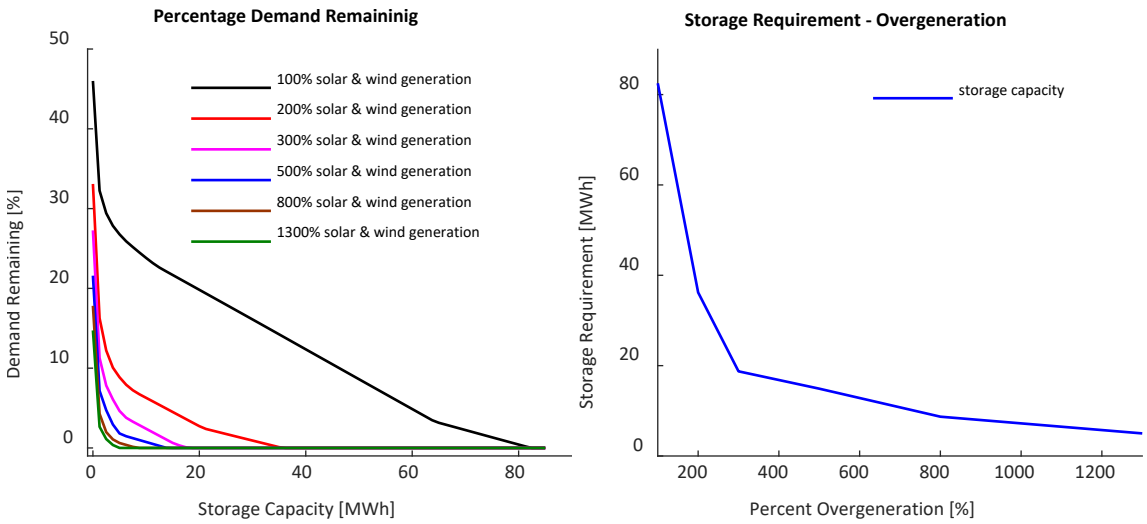

Figure 8-5. Demand remaining (a), Storage requirement (b)

Figure 8-5 (b) shows the nonlinear relationship between overgeneration and the energy storage capacity requirements to supply 100% of the annual load. It shows a significant storage decrease of 78% between the 100%-300% overgeneration scenarios and a smaller drop of 16% between 300%-1300%.

For each scenario mentioned, Figure 8-6 indicates the total self-consumption for the site which decreases from 53.8% to 6.5% as the generation is increased from 100% to 1300% of the total site demand. This is because a large portion of the generation is not getting used and it will be curtailed.

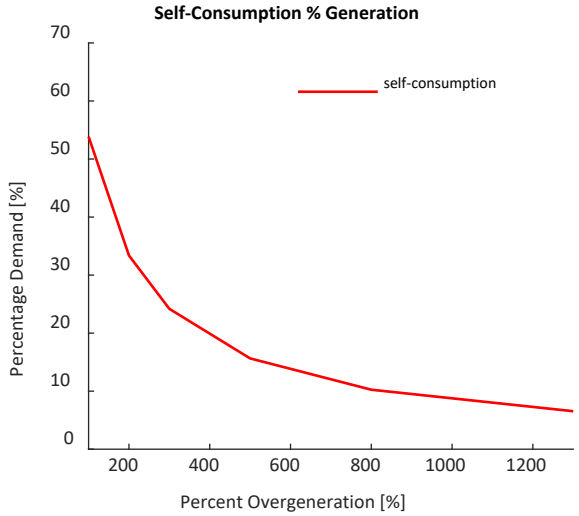

Figure 8-6. Residential self-consumption

For illustration, Figure 8-7 indicates a typical generation, load, and hybrid storage interaction across a typical year. This example is for the 200% generation scenario and 0.46 lead-acid to Li-ion storage capacity ratio. As indicated, because of large overgeneration in the summer, the battery utilisation is low, below 50 kW peak, as more of the electrical load is covered directly by

the on-site generation. In the winter months, as the ratio between generation and demand is lower, the battery supplies a larger proportion of the load. Also, although the ratio between the lead-acid and Li-ion capacities is not zero, the lead-acid cells are used only in December. This illustrates the case for hybrid battery storage described in the previous chapters, as we do not need a high-end battery specification and implicitly more expensive storage system for the last 11.5 MWh capacity to cover that period (the total storage capacity for this scenario is 36.2 MWh). Using lead-acid cells, directly connected in parallel with the Li-ion strings, the same performance can be achieved at a lower cost as detailed below.

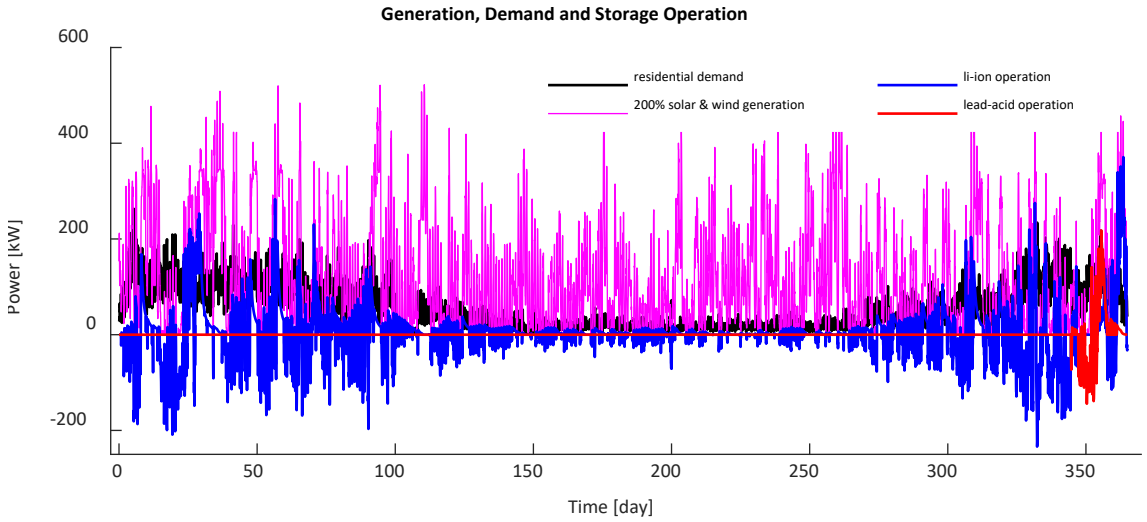

Figure 8-7. Generation and Storage for the 200%, Storage 24.7 MWh Li-ion, 11.5 MWh Lead-acid

Similarly, for illustrative purposes, Figure 8-8 shows the SoC profiles for the Li-ion and lead-acid battery strings across the year. The Li-ion storage stays above 50% SoC for most of the year, is hardly cycled during the summer, and only drops below 50% SoC in the winter months. This implies that the Li-ion strings perform almost all the short-duration cycles. The lead-acid, on the other hand, stays at 100% for most of the year and is only cycled in December. Of course, the SoC profile and the total annual cycles will change with the overgeneration scenario, and the storage ratio as detailed below.

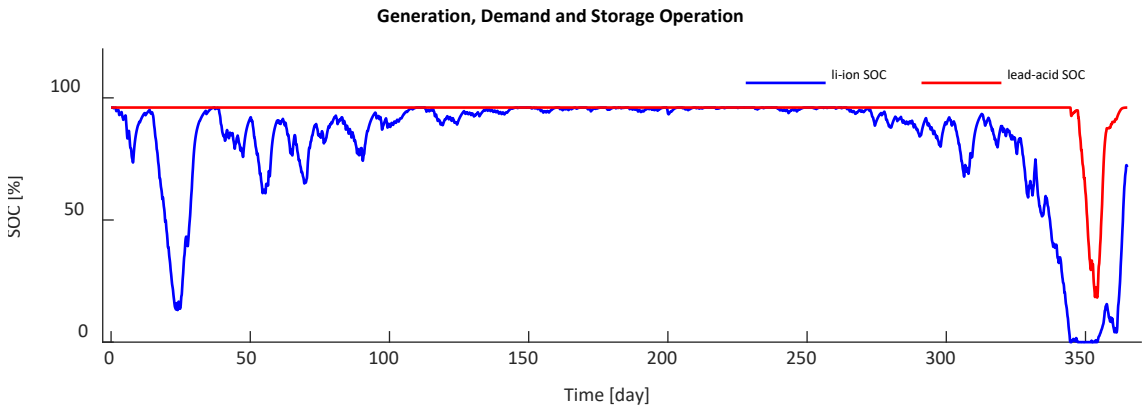

Figure 8-8. SoC profiles for Li-ion and Lead-acid

Figure 8-9 shows the annual battery utilisation, for the analysed scenarios 100-1300% of the demand load.

The first observation is that in all scenarios, the Li-ion strings have a much greater utilisation when compared with lead-acid, except for Scenario 1. This shows that the Li-ion cells are cycled harder and that the lead-acid cells operate only at specific times of the year when spikes in energy storage utilisation are required. For Scenario 1, we also observe the highest utilisation ratio of around 45.9% for the simple Li-ion only storage option (zero hybrid ratio).

The second observation is that, as we increase the lead-acid capacity of the hybrid system, the Li-ion utilisation drops across the board, but again, Scenario 1 is the outlier. In Scenario 1, the Li-ion utilisation drops from 45.8%, for a simple Li-ion option, to 18%. The lead-acid utilisation mirrors this, by increasing from zero to 27.8% for a hybrid ratio of 4. The reason for the symmetry is twofold, first, for Scenario 1, there is the highest amount of inter-seasonal storage behaviour, and secondly, it has the least amount of overgeneration. These two things require a larger MWh storage capacity when compared with the other scenarios. The two chemistries reach an equal utilisation percentage of the demand for the hybrid ratio of 2. For Scenarios 2-6, as the hybrid ratio increases, the Li-ion utilisation decreases by 8.5%, 7.3%, 4.7%, 4.12% and 3.7%. This indicates that as the overgeneration increases, there is less inter-seasonal energy transfer, and the Li-ion performs only as short short-duration storage function, covering the frequent cycling required. As expected, the lead-acid increases with the hybrid ratio, but it never exceeds 8.5%, except for Scenario 1. Also, the lead-acid utilisation values are grouped, when compared with Li-ion values which are more spread out, the maximum difference between the lowest and the highest (except Scenario 1) is 8.47%. For the Li-ion, the value is much higher, closer to 22%. These differences point again to the fact that the lead-acid strings are only used at specific times of the year when increased activity from the storage system is required.

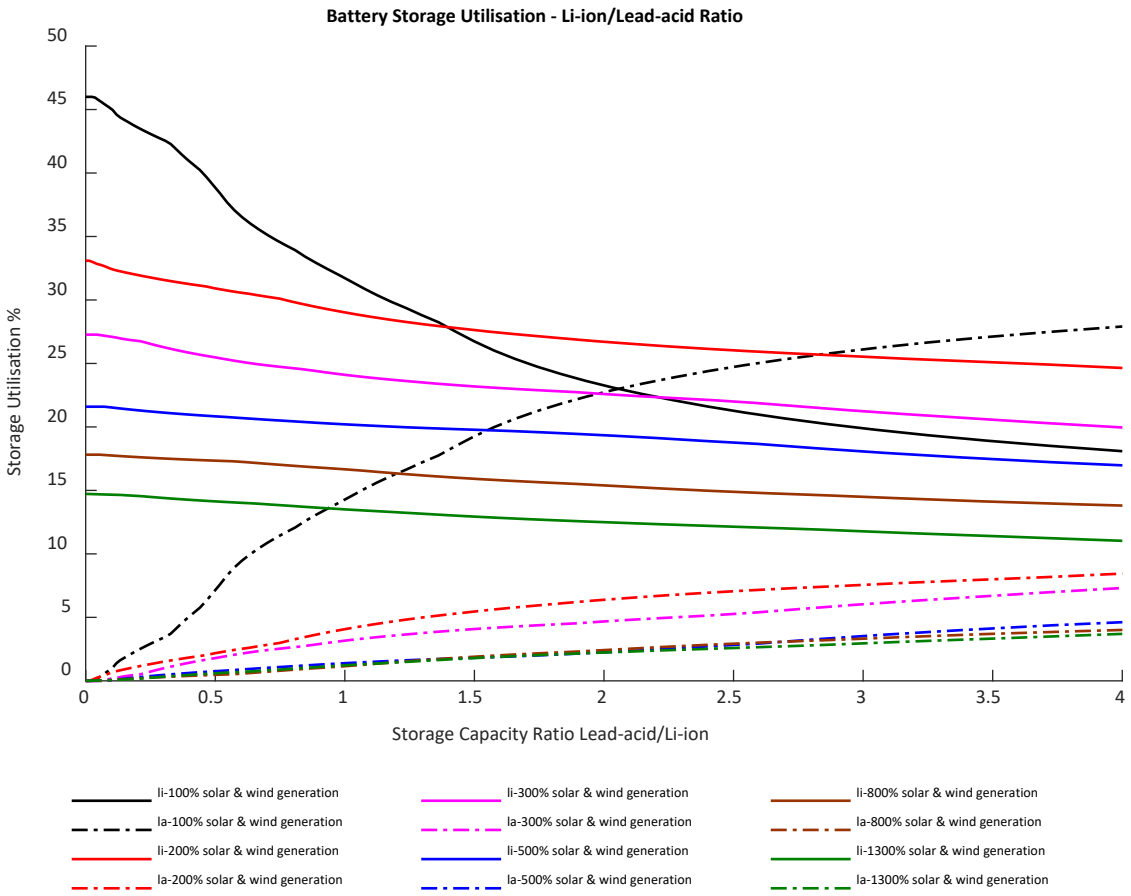

Figure 8-9. Off-grid Residential Case Study - Hybrid Battery Storage Utilisation

Figure 8-10 shows the number of cycles performed by each chemistry for Scenarios 1-6. The equivalent cycles are defined in the previous sections. The immediate observations are that the Li-ion storage is cycled harder across all scenarios and that both chemistries increase their number of cycles, especially Li-ion, with the hybrid ratio. This is not surprising, as Li-ion storage is expected to do the short cycles, and a larger hybrid ratio implies a decrease in its total capacity. Another immediate observation is that for the Li-ion, the number of equivalent cycles increases with the overgeneration capacity. This is slightly counterintuitive as the utilisation of the Li-ion strings diminishes with overgeneration. The increase in the number of cycles is because, although an increased overgeneration implies less load to be covered by the storage system, the battery storage capacity is also lower. The result is that for higher overgeneration scenarios, the Li-ion strings work harder. This is not the case for the lead-acid strings, as the number of cycles does not increase significantly with the overgeneration or the hybrid ratio. This again shows that the lead-acid strings are operated only on specific days of the year.

The number of cycles across the year is small for both chemistries. For the Li-ion strings, the lowest number is 4.7 of full equivalent cycles/year, 0.012 cycles/day, and the highest, 57 cycles/year, 0.15 cycles/day. Standard storage systems for residential applications are designed

for 1 cycle/day. This implies that, across all scenarios, the hybrid storage system is underutilised, which was expected because of the inter-seasonal nature of the residential load.

The lead-acid strings perform even a lower number of equivalent cycles, the maximum being 4.7 cycles/year for Scenario 6, hybrid ratio 4.

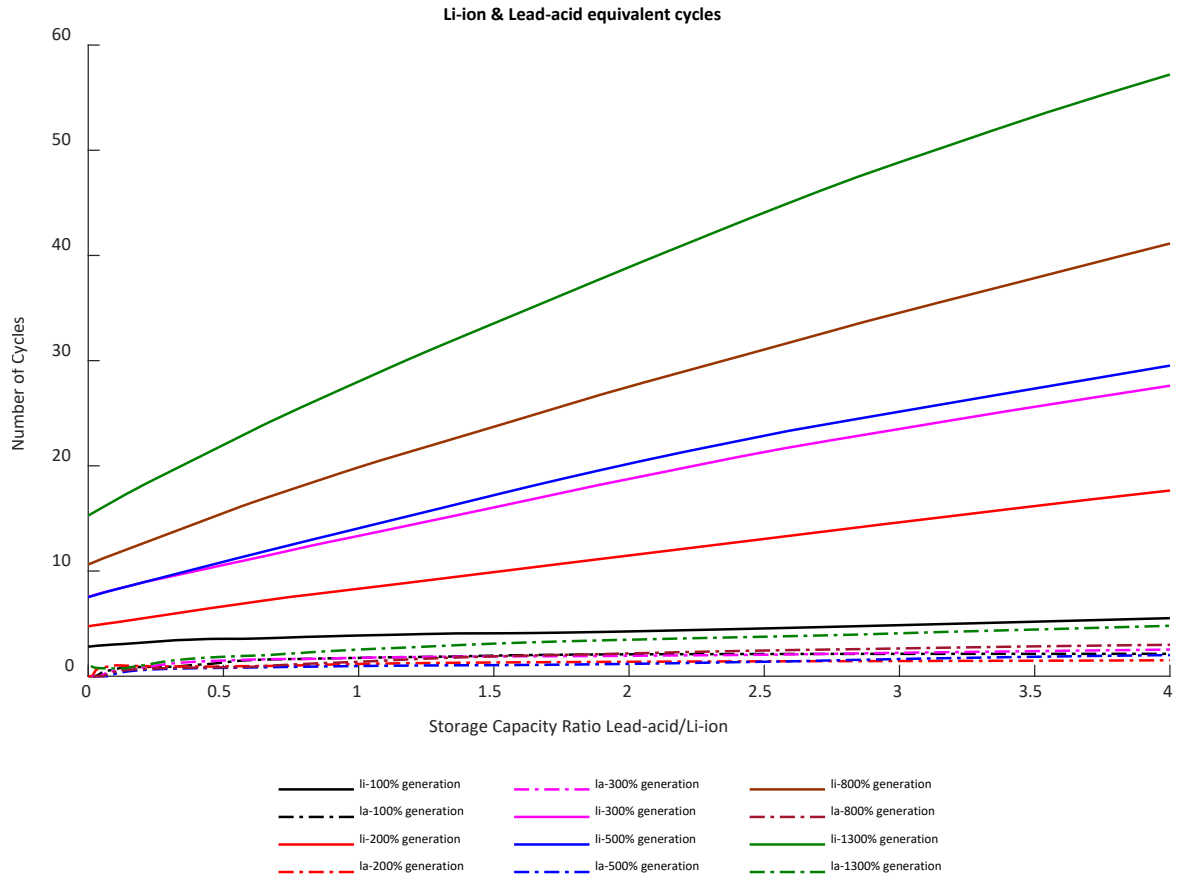

Figure 8-10. Equivalent cycles for Li-ion and lead-acid in hybrid configuration

Considering the data shown in Figure 8-9 and Figure 8-10, Scenario 1 is not recommended for hybrid ratios greater than 0.5, even if cost is not taken into account. This is because the lead-acid strings perform an insignificant number of cycles, and their utilisation increases substantially with the hybrid ratio. This means that the lead-acid strings take the inter-seasonal storage role and spend months below 100% SoC. From a practical perspective, this is not recommended as the lead-acid cells degrade faster when they remain at partial SoC for prolonged periods.

Figure 8-11 indicates the total system cost for the PV, wind and hybrid battery storage for all scenarios and all hybrid ratios considered.

The first observation is that there is a wide difference between Scenarios 1-2 and Scenarios 3-6. Generally, this is because the energy storage capacity required for the first two scenarios is much higher, as described in Figure 8-5. The highest cost, £20.1 million, is for Scenario 1, a Li-ion only

storage solution. As mentioned, this is not recommended from a technical perspective and is also challenging financially, as this implies £160.8k per property which would not be economical. For Scenario 2-6 the costs for the energy system with a single chemistry storage unit are £9.2, £5.62, £5.04, and £5.5 million pounds. The lowest cost for the simple Li-ion storage solution is Scenario 5 (800% generation).

The second observation is that a hybrid solution is always cheaper when compared with a single chemistry storage system. For each Scenario 2-6, the cost of the entire energy system drops by 25.8%, 20.6%, 14.2%, 10.7% and 4.9% as the hybrid ratio increases from zero to 4. The lowest cost overall is observed for Scenario 5. It is not surprising that the biggest energy system cost reduction is seen for Scenario 1 (25.8%) as it has the largest storage capacity overall and switching to a hybrid scenario would benefit the most.

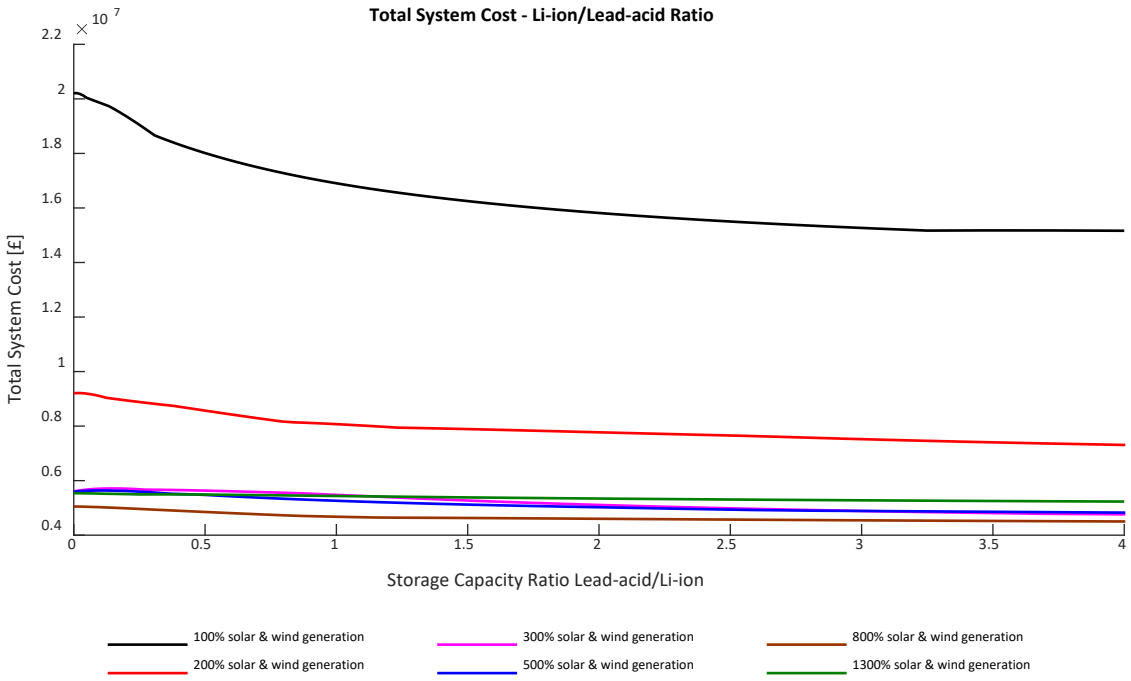

Figure 8-11. Total System Cost

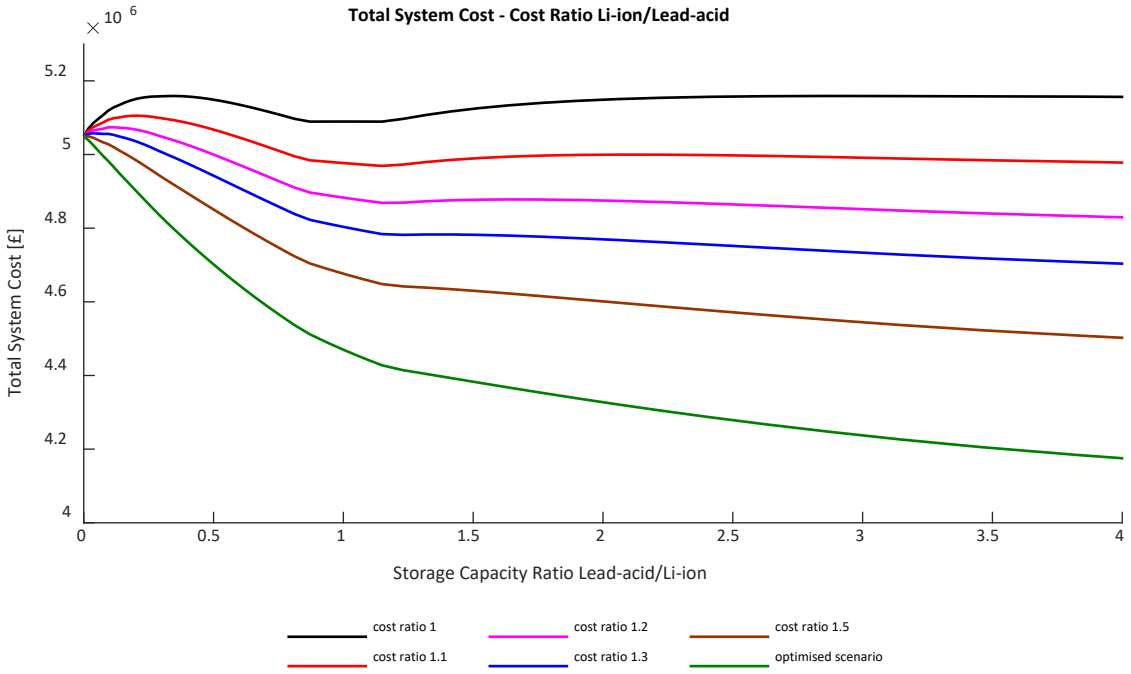

Figure 8-12. System Cost - Price Ratio Li-ion to Lead-acid

If the cost per kWh between the two chemistries is reduced, the savings potential decreases for all scenarios. To understand this, Figure 8-12 indicates the total system cost of the optimised scenario (Scenario 5) for multiple Li-ion to lead-acid cost ratios. If the kWh cost ratio between the two chemistries falls below 1.1-1.2, the cost savings when the capacity ratio is increased to 4 is less than 1%. This has been taken as a cut-off limit to justify a hybrid system from the economic perspective. As the cost per kWh of Li-ion storage approaches the lead-acid values, the system cost can increase above the single chemistry storage type. This is because the model also accounts for the price per kWh as a function of the storage size of a particular chemistry (the price per kWh for each chemistry also varies with the quantity bought). Figure 8-12 also indicates that, as the cost ratio increases, the rate of cost reduction between 0 and 1 also rises.

Table 8-1 summarise the analysed scenarios, showing the renewable installed capacity, the generation potential as a percentage of the demand, and the storage required to cover the total annual residential load.

Table 8-1. Summary table – Off-grid scenario – Residential

Scenario	Solar Capacity kW	Wind Capacity kW	Generation % annual demand	Energy Storage Capacity MWh
1	110	210	100%	82.4
2	220	220	200%	36.2
3	330	630	300%	18.5
4	550	1050	500%	14.5
5	880	1680	800%	8.75
6	1430	2730	1300%	5

Although the cost of the overall off-grid energy system can be reduced by oversizing the infrastructure, and by using hybrid battery storage technologies, it is worth mentioning, that this still requires a significant CAPEX, and from a practical perspective, it needs to be considered only when a grid connection is impossible. The cheapest option calculated is for Scenario 5 (£ 5.04 million), and this translates to £40.32 thousand per property. This is still a substantial added cost for the residential developers to consider, as a standard grid connection, with on-grid PV systems and no storage, can be achieved indicatively 4x cheaper [140].

8.2.4 On-grid Residential - Methodology

The second option analysed for the residential case study is the on-grid scenario.

Most residential developments are connected to the power distribution system, however, with the rise of embedded generation in the last decade, in the UK, securing grid connections for large residential/industrial developments can be delayed by more than a decade with major grid reinforcements costs [141]. The main reasons for this are the ageing UK grid infrastructure and the rapidly developing distributed renewable energy sources, the electrification of heat & transport and the outdated grid regulations. These trends challenge the DNO's traditional business models, and novel policies and technologies are needed. It is worth mentioning that the challenges for the network operators are not necessarily the actual quantity of electricity to be supplied but the peak demand. Overall, without considering the reserves capacities, the UK electricity grids operate at around 30% capacity factor. Getting a grid connection is fundamental to attracting economic investment in a specific area and sometimes it takes priority over the energy economics or the environmental impact.

There are four main ways of reducing the grid capacity dependency problem:

- **The off-grid option to avoid the grid connection altogether**. This was investigated in the previous section and concluded that a significant amount of overgeneration is required to

cover the demand and even with hybrid battery storage, the cost associated with it is larger when compared with grid-connected options.

- **The second option is smart load controls**. If the consumers' loads are flexible and can be shifted away from the peak times, the grid import connections required can be reduced and essentially unlock developments. Because of this, incentivising consumers to shift their electrical load for periods of low demand has become common by offering lower tariffs during off-peak hours, almost all major energy suppliers offer some form of time-of-use tariffs to achieve this [142]. The overall disadvantage of this option is the reliance on consumers and consumer behaviour to reduce and shift the demand. This adds risks to the network operation which the DNOs are reluctant to take.
- **The third option is to use on-site generation and storage, to reduce the peak grid connection requirements.** This is increasingly common, as virtually all battery storage systems suppliers provide some form of peak shaving options for their products. The advantages of communal peak shaving solutions are the system's reliability and implementation simplicity.
- **The fourth option is reducing the peak grid import requirements by reducing the demand.** This is also one of the easiest and cheapest ways to avoid major grid infrastructure reinforcements. However, its biggest disadvantage is the risk associated with the theoretical load estimation. Calculating the precise power demand profile of complex developments for a real-world scenario is impossible and no designer can guarantee that a particular set of first principles assumptions would match the real-world observations. Historically, load profiles are determined empirically but for modern, low-energy developments, there is a lack of good available data to allow load calculations in the initial stages of a development.

Considering the points raised above, this section investigates the peak shaving option for residential applications with ASHP heating to reduce the grid import requirements.

All analyses done in the modelling section use the same demand and generation data set presented above in the off-grid section as well as the same geographical location.

8.2.5 Modelling Results On-grid Scenario.

For the residential on-grid option, I've analysed five scenarios, with different grid import capacities, to understand the hybrid storage benefits vs single chemistry energy storage. The scenarios studied are indicated in Table 8-2. As for the off-grid residential analysis, the steps detailed below have been followed to model the on-grid scenario:

- **Set the power import grid connection.** As mentioned, in a constrained power capacity network, the grid import capacity needs to be reduced.
- **Set the operational data.** The operational data can be set to self-consumption or peak shaving modes or a combination of both. In the on-grid scenario, because the residential load is dominated by the winter demand, the system operates in peak shaving mode between November and April and in self-consumption mode during the summer months, April to September.
- **Set the generation profile**. The generation profile was set to 100% of the load demand with the wind and solar capacities set to two. This is common practice in on-grid applications to achieve net zero operational carbon.
- **Calculate the energy storage required.** Considering the grid-import limitation, the operational data, and the generation profile, I have calculated the storage required to cover the total annual demand.
- **Set the storage ratio.** Set the storage ratio range.
- **Calculate the hybrid storage impact on the system**. For each hybrid storage option and each grid import scenario, I have calculated the utilisation of both chemistries, the equivalent annual cycles, and the total system cost (CAPEX).

Scenario 1. In the first scenario, the grid import capacity is 50 kW, and the renewable generation is 100% of the annual load. As previously mentioned, the peak demand for the residential case study is 263 kW. The power shortfall, to cover the peak load, needs to be provided by the local generation and storage. The calculated storage requirement is 30 MWh, as indicated below.

Scenario 2-5. Similarly, for Scenarios 2 to 5, the grid import capacity is increased progressively from 100 kW to 250 kW. The renewable generation was kept to 100% of the total annual demand.

Table 8-2. Summary table – On-grid scenario – Peak Shaving, Residential

Scenario	Grid Connection kW	Wind Capacity kW	Solar Capacity kW	Energy Storage Capacity MWh
1	50	210	110	30
2	100	210	110	6.4
3	150	210	110	1.2
4	200	210	110	0.9
5	250	210	110	0.7

Figure 8-14 shows the energy storage requirements for each grid import capacity scenario. For Scenario 1, 50kW grid import capacity, the energy storage requirement is 30 MWh, 240 kWh/property, which is still generally impractical and should be considered only in extreme grid-

constrained situations. This drops rapidly to just 1.2 MWh for the 150 kW grid import capacity option. For the last two scenarios, 200 and 250 kW grid import capacity, the storage requirements are below 1 MWh.

This shows that for scenarios 3 to 5, which imply practical storage capacities of 9.6, 7.2 and 5.6 kWh/property, the grid import connection can be reduced by 42.9%, 23.9% and 4.9% from the 264 kW initially required. These are significant differences and can be fundamental to the viability of residential developments.

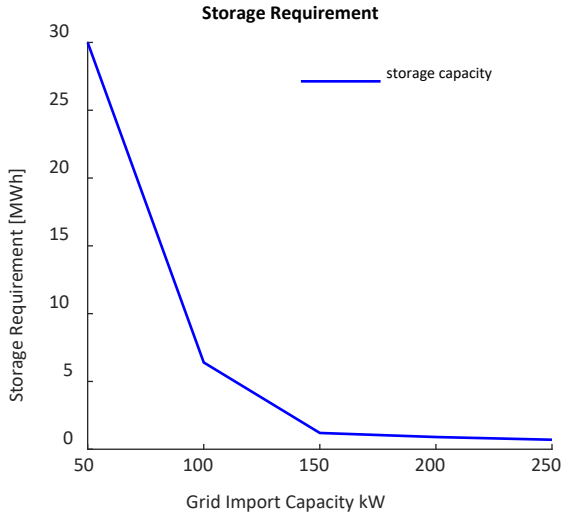

Figure 8-13. Storage Requirement – On-grid Case Study

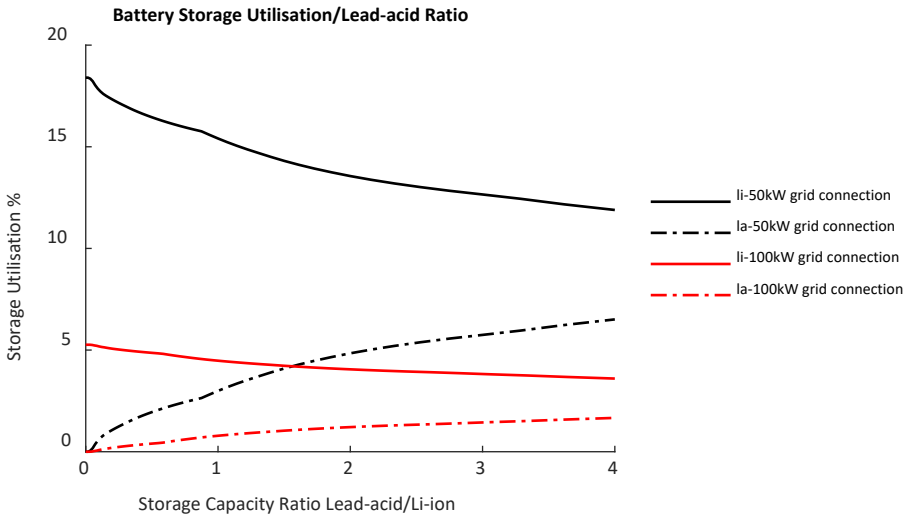

Figure 8-14. On-grid Residential Case Study - Hybrid Battery Storage Utilisation

Figure 8-14 and Figure 8-15 show the hybrid battery storage utilisation for zero to 4 lead-acid to Li-ion hybrid storage ratios. The highest hybrid storage utilisation is for Scenario 1, reaching 18.4% of the total annual load. For scenarios 2 to 5 this drops to 5.26%, 1.47%, 0.7% and 0.41%.

For Scenario 1, the lead-acid string utilisation increases from 0% to 6.5% as the hybrid ratio increases from zero to 4. This is mirrored by the Li-ion utilisation which decreased from 18.4% to 11.9%. Similarly, for scenarios 3 to 5, the lead-acid utilisation increases from zero to 1.66%, 0.52% and 0.16% as the hybrid ratio increases from zero to 4. Practically, this implies that annually, for scenarios 1 to 5, the Li-ion strings supply between 2.8 – 2.5 times the energy delivered by the lead-acid strings, even if the storage capacity between the two is increased to 4.

Overall, it's worth indicating that for scenarios 3-5, the storage system delivers less than 2% of the total annual load, and this can decrease the grid import capacity by up to 42.9% of the initial requirement.

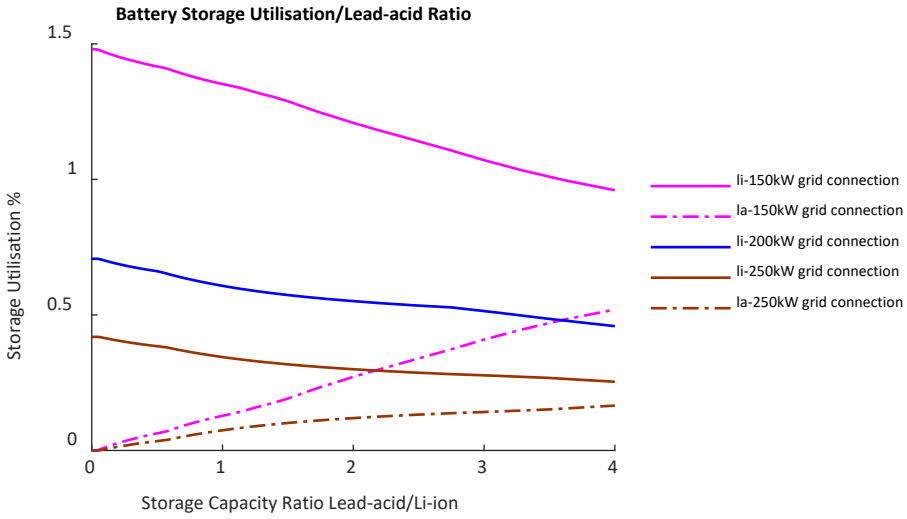

Figure 8-15. On-grid Residential Case Study - Hybrid Battery Storage Utilisation

Figure 8-16 show the equivalent cycles performed annually by the Li-ion and lead-acid strings. The first observation is that both chemistries perform less than 25 equivalent cycles per year. The Li-ion strings are cycled more often when compared with the lead-acid ones, which are cycled a maximum of 2.8 times per year. The second observation is that the Li-ion strings' equivalent cycles increase with the hybrid storage ratio and the lead-acid remains relatively constant. Like the off-grid scenario, this is because the decrease in the Li-ion storage capacity implies a higher number of equivalent cycles.

The large difference in the number of cycles performed by the two chemistries shows that the hybrid ratio can be utilised effectively in peak shaving applications.

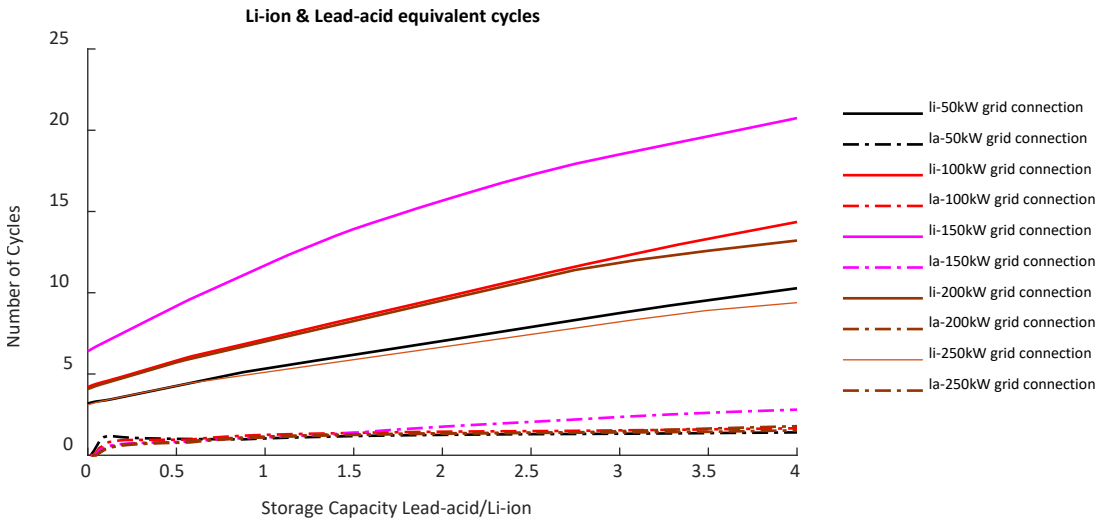

Figure 8-16. Equivalent cycles for Li-ion and lead-acid in hybrid configuration

Finally, Figure 8-17, shows the total system cost for each scenario analysed, as a function of the hybrid storage ratio. The generation and storage system cost decreases as the hybrid ratio is increased. As indicated, the largest absolute cost decrease is for Scenario 1, which indicates a drop from £7 to £5.4 million, a 22.8% cost reduction of the single Li-ion chemistry solution. As the generation system is the same across all scenarios, the percentage cost decrease is driven only by the lead-acid cost reduction and the relative value varies between generation and storage, 22.8% (Scenario 1) and 8.5% (Scenario 5). As the hybrid ratio is increased from zero to 4, for scenarios 2 to 5, the absolute values of the cost reduction, are £0.37, £0.096, £0.074, and £0.061 million. This implies savings between £488 and £12800 per property.

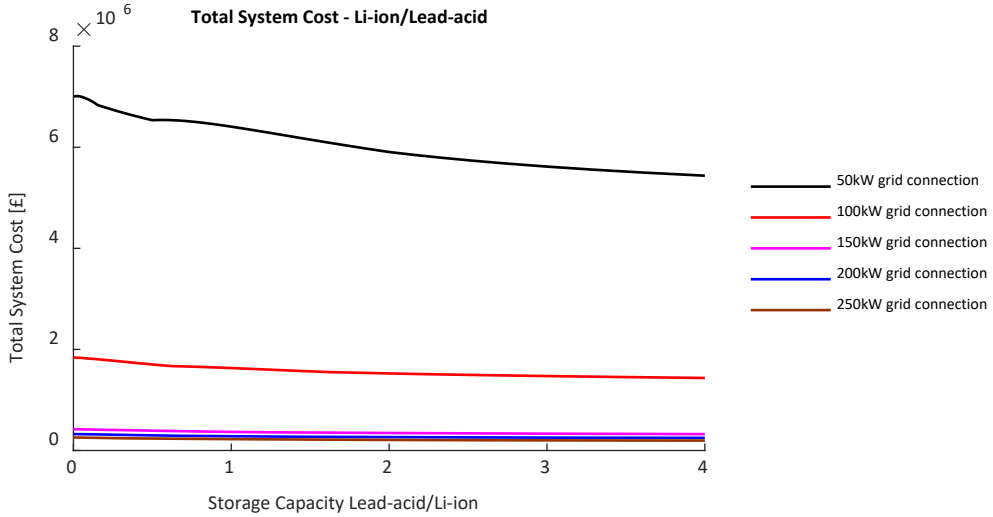

Figure 8-17. On-grid Residential Case Study, Total System Cost

8.3 Hybrid Battery System - Off-grid EV Charging

8.3.1 Introduction

The second application of the Li-ion and lead-acid hybrid battery system investigated in this thesis is an off-grid electric vehicle (EVs) charging station.

The electrification of transport is considered a settled issue, EVs will dominate personal cars and small commercial transportation, as the market share reaches nearly 10% [143]. The clean fuels will be reserved for ships and heavy goods vehicles. The UK modified its ambitious legislation to ban the sale of new petrol and diesel cars by 2030 [144], but it remains committed alongside the European Union to transport electrification by 2035 [144, 145]. While a sizeable percentage of the population is expected to charge their EV at home or at work, public chargers will be necessary to facilitate large-scale EV penetration. By 2030, estimates suggest that the UK will require between 280,000 and 480,000 public chargers [146]. Obtaining a connection to local electricity networks for EV chargers is already time-consuming and expensive, especially for high-power rapid chargers or for locations where existing electricity consumption is high. If improperly managed, these connections can put a strain on local electricity networks.

To maximise the decarbonising effect of the EV transition, the electricity used for charging must be low-carbon. However, with an increased penetration of renewable generation technologies, such as solar or wind, subsequent installation of these technologies can add challenges in terms of maintenance or grid stability due to the variability of renewable generation and the difficulty of matching supply and demand.

Hilton et al. [147, 148] suggest co-locating renewable generation, such as solar, with EV chargers to mitigate the grid impact by using renewable energy to charge the EVs. Mixing such a system with an off-vehicle energy store (OVES), the impact can be reduced further. Companies like [149] have developed small-scale off-grid EV charging stations with wind and solar. The company uses high-performance small-scale wind turbines based on F1 technology.

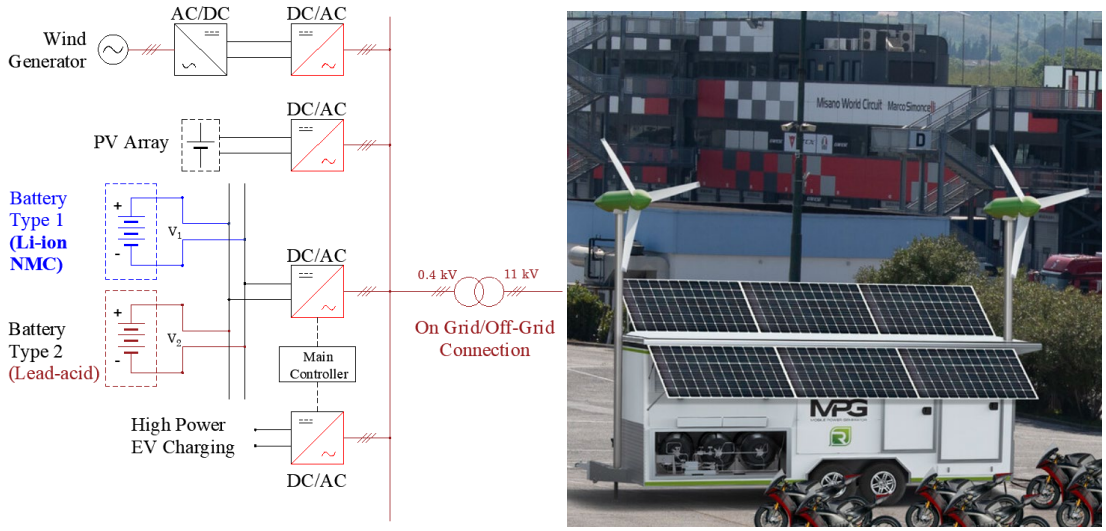

Figure 8-18. Hybrid DC-coupled Energy Storage System with Wind and Solar Generation (a) & FlowGen off-grid EV charging station (b) [149]

Figure 8-18 indicates such a system which makes use of the hybrid Li-ion and lead-acid battery system at Marwell Zoo in Hampshire, UK as a case study. Initially, an energy balance model is used to determine an appropriate size for the OVES and renewable generation capacities based on estimated EV charger use.

8.3.2 EV Charging Load profile

The electrical load profile for the EV charging station and the renewable generation curves detailed in this section was developed in collaboration with colleagues from the Future Electric Vehicle Energy networks supporting Renewables (FEVER) group at the University of Southampton, UK.

The wind and solar generation profiles were obtained using wind speed and irradiance data from Open Meteo for 2019 at Marwell Zoo, UK [150]. The wind profile was then mapped onto the power generation curves for an Aventa AV-7 wind turbine, [151], and a solar PV system with a 20% module efficiency was assumed. The system is based on a charging station with ten 7 kW chargers.

There are no existing EV chargers in place for this case study, so the charger use was modelled based on visitor arrival data for 2019 and the following assumptions:

- For 4 visitors arriving, 1 car registers in the car park.
- 3% of vehicles arriving at the car park are EVs.
- Visitors will park their cars for 4 hours while visiting the zoo.
- EVs have travelled 30 miles and only require replacement of this range when charging.

- EV efficiency of 4 miles per kWh.
- If a charger is free when an EV arrives, the EV will use the charger.
- Cars only arrive during opening hours of 10.00 am to 4.00 pm.

The hourly EV load profile was generated using the decision chart shown below in Figure 8-19.

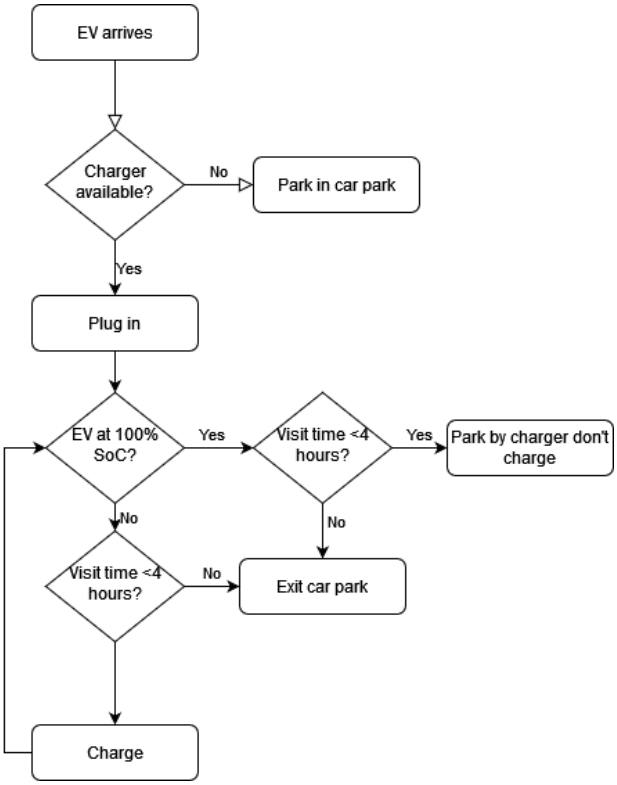

Figure 8-19. Decision chart to determine the EV charging status and LOCATION.

A typical single day EV profile is shown in Figure 8-20 and the whole profile over a year shown in Figure 8-21.

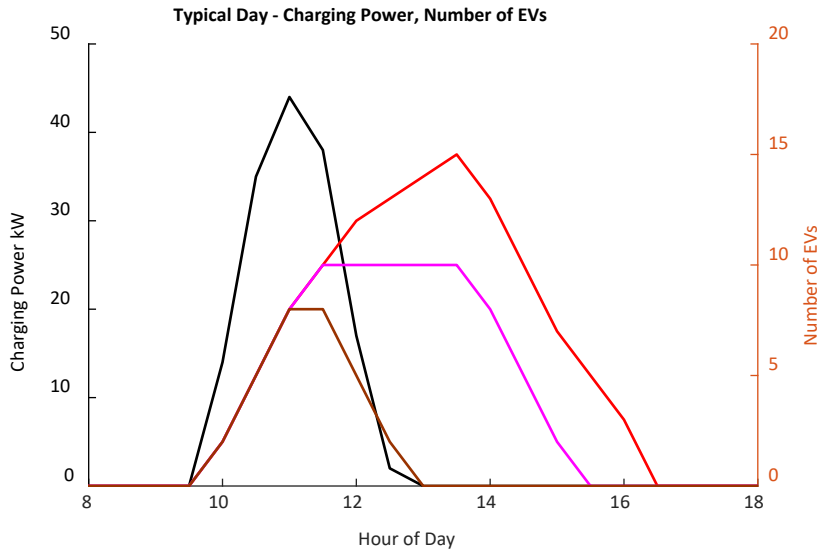

Figure 8-20. EV load with an example day (19/04/2019) showing charging power and the number of EVs parked plugged in and charging.

8.3.3 Hybrid Energy Storage Description

Based on the assumptions mentioned in the previous sections, an annual hourly EV electrical demand profile was generated. The total annual electrical demand for the site is 10,377 kWh and the hourly profile is indicated in Figure 8-21. The interaction between the EV charging demand, storage requirements, and the annual hourly wind and solar generation profiles was modelled, to understand the cost of the overall system and the storage utilisation for various generation & storage scenarios. To cover the entire annual EV electrical load using only renewable generation is not generally possible without energy storage, but in practice, a cost balance between overgeneration and hybrid storage capacity needs to be understood. This means sensitivity analysis is required between three main cost vectors: solar and wind generation (and overgeneration), the cost of Li-ion systems, and the cost of lead-acid battery storage. To understand this, the following five options have been investigated:

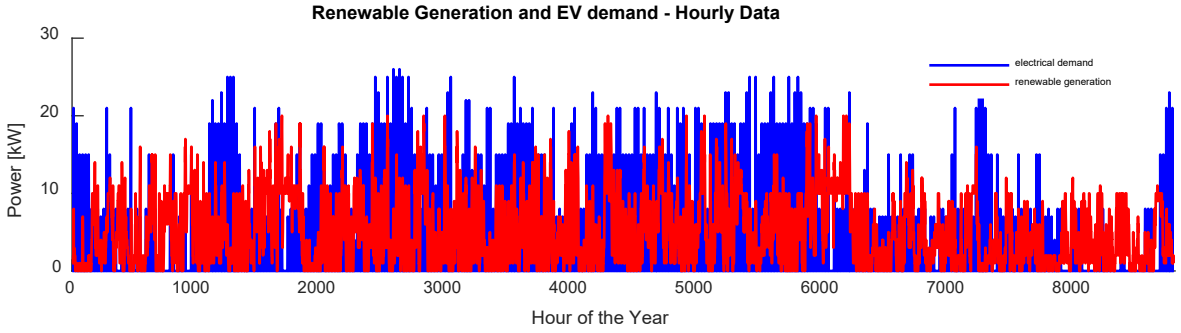

Figure 8-21. Total energy discharged hourly by the storage system.

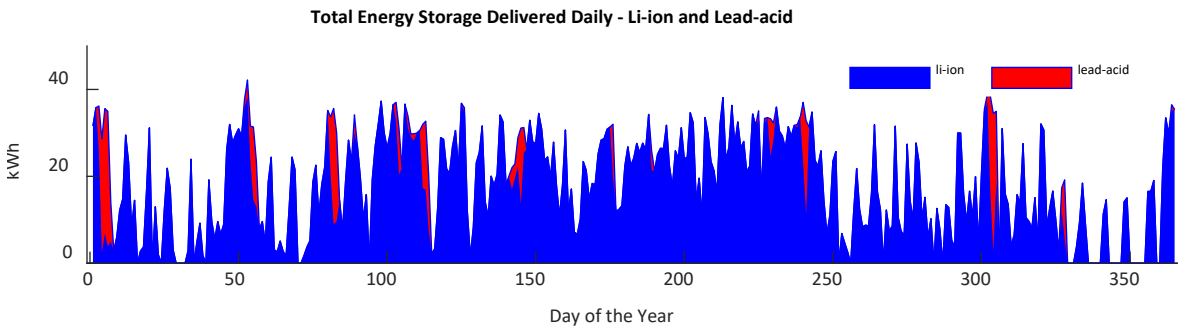

Figure 8-22. Total daily energy delivered by the energy storage system.

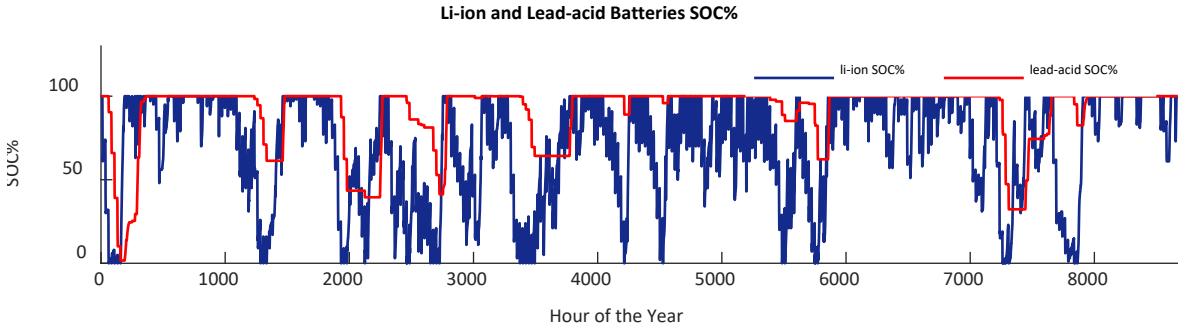

Figure 8-23. State of charge for the energy storage system across the year.

Scenario 1. In this scenario, the total annual electricity generation of wind and solar was set to 160% of the total annual EV charging demand. This accounts for 8 kW of renewable generation capacity with an equal split of 4 kW of solar PV and 4 kW of wind capacity. The 160% overgeneration has been used as a starting point from the practical perspective of considering the average round-trip efficiencies of 95% for the Li-ion and 85% for lead-acid. In this scenario, to cover the entire annual EV load only from wind and solar renewable power, a total of 206 kWh of energy storage capacity is required, assuming a max 90% depth of discharge. To test the economic performance of the different hybrid options, 17 hybrid battery storage systems have been investigated with different hybrid ratios, lead-acid kWh / Li-ion kWh, ranging from 0 (a full Li-ion option) to 5.

Scenario 2. In this scenario, the total annual renewable electricity generation is 200% of the annual EV electrical demand. For the site, this requires a generation capacity of 10 kW, 5 kW of solar, and 5 kW of wind. For the complete renewable load coverage, the total storage requirement is 191 kWh, assuming a maximum depth of discharge of 90%. Similarly, a sensitivity analysis for the lead-acid kWh / Li-ion kWh capacity ratios ranging from 0 to 5 was tested.

Scenario 3. In this scenario, the total annual renewable electricity generation is 300% of the total annual electrical EV demand. To achieve this, a total of 15.2 kW of on-site renewable capacity is required, assuming an equal split of 7.6 kW solar and 7.6 kW wind. The total storage requirement

to cover the entire EV load is 156 kWh. Sensitivity analysis was carried out for the same lead-acid kWh / Li-ion kWh storage capacity ratios.

Scenario 4. In this scenario, 600% of renewable electricity generation was considered. This translates to 30.2 kW of renewable capacity with an equal split of 15.1 kW of solar and 15.2 kW of wind. The storage requirement is 105 kWh, and similar lead-acid kWh / Li-ion kWh capacity ratios have been investigated.

Scenario 5. The last scenario considers 1200% renewable electricity generation of the total annual EV demand. This amounts to 60.4 kW of renewable capacity, 30.2 kW of solar, and 30.2 kW of wind. The storage capacity required is 105 kWh, identical to the storage requirement of Scenario 4. Increasing the total electricity generated from renewable sources beyond a certain point, the storage capacity requirements reach a plateau.

To calculate the total storage requirements and the hybrid ratios the following three steps have been followed:

- Set the renewable generation as a percentage of the total annual load requirement assuming an equal split of installed capacity between wind and solar.
- Set the hybrid storage ratio.
- Increase the total storage capacity keeping the hybrid ratio constant until the entire load can be covered by only solar, wind and storage.

Table 8-3. Renewable Generation and Hybrid Energy Storage Scenarios - Summary

Scenario	Solar kW	Wind kW	Generation % annual	Energy Storage kWh
1	4	4	160	206
2	5	5	200	191
3	7.6	7.6	300	156
4	15.1	15.1	600	105
5	30.2	30.2	1200	105

For illustration purposes, Figure 8-21, Figure 8-22, Figure 8-23, indicate the general hybrid battery storage operation for Scenario 1 and similar observations can be made for the other options. Figure 8-21 indicates the annual hourly EV demand profile plotted against 8kW of renewable wind & solar capacity. A proportion of the generation will be consumed directly by the EVs, and the rest will be stored for later usage. Figure 8-22 indicates the daily energy delivered from the energy storage system to cover the daily EV electricity demand. Generally, the Li-ion part of the hybrid system is cycled more often than the lead-acid cells. This is also illustrated in Figure 8-23, which shows the hourly SOC across the year for both Li-ion and lead-acid storage capacities.

8.3.4 Financial and Technical Assumptions

The financial and technical assumptions are identical to the residential case study.

8.3.5 Hybrid Energy Storage Analysis Results

Figure 8-24 shows the total system costs for the overall generation and hybrid storage systems scenarios plotted against various lead-acid kWh / Li-ion kWh hybrid capacity ratios.

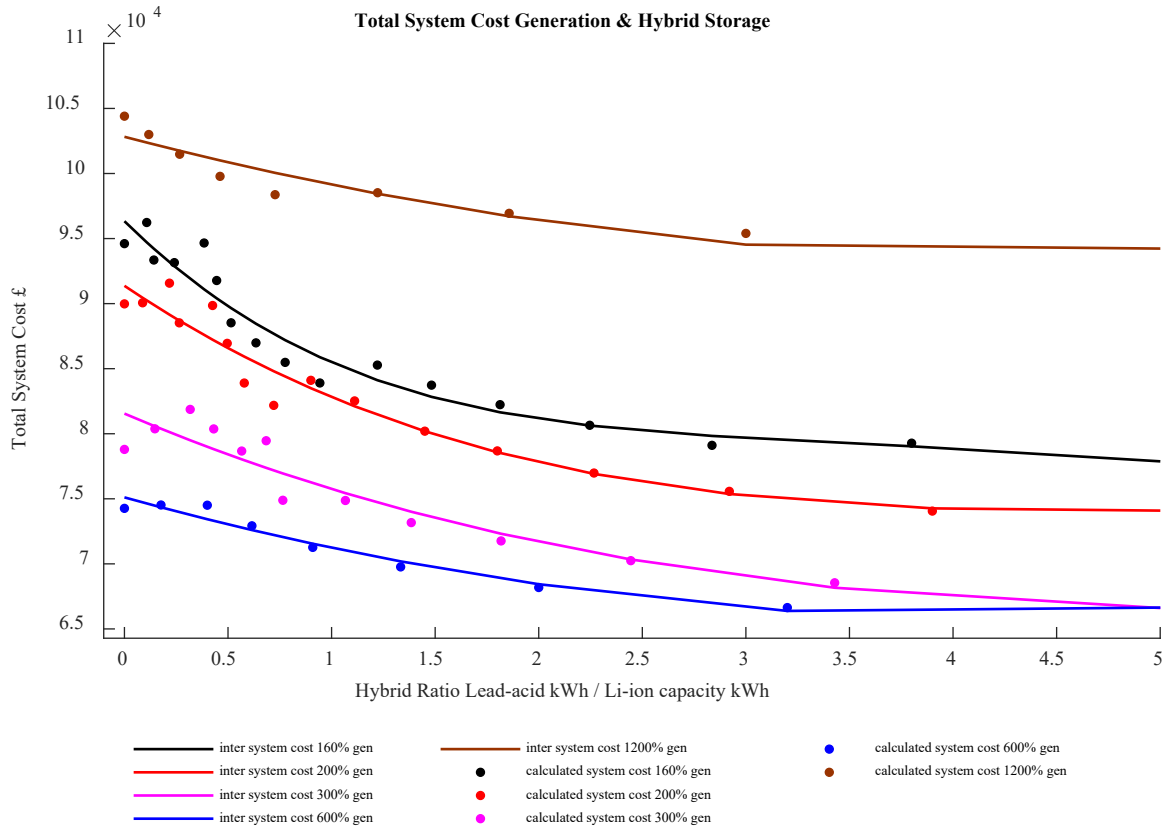

Figure 8-24. Total system cost of generation and hybrid energy store vs ratio of lead-acid to Li-ion capacity with a range of installed generation capacities

The first observation is that the cheapest option is Scenario 4 which assumes a generation profile of 30.2 kW of renewable PV and wind capacity. This amounts to a total annual energy generation of 600% of the total yearly EV electricity demand. For this scenario, the PV system cost is £11300 CAPEX and £611/year OPEX & REPEX. The 15.1 kW wind capacity cost is £18800 CAPEX and £1012/year OPEX & REPEX. The total storage capacity required for this scenario is 105 kWh. The cost associated with this depends on the ratio between the two chemistries. For the single Li-ion chemistry storage solution, the cost is £44000, which drops by 17.39% for a hybrid storage option with a storage ratio of Li-ion kWh / lead-acid kWh equal to 5. The overall generation and storage

system cost stands at a maximum of £74000 for the Li-ion only battery solution. This drops to £66500 for a hybrid system of ratio 5, a drop of 10.3%.

The second observation is that Scenario 5 is the most expensive option. Considering that it requires a similar amount of energy storage capacity to cover the entire annual EV demand, the percentage price reduction by using a hybrid storage option is slightly less than 10.3%. The total system cost, including generation and storage, drops from a maximum of £10,4400 when using a single Li-ion chemistry storage system, to £93,900 if a hybrid storage system of ratio 5 is used.

The third observation is that the biggest price reduction for switching to a hybrid storage system is for Scenario 1. This is not surprising as this requires the largest amount of storage because of its small yearly electricity generation, 160% of the total yearly demand. A large storage capacity implies that greater savings are possible for higher hybrid ratios by replacing parts of the Li-ion cells with cheaper lead-acid alternatives. For Scenario 1, the fastest price drop is achieved between the 0 and 2 hybrid storage ratios. For the simple Li-ion chemistry solution, the total system cost is £94600 and this drops to £81200 when using a hybrid option of ratio 2, a fall of 14.13% in the total cost.

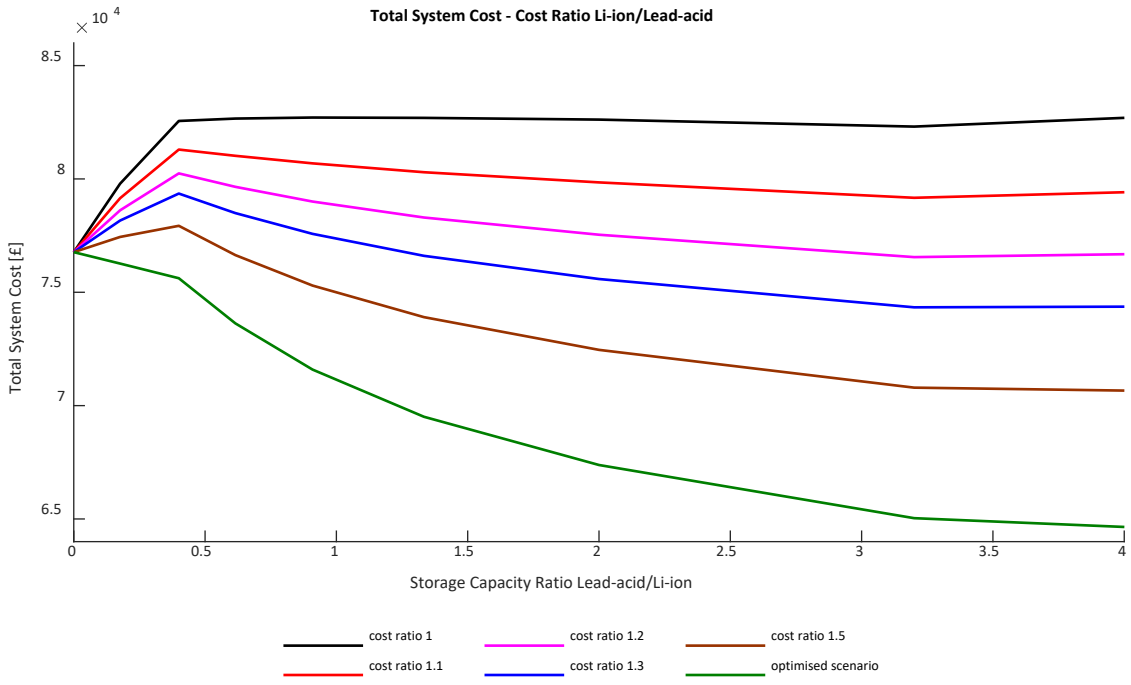

Figure 8-25. System Cost - Price Ratio Li-ion to Lead-acid

As for the residential case study, Figure 8-25 shows the total system cost for the optimised solution (Scenario 4) as a function of the kWh cost ratio between Li-ion and lead-lead. As indicated, if the cost ratio between the two chemistries falls below 1.3-1.5, the hybrid system is no longer justified, as minimum cost reductions are possible.

As shown above in Figure 8-23, during operation, the Li-ion part of the hybrid system does the frequent cycling, and the lead-acid battery strings cover the longer, intraday cycles.

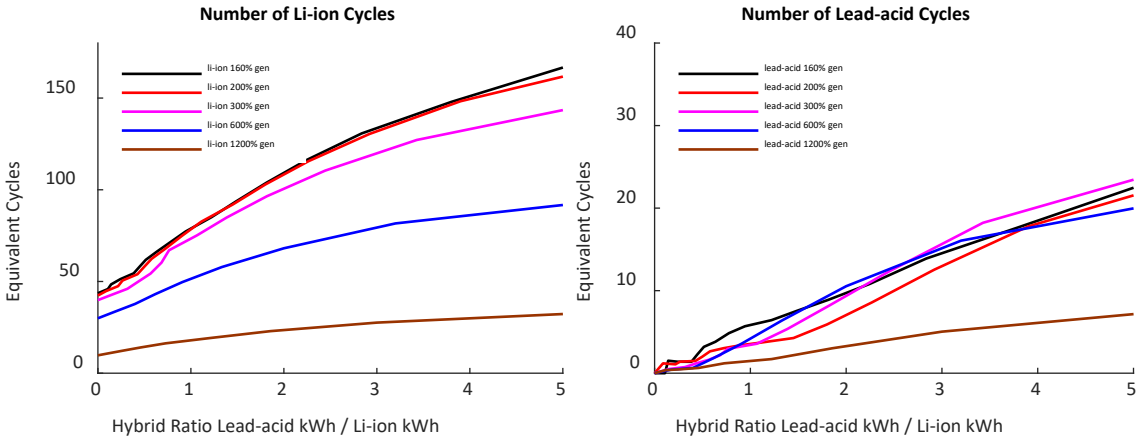

Figure 8-26. Number of cycles of Li-ion (a) and lead-acid (b) vs ratio of lead-acid to Li-ion for a range of scenarios with differing generation capacities.

Figure 8-26 shows the total equivalent cycles done by Li-ion (a) and lead-acid (b) cells across the year for each scenario investigated. For simplicity, an equivalent cycle is the total yearly energy discharged by each chemistry divided by the energy storage capacity of each chemistry, assuming a maximum of 80% depth of discharge (DOD) for Li-ion and 50% DOD for lead-acid chemistry. As indicated, for all scenarios, Li-ion does more equivalent cycles across the board. Also, Li-ion is cycled harder when the hybrid ratio increases. Taking Scenario 1 as an example, the number of Li-ion equivalent cycles increases from 44/year, for the simple Li-ion chemistry option, to 169/year for a hybrid storage system of ratio 5. Also, as we move from Scenario 1 to Scenario 2 the number of equivalent cycles decreases as less energy storage is required. However, the Li-ion cycle range indicated in Figure 8-26 has a broader spread across the different generation scenarios when compared with lead-acid. This shows that the number of short, frequent storage cycles is reduced when a larger PV and wind system is installed. The same is valid, but to a lower extent, for the longer intraday cycles.

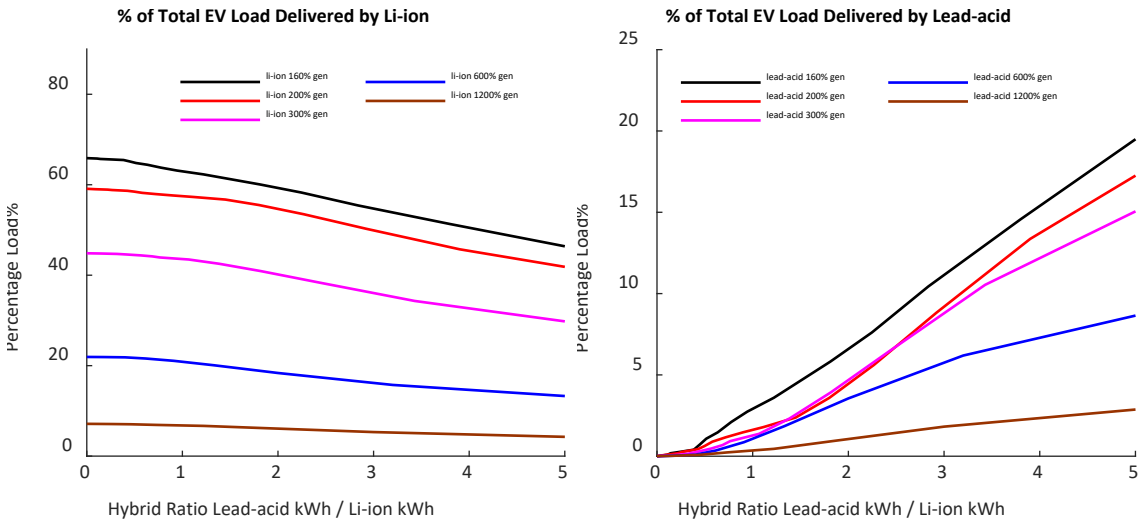

Figure 8-27. Percentage of the annual load covered separately by the Li-ion (a) and lead-acid (b) cells vs ratio of lead-acid to Li-ion for a range of scenarios with differing generation capacities.

As the annual load is covered entirely by renewable power and storage, part of the load will be covered directly by the generation, and the rest will be supplied by the storage system. Figure 8-27 indicate the battery utilisation, i.e., the percentage of the annual load covered separately by the Li-ion (a) and lead-acid (b) cells. The total storage utilisation can be as high as 65.9% for Scenario 1 and lower than 8% for Scenario 5. As indicated above, for all Scenarios 1-5, regardless of the Li-ion and lead-acid hybrid ratios, the Li-ion has a higher utilisation rate, than the lead-acid battery.

For example, in Scenario 1, Li-ion cells cover between 65.9% of the load for a pure Li-ion storage solution and 47.7% for the hybrid ratio of 5. The lead-acid reaches a utilisation rate of 20.19% for a hybrid ratio of 5. The remaining 34.1% is supplied directly by the wind and solar generation system.

At the other end of the scale, for Scenario 5, the Li-ion utilisation rate drops from 7.14% for the simple 100% Li-ion solution to 3.91% for the hybrid system with the lead-acid kWh / Li-ion kWh ratio of 5. Lead-acid, on the other hand, covers a maximum of 3.22% of the load for a hybrid ratio of 5.

8.4 Hybrid Battery Systems for Industrial Demand

8.4.1 Introduction

The next case study for the hybrid Li-ion and lead-acid battery storage system considered, is an industrial unit supplied by renewable wind and solar electricity, for both off-grid and on-grid

options. Like in the residential case study, the project is in the UK, Coedely – Ynysmaerdy area, and uses the same technologies and financial assumptions described in the previous sections.

The arrangement studied is indicated in Figure 8-28. The collocated PV, wind and hybrid storage plants are connected to an 11kV network, which feeds the industrial consumer wider network. The system can be configured using several switches in both on-grid and off-grid configurations.

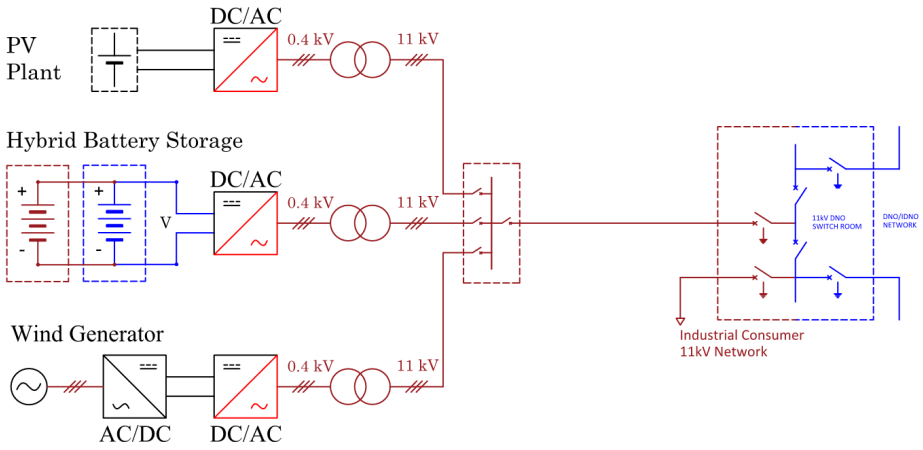

Figure 8-28. Industrial Consumer, Renewables and Storage Supply

The load profile for the industrial site was determined using publicly available data for light industrial sites [152]. The dataset was cleaned and arranged in formats to be read by the techno-economic model developed for this project. The final load factor for the electrical demand profile analysed is 47%, and the peak was scaled to 1MW. The total annual demand is 4124.4 MWh/year.

8.4.2 Off-grid Industrial Case Study – Results

Like for the residential case study, the research methodology assumes six overgeneration scenarios, 100%, 200%, 300%, 500%, 800% to 1300%, using hybrid storage with various lead-acid to Li-ion ratios between zero and 4. For each overgeneration option, I have calculated the total energy storage requirement, and based on the results, the potential for hybrid storage ratios is investigated.

Scenario 1. For Scenario 1, the overgeneration capacity is 100%, the wind & solar generate 100% of the total annual demand. The solar and wind capacities are 900 kW and 1900 kW. The ratio between the two is set to achieve, as much as possible, uniform monthly electricity generation across the year.

Table 8-4. Off-grid, industrial scenarios

Scenario	Solar Capacity kW	Wind Capacity kW	Generation % annual demand	Energy Storage Capacity MWh
1	900	1900	100%	600
2	1800	3800	200%	65
3	2700	5700	300%	45
4	4500	9500	500%	34
5	7200	15200	800%	27
6	11700	24700	1300%	19

Scenario 2. For Scenarios 2 to 6, the wind and solar capacities are increased from 200% to 1300% as indicated in Table 8-4. For each scenario, the new remaining demand profile will have to be covered by the hybrid storage system, thus offering multiple options for hybridisation.

Figure 8-29 and Table 8-4 indicate the total energy storage requirement for each scenario to achieve 100% of the annual load. As shown, there is a 9.2x decrease in the storage capacity required, when the overgeneration is increased from 100% to 200%. For scenarios 2 to 5, the energy storage required is 65, 45, 34, 27 and 19 MWh. At the same time, the self-consumption decreases from 62.2%, for Scenario 1, to 6.52% for Scenario 6.

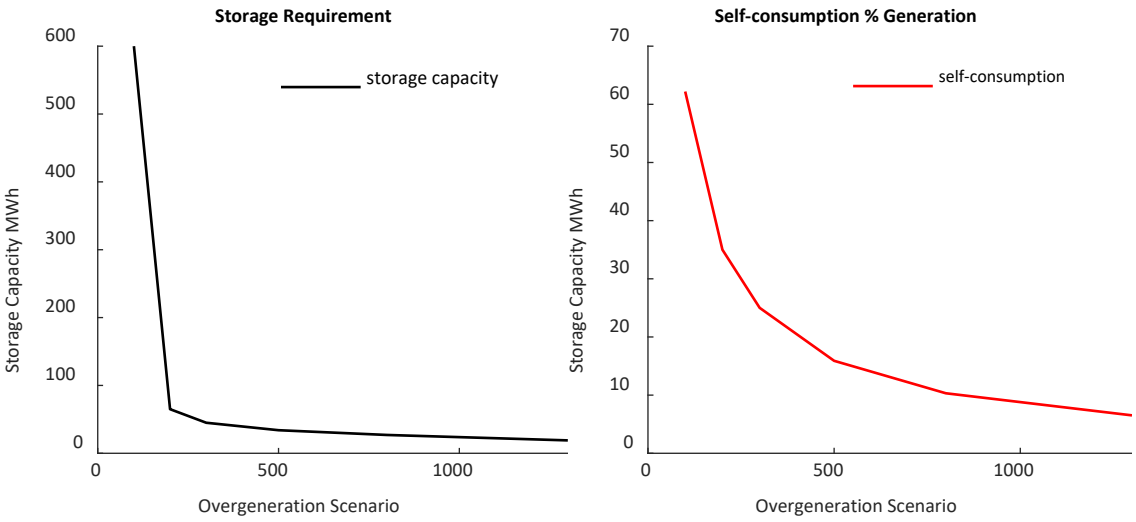

Figure 8-29. Industrial Case Study, Storage Requirements (a) and Self-consumption (b)

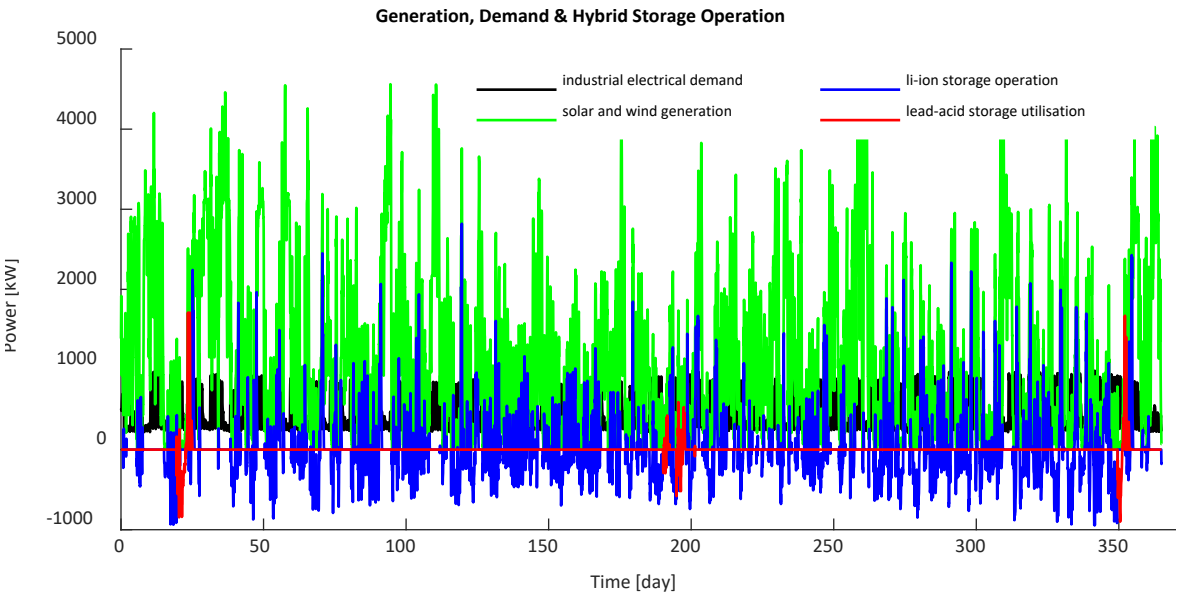

Figure 8-30. Industrial Case Study – Load Profile, Wind & Solar Generation, Hybrid Storage Operation

For illustration purposes, Figure 8-30 shows a typical annual interaction between the generation, storage, and the industrial load profile for Scenario 2, with a hybrid storage system of lead-acid to Li-ion ratio of 1. As visually observed, the Li-ion string charges and discharges daily across the year (blue), and the lead-acid chemistry is mostly inactive (red).

Figure 8-31 indicates the hybrid storage utilisation for each scenario and hybrid ratio. The first observation is that in a hybrid storage configuration, the Li-ion strings always cover a higher percentage of the annual demand when compared with the lead-acid acid, except for the first scenario which is the outlier. In Scenario 1, the large energy storage capacity required is necessary to address any seasonal electricity demand. For a non-hybrid Li-ion storage option (zero lead-acid to Li-ion hybrid storage ratio) the storage utilisation is 37.8%, 24.8%, 19.5%, 14.7%, 11.4% and 9% for Scenarios 1 to 6. At the other extreme, the Li-ion strings utilisation decreases to 21.75%, 17,65%, 14.33%, 11.96%, 9.6% and 7.26% when the hybrid ratio is increased to 4. The second observation is that the lead-acid strings utilisation doesn't increase above 7.5%, except for Scenario 1 when it reaches 16.1%, for the hybrid ratio of 4. This implies that the lead-acid strings are underutilised, and hybrid storage options can be used to decrease the overall generation and storage system cost.

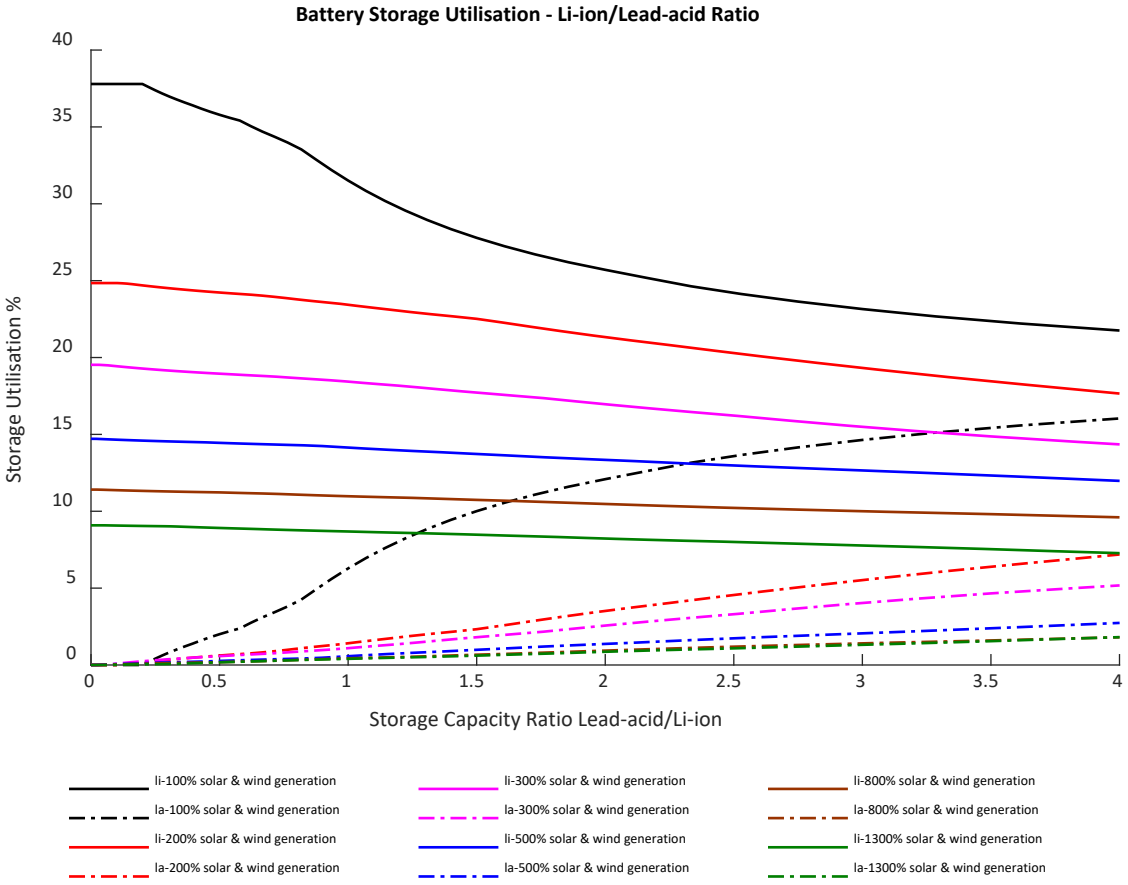

Figure 8-31. Off-grid Hybrid Battery Storage Utilisation

Figure 8-32 shows the annual equivalent cycles for both Li-ion and lead-acid strings for Scenarios 1-6. Overall, as in the previous case studies, the Li-ion strings are cycled harder, when compared with the lead-acid strings, which perform below 6.2 cycles/year, across all scenarios. In comparison, except for Scenario 1, the Li-ion chemistry performs between 16 and 82 cycles/year. It's worth mentioning that the number of Li-ion cycles increases with the hybrid ratio because the total Li-ion storage capacity is reduced. Together with the hybrid utilisation results, this shows that there are peaks in the energy storage usage profile and the hybrid Li-ion and lead-acid system can be used to reduce the overall generation and storage system cost.

Figure 8-33 shows the total cost of the off-grid solar, wind and hybrid battery storage for each scenario. The most expensive option, £142 million, is Scenario 1 (100% overgeneration), which uses a single chemistry (Li-ion) option. This is an impractical solution as a firm connection of £14.2 million/MW is 50x above what would be considered economically viable (From my experience in the UK power market, in 2022-2023, the upper limit for a connection cost, to be considered economically viable, is £0.25 million/MW). Because Scenario 1 has the highest storage capacity requirement to meet the site demand, we observe a 26.1% cost decrease

between a single chemistry storage system (hybrid ratio zero) and a hybrid storage with a ratio of 4.

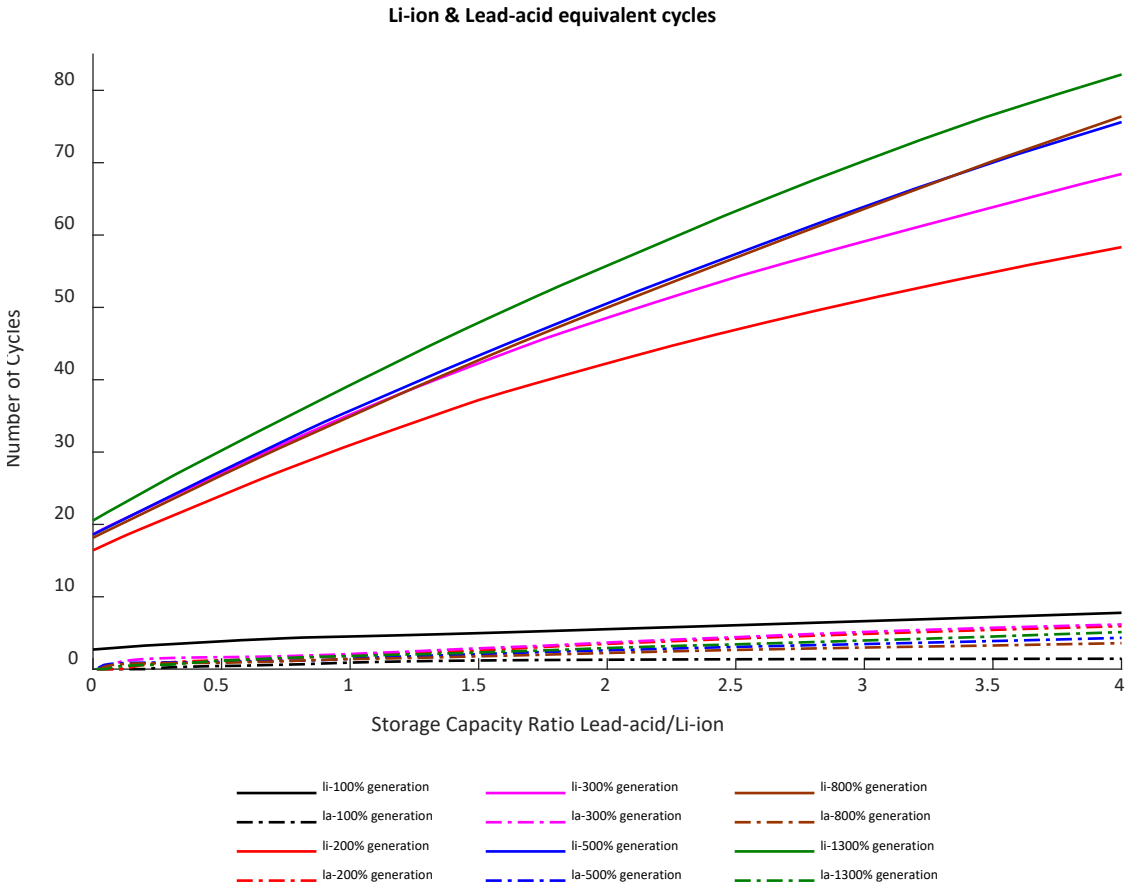

Figure 8-32. Hybrid Storage System, Off-grid – Annual Equivalent Cycles

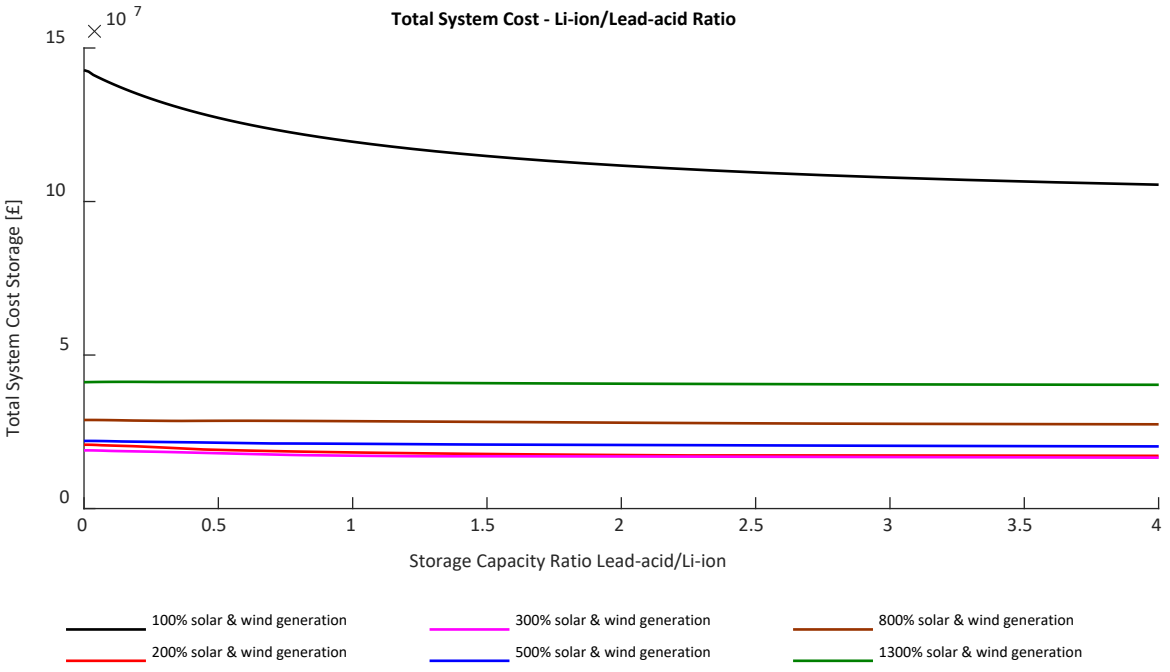

Figure 8-33. Off-grid Industrial Case Study - Total System Cost.

The cheapest generation and storage option, using a single chemistry system, is £18.9 million, for Scenario 3 (300% overgeneration). This decreases by 12.69% to £16.5 million for a hybrid lead-acid and Li-ion energy storage system of ratio 4. This is still above the practical limits and should only be considered when alternatives are not possible.

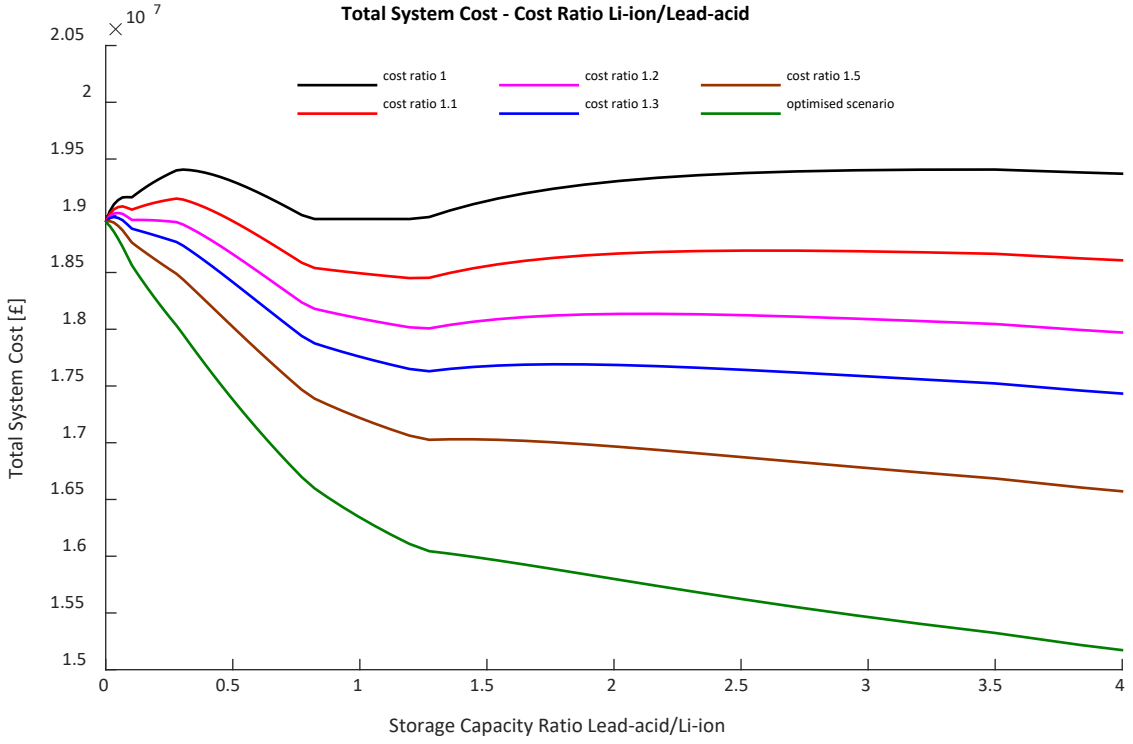

Figure 8-34. System Cost - Price Ratio Li-ion to Lead-acid

Figure 8-34 indicates the total system cost for Scenario 3 (optimised solution) as a function of the kWh cost ratio between Li-ion and lead-lead. The cost savings potential for different kWh cost ratios between the two chemistries reduces as the Li-ion price decreases. Crucially, if the cost ratio between the two chemistries falls below 1.1, the hybrid system is no longer justified, as minimum cost reductions are possible.

8.4.3 On-grid Industrial Case Study – Results

This section analyses the on-grid scenario for the industrial case study. Like the residential case investigation, the objective is to minimise the grid import connection, using local renewable and storage generation. The peak shaving application for renewable and storage is one of the four main ways to reduce the grid power import capacity. The strategy is widely used for industrial loads.

To understand this, I have analysed 5 grid import scenarios, 20%, 40% 60%, 80% and 85% of the grid connection kW import requirement if the system were to be supplied only from the local power grid. Considering the reduced load profile seasonality, the model was run using peak shaving mode across the year. For each scenario, I have calculated the storage requirement to cover 100% of the electrical demand and I analysed the usage profile for hybrid storage ratios between zero (simple Li-ion storage option) and 4. For all scenarios, the overgeneration was set to 100% and the ratio between wind to solar generation capacity, was 2.1.

The storage requirement for each grid import scenario is indicated in Table 8-5. As expected, the storage decreased from 57 MWh to 0.5 MWh as the grid import capacity increased from 200 to 850 kW.

Table 8-5. Industrial Case Study – On-grid Scenarios

Scenario	Grid Connection kW	Wind Capacity kW	Solar Capacity kW	Energy Storage Capacity MWh
1	200	900	1900	57
2	400	900	1900	22
3	600	900	1900	5.5
4	800	900	1900	0.9
5	850	900	1900	0.5

Figure 8-35 and Figure 8-36 show the hybrid battery storage utilisation for each grid import scenario. There is a significant decrease in both storage capacity & utilisation as the grid import limitation is reduced. For Scenario 1 (20% grid import capacity limitation), the maximum storage utilisation is 15.7%, and this decreases to 5.22%, 1.55%, 0.09% and 0.035% for Scenarios 2-5.

For Scenario 1, the Li-ion utilisation decreases from 15.7% (single Li-ion chemistry solution) to 9.19%. Similarly, for Scenarios 2-5, the Li-ion utilisation decreases by 3.36%, 0.66%, 0.039% and 0.016% between the same hybrid ratio range. At the same time, as the hybrid ratio is increased, the lead-acid utilisation ratio reaches 6.68%, 1.88%, 0.49%, 0.052%, and 0.018% for Scenarios 1-5. Another observation is that the relative utilisation increases between the lead-acid and Li-ion strings to above unity for the last two scenarios.

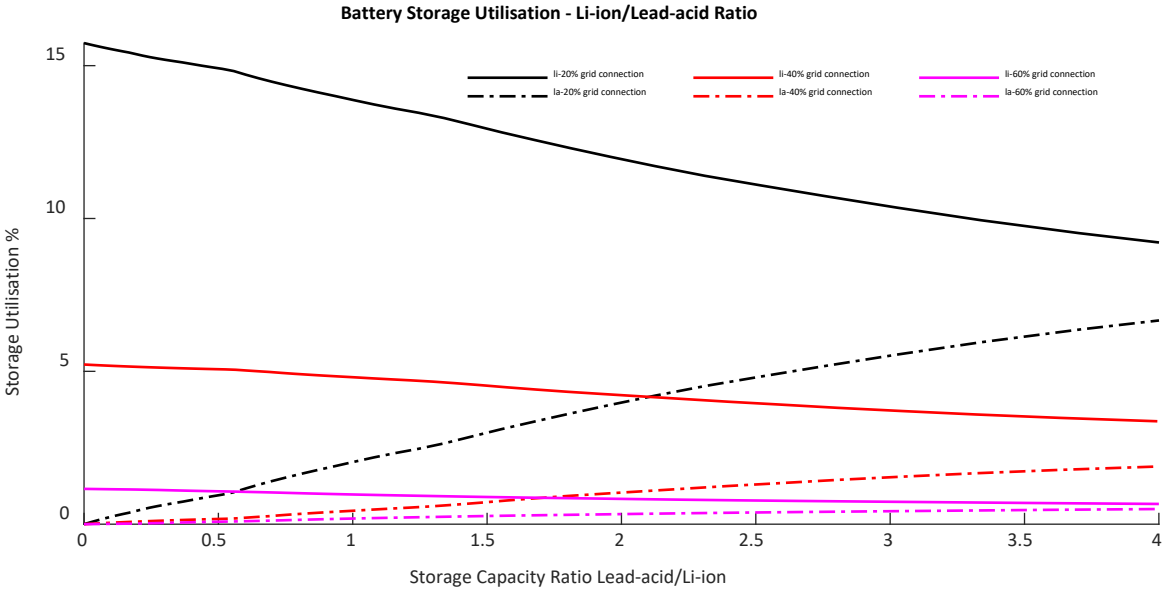

Figure 8-35. On-grid Industrial Case Study – Battery Storage Utilisation, Scenario 1-3

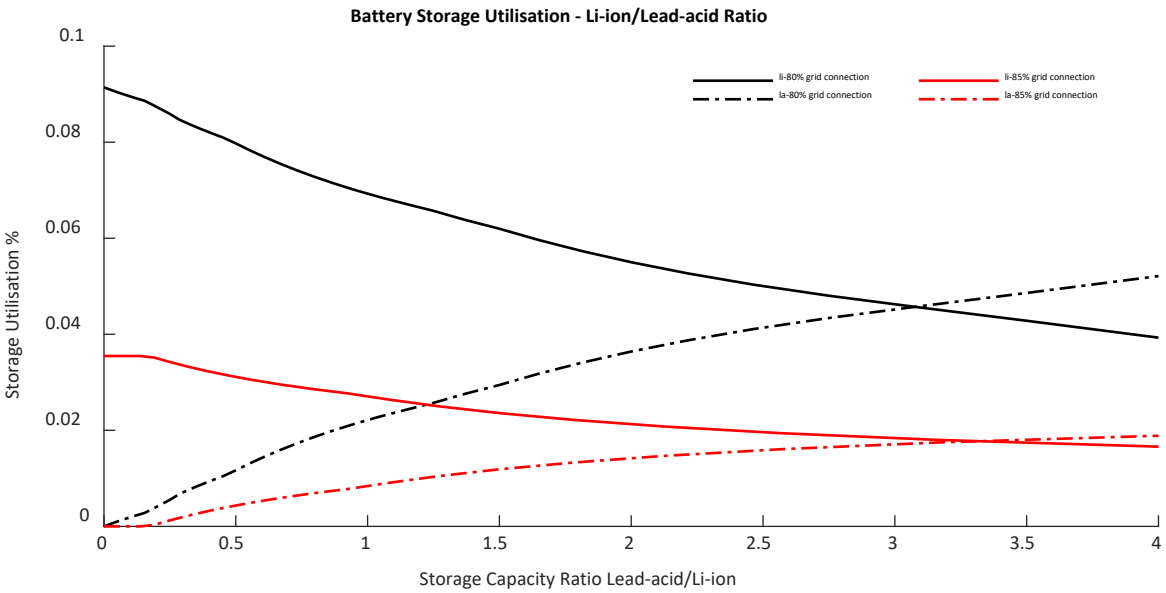

Figure 8-36. On-grid Industrial Case Study – Battery Storage Utilisation, Scenario 4-5

Figure 8-37 shows the annual equivalent cycles for the lead-acid and Li-ion strings. As in the previous cases, the Li-ion strings are cycled more often than lead-acid ones across all scenarios but, as the grid import capacity is increased, the gap between the two decreases. For Scenario 1,

Li-ion strings perform between 11.8 cycles/year, for a single chemistry energy storage solution, to 34.7 cycles per year when the hybrid ratio is increased to 4. As the grid import capacity is increased, this range is reduced to between 3 and 7.1 cycles/year. The maximum lead-acid equivalent cycles are 6.2 cycles/year. The difference between the two shows that hybrid storage systems can be used in peak shaving applications for load profiles of this type.

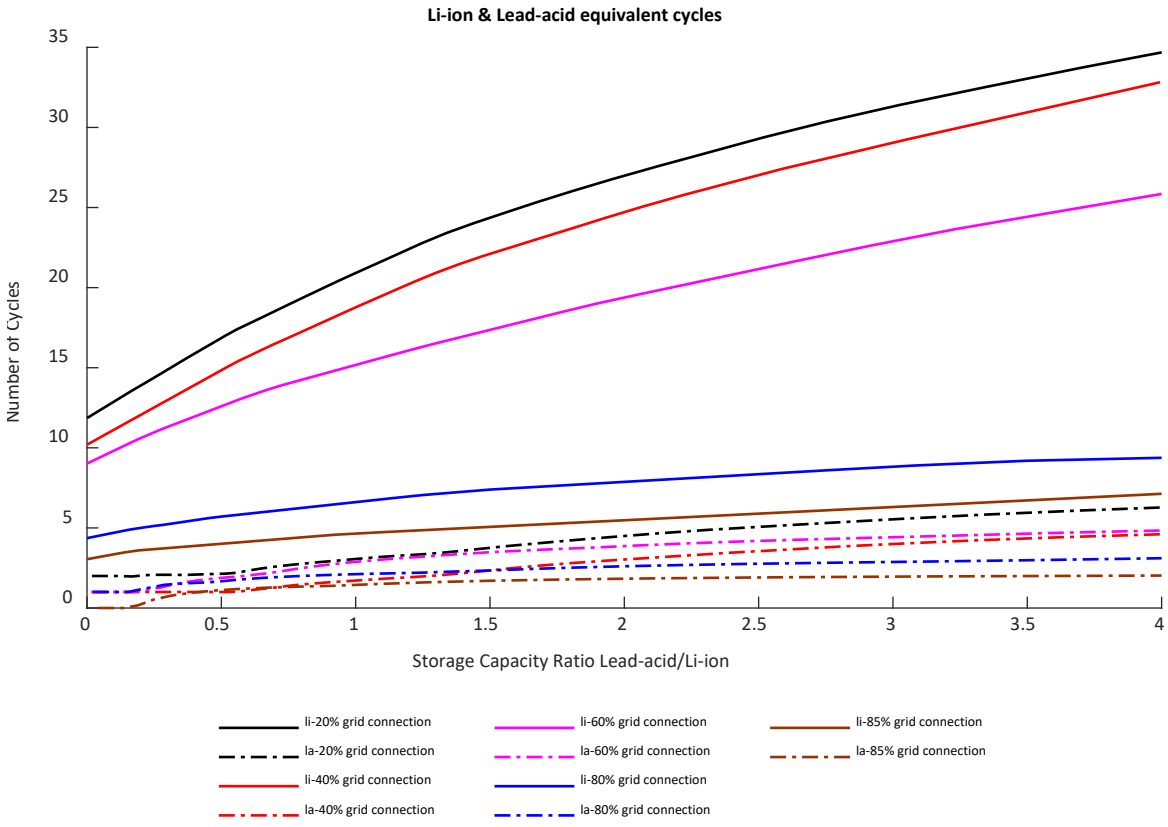

Figure 8-37. Hybrid Storage System, On-grid – Annual Equivalent Cycles

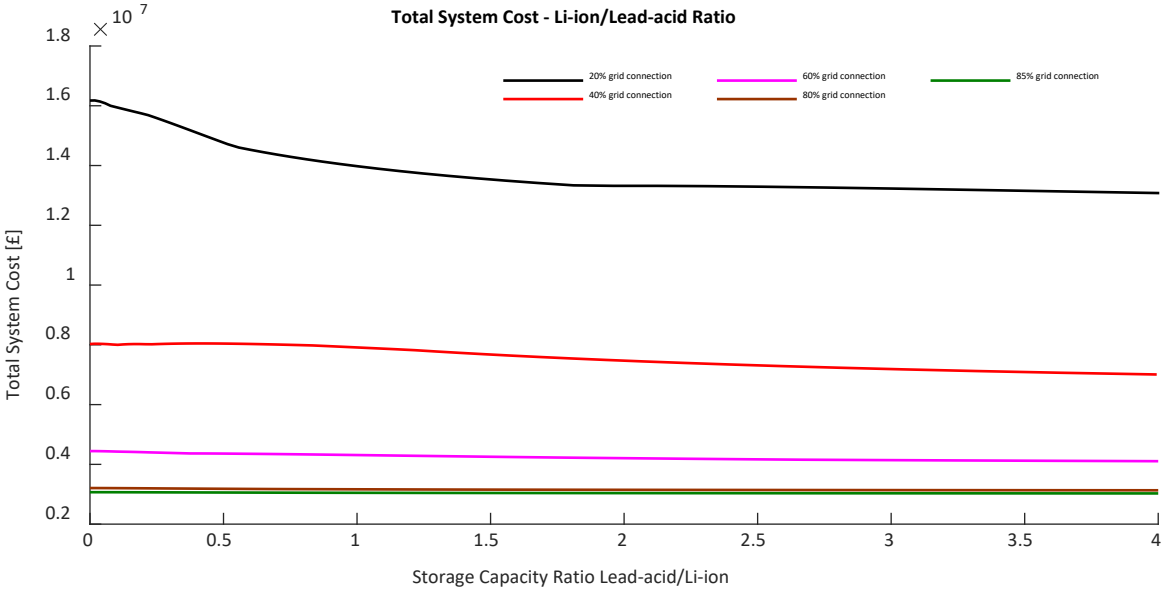

Figure 8-38. On-grid Industrial Case Study - Total System Cost.

Figure 8-38 shows the total generation and hybrid storage system cost for the on-grid, peak shaving application for the analysed grid import scenarios. As expected, Scenario 1 is the most expensive, between £13-16 million and shows the largest cost reduction of 18.75% by increasing the hybrid ratio from zero to 4. The cheapest solution is Scenario 5, £3.027-3.069 million, and benefits the least by using a hybrid solution, recording only a 1.36% cost reduction by increasing the hybrid ratio between zero and 4.

8.5 Hybrid Battery System – Front-of-the-Meter (FTM) applications

8.5.1 Introduction

The next case study considered as potential applications for the hybrid Li-ion and lead-acid energy storage system is the renewable generation FTM and plants. Apart from the cumulative storage capacity of the UPS and standby power supply applications, the FTM applications are one of the fastest-growing markets for battery storage. In the UK alone, in the last decade, this has increased from practically peripheral systems to above 3.5GW/3.5GWh storage capacity. Most of the added capacity uses Li-ion technologies but other chemistries and technologies are growing rapidly. The complete detailed market description and the operations performed by energy storage assets are beyond the purpose of this research. However, most of the FTM batteries help the National Grid balancing operations by offering services, like frequency response or by operating in different arbitrage markets. In the UK, new services are being created and modified continuously by the National Grid Electricity System Operator but, at the time of writing, most of FTM battery storage revenue streams come from Dynamic Containment Low/High and energy arbitrage in the wholesale and balancing markets.

A high-voltage architecture for a general FTM battery system is indicated in Figure 8-39. This usually includes a series of containerised battery storage systems, connected to dedicated transforms, which raise the voltage to the local available DNO network connection points. In the UK, the FTM systems are connected at all voltage levels, from 11kV to 400kV. The energy storage capacities have also increased in the last decade, reaching hundreds of MWh as of December 2023.

The vast majority of the FTM projects, including wind, solar or battery storage plants are standalone units. However, in recent years, due to grid connection restrictions, the FTM colocation option has gained increasing attention and almost all new renewable & storage projects include some form of asset colocation. The main advantages of this are the grid connection sharing and the synergy between the generation and on-site energy storage. The grid connection sharing is possible due to the complementary nature of wind & solar generation profiles and the battery storage operating schedules. Generally, when the national grid generation outstrips demand, the grid frequency increases and based on the frequency variations, the battery storage (located next to PV or wind plants) charges directly from the on-site renewables, without utilising the grid connection. When the opposite happens and the demand outstrips supply because of the shortfall in renewable generation, the frequency decreases and the discharge battery functions are activated. This is possible because the grid export capacities are underutilised at that time (shortfall in renewable generation). These complementary operation profiles for both generators and storage, alongside the grid connection restrictions, make colocation projects the cheapest and quickest way to expand the renewable and storage capacities without major transmission and distribution grid reinforcements.

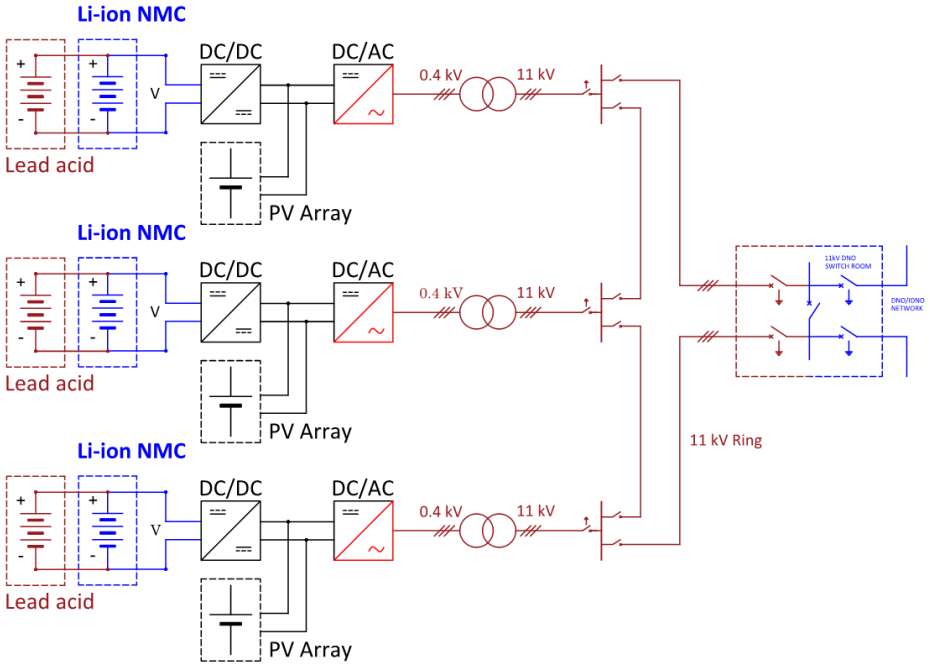

Figure 8-39. FTM, Collocated PV and Hybrid Battery Storage

A particular colocation option is the DC-coupled, PV and battery storage systems, with an oversized DC:AC ratio. Usually, the PV plants export according to some form of power purchase agreement structure and the FTM battery storage system operates in frequency services markets. There are multiple reasons why a DC-coupled system is actively being investigated.

First, there are multiple advantages to using an oversized DC:AC ratio:

- The MW rating of a PV plant is the DC rating (DC nameplate capacity) of the cumulative DC PV power output (datasheet info of the PV panels). The output rating, however, is calculated at standard test conditions (STC), which rarely occur in practice. An increased DC:AC ratio implies installing more DC capacity when compared with the inverter AC rating to account for the differences in real operation conditions.

- The DC power available varies with a myriad of factors like temperature (The PV power output decreases with the ambient temperature rise. Ground-mounted PV plants have generally better ventilation when compared with roof-mounted systems and the energy generated per kW hour can be higher over the system lifetime, shading, orientation, cable lengths, PV degradation and cleanness factors for specific geographic areas.

- The AC rating of PV plants is the sum of the maximum continuous power output of the inverters. Because of the DC/AC conversion, the real DC power is reduced further. The AC power depends on the inverter efficiency, which in turn depends on the inverter loading. An inverter typically has 75-80% efficiency if it operates at below 5% of its nameplate capacity (which occurs in the early mornings and late evenings). The peak PV inverter efficiency is above 95-97%, but in practice, the system operates at varying efficiencies. Temperature and degradation also impact the overall inverter efficiency and lifetime.

These mean that the real DC power available over time is almost always less when compared with the DC nameplate rating of a PV plant. Considering the above observations, it makes sense, economically and technically, to increase the DC:AC power installed. Increasing the DC:AC ratio implies potential clipping (DC power generated is higher than the AC inverter rating. In this situation the inverter will automatically limit its output if the battery is fully charged) if the battery storage system is not sized correctly.

Secondly, a DC-coupled system helps the grid integration process of a colocation system, as the fault contributions are reduced, and the actual power operating in parallel with the grid is lower, when compared with simple AC-coupled systems. A lower power capacity operating in parallel can potentially reduce the maximum power swing and the subsequent impact on the power network.

The topology of the collocated PV and hybrid storage system analysed in this section is indicated in Figure 8-39. The battery systems are connected to a common DC voltage bus via DC/DC converters, and the outputs of the shared inverters feed step-up transformers, interconnected on the high voltage side.

8.5.2 Methodology

To investigate the viability of hybrid Li-ion and lead-acid energy storage systems for FTM applications, I have tested two generic options, a standalone FTM hybrid battery system and a PV & hybrid storage colocation option.

As explained in the previous methodology chapter, the battery operation profile, market prices, the grid export limitation and the interaction between the system components have been optimised to maximise revenue, using a specialised software, widely used in the industry for FTM optimisation. The resulting, optimised, site output power profile, the PV generation and import limitations have been fed into the techno-economic model developed during this research and analysed using hybrid storage options.

The size of the FTM plants developed in Gridcog are for typical small to medium-size FTM applications and the model inputs are the following:

- **Connection size**: The import/export grid connection size was limited to 10MW. This was an arbitrary choice as scaled results can be achieved using higher grid connection power ratings.
- **Markets**: I have designed the arrangement so that both systems, standalone and colocation, can work in GB Balancing Market, GB Dynamic Containment High, and GB Dynamic Containment Low.
- **DNO tariffs**: For both applications, I have used a standard DNO red, amber, and green, network tariff (HV Band 2: nighttime 0.058p/kWh for 22:00-07:00, daytime 0.334p/kWh for 08:00-15:00 & 20:00-22:00 and red 2.853p/kWh for 16:00-19:00).
- **Frequency**: For both applications, the battery storage systems are allowed to do as many daily cycles are possible to maximise the revenue potential.
- **Inverter arrangement**: As explained, for the PV and battery storage colocation system, a DC-coupled system was implemented in Gridcog.
- **PV plant (only for colocation option)**: For the colocation plant, I have used a standard 150% DC:AC ratio, and 35 degrees south facing for the PV plant. The PV plant uses typical UK power purchase agreement rates of 12p/kWh to export power to the grid. Also, I used

standard losses and degradation rates for the PV panels, 11% losses and 0.4% degradation per year.

- **Battery size**: For both FTM systems, I have modelled the following battery storage capacities: ranging from 10MW/10MWh, 10MW/20MWh, 10MW/40MWh and 10MW/60MWh (1, 2, 4 and 6-hour duration).

The scenarios analysed for the FTM options are indicated in Table 8-6.

Table 8-6. FTM scenarios

Scenario	Grid Connection (and inverter size) MW	Solar Capacity (only for colocation) MW	Storage Capacity MW & MWh
1	10	15	10/10MWh
2	10	15	10/20MWh
3	10	15	10/40MWh
4	10	15	10/60MWh

For illustration purposes, Figure 8-40 to Figure 8-43 show the wholesale, balancing and dynamic containment market prices used in this investigation. All electricity prices are based on the 2023 UK market conditions.

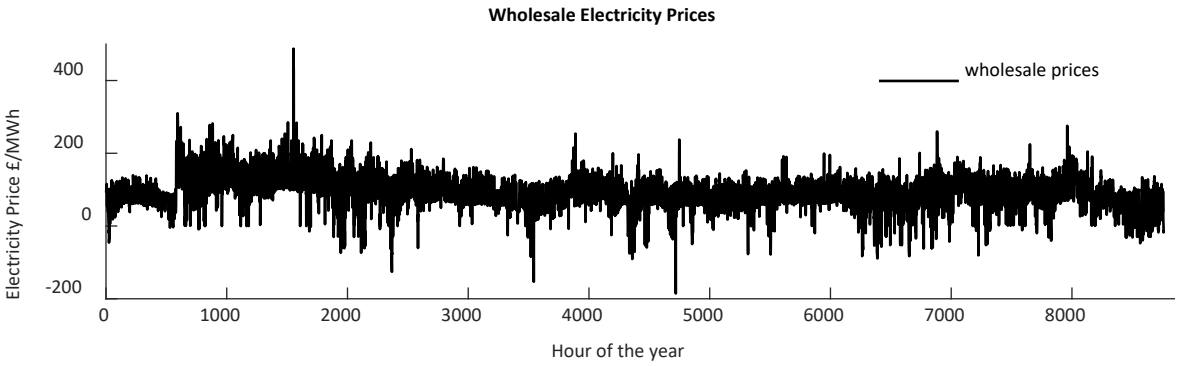

Figure 8-40. UK Wholesale Electricity Prices 2023

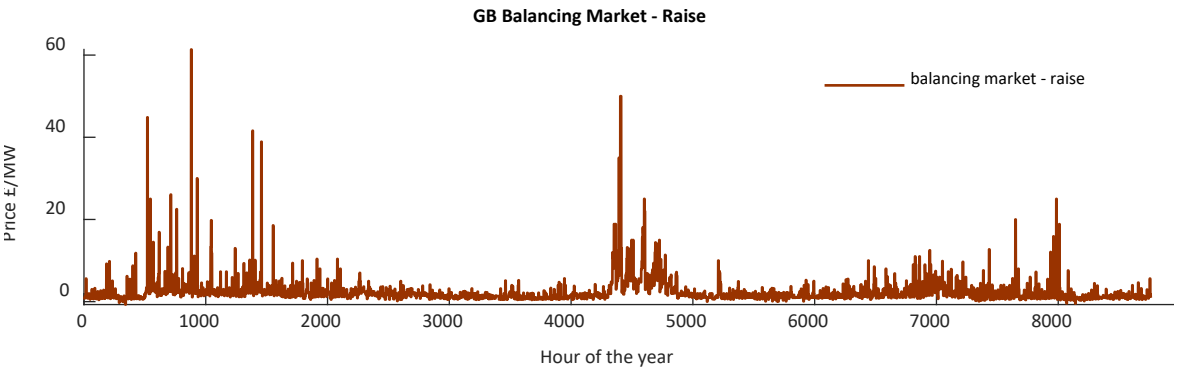

Figure 8-41. UK Balancing Market – Raise Price

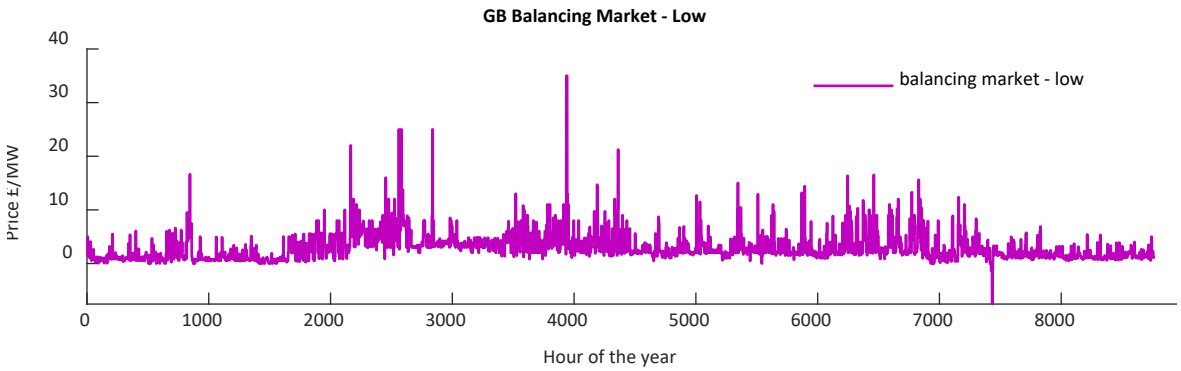

Figure 8-42. UK Balancing Market – Low Price

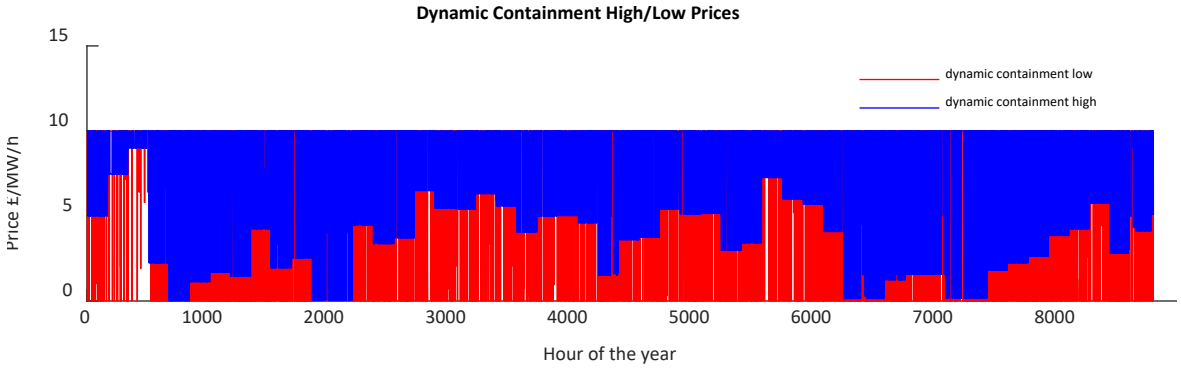

Figure 8-43. UK Dynamic Containment High & Low

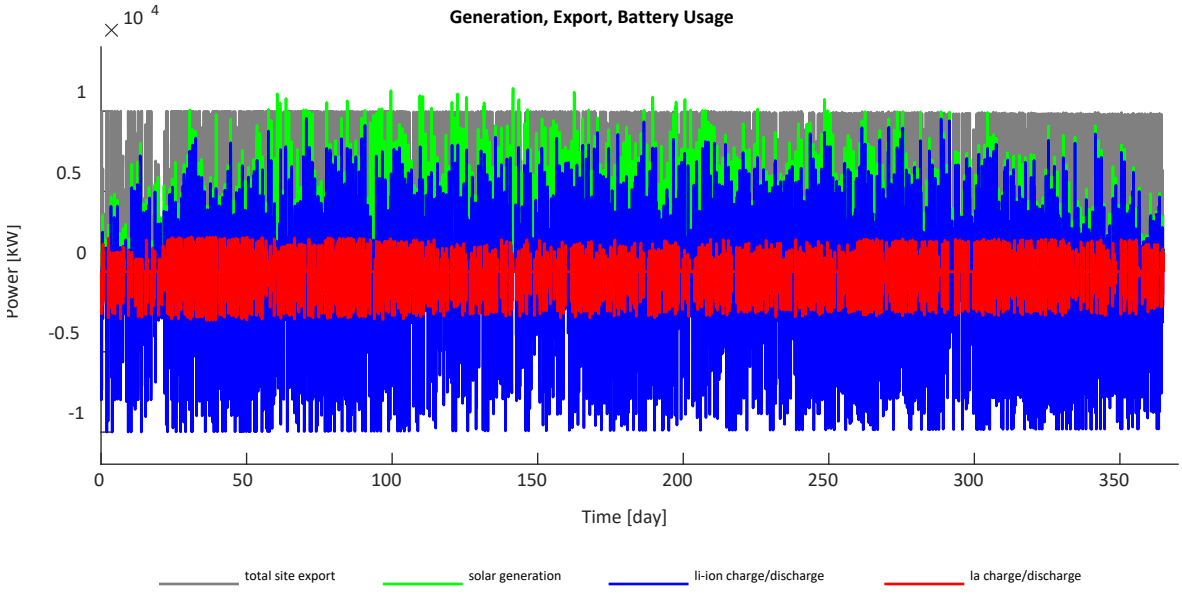

Figure 8-44. Typical Solar Generation, Site Export and Hybrid Battery Operation

Similarly, for illustration purposes, Figure 8-44 shows the operation profile of a typical colocation FTM plant analysed in this thesis, 15MW PV and 10MW/10MWh hybrid storage with a ratio of 1. As shown, site export is limited to 10MW import/export and optimising the system operation to

maximise the system revenue results in a complex interaction between the various operating system components profiles.

8.5.3 PV & Storage Colocation – FTM Case Study

As mentioned, for the colocation PV and hybrid storage case study, a 15MW PV plant, collocated with four battery storage scenarios, 10MW/10MWh, 10MW/20MWh, 10MW/40MWh and 10MW/60MWh, have been investigated to determine the hybridisation potential for these storage application types. For each storage capacity, I have analysed the hybrid lead-acid and Li-ion storage potential by varying the hybrid ratio from zero (single Li-ion storage option) to 4 and I calculated the storage utilisation and the potential number of equivalent cycles done by each chemistry string.

Figure 8-45 (a & b) shows the annual Li-ion and lead-acid equivalent cycles. The first observation is that the Li-ion strings' cycling decreases as the energy storage duration is increased and rises as the hybrid ratio is increased. For Scenario 1 (1-hour duration, 10MW/10MWh), the Li-ion cells do 760 cycles/year, for a simple Li-ion storage solution, and 1042 cycles/year when the hybrid ratio is increased to 4. Similar trends are observed for the 2h, 4h and 6h storage duration. For Scenario 4 (10MW/10MWh, 6h duration), the Li-ion strings perform between 341 and 600 cycles/year when the hybrid ratio is varied between zero and 4. Figure 8-45 (b) indicates the lead-acid cycling profile as the hybrid ratio is increased from zero to 4. The second observation is that the lead-acid strings are cycled much harder when compared with the previous case studies. Averaged across all hybrid ratios, it’s close to half the number of Li-ion cycles for all scenarios. As indicated, the lead-acid cycling increases sharply before levelling off. For Scenario 1, the number of lead-acid cycles increases from zero to 667 cycles/year, before decreasing to 436 cycles/year, when the hybrid ratio is increased to 4. Similar results are indicated for Scenarios 2-4.

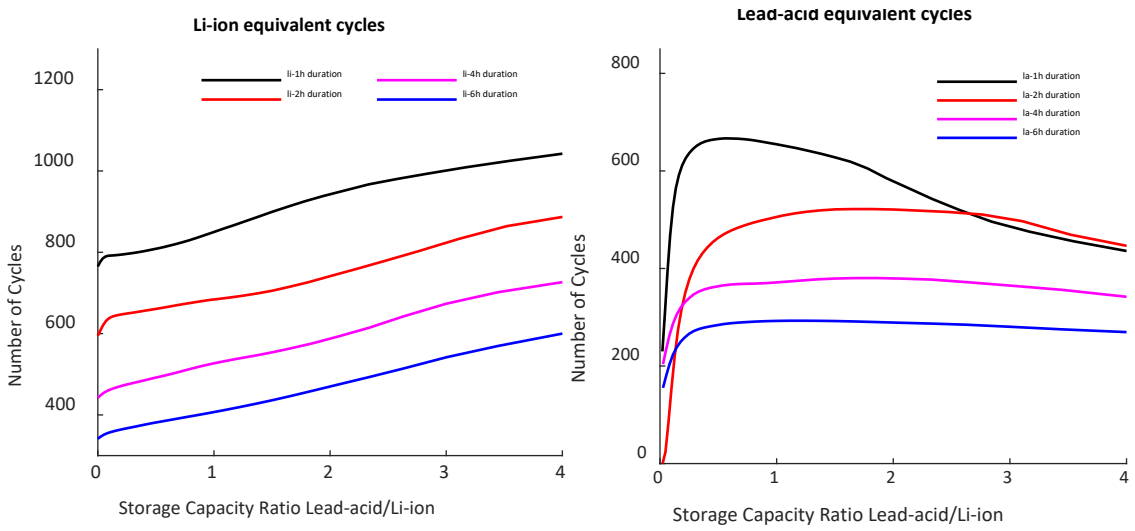

Figure 8-45. Li-ion and Lead-acid Annual Equivalent Cycles

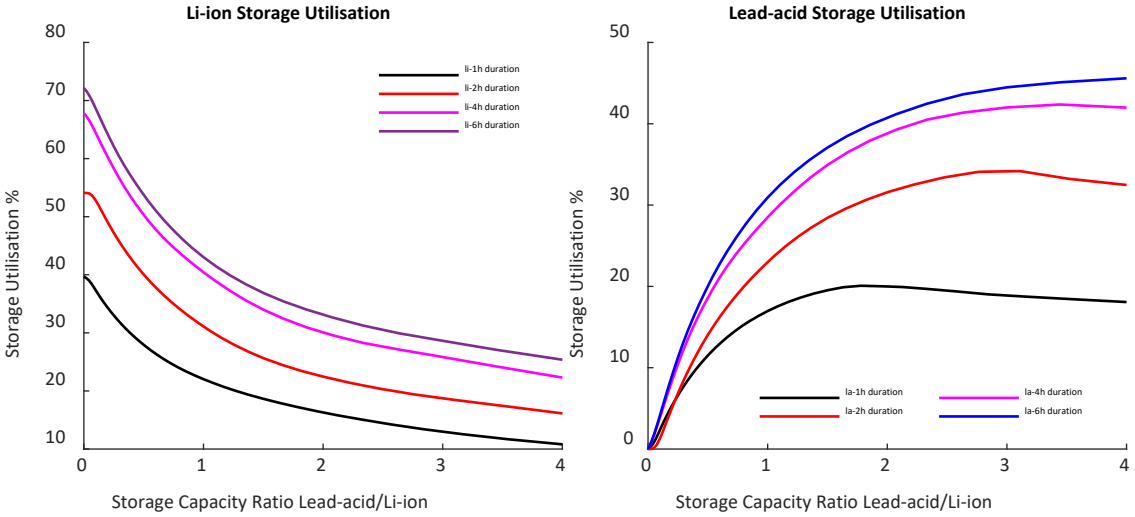

Figure 8-46. Hybrid Battery Storage Utilisation

Figure 8-46 (a & b) indicate the storage utilisation for each chemistry. As the storage duration is increased from 1h to 6h, the battery system exports to the grid between 39% to 72% of the annual energy delivered to the network. This implies that the direct solar export decreases as the storage capacity increases, indicating more PV generation is captured and transferred in the frequency and balancing markets. The lead-acid utilisation mirrors the decrease in Li-ion utilisation.

These results, and the high lead-acid utilisation and increased number of cycles per year, show that the potential for hybrid storage is not recommended. This is mainly because the storage discharge profile is relatively constant across the year and with no major peaks, the lead-acid string is cycled like the Li-ion. As a visual example, Figure 8-44, shows a typical lead-acid charge/discharge profile for the colocation configuration - 15MW PV and 10MW/10MWh hybrid storage of lead-acid to Li-ion ratio of 1. This, along with Figure 8-45 and Figure 8-46, visually shows that the lead-acid strings would be charged and discharged across the year for FTM applications,

and this reduces the potential for hybrid storage. As explained in the previous chapters, the hybrid system makes sense, economically and technically, when there is a variable storage utilisation profile across the year which would allow us to use a cheaper, lower specification battery technology.

8.5.4 Standalone Battery Storage – FTM Case Study

This section shows the results of investigating the hybrid storage option for a standalone FTM battery storage application. Like the colocation case study, I have analysed four scenarios, 10MW/10MWh, 10MW/20MWh, 10MW/40MWh and 10MW/60MWh using hybrid ratios between zero and 4.

Figure 8-47 (a & b) shows the annual equivalent cycles for the lead-acid and Li-ion strings. The first observation is that, like for the colocation case, both chemistries perform, on average, an increased number of annual equivalent cycles across the hybrid ratios, when compared with residential and industrial case studies. For Scenario 1, the Li-ion is cycled between 725 and 960.8x per year, as the hybrid ratio is increased from zero to 4. Similar trends are observed for the remaining Scenarios 2-4. As expected, the 6-hour duration storage option does the least number of cycles, ranging between 386 and 716 cycles/year. The lead-acid strings behave similarly to the colocation test, increasing sharply as the hybrid ratio is increased, and levelling off depending on the scenario.

For Scenario 1, the peak numbers of cycles (641 cycles/year) are delivered when the hybrid ratio reaches 1.5. As the storage duration is increased, the peaks for the equivalent cycle curves occur between 0.4 and 1.6 hybrid ratio, and the profiles flatten. Scenario 4 does a peak of 315 cycles/year and decreases slightly to 295 cycles per year as the hybrid ratio is increased to 4.

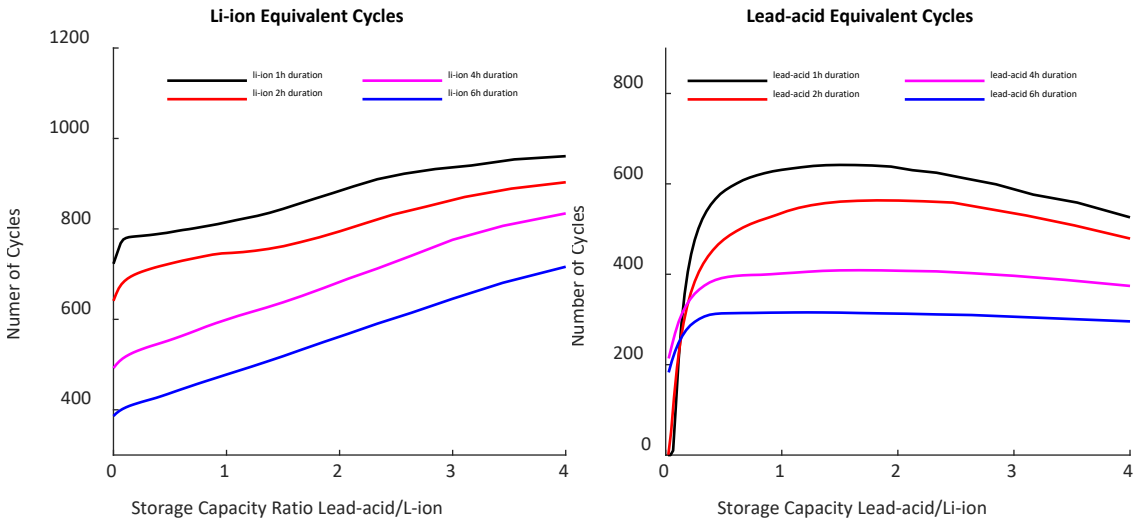

Figure 8-47. Li-ion and Lead-acid Annual Equivalent Cycles

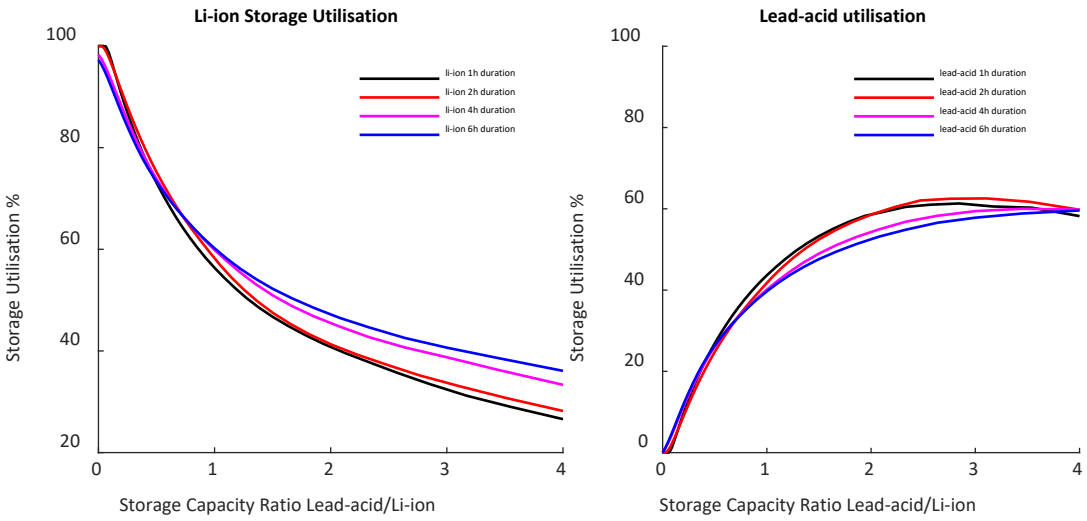

Figure 8-48. Hybrid Battery Storage Utilisation

Figure 8-48 (a & b), shows the hybrid storage utilisation and ratio for both Li-ion and lead-acid strings. For Scenarios 1-4, the Li-ion utilisation ratio decreases from 100% to 26.6%, 28.1%, 33.3% and 36% of the total annual grid export, as the hybrid ratio increases from zero to 4. The lead-acid cells mirror this.

Both data sets shown in Figure 8-47 and Figure 8-48 indicate that, in the current UK markets, the hybrid Li-ion and lead-acid system is not recommended for the standalone FTM applications. This is because the annual energy storage profile is practically equally spread across the year. This implies no major peaks to be covered by the lead-acid strings and any hybridisation would force an increased number of cycles for both chemistries. The results are based on the current market scenarios, and any future commercial arrangements might impose a different operational charge/discharge profile, providing opportunities for hybridisation.

8.6 Hybrid Battery System – Micro Hydro & PV applications

8.6.1 Introduction Floating Solar PV (FPV)

The last case study considered is the hybrid Li-ion and lead-acid storage option for hydropower and PV plants.

As explained in the previous chapters, alongside the obvious clean energy generation potential, the two biggest drawbacks of renewable technologies are the low energy density and the variable generation output. As argued throughout this thesis, the variable generation output can be addressed using energy storage, interconnection, and geographical diversification. The low energy density issue can be solved using previously vacant spaces like remote and offshore areas for wind generation as well as rooftops, building integration, deserts, and non-agricultural land

for ground-mounted solar generation. Additionally, because the photovoltaic systems are flexible and can be installed practically everywhere, combining photovoltaic generation with other industries can result in mutual benefits. For example, the use of PV systems in farming and agriculture (agrivoltaics) can improve land use revenue and reduce water usage. One option for PV plant integration is floating solar technologies (FPV) which implies installations on the existing hydropower lakes, natural and artificial waterways, canals, wastewater treatment lakes and even coastal areas as indicated in Figure 8-49.

Floating solar plants have increased at an average annual rate of 8-8.5% since 2007. The total world FPV capacity reached 3.9 GW in 2022 [153]. This is expected to increase dramatically to 30GW by 2030, predicting to achieve one of the fastest renewable generation growth rates, as GW-scale plants are under construction worldwide, like the Saemangeum Floating Solar Power Project, South Korea [154].

Figure 8-49. Canoe Brook Reservoir FPV Plant (8.9MW), USA and Dezhou Dingzhuang FPV (320MW), China [154, 155]

The FPV and hydropower have attractive mutual technical advantages when compared with traditional ground-based or roof-mounted solar PV plants. Some of these are listed below.

- Strong reduction of land occupancy.

The first obvious advantage of FPV technologies is that they do not take up land, especially in countries where land is expensive, like Singapore or the UK. This way, power generation avoids the politically sensitive competition with agricultural production or housing developments. The land leasing arrangements are easier and potentially cheaper in theory, as there is usually one owner of a particular water area. Another land-related advantage is that it does not depend on topology. This implies that large-scale PV generation can be deployed even in mountainous locations [156, 157].

- Installation and decommissioning.

The second advantage of FPV plants is that they are easier to install and decommission. This is because there are no fixed structures, like foundations for ground-based systems, and because the floating systems are modular [156, 157].

- Water saving and water quality.

Covering water bodies with solar panels reduces evaporation and improves the water quality. In the most arid areas, like Australia, it is estimated that the annual water evaporation can be as high as 40% of the total water storage capacity [158, 159]. This can improve the overall economic sustainability, especially in areas where drinking and irrigation water is scarce [156, 157, 160, 161].

FPV plants also discourage algae growth, which increases the cost of the water treatment processes.

- Cooling and tracking.

The PV plant outputs decrease as the operating ambient temperature increases. Another advantage of the FPV systems is the increased energy generation due to additional water-cooling effects on the generation system. This is because the ambient air is cooled above the water surface due to evaporation and better ventilation (the air movement above the water bodies due to the temperature between the surrounding land areas and the water surfaces tends to also be higher). The resulting cooling effect can increase energy production by over 10%, depending on the local climate [162].

The floating structures of the FPV plants are mobile and tracing systems can be implemented at a lower cost when compared with ground-based systems, which require complicated mechanical moving parts. Studies show that with simple N-S tracking systems and the additional cooling benefits, the energy generation of an FPV can be increased by 23-27% when compared with ground-mounted PV [162-164].

- Hybrid system integration.

FPV farms can be integrated with existing power stations, especially offshore wind and hydropower. The main advantages of this are the grid connection sharing and the complementary nature of the wind, hydropower generation and solar generation profiles. Additional advantages can be achieved if the FPV plant is coupled with pumped hydro storage [156, 157].

- Environmental benefits.

The FPV plants have a lower environmental footprint as no concrete foundations, steel structures or heavy equipment are required. The floating systems are made of HDPE material which is widely used in the water distribution industry and can be recycled.

- Synergy with fishing.

FPV plants have been used in fish farms and additional benefits related to fish growth cycles can be obtained [165-169].

Alongside the advantages mentioned above, the FPV plants bring additional challenges related to increased maintenance difficulty, potential corrosion increases, and the need for improved

electrical safety. However, the slightly increased capital cost, $0.8-1.2/W (4-8% higher than ground-based systems), is offset entirely by the improved energy generation. Comprehensive studies like [156] find that, even without the additional benefits mentioned, there is almost no difference in the LCOE between ground-mounted PV and FPV systems.

The work presented in this section of the thesis will analyse the hydropower & FPV systems coupled with hybrid battery storage systems. Studies like [156, 157] show that hydropower, especially pumped hydro, could benefit most from FPV hybridisation. In [160] it is indicated that only 10% coverage of the existing hydropower reservoirs with FPV plants could replace the entire fossil fuel electricity generation. On top of the advantages mentioned above, the FPV increases the power and energy density of hydropower plants. The average world power and energy densities for hydropower systems are 4 W/m^2 and 19.2 kWh/year/m^2. Using FPV, this can be increased to a conservative 120 W/m2 and 150 kWh/year/m^2. This implies a higher capacity factor due to the complementary nature of hydropower and solar generation. In practice, the grid connection size and the energy storage capacity can limit the practical FPV power installed [157]. An analysis of the 20 largest hydro plants concludes that an average of 2-3% FPV coverage could increase the total annual generation by 27-45% [157].

Figure 8-50. Floating solar panels on the surface of the Hapcheon Dam in South Korea (40.32 MW) and Queen Elizabeth II Reservoir floating solar (6.3 MW) [170, 171]

8.6.2 Micro Hydro, PV & Hybrid Storage Plant Description

To understand the synergy between hydropower, PV and hybrid battery storage, a complete system was designed to capture these three elements. The micro hydro plant is based on a real case study I designed during this research project.

The PV, hybrid battery storage and micro hydro plant proposals are located in Dare Valley Country Park. This is a public area covering around 200ha consisting of woodland, pastures, play areas, camping sites, walking trails and a built area. The land is publicly owned by the Rhondda Cynon

Taff County Borough Council. The small building complex is on the eastern side of the site, next to the entrance, and contains a hotel, café, and other facilities. The electrical load of these facilities was considered in this thesis to be electrified using the hybrid power system.

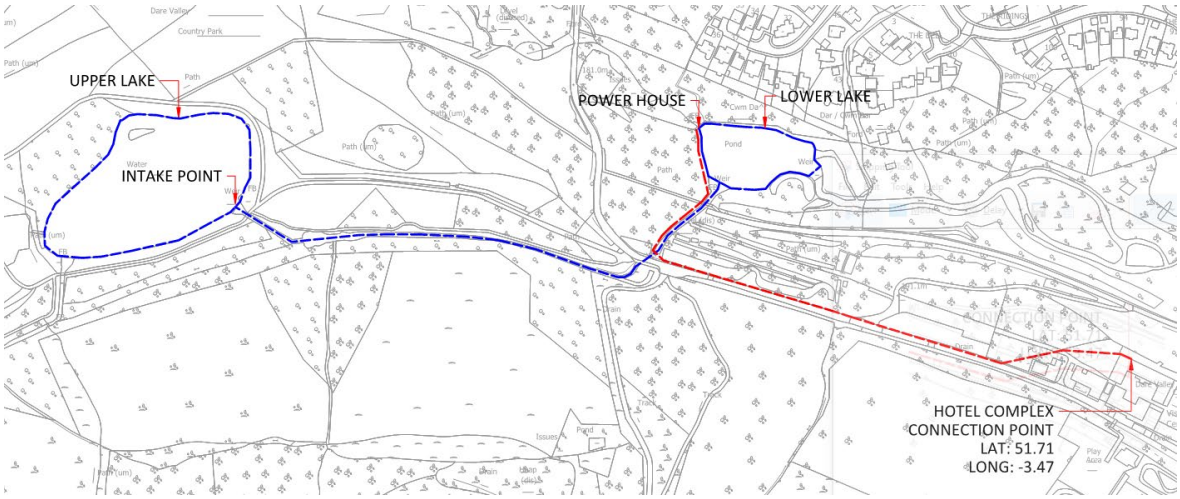

Figure 8-51. Micro Hydro site overview

The Dare River flows through the site and two artificial ponds are located along the river, northeast of the hotel complex, as indicated in Figure 8-51. The stream between the two ponds is an artificial waterway, as well as the stepped waterfall before the stream ends in the lower pond. Figure 8-51 shows the general site arrangement, indicating the two ponds and the building complex. The wide site can be accessed by a series of tarmac roads and footpaths, both lakes being easily accessible.

The micro hydro scheme makes use of the stream between the ponds and the height difference between the upper and lower ponds, as indicated in Figure 8-51. A proportion of the stream flow was abstracted using a weir system, run through a penstock to the lower-level lake where the turbine and generator are located (Figure 8-51).

I surveyed the site to determine the best point of connection, the LV cable route, measured the distances between the potential powerhouse and the point of connection and calculated the head difference (m) between the upper and lower lake as well as the penstock length. All of these are crucial for the hydropower generation profile. The survey was done using a drone to determine the best penstock and power cable routes. I have used desktop tools to calculate the elevation difference and checked the data with third-party on-site GPS-based measurements. The measurement errors of the total gross head available are assumed to be 3% and 5% for the distances between the powerhouse and the connection point.

The total available gross head was measured to be 29.9 meters between the upper weir location and the lower lake. The penstock length, based on the route indicated in Figure 8-51, was estimated to be around 381m.

The distance between the powerhouse and the connection point, which dictates the length of the main power cable, was calculated to be 460-470m. The existing hotel electrical supply is a standard three-phase, 400V system, and there are spare ways on the main LV panel for another 200A breaker necessary for the micro hydro and FPV generation system. Based on the size of the incoming cable, the connection for the hotel was approximated to be around 150 kVA.

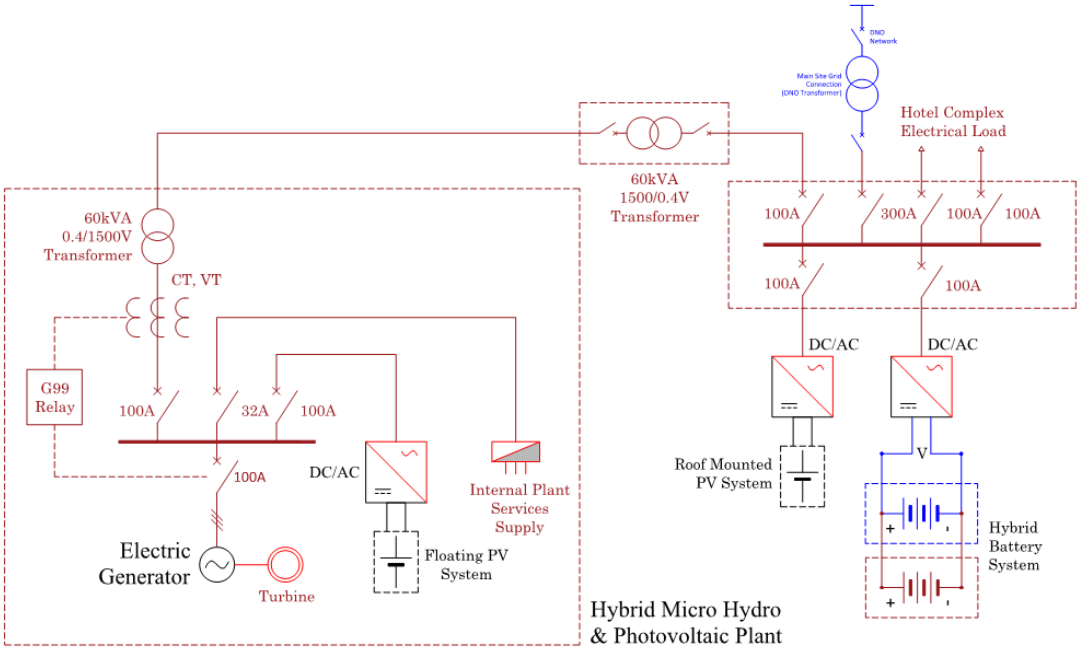

Figure 8-52. Micro Hydro with FPV, Roof-mounted PV and Hybrid Storage Schematic

Figure 8-52 shows the electrical schematic of the plant. The synchronous hydroelectric generator, powered by the turbine, and the FPV plant inverters feed into a central three-phase panel board.

In this thesis, I considered only crossflow turbines because of the relatively low head of the system and simple design, which makes them easy to install, operate, and maintain [172]. This also makes them cost-effective, especially for small-scale installations. They can also operate at efficiencies up to 80% across a wide range of flow rates. Usually, the manufacturers offer packaged solutions for the turbine generator arrangements. I have based all the turbine calculations in this thesis on the CINK Hydro-Energy turbine/generator arrangement, the technical details of which are indicated in the Appendix [173].

As the power is generated at low voltage, there is a need for a step-up voltage transformer to transmit power to the demand point with minimum losses. Considering that an 11kV system

would not be practical for the power ratings discussed, I considered a maximum of 1.5kV ‘transmission system’. The main power cable terminates in a step-down transformer at the consumer and eventually is connected to the main distribution panel of the hotel complex. The hybrid battery system and the roof-mounted PV are connected via inverters to the consumer distribution board as indicated. Figure 8-52 also indicates the DNO supply for the site, which is done via a pole-mounted 0.4/11kV transformer. For both electric panels indicated, LV feeders are supplying the main electrical loads as well as the plant's internal services.

The FPV plant is indicated in Figure 8-53. The overall arrangement is south-facing, with 10% horizontal inclination. The FPV was only considered for the lower lake because of the distance limitations between the upper lake and the powerhouse. Figure 8-54 shows the roof mounted PV system for the hotel complex. As indicated, this includes several roof areas with different orientations, south-west, south-east and south-facing systems. I have based all PV calculations for the roof mounted system and FPV on Q.PEAK DUO ML-G11S photovoltaic panels series.

Figure 8-53. Floating Solar Plant (FPV), Lower Lake

Figure 8-54. Roof mounted PV, Hybrid Battery Storage, Dare Valley Country Park Hotel

In terms of the civil engineering design, the intake weir design uses a system of one 'V' and two rectangular notches to regulate the water flow. The two rectangular notches are separated by a narrow concrete structure, and the ratio between the widths of the two determines the abstraction ratio for the micro hydro plant. The 'V' notch guarantees the minimum hands-off flow based on the Dare River flow duration curve.

The penstock uses HDPE technology has been assessed to be the most suitable. The size and specifications of the pipe are the following: size (OD) - 500mm, material strength - PE100, pressure nominal - PN10 and water pressure resistance - 10 bar.

8.6.3 Generation data for Micro Hydro and PV

To calculate the final generation profile for the micro hydro and PV/FPV system, I have used three main data sets:

- The flow duration curve data for the Dare River.
- The efficiency data for the electrical power equipment.
- Solar data for the Dare Valley area.

The annual and monthly flow duration curves for the Dare River were initially calculated using Low Flows software and later revised by Natural Resources Wales (NRW). This research project uses the recommended NRW flow data, indicated in the Appendix. Once the flow data curve is established, any hydropower system relies on an abstraction scenario which allows for a certain percentage of the river flow, above the hands-off flow (the minimum river flow rate necessary for aesthetic reasons and other environmental requirements), to be used for power generation. The maximum flow rate can't be more than the average annual flow rate. The abstraction scenario modelled for the research is the 60/40% option, which implies 60% of the river flow rate, above the hands-off rate and lower than the annual average, can be used for power generation. Additional abstraction options are possible, but this is considered industry standard.

Using the data for the 60/40% abstraction scenario, three categories of data have been generated:

- Total annual energy generated.
- Monthly energy generated.
- Hourly energy generated assuming a constant capacity factor across each month.

In an ideal scenario, the power generation profile is directly determined based only on the flow data and the system head. However, in practice, a set of efficiency losses is introduced across

the energy transformation process. I have considered the main six main categories of losses which occur across the transformation chain:

- Head loss in the penstock and across the pipe valves.
- Turbine losses.
- Electrical Generator losses.
- Step-up transformer losses.
- Low voltage cable losses.
- Step-down transformer losses.

The penstock head losses have been calculated using Equation 8-1 [172]. The calculations consider the additional losses due to valves and inlet points, but they ignore the evolution of the penstock losses over the lifetime of the system.

$$S = \frac{h_f}{L} = \frac{10.67Q^{1.852}}{C^{1.852}d^{4.8704}};$$ Equation 8-1

S – hydraulic slope

h_f – head loss in meters

L – length of pipe in meters

Q – volumetric flow rate m3/s

C – pipe roughness coefficient, 140 for HDPE

d – inside pipe diameter in meters

Like the penstock losses, the turbine, electrical generator, step-up and step-down transformers as well as the cable losses, vary with the load factor of the system. All these losses are too complex to be determined analytically and are usually determined experimentally and provided by the manufacturers. Figure 8-55 indicates the efficiency data for the turbine, generator, and transformers as a function of the loading factor.

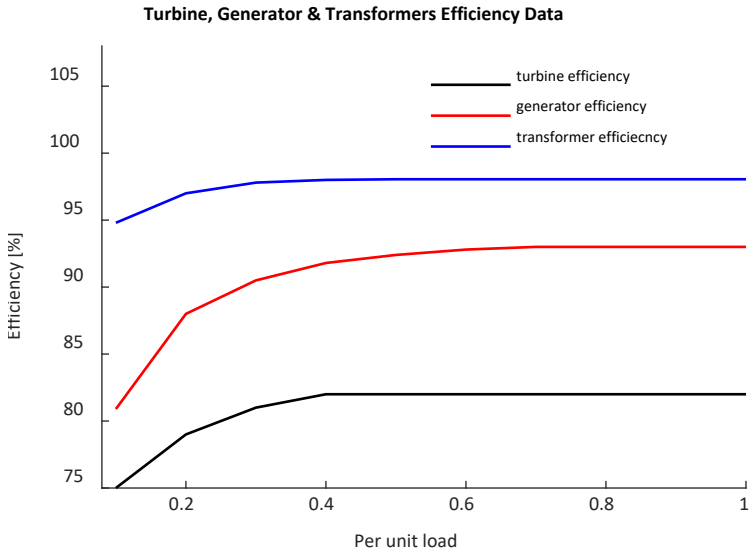

Figure 8-55. Efficiency Data

8.6.4 Modelling Results

To show the operation principles of the micro hydro, PV (FPV & roof mount) generation coupled with a hybrid storage system, this section details a typical off-grid scenario analysed in this work.

The option used as an example assumes a hydro generation plant power rating of 50 kW, working in parallel with a combined 135 kW PV generation system, and a hybrid energy storage of 7 MWh (2 MWh of Li-ion and 5 MWh of lead-acid directly connected at the DC bus as indicated in Figure 8-52).

Figure 8-56 shows the annual hourly generation profile for the hydro plant and the solar system. The hydro generation profile was calculated as described in the previous section and the solar generation profile was derived using site-specific data, considering the orientation, angles, and shading of the PV panels for the FPV and roof-mounted sections. The final hydro profile considers the river flows, the abstraction rate, and the losses along the energy transformation chain (penstock, valves, turbine, transformers, and cable losses). The micro hydro power generation profile is limited to 50 kW for practical considerations.

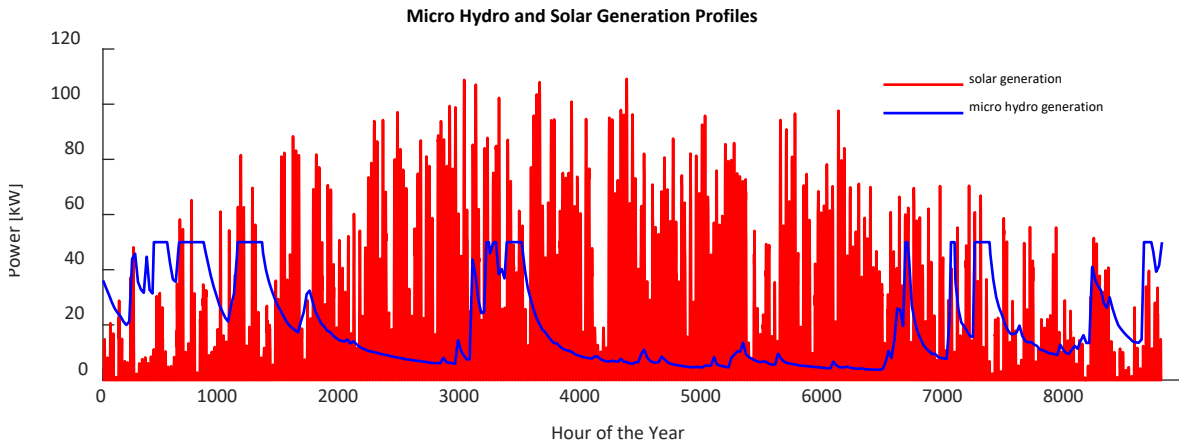

Figure 8-56. Micro hydro and PV generation profiles

As shown in Figure 8-57 (a) and mentioned in the previous section, the monthly generation profiles for the PV and the hydro system are complementary, the PV generation dominates the summer months, and the hydro system the winter period. This implies that the combined solar and hydro generation output has a reduced seasonal variation when compared with either hydro or PV in standalone configurations. Figure 8-57 (b) shows the total monthly generation profile and the monthly site electrical demand. This implies that the seasonal storage required in off-grid configurations can be reduced by manipulating the ratio between the two generating technologies to achieve a relatively constant monthly generation profile.

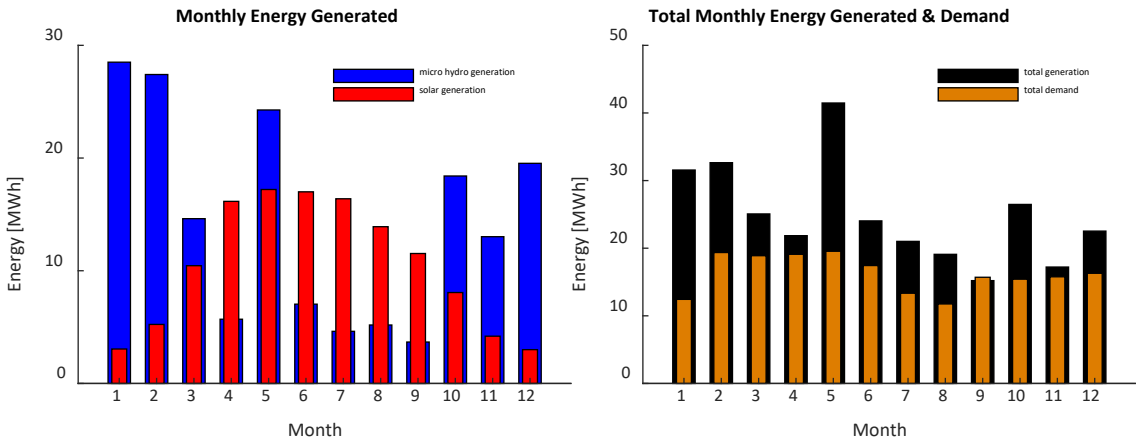

Figure 8-57. Monthly energy generation (a) and Total monthly generation and demand (b)

The hourly annual demand for the Dare Valley site is indicated in Figure 8-58. The total generation system described will produce 150% of the annual demand. As in the previously analysed cases, oversizing the generation is a simple option to reduce the energy storage requirements and the overall cost of the energy system.

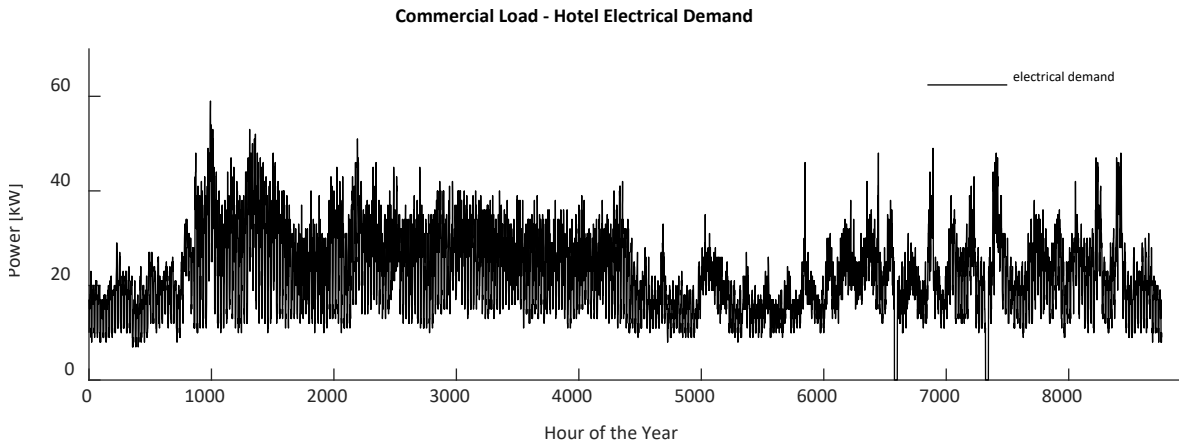

Figure 8-58. Dare Valley electrical demand.

Even if the generation system is oversized to 150% of the site load, it cannot cover the total demand without using energy storage, as the generation profile does not always match the demand. For the example scenario discussed, the total storage required is 7 MWh.

If a hybrid Li-ion and lead-acid system is used, the hourly charge/discharge profile of the system is shown in Figure 8-59. As indicated, the Li-ion strings are utilised throughout the year. This is not the case for the lead-acid cells. Annual energy flows show that 54% of the total generation is directly consumed on-site, covering 81.55% of the demand. The remaining load is covered by the hybrid storage system, 16.72% is supplied by the Li-ion, and 1.71% by the lead-acid strings.

The storage operation is also shown in Figure 8-60. The Li-ion SoC varies across the year, but the lead-acid cells stay at 100% SoC and discharge only for the peak storage demand.

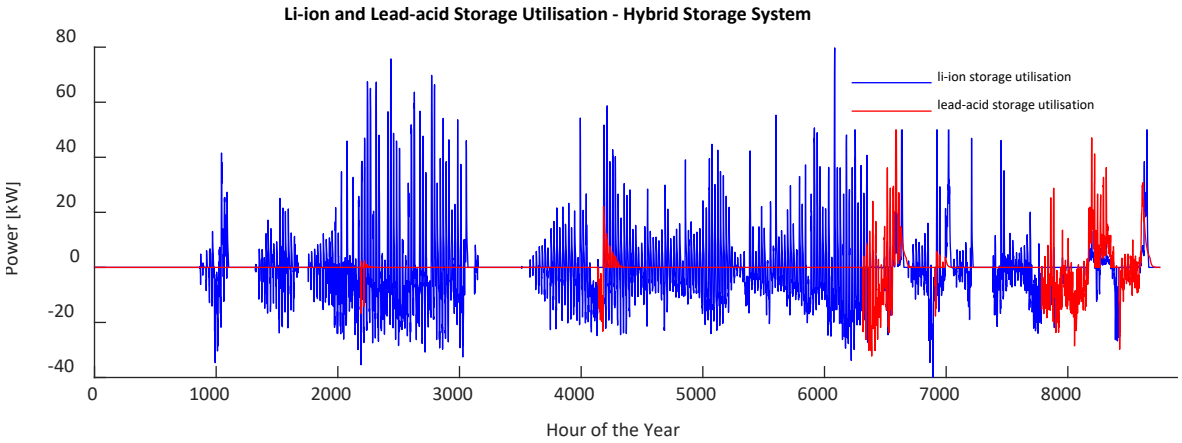

Figure 8-59. Hybrid Energy Storage charge/discharge annual power profile

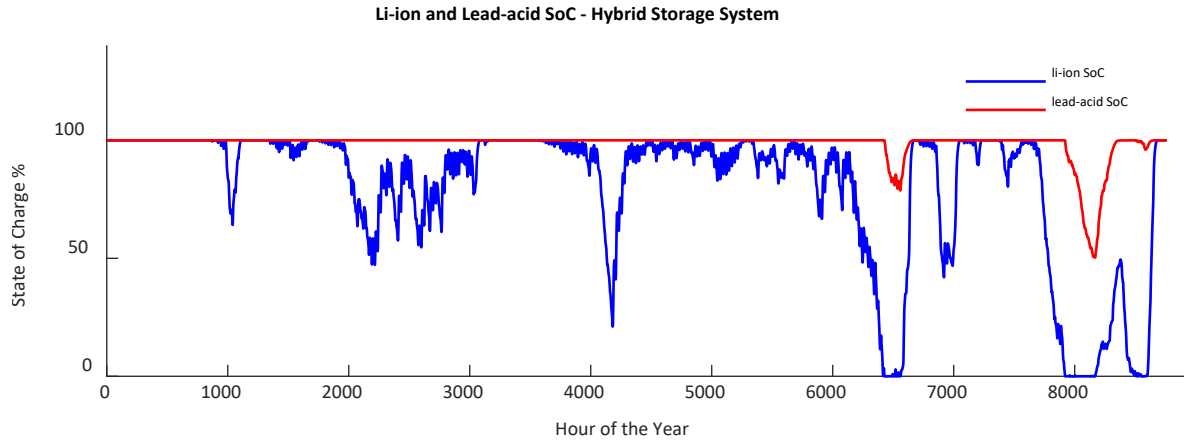

Figure 8-60. Hybrid Energy Storage SoC evolution across the year

Like Figure 8-59 and Figure 8-60, Figure 8-61 shows the cumulative energy delivered by each chemistry. This also shows that the Li-ion strings are cycled across the year, and the lead-acid batteries are used only in specific peak storage utilisation.

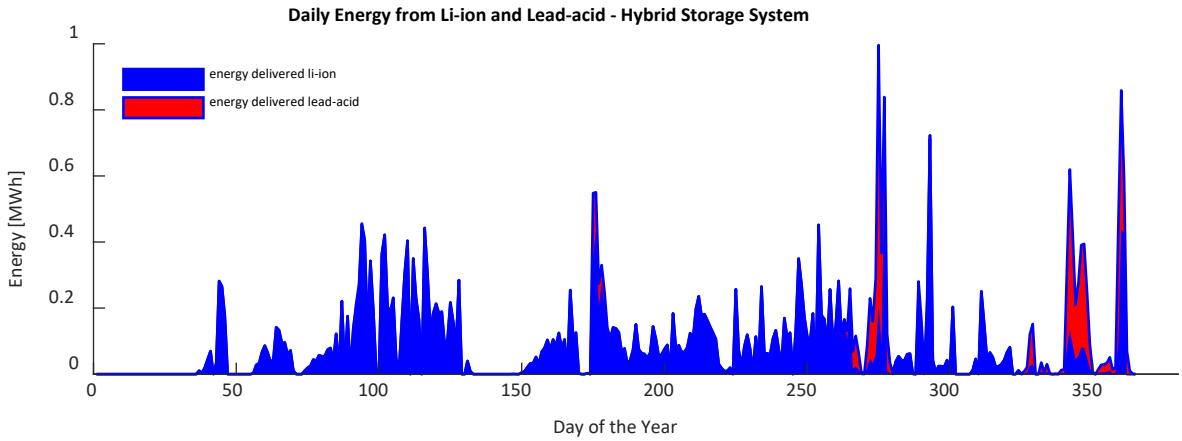

Figure 8-61. Total energy storage demand profile

Like the previous case studies, the example analysed shows that from a total of 7 MWh energy storage capacity, 5 MWh is underutilised, only cycled during peak storage requirements. A simple energy storage system based only on Li-ion batteries implies that a high-performance technology is idle for most of the year, which reduces the economic performance of the total energy system. A hybrid configuration allows the design flexibility to size the system for the specific load profile. This reduces the cost involved as detailed below.

Several overgeneration scenarios have been analysed to determine the hybrid storage potential for the off-grid micro-hydro & FPV arrangement as indicated in Table 8-7. The overgeneration scenarios assume renewable generation of 100% to 1300% of the total annual demand. To increase the generation, I have varied only the solar capacity as the micro hydro system is fixed to 50kW (Scaling the hydro potential is not economically and technically possible.).

Table 8-7. Overgeneration Scenarios - micro hydro & FPV

Scenario	Solar Capacity kW	Hydro Capacity kW	Generation % annual demand	Energy Storage Capacity MWh
1	30	50	100%	32.8
2	235	50	200%	2.8
3	445	50	300%	1
4	865	50	500%	0.61
5	1700	50	800%	0.43
6	2530	50	1300%	0.4

Assuming the overgeneration scenarios indicated, Figure 8-62 (a), show the combined solar and hydro self-consumption as a percentage of the total generation as well as the energy storage requirements to supply 100% of the annual demand. As shown in Figure 8-62 (b), the largest storage requirement is for Scenario 1, and the 32 MWh storage suggested covers any load seasonality. The storage capacity decreases dramatically as the overgeneration is increased. Between scenarios 1 and 2, the storage requirements decrease by 91.4% to 2.8 MWh. However, between scenarios 2 and 6, the storage decreases from 2.8 to 0.4 MWh, an 85.7% reduction.

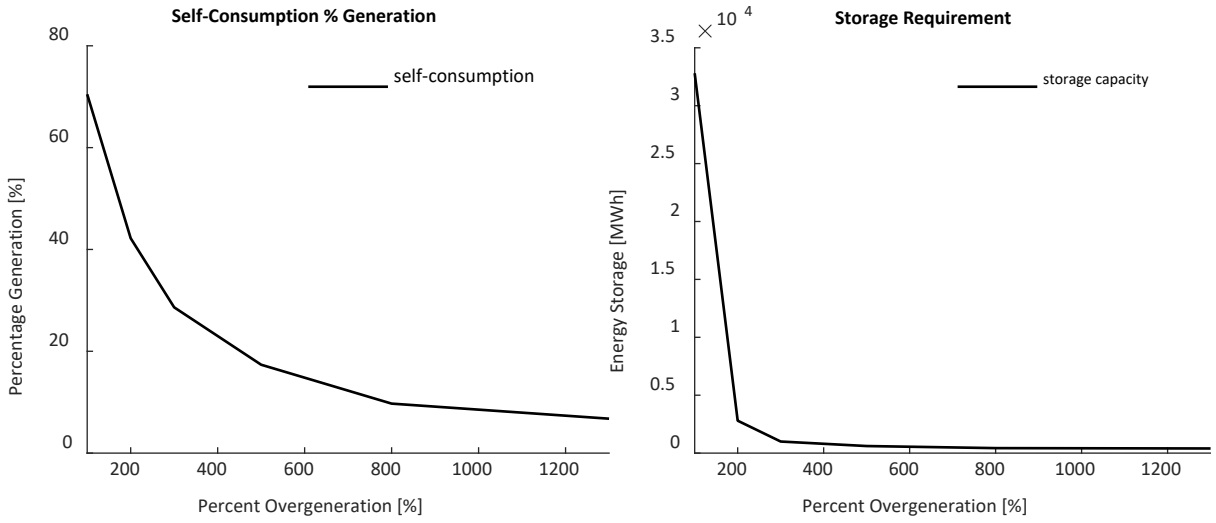

Figure 8-62. Self-consumption as % of the total generation (a) and storage requirements (b) for the micro hydro & FPV

The hybrid storage utilisation of each string, as a function of the hybrid storage ratio, is shown in Figure 8-63. The first observation is that, except in Scenario 1, the Li-ion strings always supply a larger percentage of the total annual site load when compared with the lead-acid, even when the hybrid Li-ion/lead-acid capacity ratio is increased to 4. Scenario 1 is the only one where the lead-acid utilisation is greater than the Li-ion as the hybrid ratio is increased above 1.6. This is due to the increased energy transferred between months when exactly 100% of the load is generated.

The maximum Li-ion utilisation is for Scenario 1, hybrid ratio zero (single Li-ion storage option), when the Li-ion strings supply 28% of the annual load. At the other extreme, the lowest total storage utilisation is 14.29% for Scenario 6. This shows that even if the overgeneration is increased by 13x of the annual demand, energy storage is still required. The second observation is that the maximum lead-acid utilisation (except Scenario 1) is 5.6% for Scenario 6. This indicates the potential for hybrid storage.

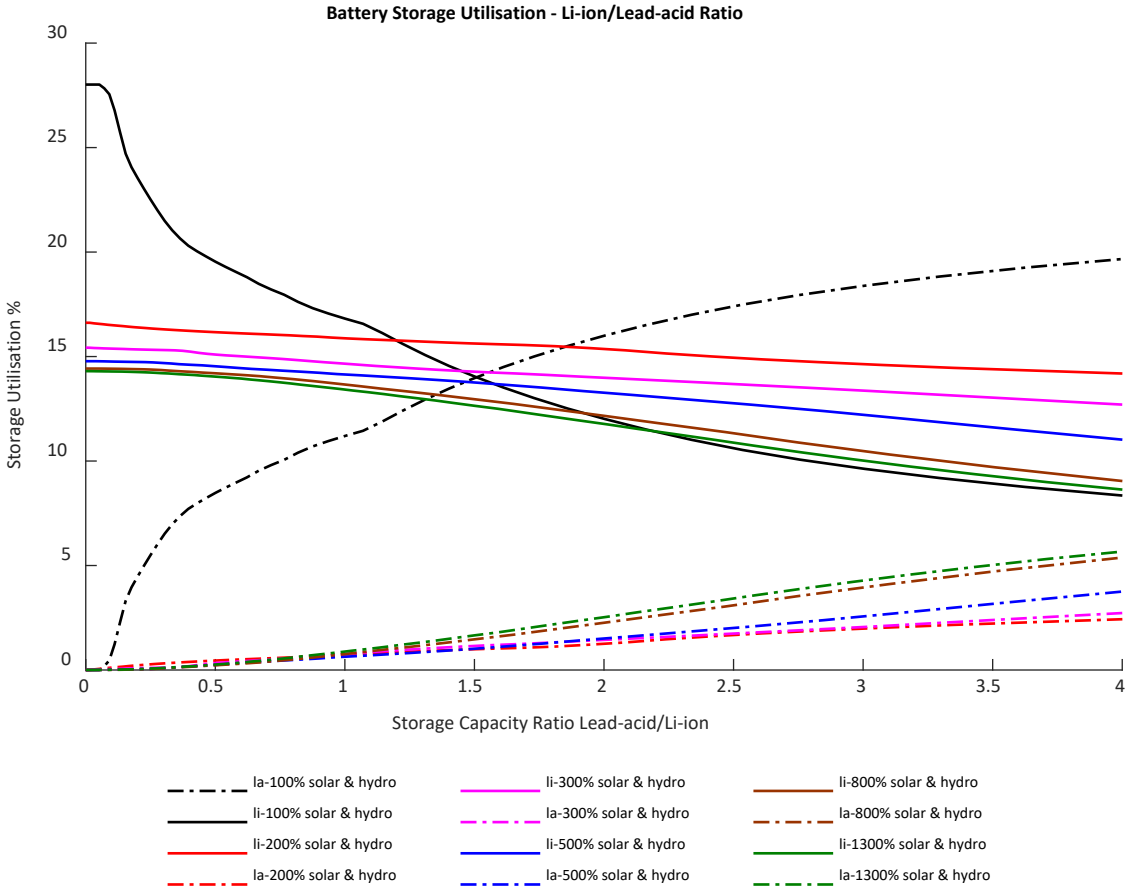

Figure 8-63. Hybrid Battery Storage Utilisation

Figure 8-64 shows the equivalent cycling performed by each chemistry string. The first observation is that the Li-ion chemistry is always cycled harder when compared with the lead-acid. As the hybrid ratio is increased from zero to 4, the Li-ion number of annual cycles also increases. The maximum cycles performed by the Li-ion strings is 218.9 cycles/year for Scenario 6 (0.59 cycles/day). The second observation is that the lead-acid strings do not increase above 36 equivalent cycles per year (0.09 cycles per day) across all scenarios. This also demonstrates the hybrid storage potential.

Scenario 1 is the only case when the Li-ion performs almost the same number of cycles as lead-acid. This is because both chemistries work as seasonal storage systems.

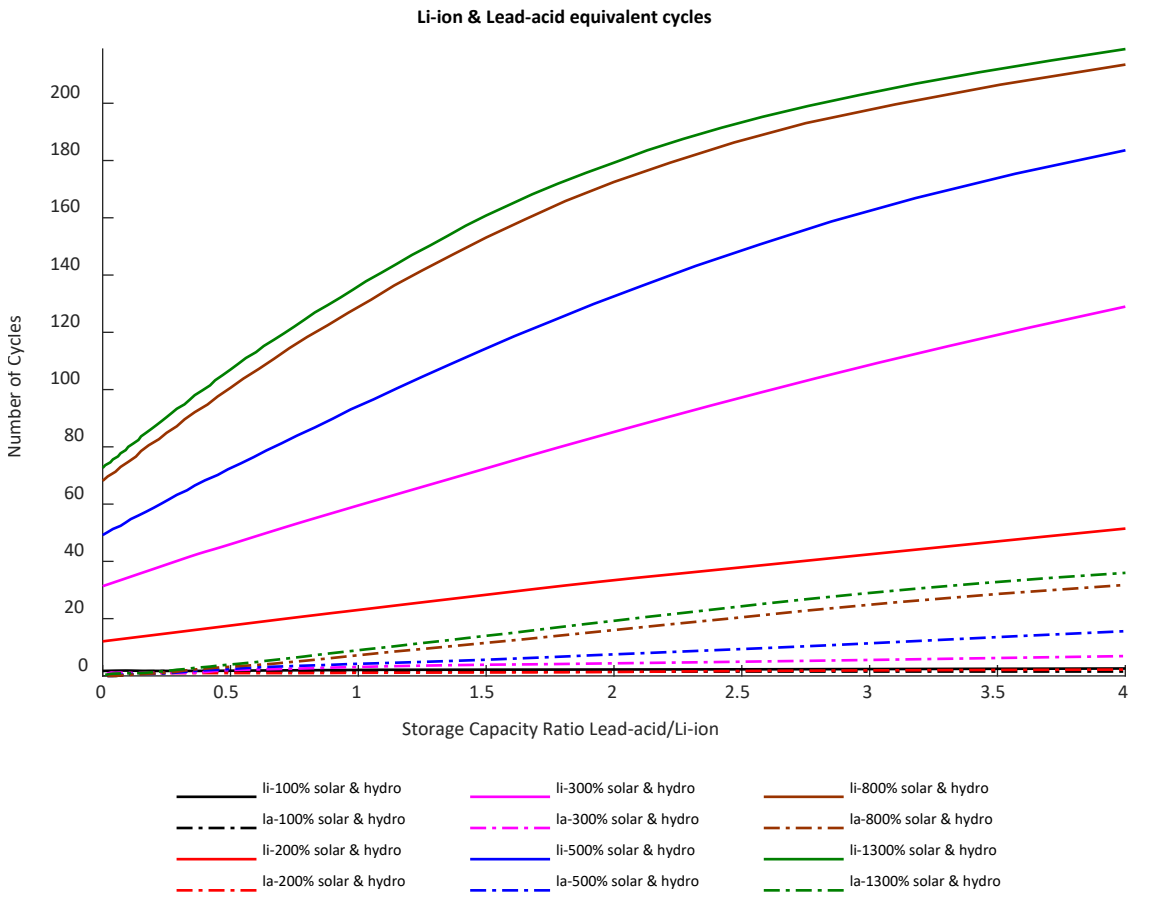

Figure 8-64. Li-ion & Lead-acid equivalent cycles

The overall system cost for each scenario and hybrid ratio is shown in Figure 8-65. Like in the previous cases, we observe that there are two ways to decrease the CAPEX for the off-grid renewable system, by increasing the overgeneration and by using hybrid storage. Using the Li-ion single chemistry storage system, the cheapest option is Scenario 5 (500% overgeneration), £1.282 million. When hybrid storage is used (ratio 4), Scenario 3 is the cheapest, £1.218 million. The biggest cost reduction obtained using hybrid storage depends on the storage cost as a proportion of the total energy system CAPEX. As scenario 1 has the highest storage requirement, the biggest cost reduction of 20.8% can be achieved as the hybrid ratio is increased from zero to 4. For scenarios 2-6, the cost reduction potential using hybrid storage is 10.9%, 6.2%, 4%, 2.3% and 1.7%. When comparing this with the previous case studies, we observe a lower cost reduction potential, and this is mainly because the CAPEX of hydro/kW is higher when compared with wind and solar.

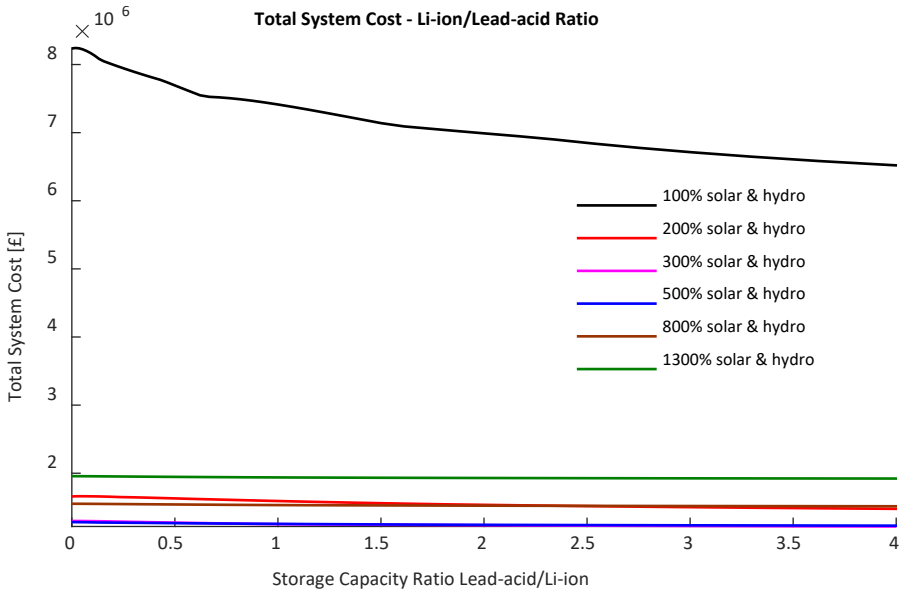

Figure 8-65. Total energy system cost.

As for the other scenarios, Figure 8-66 indicates the sensitivity analysis of the total system cost for Scenario 3 (optimised solution) to the kWh cost ratio between the two chemistries. The cost savings potential for different kWh cost ratios between the two chemistries reduces as the Li-ion price decreases. If the cost ratio between the two chemistries falls below 1.1-1.2, the hybrid system is no longer justified, as minimum cost reductions are possible.

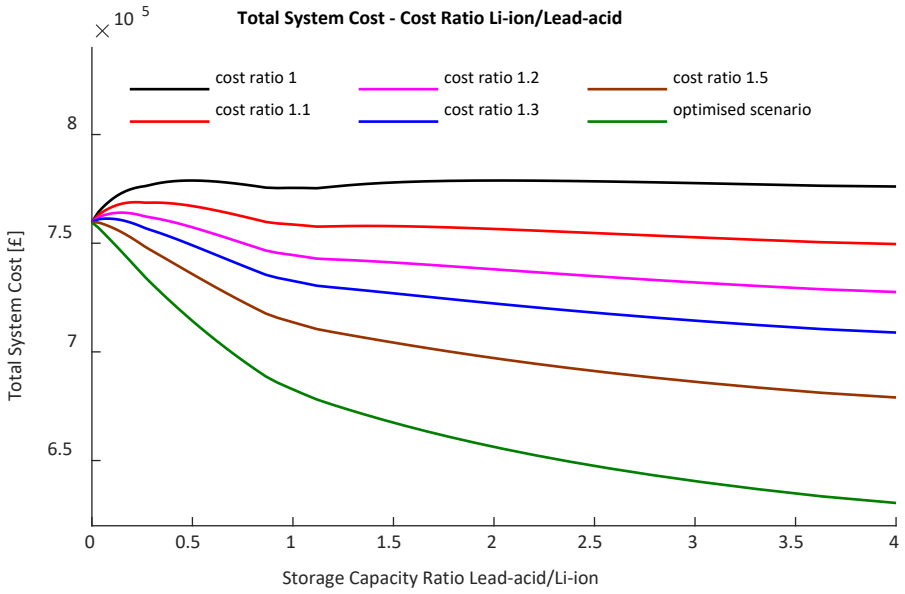

Figure 8-66. System Cost - Price Ratio Li-ion to Lead-acid

8.7 Conclusions

8.7.1 Residential Case Study – Conclusions

The first case study discussed in this chapter is a residential development of 125 properties, ASHP heated, powered by wind and solar, and supported by a hybrid Li-ion and lead-acid energy storage system. The analysis is done for off-grid and on-grid options. Across all overgeneration and grid import options, without storage, the on-site generation can't supply 100% of the annual load required, and energy storage systems are required to work alongside the wind and solar generators. The analysis shows the techno-economic parameters of the hybrid storage system for each scenario and hybrid storage ratio.

For the off-grid option, six overgeneration scenarios, 100%, 200%, 300%, 500, 800% and 1300% (Scenario 1-6), are studied and I've shown that even for the extreme 1300% case, the energy storage system must cover 14.7% of the annual demand. For Scenarios 1 to 5, the storage supplies 45.8%, 33%, 27.2%, 21.5%, and 17.8%. of the total annual demand.

The results show that when using hybrid battery storage, the utilisation by each chemistry depends on the overgeneration scenario. For the extreme case, if the hybrid ratio is increased to 4, the lead-acid will cover 27.8%, 8.5%, 7.3%, 4.7%, 4.12% and 3.7% of the demand for Scenarios 1-6. At the same time, Li-ion utilisation will decrease to 18%, 24.5%, 19.9%, 16.8%, 13.68% and 11%. Also, the lead-acid strings perform a maximum of 4.7 equivalent cycles/year (hybrid ratio increased to 4) and the Li-ion between 4.7 and 57 cycles/year. Except for Scenario 1, this implies that the hybrid solutions can be used to reduce the overall system cost.

The cheapest solution for the off-grid option is Scenario 5 (800% overgeneration scenario). If a simple Li-ion chemistry solution is used with the wind and solar generators, the total system cost would be £5.04 million. If a hybrid solution is to be used, the cost can be reduced by a further 10.7% as the hybrid ratio is increased from zero (simple Li-ion solution) to 4. Overall, the cost for Scenario 5 would add £40.32 thousand per property since the storage required is 32 kWh/property.

For the residential on-grid option, I investigated the sizing of hybrid Li-ion and lead-acid battery storage solutions to reduce the grid import requirements by operating the renewables and storage system in peak shaving mode. For the same residential profile and 100% overgeneration (210kW wind generation and 110kW PV), I have analysed 5 grid import scenarios with the import power restrictions of 50, 100, 150, 200 and 250kW (the peak demand is 263kW), and for each, I have calculated the hybridisation potential.

The results show that for Scenario 1 (50 kW grid import), the storage required is 30 MWh. This decreases dramatically to more practical sizes of 6.4, 1.2, 0.9 and 0.7 MWh as the grid import capacity is increased. For Scenarios 3-5 (150-250 kW grid import), the storage required is 9.7, 7.2 and 5.6 kWh / property and this achieves a peak reduction of 42.9%, 23.9% and 4.9%.

For the peak shaving application, the total battery utilisation is lower when compared with the off-grid option, decreasing from 18% to 5.26%, 1.47%, 0.7% and 0.41% for Scenarios 3-5. For the lead-acid strings, the utilisation rate relates to 2.8-2.5x less annual energy delivered when compared with Li-ion strings. Also, this means that even with a modest, less than 2% of the total annual load required, a storage system can reduce the peak grid import power requirements by 42.9%.

As the overgeneration scenario is 100%, for each scenario analysed, the system cost can be reduced by 22.8% if the hybrid storage system is used.

8.7.2 EV Case Study – Conclusions

The second case study is an off-grid EV charging station for the Maxwell Zoo car park.

The model generates an annual hourly load profile for EV charging stations. This has been analysed against the local PV & wind generation profiles to understand how much of the load can be covered directly by on-site generation, the sizing of the storage system required for fully off-grid solutions, the interaction between the hybrid storage system and the EV load profile and the cost of the overall system. Like the residential case study, five scenarios were run with varying renewable overgeneration from 160% to 1200% of the required energy demand over a year. For each scenario, several energy storage solutions were tested with the ratio of lead-acid to Li-ion capacity between 0 and 5.

The modelling shows that energy storage is critical in covering an EV load profile with only wind and solar generation. For Scenario 1, only 34% of the total EV load can be covered by the on-site renewables. Even for Scenario 5, when the generation system is oversized to 1200% of the annual EV load required, there is still around 7.14% of the load which needs to be supplied by an energy storage system.

The modelling calculates the hybrid storage system over the whole year, showing the cycling behaviour of Li-ion and lead-acid. The Li-ion does most of the frequent, short-duration cycles and lead-acid the long-duration ones. For the extremes, in Scenario 1 – hybrid ratio 5 and 160% overgeneration, the Li-ion cells do an equivalent of 0.46 cycles/day (169 cycles/year), contrary to lead-acid, which does 7x less cycling, 0.06 cycles/day (23.2 cycles/year). As the overgeneration increases, most of the short-duration cycles are covered by the PV & wind, for example, in

Scenario 5 – hybrid ratio 5, Li-ion cells performed only 34 equivalent cycles/year (0.09 cycles/day) and lead-acid only 7.8 cycles/year (0.02 cycles/day).

The modelling also shows that cost reduction of battery energy storage systems is possible by using DC-coupled hybrid Li-ion and lead-acid arrangements. The fundamental underlying philosophy of this is that of using cheaper batteries for the long-duration energy storage peaks. This reduces the overall cost of the system by not 'oversizing' the storage system. The rate of cost reductions as a function of the hybrid ratio depends on the storage size required. For the cases analysed, the sharpest cost reductions of around 14% from the initial values were calculated for Scenario 1, between hybrid ratios 0–2. However, the scenario with the lowest system cost overall, including generation and battery storage, was the option with 600% overgeneration and 115 kWh of storage (5 kWh Li-ion and 110 kWh lead-acid). This is around £74000 for the Li-ion only battery solution and £66500 for a hybrid system with a ratio of lead-acid to Li-ion capacity of 5. This shows that for a fully optimised generation and battery storage solution, the hybrid system alone can further reduce the overall system cost by up to 10.1%. However, in practice, it's very difficult to predict the exact EV load profile so it's unlikely that a fully optimised ratio of generation and hybrid battery storage (with the additional optimised hybrid ratio) can be accurately calculated. For large battery storage systems, however, even a few per cent in cost reduction can bring hundreds of thousands of pounds in savings.

8.7.3 Industrial Case Study – Conclusions

For the industrial case study, I have used a real-world electrical demand data set for industrial buildings to test the viability of hybrid Li-ion and lead-acid storage systems. The final load profile is a compilation of multiple industrial buildings' half-hourly electrical demand data with different capacity factors (the final capacity factor is 47%). The peak power demand for the case study is 1 MW.

Like the residential case study, I have analysed an off-grid option, with six different overgeneration scenarios 100%, 200%, 300%, 500, 800% and 1300% to supply 100% of the annual demand. For the on-grid solution, the renewables and storage system are used in peak shaving mode, to minimise the grid connection size. I have analysed 5 grid-constrained scenarios, 20%, 40%, 60%, 80% and 85% of the peak demand.

The off-grid results show that across all overgeneration scenarios, energy storage systems are still required to cover a portion of the demand. For Scenarios 1-6, the energy covered by the storage system is 37.8%, 24.8%, 19.5%, 14.7%, 11.4% and 9%. If hybrid storage systems are used, for the same scenarios, the Li-ion strings will deliver, in a hybrid configuration of ratio 4, 21.75%, 17,65%, 14.33%, 11.96%, 9.6% and 7.26% of the annual load. Except for Scenario 1, the

lead-acid strings are always cycled less than Li-ion and perform a maximum of 6.2 cycles/year. This implies maximum storage utilisation rates of 7.15%, 5.17%, 2.74%, 1.8% and 1.74% for Scenarios 2-6 (200%-1300%). On the other hand, the Li-ion strings deliver between 16 and 82 cycles per year.

These utilisation values show that the energy storage discharge profile is not uniform across the year and hybrid options can be considered to reduce the capital cost. If a standard Li-ion energy storage system is used for the overall renewable and storage system, the lowest cost option is £18.9 million, for the 300% overgeneration (Scenario 3). This can be reduced further by a maximum of 12.69% using hybrid storage of ratio 4.

For the on-grid solution, I have analysed 5 grid import scenarios, 20%, 40%, 60%, 80% and 85% (Scenarios 1-6) of the maximum load peak power requirement. Across these, the storage systems deliver 15.7%, 5.22%, 1.55%, 0.09% and 0.035% of the annual demand. Using the hybrid Li-ion and lead-acid system, for each grid import scenario, the lead-acid strings deliver a maximum of 6.68%, 1.88%, 0.49%, 0.052%, and 0.018% of the load requirement. In terms of cycling, the Li-ion strings deliver between 11.8 and 34.7 equivalent cycles per year. On the other hand, lead-acid delivers only 6.2 cycles per year. The utilisation rates and the number of equivalent cycles indicate that there is a variable energy storage discharge profile, and the hybrid system can be used to reduce the storage cost.

The cost analysis shows that, in comparison with a single Li-ion chemistry storage system, for each grid import scenario, between 1.36% - 18.75% cost reduction is possible. Although impractical because of its large storage requirements, the biggest cost reduction is observed for Scenario 1 (18.75%).

8.7.4 FTM Case Study – Conclusions

For the FTM case study, two 10MW grid-constrained plant options have been investigated as potential applications for the hybrid Li-ion and lead-acid system. The first is a collocated, DC-coupled, 15MW solar PV plant with a 150% DC:AC ratio, and the hybrid battery storage plant. The second is a standalone FTM battery storage using hybrid options. Both plant options have been optimised and modelled to maximise annual revenue by operating the storage in the UK frequency services, balancing markets and the PV plant in a standard power purchase agreement. The optimisation process was done using the 2023 UK dynamic containment and balancing market data. For each option, four battery storage systems of different capacities, 10MW/10 MWh, 10MW/20 MWh, 10MW/40 MWh and 10MW/60 MWh have been studied to understand the number of cycles each chemistry would have to perform in a hybridised system.

The FTM study concludes that for the PV and hybrid system colocation, the Li-ion delivers 760, 595, 442 and 341 equivalent cycles per year for the simple Li-ion option of 1h, 2h, 4h and 6-hour battery storage capacity. As the hybrid ratio is increased, the Li-ion cycling increases, and it reaches 1042, 887, 726, and 600 cycles per year when the hybrid ratio is increased to 4. Although the lead-acid strings are not cycled as often, they still deliver on average, across all hybrid ratios, 545, 443, 265, and 257 cycles per year.

As the storage duration increases from one to six hours, the battery storage system delivers an increasing portion of the energy exported to the grid, which increases from 38%, for the 1h duration, to 72% for the 6-hour storage duration. This is mainly driven by an increasing amount of battery charging from the grid but also the energy transfers in the DC-coupled configuration.

Similarly, for the standalone battery storage system, for the non-hybrid option (single Li-ion chemistry), the storage performs 725, 641, 492 and 386 equivalent cycles per year for the 1h, 2h, 4h and 6-hour duration. At the other extreme, as the hybrid ratio increases to 4, the Li-ion strings perform 960.8, 903, 834 and 716 equivalent cycles per year. For the lead-acid strings, beyond 0.1 hybrid ratio, the average number of annual cycles is 545, 490, 380 and 306 cycles per year for each storage duration analysed. As this is a standalone FTM battery, 100% of the grid utilisation is due to the battery storage operation.

The comparison between the colocation option and the standalone battery system shows that generally (except the 1-hour duration option), the battery storage is utilised more in the standalone system. This is not surprising as the grid must accommodate the PV export in the collocated configuration, which limits the grid space and subsequently the battery charge/discharge operation. The same is valid for the hybrid options which shows that both chemistries perform more cycles per year.

Most importantly, the analysis shows that the energy storage profile is relatively flat across the year, and this does not favour the use of hybrid options. This is indicated by the increased number of lead-acid cycles if the hybrid ratio is greater than 0.1.

8.7.5 Case Studies Summary

Table 8-8 shows the economically optimised scenarios across the analysed case studies, the cost-saving potential if a hybrid storage solution is used, the feasibility of hybrid storage systems and the maximum cost savings potential if no significant overgeneration is possible.

As explained in this chapter, the saving potential of switching from a simple Li-ion storage solution to a hybrid Li-ion and lead-acid depends on the load profile, the cost of energy storage as a share of the total system cost and the cost ratio between the two battery technologies. For

the economically optimised scenarios, the comparison shows that the cost savings vary between 1.36% to 12.69%. In all case studies, the maximum cost reduction possible is for Scenario 1 and, when compared with a single chemistry solution, it can be up to 26.1%. As explained, this is because the energy storage requirements and cost are the largest, and thus the potential for savings is also greater. The minimum price ratio between Li-ion and lead-acid, which justifies the hybrid storage usage, varies between 1.1 to 1.5. If the price ratio between the two chemistries decreases below the indicated limits, a hybrid solution is not justified economically.

Table 8-8 Case Studies Summary

Case Study	Optimised Scenario	Hybrid Storage Cost Savings	Maximum Hybrid Storage Cost Savings	Minimum Price Ratio
Residential off-grid	**Scenario 5:** - 880 kW PV - 1.68 MW Wind - 8.75 MWh Storage	10.7% (Scenario 5, optimised scenario)	25.8% (Scenario 1)	1.1-1.2
Residential on-grid	**Scenario 5:** - 250 kW grid - 110 kW PV - 210 kW Wind - 0.7 MWh Storage	8.5% (Scenario 5, optimised scenario)	22.8% (Scenario 1)	1.1-1.2
EV Charging off-grid	**Scenario 4:** - 15.1 kW PV - 15.1 kW Wind - 0.105 MWh Storage	10.3% (Scenario 4, optimised scenario)	14.3% (Scenario 1)	1.3-1.5
Industrial off-grid	**Scenario 3:** - 2.7 MW PV - 5.7 MW Wind - 45 MWh Storage	12.69% (Scenario 3, optimised scenario)	26.1% (Scenario 1)	1.1
Industrial on-grid	**Scenario 5:** - 850 kW Grid - 1900 kW PV - 900 kW Wind - 0.5 MWh Storage	1.36% (Scenario 5, optimised scenario)	18.75% (Scenario 1)	1.1
FTM PV & Storage Colocation	Not feasible	Not feasible	Not feasible	Not feasible
FTM Storage Colocation	Not feasible	Not feasible	Not feasible	Not feasible
Micro Hydro with PV & Hybrid Storage	**Scenario 3:** - 445 kW PV - 50 kW Micro Hydro - 1 MWh Storage	6.2% (Scenario 3, optimised scenario)	20.8% (Scenario 1)	1.1-1.2

Chapter 9 Conclusions

This thesis begins by introducing the current energy challenges and explains why energy storage is fundamental to a future powered by clean, renewable energy systems. Particularly, in the power systems sector, battery storage is increasingly used for power system stabilisation, balancing and energy arbitrage.

The literature review sections indicate that there is a wide academic literature and real-world applications of hybrid storage, particularly hybrid battery systems, but most of these use active control systems to schedule the power and energy sharing between the technologies used. The literature also shows that, generally, directly connected hybrid systems are not advisable, as different technologies have different voltage operating profiles, and this can result in underutilisation and uneconomical solutions. In the worst case, if the directly connected battery systems are sized incorrectly, it can lead to unstable, dangerous overcharging and runaway effects.

However, this research project shows that the Li-ion (NMC) and lead-acid (VRLA) hybrid battery systems have complementary operating voltage profiles, which allow them to be used successfully in passive, directly connected configurations. As detailed below, the conclusions of this work show that the solution is not only stable but also offers charge/discharge control over the system strings, which is not usually the case for passive architectures. The hybrid system proposed is also cheaper, between 1.36% to 26.1% depending on the applications, and more environmentally friendly when compared with simple Li-ion based options, due to lead-acid batteries' recyclability.

Apart from a few attempts listed in the literature review section, there is no comprehensive research investigating the directly connected NMC and VRLA battery systems. There is a gap in the literature regarding the overall operation of such systems, specifically about the round-trip efficiency, general hybrid behaviour, the energy transferred between the strings and examples of real-world studies.

The work undertaken during this research project fills this gap by answering the following questions:

- What are the hybrid characteristics of directly coupled, hybrid NMC and VRLA systems?
- Can the instantaneous hybrid behaviour be modelled using equivalent circuits?
- How do hybrid battery systems perform over time in real-world applications?
- What storage applications are best suited for hybrid lead-acid and Li-ion systems and what are the associated techno-economic parameters?

The initial set of experimental results presented in Chapter 5, addresses the first question by analysing the performance of five hybrid Li-ion and lead-acid battery energy storage systems to understand the directly connected hybrid behaviour and the benefits of such systems. This was done by comparing various charge/discharge parameters across different hybrid systems with different numbers of strings and voltage levels.

The overarching conclusion is that the hybrid, directly connected, Li-ion and lead-acid battery storage systems are possible as the arrangement is stable, and the voltage profiles of the two chemistries allow for semi-active string control without power converters (it allows for Li-ion and lead-acid strings groups to discharge independently, one after the other). This implies that part of the Li-ion energy capacity can be cycled independently of the lead-acid thus offering the advantage of limiting the additional cost generally associated with hybrid systems.

The first major conclusion of this study is that both, the total energy available from a hybrid system as well as the energy available independently for frequent cycling, are mainly driven by the number of lead-acid strings and the charge/discharge C rates. The number of strings modifies the total energy available by changing the equivalent electrical resistance and the subsequent dynamics of each battery string. The Li-ion energy available for independent cycling can reach around 75-80% of the total Li-ion capacity available when coupled in hybrid configurations, but this happens for C rates below 0.2C. On average, across 0.2-1C rates, each extra lead-acid string reduces the independent Li-ion capacity by around 8%. The total Li-ion energy available does not change on average with the number strings, if the system is discharged below 10% DoD for the lead-acid, the Li-ion energy available is practically the same across all different configurations analysed. However, the total energy available from the hybrid system depends on the lead-acid capacity, more strings imply less current per string for the same discharge current, and this means more energy available for cycling.

The second set of conclusions is related to the round-trip efficiency of the entire system. Again, the number of lead-acid strings relative to the Li-ion ones plays a crucial role. If we increase the number of Li-ion strings, the round-trip efficiency of the hybrid system, when only the Li-ion is cycled, is close to the standalone Li-ion efficiency values of 90-91% for the analysed cells. However, as the number of lead-acid strings is increased, the round-trip efficiency of the system drops by 10-11% per lead-acid string added. The measured round-trip efficiency value for the 1LI&3LA system, when only the Li-ion is cycled, drops to 68%. This happens because the lead-acid activity increases in the A-X region (Chapter 5), with each added string. If the system is discharged below 10% DoD for the lead-acid string, the round-trip efficiency comes close to the overall 86-87%, which is relatively the same across the analysed systems.

The third observation is that the charge and energy transfers between the two chemistries are mainly driven by the number of Li-ion strings. The measured peak energy transferred between the strings is less than 7% of the total Li-ion energy independently available, and less than 1-2.5% of the total energy available. Also, increasing the number of lead-acid strings, or the voltage of the whole system, does not modify peak transient currents and the peak energy transferred between the strings.

Finally, the analysis done in Chapter 5 briefly discusses the intermittent charging process and its effects on the overall performance of the system. The analysis indicates that energy & charge can be transferred between the strings during charging. This changes the round-trip efficiency of the complete (inverter & battery cells) hybrid storage system.

In Chapter 6, I discussed the modelling of the hybrid, directly connected lead-acid and Li-ion energy storage system. The study uses equivalent circuit theory to model the hybrid behaviour and presents the complete process of battery testing, parameters extractions and model building of hybrid Li-ion and lead-acid directly connected systems at the DC bus. As observed during lab testing and later during on-site trials, the operation of the hybrid system allows for the Li-ion strings to be operated independently of the lead-acid, and this offers passive control over the discharge process. I have used MATLAB/Simulink to model the hybrid behaviour and understand how it performs when compared with the experimental data.

The analysis is done by comparing the simulation and the experimental data of a 48V 1LI&1LA system. The modelled results indicate that the average dynamic circulation currents between the strings can be modelled with 90% accuracy, except when the system is discharged to the 20-30% lead-acid DoD range. The comparison is made based on the total energy transferred during the rest period. The discrepancies between the experimental and the simulated values, in the 20-30% lead-acid DoD, are due to the difficulty in modelling the lead-acid cells at high SoC. More advanced models are required to capture the complex lead-acid chemistry in this SoC interval.

The round-trip efficiency and the total charge / discharged energy, as a function of the DoD, can also be predicted with 91% accuracy.

The simulated values for the Li-ion energy available for independent cycling overestimate the experimental values by 10% if the lead-acid is discharged between 10-50%. If the system is operated only in the A-B region, the lead-acid is kept at 100% SoC, the total Li-ion energy can be predicted with 95% accuracy.

To understand the behaviour at different voltage levels and for systems with different numbers of strings, I compared 9 hybrid systems at 48V, 240V and 480V in terms of the circulation currents and energy efficiency. The modelled results suggest that the circulation currents vary with the

lead-acid DoD but do not increase with the system voltage. The energy transferred, however, varies linearly with the DC bus voltage increase. For hybrid systems with multiple strings, the simulation shows that increasing the number of lead-acid strings reduces the transient currents and the energy transferred between the strings. The peak energy transferred decreases on average by 29% for each lead-acid string added. If the Li-ion strings are increased, the opposite happens.

The energy efficiency of the systems depends on the ratio between the Li-ion and the lead-acid charged/discharged energy and the system's DoD. If the system is discharged between 10-50% DoD for the lead-acid strings, the average modelled efficiency varies between 85% and 95% for different Li-ion to lead-acid ratios. The model fails to predict the efficiency drop when the lead-acid strings dominate and only the Li-ion is cycled, A-B region.

Overall, the work undertaken in trying to model the hybrid behaviour, shows that the hybrid Li-ion and lead-acid systems (directly connected), can partially be modelled using simple equivalent circuit theory for general system sizing.

In Chapter 7, I have shown that the dual chemistry Li-ion and lead-acid hybrid storage system is stable over time and can work successfully in real-world applications, without power converters. This was done by monitoring a BTM hybrid Li-ion and lead-acid demonstrator project (100kW system). As expected, the interaction between the two chemistries shows that I can discharge the Li-ion strings independently of the lead-acid one, thus providing semi-control of the strings.

The overall system round-trip efficiency depends on the ratio of Li-ion and lead-acid capacity and the depth of discharge of the overall system. As the system has 3 Li-ion strings and 1 of lead-acid batteries, the calculated average round-trip efficiency across the analysed tests is 90% and the average energy discharged by the system is 210 kWh, 138 kWh being delivered by the lead-acid and 75 kWh by the Li-ion strings.

In real-world applications, the energy transfer between the strings due to different dynamic time constants of the two chemistries depends on the charge stopping point (point C, final SoC point when the system charger is on) and to a lesser extent on the discharge point F (the SoC point when the load current is zero). For the analysed system, the average Li-ion to lead-acid energy transfer during the charging process is 13 kWh, 5.5% of the total charged energy. The average lead-acid to li-in energy transfer during discharge is 5.2 kWh, 2.47% of the total discharged energy.

During discharge, the Li-ion strings provide most of the power between points D-E (discharge interval between 100% and when the power delivered by both strings equalises). The data shows that around 93% of the total Li-ion discharged energy takes place before the lead-acid and Li-ion power share equalises (point E). This is important as it allows the Li-ion strings to be cycled

practically independent of lead-acid and can take most of the short charge/discharge cycles thus protecting the lead-acid.

Building on the Chapter 5, 6 and 7 results, Chapter 8, addresses the last research question of this thesis regarding the hybrid Li-ion and lead-acid battery storage sizing and applications. Five case studies, residential, industrial, EV charging, FTM and commercial with micro hydro, are analysed to determine the hybrid system sizing based on different load profiles. For each case study, I have analysed different scenarios in terms of overgeneration, on-grid/off-grid options and the FTM energy storage duration in either colocation or standalone applications. To determine this, I have used a techno-economic model to test the storage hybridisation possibility. The load profiles and the case studied discussed use real-world data (except for the EV off-grid charging station load profile).

For the first case study, I analysed a residential development of 125 properties, ASHP heated, powered by wind and solar, and supported by the hybrid Li-ion and lead-acid energy storage system. The analysis is done for off-grid and on-grid options. Across all overgeneration and grid import options, the on-site generation without storage can't supply 100% of the annual load required, and energy storage systems are required to work alongside the wind and solar generators. The analysis shows the techno-economic parameters of the hybrid storage system for each scenario and hybrid storage ratio.

For the off-grid option, six overgeneration scenarios, 100%, 200%, 300%, 500, 800% and 1300% (Scenarios 1-6), are studied and I've shown that even for the extreme 1300% case (Scenario 6), the energy storage system still needs to cover 14.7% of the annual demand. For Scenarios 1 to 5, the storage system supplies 45.8%, 33%, 27.2%, 21.5%, and 17.8%. of the total annual demand.

The results show that when using hybrid battery storage, each chemistry utilisation depends on the overgeneration scenario. For the extreme hybrid ratio (the hybrid ratio is increased to 4), for Scenarios 1- 6, the lead-acid will cover 27.8%, 8.5%, 7.3%, 4.7%, 4.12% and 3.7% of the total electrical demand. At the same time, the Li-ion utilisation will decrease to 18%, 24.5%, 19.9%, 16.8%, 13.68% and 11%. Also, the lead-acid strings perform a maximum of 4.7 equivalent cycles/year (hybrid ratio increased to 4) and the Li-ion between 4.7 and 57 cycles/year. Except for Scenario 1, this implies that hybrid solutions can be used to reduce the overall system cost.

The cheapest solution for the off-grid option is Scenario 5 (800% overgeneration scenario). If a simple Li-ion chemistry solution is used with the wind and solar generator, the total system cost would be £5.04 million. If a hybrid solution is to be used, the cost can be reduced by a further 10.7% as the hybrid ratio is increased from zero (simple Li-ion solution) to 4. Overall, the cost for

Scenario 5 would add £40.32 thousand per property since the storage required is 32 kWh/property.

For the residential on-grid option, I investigated the sizing of hybrid Li-ion and lead-acid battery storage solutions to reduce the peak grid import requirements by operating the renewables and storage system in peak shaving mode. For the same residential profile and 100% overgeneration (210kW wind generation and 110kW PV), I have analysed 5 grid import scenarios with the import restrictions of 50, 100, 150, 200 and 250kW (the peak demand is 263kW) and for each, I have calculated the hybridisation potential.

The results show that for Scenario 1 (50kW grid import), the storage is required 30 MWh. This decreased dramatically to more practical sizes of 6.4, 1.2, 0.9 and 0.7 MWh as the grid import capacity is increased. For Scenarios 3-5 (150-250 kW grid import capacities), the storage required is 9.7, 7.2 and 5.6 kWh / property, and this achieves a peak power reduction of 42.9%, 23.9% and 4.9%.

For the peak shaving application, the total battery utilisation is lower when compared with the off-grid options, decreasing from 18% to 5.26%, 1.47%, 0.7% and 0.41% for Scenarios 3-5. For the lead-acid strings, the utilisation rate relates to 2.8-2.5x less annual energy delivered when compared with the Li-ion strings. Also, this means that even with modest storage, less than 2% of the total load required, a storage system can reduce the grid import power requirements by 42.9%.

As the overgeneration scenario is 100%, for each scenario analysed, the system cost can be reduced by a maximum of 22.8% if the hybrid storage system is used.

For the off-grid EV charging station case study, I have modelled the Maxell Zoo (UK) car park.

The model generates an annual hourly load profile for EV charging stations. This has been analysed against the local PV & wind generation profiles to understand how much of the load can be covered directly by on-site generation, the sizing of the storage system required for fully off-grid solutions, the interaction between the hybrid storage system and the EV load profile and the cost of the overall system. Five scenarios were run with varying renewable overgeneration from 160% to 1200% of the required energy demand over a year. For each scenario, several energy storage solutions were tested with the ratio of lead-acid to Li-ion capacity between 0 and 5.

The modelling shows that energy storage is critical in covering an EV load profile with only wind and solar generation. For Scenario 1, only 34% of the total EV load can be covered by the on-site renewables. Even for Scenario 5, when the generation system is oversized to 1200% of the annual

EV load required, there is still around 7.14% of the load which needs to be supplied by an energy storage system.

The modelling calculates the hybrid storage system over the whole year showing the cycling behaviour of Li-ion and lead-acid. The Li-ion does most of the frequent, short-duration cycles and lead-acid the long-duration ones. For the extremes, in Scenario 1 – hybrid ratio 5 and 160% overgeneration, the Li-ion cells do an equivalent of 0.46 cycles/day (169 cycles/year), contrary to lead-acid, which does 7x less cycling, 0.06 cycles/day (23.2 cycles/year). As the overgeneration increases, most of the short-duration cycles are covered by the PV & wind, for example, in Scenario 5 – hybrid ratio 5, Li-ion cells performed only 34 equivalent cycles/year (0.09 cycles/day), and lead-acid only 7.8 cycles/year (0.02 cycles/day).

The modelling also shows that cost reduction of battery energy storage systems is possible by using directly connected hybrid Li-ion and lead-acid arrangements. The fundamental underlying philosophy of this is that of using cheaper batteries for the long-duration energy storage peaks. This reduces the overall cost of the system by not 'oversizing' the system. The rate of cost reductions as a function of the hybrid ratio depends on the storage size required. For the cases analysed, the sharpest cost reductions of around 14.3% from the initial values were calculated for Scenario 1, between hybrid ratios 0–2. However, the scenario with the lowest system cost overall, including generation and battery storage, was the option with 600% overgeneration and 115 kWh of storage (5 kWh Li-ion and 110 kWh lead-acid). This is around £74000 for the Li-ion only battery solution and £66500 for a hybrid system with a ratio of lead-acid to Li-ion capacity of 5. This shows that for a fully optimised generation and battery storage solution, the hybrid system alone can further reduce the overall system cost by up to 10.3%. However, in practice, it's very difficult to predict the exact EV load profile so it's unlikely that a fully optimised ratio of generation and hybrid battery storage (with the additional optimised hybrid ratio) can be accurately calculated. For large battery storage systems, however, even a few per cent in cost reduction can bring hundreds of thousands of pounds in savings.

For the industrial case study, I have used a real-world electrical demand data set for industrial buildings to test the viability of hybrid Li-ion and lead-acid storage systems. The final load profile is a compilation of multiple industrial buildings' half-hourly electrical demand data with different capacity factors (the final capacity factor being 47%). The peak power demand for the case study is 1 MW.

Like the residential case study, I have analysed an off-grid option, with six different overgeneration scenarios 100%, 200%, 300%, 500, 800% and 1300% to supply 100% of the annual demand. For the on-grid solution, the renewables and storage system are used in peak shaving mode to

minimise the grid connection size. I have analysed 5 grid-constrained scenarios, 20%, 40%, 60%, 80% and 85% of the peak demand.

The off-grid results show that across all overgeneration scenarios, energy storage systems are still required to cover a portion of the demand. For Scenarios 1-6, the energy covered by the storage system is 37.8%, 24.8%, 19.5%, 14.7%, 11.4% and 9%. If hybrid storage systems are used, for the same scenarios, the Li-ion strings will deliver, in a hybrid configuration of ratio 4, 21.75%, 17,65%, 14.33%, 11.96%, 9.6% and 7.26% of the annual load. Except in Scenario 1, the lead-acid strings are always cycled less than Li-ion and perform a maximum of 6.2 cycles/year. This implies maximum storage utilisation rates of 7.15%, 5.17%, 2.74%, 1.8% and 1.74% for Scenarios 2-6 (200%-1300%). On the other hand, the Li-ion strings deliver between 16 and 82 cycles per year.

These utilisation values show that the energy storage discharge profile is not uniform across the year and hybrid options can be considered to reduce the capital cost. If a standard Li-ion energy storage system is used for the overall renewable and storage system, the lowest cost option is £18.9 million, for the 300% overgeneration (Scenario 3). This can be reduced further by a maximum of 12.69% for a hybrid system of ratio 4.

For the on-grid solution, I have analysed 5 grid import scenarios, 20%, 40%, 60%, 80% and 85% (Scenarios 1-6) of the maximum load peak requirement. Across these, the storage systems deliver 15.7%, 5.22%, 1.55%, 0.09% and 0.035% of the annual demand. Using the hybrid Li-ion and lead-acid system, for each grid import scenario, the lead-acid strings deliver a maximum of 6.68%, 1.88%, 0.49%, 0.052%, and 0.018% of the load requirement. In terms of cycling, the Li-ion strings deliver between 11.8 and 34.7 equivalent cycles per year. On the other hand, lead-acid delivers only 6.2 cycles per year. The utilisation rates and the number of equivalent cycles indicate that there is a variable energy storage discharge profile, and the hybrid system can be used to reduce the storage cost.

The cost analysis shows that, in comparison with a single Li-ion chemistry storage system, for each grid import scenario, between 1.36% - 18.75% cost reduction is possible. Although impractical because of its large storage requirements, the biggest cost reduction is observed for Scenario 1 (18.75%).

For the FTM case study, two 10MW grid-constrained plant options have been investigated as potential applications for the hybrid Li-ion and lead-acid systems. The first is a collocated, DC-coupled, 15MW solar PV plant with a 150% DC:AC ratio, and the hybrid battery storage plant. The second is a standalone FTM battery storage using hybrid options. Both plant options have been optimised and modelled to maximise annual revenue by operating the storage in the UK

frequency services, balancing markets and the PV plant in a standard power purchase agreement. The optimisation process was done using the 2023 UK dynamic containment and balancing market data. For each option, four battery storage systems of different capacities, 10MW/10MWh, 10MW/20MWh, 10MW/40MWh and 10MW/60MWh have been studied to understand the number of cycles each chemistry would have to perform in a hybridised system.

The FTM study concludes that for the PV and hybrid system colocation, the Li-ion delivers 760, 595, 442 and 341 equivalent cycles per year for the simple Li-ion option of 1h, 2h, 4h and 6-hour battery storage capacity. As the hybrid ratio is increased, the Li-ion cycling increases and it reaches 1042, 887, 726, and 600 cycles per year when the hybrid ratio is increased to 4. Although the lead-acid strings are not cycled as often, they still deliver on average, across all hybrid ratios, 545, 443, 265, and 257 cycles per year.

As the storage duration increases from one to six hours, the battery storage system delivers an increasing portion of the energy exported to the grid, which increases from 38% for the 1-hour duration to 72% for the 6-hour storage duration. This is mainly driven by an increasing amount of battery charging from the grid but also from the energy transfers in the DC-coupled configuration.

Similarly, for the standalone battery storage system, for the non-hybrid option (single Li-ion chemistry) the storage performs 725, 641, 492 and 386 equivalent cycles per year for the 1h, 2h, 4h and 6-hour duration. At the other extreme, as the hybrid ratio increases to 4, the Li-ion strings perform 960.8, 903, 834 and 716 equivalent cycles per year. For the lead-acid strings, beyond 0.1 hybrid ratio, the average number of annual cycles is 545, 490, 380 and 306 cycles per year for each storage duration analysed. As this is a standalone FTM battery, 100% of the grid utilisation is due to the battery storage charge/discharge.

The comparison between the colocation option and the standalone battery system shows that generally (except the 1-hour duration option), the battery storage is utilised more in the standalone system. This is not surprising as the grid must accommodate the PV export in the collocated configuration, which limits the grid capacity space and subsequently the battery charge/discharge operation. The same is valid for the hybrid options, which show that both chemistries perform more cycles per year.

Most importantly, the analysis shows that the energy storage profile is relatively flat across the year, and this does not favour the use of hybrid options. This is indicated by the increased number of lead-acid cycles if the hybrid ratio is greater than 0.1.

Analysing the case studies presented above, I conclude that the hybrid Li-ion and lead-acid system is technically suitable for applications where the interaction between the generation and the load profile results in an irregular annual discharge profile for the energy storage system. This

is the case for the residential (off-grid and on-grid options), industrial (off-grid and on-grid options) and off-grid EV charging stations. Although not all solutions presented above are viable from an economic perspective, cost reduction is possible using hybrid storage systems.

For the current UK frequency and balancing markets environments, the FTM applications are not suitable for the hybrid storage system. This is mainly because the daily storage operation profiles are constant across the year, and it does not provide opportunities for low-cost battery technologies to capture the storage peaks.

Chapter 8 ends by comparing the optimised energy generation and storage scenarios for each case study in terms of cost-saving potential versus the maximum possible for the minimum overgeneration scenario. The minimum cost ratio between Li-ion and lead-acid below which the hybrid storage does not provide cost reductions is also compared. Depending on the case study, the minimum cost ratio varies between 1.1 and 1.5.

9.1.1 Further Work

This section describes the main future work related to the hybrid battery system described in this thesis. There are multiple directions of further studies which include aspects related to battery modelling, experimental testing or power electronics developments.

The first possible work is to continue to test the lab-based hybrid storage system for a more in-depth understanding of the directly connected battery system operation. The results presented in this thesis provide a solid foundation, but further work is required to have a complete understanding of the hybrid system proposed. The first set of tests could be related to the experimental characteristics of the hybrid system operated for a variable load profile. This will determine the efficiency, degradation and the energy and charge transferred between the strings for a more complex charge/discharge profile. This implies programming the electronic load and the battery charger to generate realistic operating profiles, like a standard residential demand curve with PV generation. The current lab arrangement could be modified to allow the electronic load and the power supply to be controlled via MATLAB, with the help of which more complicated charge/discharge profiles could be implemented. For a dynamic load profile, the charge transferred between the strings will be different, and this will provide further insights into the round-trip efficiency and the system degradation.

The second possible set of lab tests is to calculate the degradation for different boost voltage levels for the lead-acid battery. In this thesis, the maximum voltage for the lead-acid cells was 2.35 V/cell and this is linked to the maximum voltage range for the Li-ion operation. This can be increased, to provide a wider voltage range for the independent Li-ion operation. However, if the

lead-acid cells are constantly maintained at boost voltage, possible degradation effects need to be considered. This, however, has not been tested, especially using a dynamic profile when the actual operation of the system in the boost voltage range is only temporary. The complexity of the dynamic load profile can include PV and wind generation charging profiles and dynamic discharge loads. Like the issues mentioned above, further insight is possible for the actual system operating profile with multiple power generation sources.

The third set of tests is related to the temperature impact on the system. All tests done during this research were performed at room temperature. However, additional insights are possible into the system operation over a range of extreme temperatures.

The fourth set of tests is related to the charging methodology. The results regarding the charging strategy presented in the thesis are just an introduction to the topic, and further research is required to determine the most energy-efficient charging strategy for the hybrid system. One possible future research direction is to build a completely new lab-based arrangement, with a dedicated smart charger and test how the energy transferred from the Li-ion strings to the lead-acid impacts the overall round-trip efficiency. The tests can be performed for constant current charging at different C rates or for dynamic profiles. One testing strategy could be pulse charging during the CV period of the charging process. As shown in this thesis, if the current is interrupted and the system is rested, the energy transferred from the Li-ion to the lead-acid can improve the overall round-trip efficiency. However, this was not tested for pulse current charging. Another direction could be to determine if the proposed pulse charging strategy impacts the system degradation. The effect of this would be small and a few years of operation will be required to determine this.

The second major possible workstream is related to the ADEPT system. There are a few options to continue the research started for the pilot project. One possible option is related to the degradation study. One could continue to cycle the hybrid storage system for another 4-5 years to have a complete understanding of the system degradation, as the data presented in the thesis covers only the first years of operation. Apart from the ADEPT data presented in this thesis, there is no research on how the current sharing, the discrimination between the Li-ion and the lead-acid strings or the system dynamics will look like when the system moves beyond 2-3% and up to 20% degradation. Also, the testing conditions done for this research are for peak shaving and discharging the system at constant power during peak hours. This can be improved by using dynamic time-of-use tariffs for the consumer. This way, the discharging will not be done at constant power. Also, if a significant amount of solar is connected to the system, the battery can work in colocation mode, and the long-term effects of a more variable profile can be studied.

Another possible research project is to install additional equipment in the battery container to allow access to the frequency services and balancing markets. The connection can be done via an aggregator. This will allow investigations into the degradation and the feasibility of hybrid battery systems for front-of-the-meter applications. Currently, in this thesis, I have only done this from the modelling perspective, which indicates that the hybrid system investigated is not suitable for frequency response applications. The experimental data can validate the modelling results.

Colocation of the hybrid storage system with PV or wind generation for a particular load profile could be another work stream. This will be able to validate and test the modelling results presented in Chapter 8.

Finally, another research direction for the ADEPT hybrid storage system is to be cycled for another 4-5 years. During this time, one could test periodically in the lab the Li-ion and lead-acid cells to obtain the equivalent circuit parameters. This will determine the ECM parameter evolution over time and at the end of life. Also, impedance spectroscopy can show how the cells degrade differently than in standard battery operation conditions. The results obtained can be integrated into the MATLAB model developed to increase the accuracy of the system modelling.

The modelling of the hybrid behaviour can also be improved. As explained in the thesis, the modelling done so far to predict the transient hybrid behaviour, the current sharing and the round-trip efficiency, is not accurate across the entire SoC range of the hybrid storage system. Additionally, I concluded that the ECM method is not precise enough to model the hybrid behaviour in the transient region, and a completely new approach could provide improved results. As explained, this is especially true for the B-X-C region (Chapter 5) due to the complicated lead-acid chemistry at high SoC. One possible solution is to build more advanced electrochemical models for both chemistries to predict the lead-acid behaviour in the high SoC region and up to the boost voltage.

Further work can also include improvements to the techno-economic calculations done for the hybrid storage sizing. The existing model can be refined by adding improved functions to approximate the empirical hybrid behaviour. The current techno-economic model does not account for the dynamic effects of the hybrid system. The simplest way to implement this is to link the two models developed for this thesis, the Simscape/MATLAB model described in Chapter 6 and the techno-economic model used in Chapter 8. The Simscape/MATLAB model can be called from the main file when the charge/discharge conditions predict circulation currents. The second improvement to the techno-economic model is the addition of the round-trip efficiency of the A-B region. Currently, the model uses the separate round-trip efficiencies of the Li-ion and lead-acid cells but not the combined values. As explained, this is difficult to predict due to the

complex nature of the system, but simple look-up tables can be used. The fourth set of improvements is to integrate an experimental degradation profile for the hybrid arrangement and self-discharge functions, especially for the lead-acid. Currently, the model includes this, but the degradation is based on the existing literature for the separate Li-ion and lead-acid based systems. The final suggestion to improve the techno-economic model is to implement charging strategies specific to the hybrid model. These can include pulse charging methods for the CV mode.

Another set of investigations which can build on the existing research is to determine the ion diffusion rates for both battery types and propose alterations to the cell's designs to match the dynamic response and minimise the circulation currents. If electrochemical models are used to improve the understanding of the hybrid behaviour, the same models can dictate the ion diffusion rates for the two chemistries. This can inform the cell manufacturing specifically for the hybrid system.

Although the focus of the thesis is the directly connected Li-ion and lead-acid hybrid systems, a further line of work could be to investigate an inverter/charger design which also monitors the string currents to anticipate the hybrid behaviour and minimise the transient energy transfers between the strings. This can be done by developing power electronics equipment connected in series with each string type and adjusting the voltage to eliminate the voltage difference and thus minimise the circulating currents.

9.1.2 Project legacy

1. The hybrid storage system is investigated further at the University of Southampton as part of the FEVER programme (Future Electric Vehicle Energy Networks supporting Renewables). The project aims to develop an off-grid EV charging station using renewable generation and the hybrid Li-ion and lead-acid system.
2. Following a presentation on this work at the Asian Battery Conference, the battery system manufacturer, Battery Energy Power Solutions Pty Ltd (Australia) took the idea further to analyse LFP and VRLA hybrid battery options. I have briefly corresponded with them and compared our results.

Appendix A Li-ion and Lead-acid Data

9.1.3 Li-ion and Lead-acid Parameters

9.1.3.1 Li-ion parameters

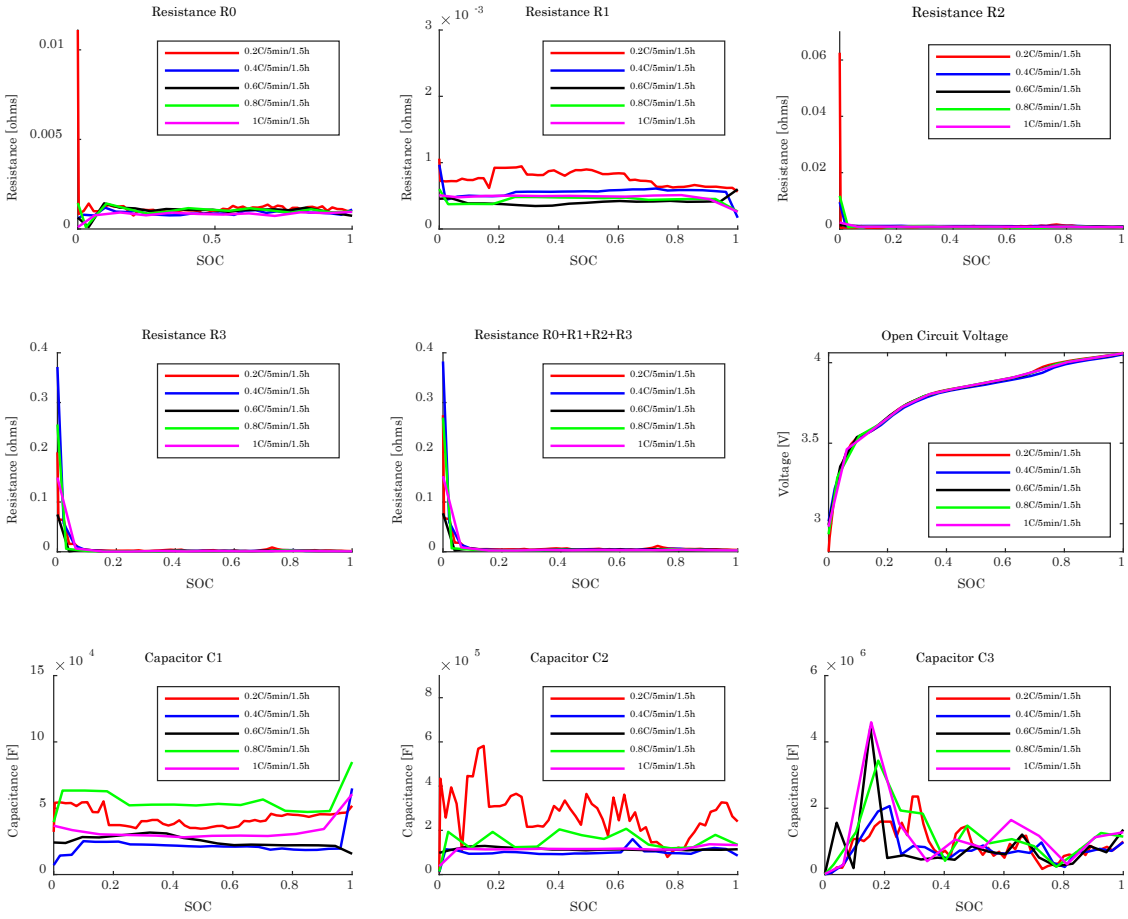

9.1.3.2 Li-ion parameters comparison

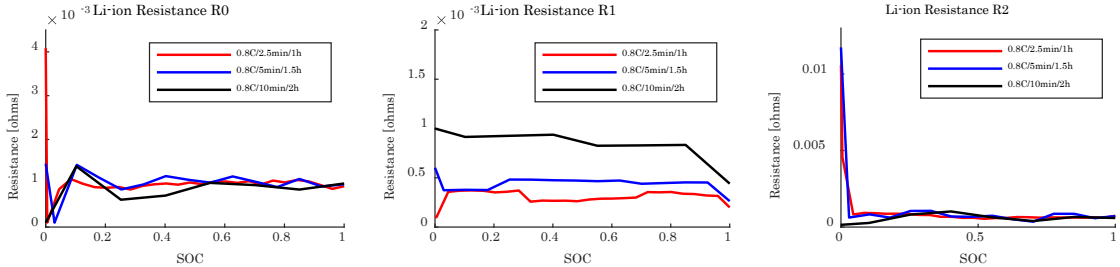

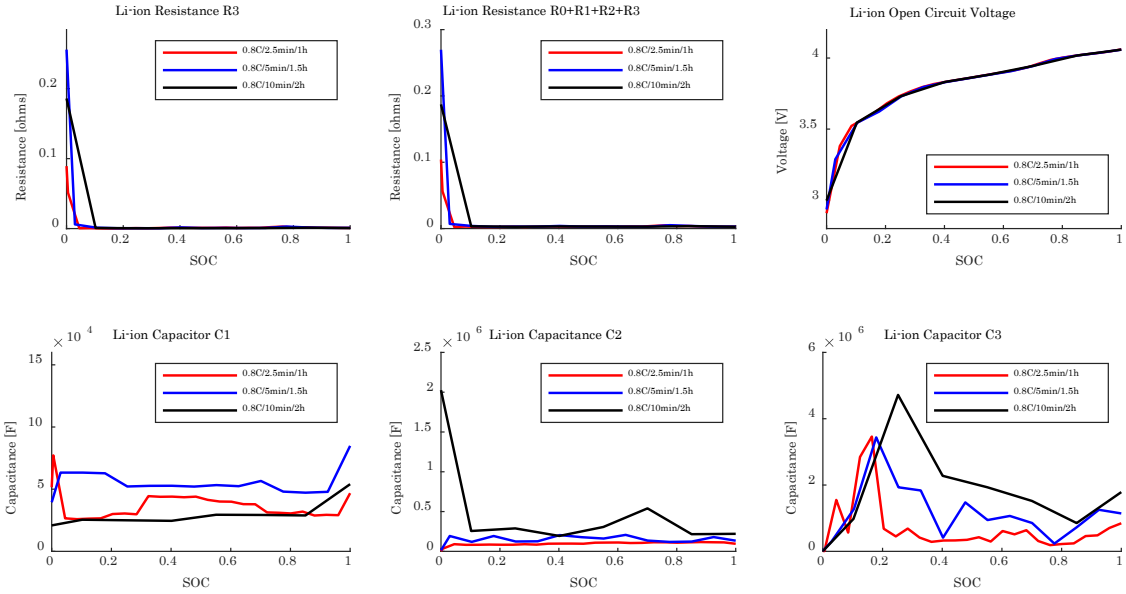

9.1.3.3 Lead-acid parameters overview

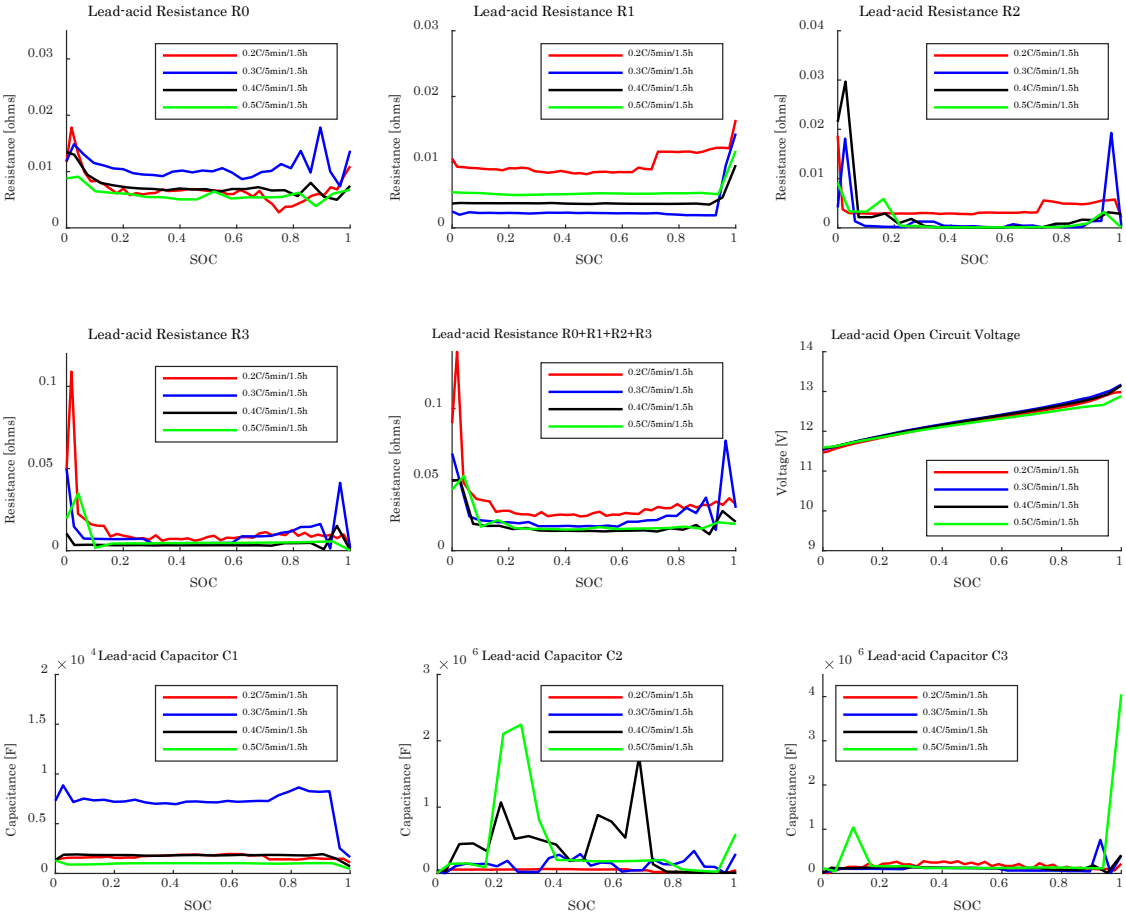

9.1.3.4 Lead-acid parameters comparison

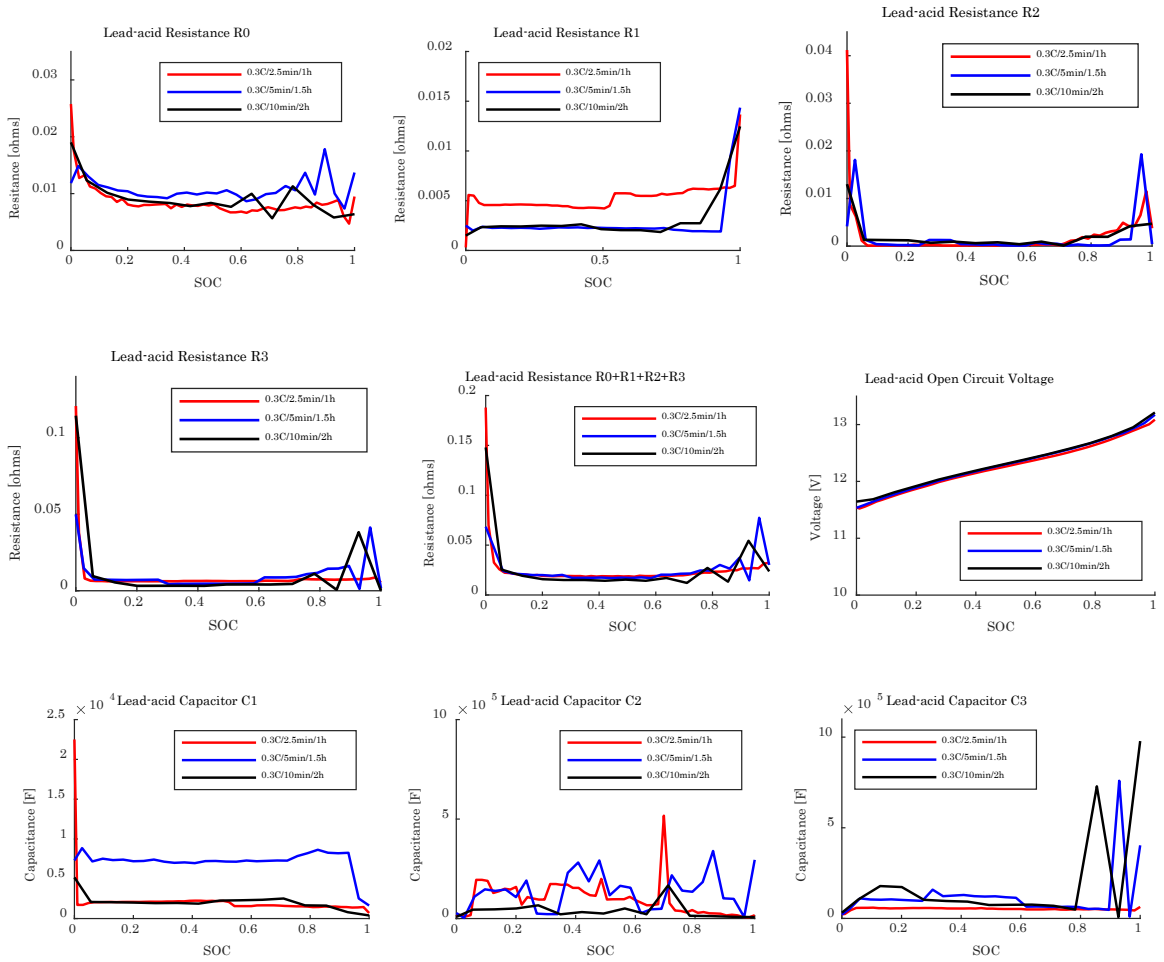

9.1.4 Li-ion and Lead-acid Battery Cost

name		2.5kW, 5kWh	5kW, 10kWh	10kW, 20kWh	15kW, 30kWh	50kW, 106kWh	100kW, 213kWh	250kW, 530kWh	0.5MW, 1MWh	1MW, 2MWh
Capacity	kW	2.50	5.00	10.00	15.00	50.00	100.00	250.00	500.00	1000.00
Effective Charge Capacity	kWh	5.00	10.00	20.00	30.00	106.00	213.00	530.00	1000.00	2000.00
Round-trip Efficiency	%	85.00	85.00%	85.00%	85.00	85.00%	85.00%	85.00%	85.00%	85.00%
Cycles	no.	2000	2000	2000	2000	2000	2000	2000	2000	2000
CAPEX	£/kW	666.67	633.33	620.00	616.67	600.00	566.67	520.00	473.33	436.67
$O\&M_{fixed}$	£/MW	20.00	19.00	18.60	18.50	18.00	17.00	15.60	14.20	13.10
Service Life	years	11.00	11.00	11.00	11.00	11.00	11.00	11.00	11.00	11.00
$REPEX_{annualised}$	£/kW/year	24.24	23.03	22.55	22.42	21.82	20.61	18.91	17.21	15.88

name		2.5kW, 5kWh	5kW, 10kWh	10kW, 20kWh	15kW, 30kWh	50kW, 106kWh	100kW, 213kWh	250kW, 530kWh	0.5MW, 1MWh	1MW, 2MWh
Capacity	kW	2.50	5	10	15	50	100	250	500	1,000
Effective Charge Capacity	kWh	5	10	20	30	106	213	530	1,000	2,000
Round-trip Efficiency	%	95%	95%	95%	95%	95%	95%	95%	95%	95%
Cycles	no.	5,000	5,000	5,000	5,000	5,000	5,000	5,000	5,000	5,000
CAPEX	£/kW	£1,000	£950	£930	£925	£900	£850	£780	£710	£655
$O\&M_{fixed}$	£/MW	£30	£29	£28	£28	£27	£26	£23	£21	£20
Service Life	years	11	11	11	11	11	11	11	11	11
$REPEX_{annualised}$	£/kW/year	£36.36	£34.55	£33.82	£33.64	£32.73	£30.91	£28.36	£25.82	£23.82

Bibliography

1. Adelman, J., *Worlds Together, Worlds Apart - A History of the World from the Beginnings of humankind to the Present* Vol. 1. 2011: W. W. Norton & Company. 993.
2. Schwab, K., *The Fourth Industrial Revolution*. 2016: World Economic Forum. 172.
3. BP, *BP Statistical Review of World Energy*. 2022: UK. p. 61.
4. IEA, *World Energy Outlook - 2023*. 2023. p. 661.
5. IPCC, *Climate Change 2014 - Synthesis Report*. 2015, IPCC: Geneva, Switzerland.
6. IPCC, *IPCC Special Report on Global Warming of 1.5°C*. 2018, IPCC: Geneva, Switzerland. p. 630.
7. Hickel, J., *Less is more: How degrowth will save the world*. 2020: Random House.
8. Bashmakov, I., *Three laws of Energy Transitions.* Energy Policy, 2007. **35**(7): p. 3583–3594.
9. Helm, D., *The Carbon Crunch*. Second ed. Vol. 1. 2015: Yale University Press. 282.
10. Helm, D., *Burn Out*. -, ed. -. Vol. 1. 2018: Yale University Press. 281.
11. Statista. *Global gross domestic product (GDP)*. 2023; Available from: https://www.statista.com/statistics/268750/global-gross-domestic-product-gdp/.
12. CarbonBrief. *CarbonBrief*. 2023 2023]; Available from: https://www.carbonbrief.org/mapped-worlds-coal-power-plants.
13. REN21, *Key Messages for Decision Makers*. 2021, REN21. p. 32.
14. IRENA, *Renewable Power Generation Costs in 2020*. 2021: Abu Dhabi. p. 180.
15. BEIS, *Modelling 2050: Electricity System Analysis*. 2020, BEIS: UK. p. 35.
16. (IRENA), I.R.E.A., *Renewable Capacity Statistics 2023*. 2023: IRENA.
17. Governement, H., *Building our Industrial Strategy*. 2017, HM Governement: UK. p. 132.
18. Governement, H., *Industrial Strategy - Building a Britain fit for the future*. 2017, HM Government: UK. p. 256.
19. Schill, W.-P. and A. Zerrahn, *Long-run power storage requirements for high shares of renewables: Results and sensitivities.* Renewable and Sustainable Energy Reviews, 2018. **83**: p. 156-171.
20. Zerrahn, A., W.-P. Schill, and C. Kemfert, *On the economics of electrical storage for variable renewable energy sources.* European Economic Review, 2018. **108**: p. 259-279.
21. AURORA, *Long duration electricity storage in GB*. 2022, Aurora Energy Research: United Kingdom. p. 43.
22. Ltd, D.K., *The Benefits of Pumped Storage Hydro to the UK*. 2016: UK. p. 43.

23. Media, S. *UK Battery Storage Project Database*. 2022; Available from: https://marketresearch.solarmedia.co.uk/products/uk-battery-storage-project-database-report.

24. IRENA, E.T., Thomas Nikolakakis, Carlos Fernandez and Aakarshan Vaid (IRENA), Ann Yu, Vinayak Walimbe and Mark Tinkler (Customized Energy Solutions, Ltd), and Randell Johnson (acelerex), *Electricity Storage Valuation Framework*. March 2020, IRENA.

25. IEA. *Grid-scale Storage*. 2023; Available from: https://www.iea.org/energy-system/electricity/grid-scale-storage.

26. IRENA, E.S., *Renewables: Costs and Market to 2030*. 2017, October.

27. Ahmed F. Zobaa, P.F.R. and S.H.E.A.A.a.S.N. Afifi, *Energy Storage at Different Voltage Levels*. Vol. 1. 2018, UK: IET. 354.

28. Frank S. Barnes, J.G.L., *Large Energy Storage Systems*. Vol. 1. 2011: CRC Press Taylor & Francis Group. 254.

29. Sabihuddin, S., A.E. Kiprakis, and M. Mueller, *A numerical and graphical review of energy storage technologies*. Energies, 2015. **8**(1): p. 172-216.

30. Moseley, P.T. and J. Garche, *Electrochemical energy storage for renewable sources and grid balancing*. 2014: Newnes.

31. Xue, X., K. Cheng, and D. Sutanto. *Power system applications of superconducting magnetic energy storage systems*. in *Fourtieth IAS Annual Meeting. Conference Record of the 2005 Industry Applications Conference, 2005.* 2005. IEEE.

32. Shinichi, M., *Development of Superconducting technologies for the Smart Grid*. Furukawa Review, 2013(43).

33. Kim, B.K., et al., *Electrochemical supercapacitors for energy storage and conversion*. Handbook of Clean Energy Systems, 2015: p. 1-25.

34. Warner, J., *Handbook of lithium-ion battery pack design, chemistry, components, types and terminology*. Vol. 1. 2015, USA: Elsevier Inc, 225 Wyman Street, Waltham, MA 02451. 263.

35. Luo, X., et al., *Overview of current development in electrical energy storage technologies and the application potential in power system operation*. Applied energy, 2015. **137**: p. 511-536.

36. Mortimer, R.G., *Physical Chemistry*. Third Edition ed. Vol. 1. 2008, USA: Elsevier Academic Press. 1301.

37. Albright, G., J. Edie, and S. Al-Hallaj, *A comparison of lead acid to lithium-ion in stationary storage applications*. Published by AllCell Technologies LLC, 2012.

38. Korthauer, R., *Lithium-Ion Batteries: Basics and Applications*. 2017, Germany: Springer-Verlag GmbH Germany.

39. MEDIA, S. *UK Battery Storage Project Database Report*. 2020 [cited 2020; Available from: https://marketresearch.solarmedia.co.uk/products/uk-battery-storage-project-database-report.

40. ABB, *World's Largest Battery Energy Storage System*. 2009, ABB: USA. p. 4.

41. Doughty, D.H., et al., *Batteries for Large-Scale Stationary Electrical Energy Storage*. Electrochemical Society Interface, 2010: p. 49.

42. Chalamala, B.R., et al., *Redox flow batteries: an engineering perspective*. Proceedings of the IEEE, 2014. **102**(6): p. 976-999.

43. Weber, A.Z., et al., *Redox flow batteries: a review*. Journal of Applied Electrochemistry, 2011. **41**(10): p. 1137.

44. Alotto, P., M. Guarnieri, and F. Moro, *Redox flow batteries for the storage of renewable energy: A review*. Renewable and Sustainable Energy Reviews, 2014. **29**: p. 325-335.

45. Yuasa, G. *GS Yuasa Batteries Industrial Range*. 2024; Available from: https://www.yuasa.co.uk/batteries/industrial.html.

46. Bača, P., et al., *Heat Effects during the Operation of Lead-Acid Batteries*. Batteries, 2024. **10**(5): p. 148.

47. Catherino, H.A., F.F. Feres, and F. Trinidad, *Sulfation in lead–acid batteries*. Journal of Power Sources, 2004. **129**(1): p. 113-120.

48. Sharpe, T. and R. Conell, *Low-temperature charging behaviour of lead-acid cells*. Journal of applied electrochemistry, 1987. **17**(4): p. 789-799.

49. Alshabib, K.R. and T. Tural. *Temperature Effect on Performance Parameters of Valve Regulated Lead Acid (VRLA) Batteries: An Experimental Study for off-grid system*. in *2022 Saudi Arabia Smart Grid (SASG)*. 2022. IEEE.

50. Bhatt, J.M. *Experimental Study About Effect of Temperature on Performance Parameters of Valve Regulated Lead Acid (VRLA) Battery*. in *2019 IEEE International Conference on Sustainable Energy Technologies and Systems (ICSETS)*. 2019. IEEE.

51. Ma, S., et al., *Temperature effect and thermal impact in lithium-ion batteries: A review*. Progress in Natural Science: Materials International, 2018. **28**(6): p. 653-666.

52. Leng, F., C.M. Tan, and M. Pecht, *Effect of temperature on the aging rate of Li ion battery operating above room temperature*. Scientific reports, 2015. **5**(1): p. 12967.

53. Leng, F., et al. *The effect of temperature on the electrochemistry in Lithium-ion batteries*. in *2014 International Symposium on Next-Generation Electronics (ISNE)*. 2014. IEEE.

54. Razi, M.F.I.M., et al., *Li-NMC Battery Internal Resistance at Wide Range of Temperature*. Journal of Advanced Research in Fluid Mechanics and Thermal Sciences, 2022. **99**(1): p. 9-16.

55. Lou, T.T., et al., *The internal resistance characteristics of lithium-ion battery based on HPPC method*. Advanced materials research, 2012. **455**: p. 246-251.

56. Łebkowski, A., *Temperature, overcharge and short-circuit studies of batteries used in electric vehicles*. Przeglad Elektrotechniczny, 2017. **1**(5): p. 69-75.

57. Lv, S., et al., *The influence of temperature on the capacity of lithium ion batteries with different anodes*. Energies, 2021. **15**(1): p. 60.

58. Teliz, E., C. López-Vázquez, and V. Díaz, *Degradation study for 18650 NMC batteries at low temperature*. Electrochimica Acta, 2024. **475**: p. 143540.

59. Spitthoff, L., P.R. Shearing, and O.S. Burheim, *Temperature, ageing and thermal management of lithium-ion batteries*. Energies, 2021. **14**(5): p. 1248.

60. Zülke, A., et al., *High-energy nickel-cobalt-aluminium oxide (NCA) cells on idle: anode-versus cathode-driven side reactions*. Batteries & Supercaps, 2021. **4**(6): p. 934-947.

61. Lam, V.N., et al., *A decade of insights: Delving into calendar aging trends and implications*. Joule, 2025. **9**(1).

62. Yuksel, T. and J.J. Michalek, *Effects of regional temperature on electric vehicle efficiency, range, and emissions in the United States*. Environmental science & technology, 2015. **49**(6): p. 3974-3980.

63. Hemmati, R. and H. Saboori, *Emergence of hybrid energy storage systems in renewable energy and transport applications–A review*. Renewable and Sustainable Energy Reviews, 2016. **65**: p. 11-23.

64. Farhadi, M. and O. Mohammed, *Energy storage technologies for high-power applications*. IEEE Transactions on Industry Applications, 2015. **52**(3): p. 1953-1961.

65. Lain, M.J., J. Brandon, and E. Kendrick, *Design Strategies for High Power vs. High Energy Lithium Ion Cells*. Batteries, 2019. **5**(4): p. 64.

66. Hajiaghasi, S., A. Salemnia, and M. Hamzeh, *Hybrid energy storage system for microgrids applications: A review*. Journal of Energy Storage, 2019. **21**: p. 543-570.

67. Chong, L.W., et al., *Hybrid energy storage systems and control strategies for stand-alone renewable energy power systems*. Renewable and sustainable energy reviews, 2016. **66**: p. 174-189.

68. Dougal, R.A., S. Liu, and R.E. White, *Power and life extension of battery-ultracapacitor hybrids*. IEEE Transactions on components and packaging technologies, 2002. **25**(1): p. 120-131.

69. Grün, T., et al., *Passive Hybrid Storage Systems: Influence of circuit and system design on performance and lifetime*. Energy Procedia, 2018. **155**: p. 336-349.

70. Ma, T., H. Yang, and L. Lu, *Development of hybrid battery–supercapacitor energy storage for remote area renewable energy systems*. Applied Energy, 2015. **153**: p. 56-62.

71. Bentley, P. and D.A. Stone. *The parallel combination of a valve regulated lead acid cell and supercapacitor for use as a hybrid vehicle peak power buffer*. in *2005 European Conference on Power Electronics and Applications*. 2005. IEEE.

72. Ise, T., M. Kita, and A. Taguchi, *A hybrid energy storage with a SMES and secondary battery*. IEEE Transactions on Applied Superconductivity, 2005. **15**(2): p. 1915-1918.

73. Dambone Sessa, S., et al., *Li-Ion Battery-Flywheel Hybrid Storage System: Countering Battery Aging During a Grid Frequency Regulation Service*. Applied Sciences, 2018. **8**(11): p. 2330.

74. F. Burke, A.F., J. Bracken, *Flywheel-Battery Hybrid for Grid Stability*. 2017, Schwundrad Energie.

75. Becker, J., et al., *Dimensioning and optimization of hybrid li-ion battery systems for EVs*. World Electric Vehicle Journal, 2018. **9**(2): p. 19.

76. Lemofouet, S. and A. Rufer. *Hybrid energy storage system based on compressed air and super capacitors with MEPT (maximum efficiency point tracking)*. in *IPEC 2005: International Power Electronics Conference*. 2005.

77. Zhao, P., Y. Dai, and J. Wang, *Design and thermodynamic analysis of a hybrid energy storage system based on A-CAES (adiabatic compressed air energy storage) and FESS (flywheel energy storage system) for wind power application*. Energy, 2014. **70**: p. 674-684.

78. Thounthong, P., S. Raël, and B. Davat, *Control strategy of fuel cell/supercapacitors hybrid power sources for electric vehicle*. Journal of Power Sources, 2006. **158**(1): p. 806-814.

79. Sander, M., et al., *LIQHYSMES storage unit–Hybrid energy storage concept combining liquefied hydrogen with Superconducting Magnetic Energy Storage*. International journal of hydrogen energy, 2012. **37**(19): p. 14300-14306.

80. Jiang, Z., et al., *Design and experimental tests of control strategies for active hybrid fuel cell/battery power sources*. Journal of power sources, 2004. **130**(1-2): p. 163-171.

81. Zimmermann, T., et al., *Review of system topologies for hybrid electrical energy storage systems*. Journal of Energy Storage, 2016. **8**: p. 78-90.

82. Waag, W., S. Käbitz, and D.U. Sauer, *Experimental investigation of the lithium-ion battery impedance characteristic at various conditions and aging states and its influence on the application*. Applied energy, 2013. **102**: p. 885-897.

83. Chen, Z. *High pulse power system through engineering battery-capacitor combination*. in *Collection of Technical Papers. 35th Intersociety Energy Conversion Engineering Conference and Exhibit (IECEC)(Cat. No. 00CH37022)*. 2000. IEEE.

84. Sikha, G. and B.N. Popov, *Performance optimization of a battery–capacitor hybrid system*. Journal of Power Sources, 2004. **134**(1): p. 130-138.

85. Chuan, Y., C. Mi, and M. Zhang, *Comparative study of a passive hybrid energy storage system using lithium ion battery and ultracapacitor*. World Electric Vehicle Journal, 2012. **5**(1): p. 83-90.

86. Song, Z., et al., *A comparison study of different semi-active hybrid energy storage system topologies for electric vehicles*. Journal of Power Sources, 2015. **274**: p. 400-411.

87. Christian Julien, A.M., Ashok Vijh, Karim Zaghib, *Lithium Batteries - Science and Technology*. Vol. 1. 2016, New York: Springer International Publishing.

88. Quinn, J.B., et al., *Energy density of cylindrical Li-ion cells: A comparison of commercial 18650 to the 21700 cells*. Journal of The Electrochemical Society, 2018. **165**(14): p. A3284-A3291.

89. Burke, A. and M. Miller, *The power capability of ultracapacitors and lithium batteries for electric and hybrid vehicle applications*. Journal of Power Sources, 2011. **196**(1): p. 514-522.

90. Takeda, K., et al. *Design of hybrid energy storage system using dual batteries for renewable applications*. in *2014 IEEE PES General Meeting| Conference & Exposition*. 2014. IEEE.

91. Dascalu, A., et al., *Performance of a hybrid battery energy storage system*. Energy Reports, 2022. **8**: p. 1-7.

92. Chung, S. and O. Trescases, *Hybrid energy storage system with active power-mix control in a dual-chemistry battery pack for light electric vehicles*. IEEE Transactions on Transportation Electrification, 2017. **3**(3): p. 600-617.

93. Chung, S., *Hybrid Lead-Acid/Lithium-Ion Energy Storage System with Power-Mix Control for Light Electric Vehicles*, in *Electrical and Computer Engineering*. 2016, University of Toronto: Canada. p. 95.

94. Thien, T., et al. *Planning of grid-scale battery energy storage systems: Lessons learned from a 5 MW hybrid battery storage project in Germany*. in *Proc. BATTCON Int. Battery Conf*. 2015.

95. Schweer, D., A. Maaz, and A. Moser. *Optimization of frequency containment reserve provision in M5BAT hybrid battery storage*. in *2016 13th International Conference on the European Energy Market (EEM)*. 2016. IEEE.

96. (NEDO), N.E.a.I.T.D.O. *Demonstration Project in Germany Large-Scale Hybrid power storage System Starting to Operate in November*. 2018 2020]; Available from: https://www.nedo.go.jp/english/news/AA5en_100396.html.

97. Oxford, E.S. *Hybrid battery*. 2021; Available from: https://energysuperhuboxford.org/technologies/battery-energy-storage/.

98. PressCenter. *Bosch: Double battery for energy storage facility in Braderup*. 2014; Available from: https://presscenter.com/bosch-double-battery-for-energy-storage-facility-in-braderup/.

99. Held, L., et al., *Grid-friendly operation of a hybrid battery storage system*. 2019.

100. Hitachi, L. *Poland's largest hybrid battery energy storage system commences full-scale technology demonstration*. 2020; Available from: https://www.hitachi.eu/en/poland-largest-hybrid-battery-energy-storage-system.

101. HOPPECKE. *On the grid: innovative HOPPECKE hybrid storage system successfully commissioned*. 2017; Available from: https://www.hoppecke.com/de/stories/show/am-netz-innovativer-hoppecke-hybrid-grossspeicher-erfolgreich-in-betrieb-genommen/.

102. GS-Yuasa. *GS Yuasa power the world's first container dual chemistry energy storage system*. 2019; Available from: https://www.yuasa.co.uk/2019/01/gs-yuasa-power-the-worlds-first-container-dual-chemistry-energy-storage-system/.

103. Yuasa, G. *GS Yuasa Hybrid Battery for EV Charging Station - Portsmouth Port*. 2021; Available from: https://www.yuasa.co.uk/2020/10/gs-yuasa-batteries-installed-in-ground-breaking-portsmouth-port-electric-vehicle-charging-station/.

104. BOS. *BOS-LE300*. 2021; Available from: https://www.bos-ag.com/products/le300/.

105. Elkadragy, M.M. *Off-Grid Hybrid Systems Techno-Economic Study*. 2020; Available from: https://ae4h.org/projects/ohres.

106. Elkadragy, M.M., et al., *Off-grid and decentralized hybrid renewable electricity systems data analysis platform (OSDAP): A building block of a comprehensive techno-economic approach based on contrastive case studies in Sub-Saharan Africa and Canada*. Journal of Energy Storage, 2021. **34**: p. 101965.

107. Elkadragy, M.M., et al. *Contrastive Techno-Economic Analysis Concept for Off-Grid Hybrid Renewable Electricity Systems Based on comparative case studies within Canada and Uganda*. in *Proceedings of the 3rd International Hybrid Power Systems Workshop, Tenerife, Spain*. 2018.

108. Bestmag. *GS Yuasa dual-chemistry BESS installed in multi-technology energy centre at UK's Royal Mint*. 2023; Available from: https://www.bestmag.co.uk/gs-yuasa-dual-chemistry-bess-installed-in-multi-technology-energy-centre-at-uks-royal-mint/.

109. Nio. *NIO Launches the Standard-Range Hybrid-Cell Battery*. 2021; Available from: https://www.nio.com/news/nio-launches-standard-range-hybrid-cell-battery.

110. Randall, C. *Nio introduces new battery pack combining NMC & LFP cells*. 2021; Available from: https://www.electrive.com/2021/09/24/nio-introduces-new-battery-pack-combining-nmc-lfp-cells/.

111. Ruddock, D. *NIO wants to lower its EV prices even more using LFP*. 2023; Available from: https://electrek.co/2023/12/11/nio-wants-to-lower-its-ev-prices-even-more-using-lfp/#:~:text=Currently%2C%20the%20company%20uses%20NMC,LFP's%20poor%20cold-weather%20performance.

112. One. *Gemini Dual-Chemistry Battery Powers BMW iX 608 Miles*. 2023; Available from: https://one.ai/dual-chemistry-gemini-battery-powers-bmw-ix-608-miles-on-a-single-charge.

113. Abuelsamid, S. *Our Next Energy Dual-Chemistry Battery Achieves Over 600-Mile Range*. 2023; Available from: https://www.forbes.com/sites/samabuelsamid/2023/11/30/our-next-energy-dual-chemistry-battery-achieves-over-600-mile-range/.

114. Hanley, S. *BMW iX With ONE Battery Pack Drives 978 Km On Single Charge*. 2023; Available from: https://cleantechnica.com/2023/12/04/bmw-ix-with-one-battery-pack-drives-978-km-on-single-charge/.

115. LUTZ, H. *Our Next Energy develops EV battery with 608-mile range for BMW iX*. 2023; Available from: https://www.autonews.com/mobility-report/our-next-energy-develops-608-mile-range-ev-battery-bmw-ix.

116. Zhang, C., et al., *Online estimation of battery equivalent circuit model parameters and state of charge using decoupled least squares technique*. Energy, 2018. **142**: p. 678-688.

117. Instruments, G. *Electrochemical Impedance Spectroscopy*. 2008; Available from: https://www.gamry.com/application-notes/.

118. Pavlov, D., *Lead-acid batteries: science and technology*. 2011: Elsevier.

119. Peter Atkins, J.D.P., *Physical Chemistry*. 8th ed. Vol. 1. 2006, New York: W. H. Freeman and Company. 1021.

120. Cole, K.S. and R.H. Cole, *Dispersion and absorption in dielectrics I. Alternating current characteristics*. The Journal of chemical physics, 1941. **9**(4): p. 341-351.

121. Lasia, A., *Electrochemical Impedance Spectroscopy and its Applications*. Vol. -. 2014, New York Heidelberg Dordrecht London: Springer. 365.

122. Rodgers, D.B. *The Constant Phase Element (CPE)*. 2012; Available from: http://consultrsr.net/resources/eis/cpe1.htm.

123. Plett, G.L., *Battery Management Systems - Battery Modeling*. Battery Modeling. Vol. Volume I. 2015, US: Artech House 685 Canton Street Norwood, MA 02062. 343.

124. Plett, G.L., *Battery Management Systems - Equivalent-Circuit Methods*. Vol. II. 2016, 685 Canton Street Norwood, MA 02062: Artech House. 329.

125. Feng, J., Y. He, and G. Wang, *Comparison study of equivalent circuit model of Li-Ion battery for electrical vehicles*. Res. J. Appl. Sci. Eng. Technol, 2013. **6**: p. 3756-3759.

126. He, H., R. Xiong, and J. Fan, *Evaluation of lithium-ion battery equivalent circuit models for state of charge estimation by an experimental approach*. energies, 2011. **4**(4): p. 582-598.

127. Jiunchun Jiang, C.Z., *Fundamentals and Applicaitons of Lithium-Ion Batteries in Electric Drive Vehicles*. Vol. 1. 2015, Beijing Jiaotong University, China: John Wiley & Sons Singapore Pte. Ltd. 299.

128. Liu, X., W. Li, and A. Zhou, *PNGV equivalent circuit model and SOC estimation algorithm for lithium battery pack adopted in AGV vehicle*. Ieee Access, 2018. **6**: p. 23639-23647.

129. Wei, X., X. Zhao, and Y. Yuan. *Study of equivalent circuit model for lead-acid batteries in electric vehicle*. in *2009 International Conference on Measuring Technology and Mechatronics Automation*. 2009. IEEE.

130. Zhang, X., W. Zhang, and G. Lei, *A review of li-ion battery equivalent circuit models*. Trans. Electr. Electron. Mater, 2016. **17**(6): p. 311-316.

131. Zhang, L., et al., *Comparative research on RC equivalent circuit models for lithium-ion batteries of electric vehicles*. Applied Sciences, 2017. **7**(10): p. 1002.

132. Li, S. and X. Cheng. *A comparative study on RC models of lithium-ion battery*. in *2014 IEEE Conference and Expo Transportation Electrification Asia-Pacific (ITEC Asia-Pacific)*. 2014. IEEE.

133. Intelligence, W.P.E.-M. *Mynydd Portref - Wind Farm*. 2023; Available from: https://www.thewindpower.net/windfarm_en_18838_mynydd-portref.php.

134. Energy, R. *The UK's first consumer owned wind farm*. 2022; Available from: https://rippleenergy.com/our-projects/graig-fatha.

135. Yuasa, G. *GS Yuasa batteries set the gold standard in sustainable energy as new Royal Mint Energy Centre is unveiled*. 2023; Available from: https://www.yuasa.co.uk/2023/08/gs-yuasa-batteries-set-the-gold-standard-in-sustainable-energy-as-new-royal-mint-energy-centre-is-unveiled/.

136. Atlas, G.W. *Wind Data*. 2023; Available from: https://globalwindatlas.info/en/.

137. SolarEdge. 2023; Available from: https://www.solaredge.com/en/products/software-tools/designer.

138. Catapult, E.S. *Electrification of Heat UK demonstration project*. 2022; Available from: https://es.catapult.org.uk/project/electrification-of-heat-demonstration/.

139. Centre, U.E.D. *BEIS Electrification of Heat Project - Property, Design and Installation Information*. 2022; Available from: https://ukerc.rl.ac.uk/DC/cgi-bin/edc_search.pl?GoButton=Detail&WantComp=284&&RELATED=1.

140. NGED. *Budget Estimate*. 2023; Available from: https://connections.nationalgrid.co.uk/budget-estimate/.

141. Government, H. *PM speech on Net Zero: 20 September 2023*. 2023; Available from: https://www.gov.uk/government/speeches/pm-speech-on-net-zero-20-september-2023.

142. Octupus. *Agile Tariff*. 2023; Available from: https://octopus.energy/smart/agile/.

143. IEA, *Global EV Outlook 2022*. 2022: Paris.

144. UK Government, *Transitioning to zero emission cars and vans: 2035 delivery plan*. 2021.

145. European Commission, *European Commission - Press release: Zero emission vehicles: first 'Fit for 55' deal will end the sale of new CO2 emitting cars in Europe by 2035*. 2022: Brussels.

146. Competition & Markets Authority, *Electric Vehicle Charging market study*. 2021.

147. Hilton, G., et al., *The case for energy storage installations at high rate EV chargers to enable solar energy integration in the UK–An optimised approach*. Journal of Energy Storage, 2019. **21**: p. 435-444.

148. Hilton, G., et al., *Dynamic charging algorithm for energy storage devices at high rate EV chargers for integration of solar energy*. Energy Procedia, 2018. **151**: p. 2-6.

149. DKSH. *FlowGen - Wind Turbine Systems*. 2023; Available from: https://www.dksh.com/global-en/products/iap/flowgen-technology.

150. *Open-Meteo*. 2023 [cited 2023 06/03]; Available from: https://open-meteo.com/.

151. Wind turbine models. *Aventa AV-7*. 2023 [cited 2023 06/03]; Available from: https://en.wind-turbine-models.com/turbines/1529-aventa-av-7.

152. Braeuer, F., *Load profile data of 50 industrial plants in Germany for one year*. Zenodo, Jun, 2020. **17**.

153. Silalahi, D.F. and A. Blakers. *Global atlas of marine floating solar PV potential*. in *Solar*. 2023. MDPI.

154. Technology, P. *Power plant profile: Saemangeum Floating Solar Power Project, South Korea*. 2023; Available from: https://www.power-technology.com/marketdata/power-plant-profile-saemangeum-floating-solar-power-project-south-korea/?cf-view.

155. Magazine, P. *Floating solar powers water treatment plant in New Jersey*. 2023; Available from: https://pv-magazine-usa.com/2023/06/07/floating-solar-powers-water-treatment-plant-in-new-jersey/.

156. Singapore, S.E.R.I.o., *Where Sun Meets Water Floating: Solar Market Report*. 2019, World Bank: USA.

157. Rosa-Clot, M., *Floating PV plants*. 2020: Academic Press.

158. Helfer, F., C. Lemckert, and H. Zhang, *Impacts of climate change on temperature and evaporation from a large reservoir in Australia*. Journal of hydrology, 2012. **475**: p. 365-378.

159. Tian, W., et al., *Estimation of global reservoir evaporation losses*. Journal of Hydrology, 2022. **607**: p. 127524.

160. Almeida, R.M., et al., *Floating solar power could help fight climate change—let's get it right*. Nature, 2022. **606**(7913): p. 246-249.

161. Magazine, P. *Solar over canal study announced in California*. 2022; Available from: https://pv-magazine-usa.com/2022/02/08/solar-over-canal-study-announced-in-california/.

162. Sukarso, A.P. and K.N. Kim, *Cooling effect on the floating solar PV: Performance and economic analysis on the case of west Java province in Indonesia*. Energies, 2020. **13**(9): p. 2126.

163. Tina, G.M., et al., *Economic comparison of floating photovoltaic systems with tracking systems and active cooling in a Mediterranean water basin*. Energy for Sustainable Development, 2023. **76**: p. 101283.

164. Tina, G.M. and F.B. Scavo, *Energy performance analysis of tracking floating photovoltaic systems*. Heliyon, 2022. **8**(8).

165. Aquacuture, W. *World's first wind and solar-powered offshore aquaculture project completed in China*. Nov 2023; Available from: https://weareaquaculture.com/news/aquaculture/worlds-first-wind-and-solar-powered-offshore-aquaculture-project-completed-in-china#:~:text=When%20Shanghai%20Electric%20announced%20a,realize%20the%20shared%20use%20of.

166. Santos, B. *Floating solar tech for aquaculture*. 2023; Available from: https://www.pv-magazine.com/2023/01/04/floating-solar-tech-for-aquaculture/.

167. Fishfarmingexpert. *Floating solar power plant now on the market*. 2022; Available from: https://www.fishfarmingexpert.com/inseanergy-salmon-farming-solar-power/floating-solar-power-plant-now-on-the-market/1429024.

168. Fishfarmingexpert. *Solar lights 'improve fish growth and feed conversion'*. 2021; Available from: https://www.fishfarmingexpert.com/philips-pond-lights-signify/solar-lights-improve-fish-growth-and-feed-conversion/1373381.

169. Solar, T. *Trina Solar's modules powered 100MW fishery PV project with high-performance*. 2023; Available from: https://www.trinasolar.com/en-glb/resources/newsroom/matrina-solars-modules-powered-100mw-fishery-pv-project-high-performance.

170. Technology, P. *Power plant profile: Hapcheon Dam Floating Solar Power Project, South Korea*. 2023; Available from: https://www.power-technology.com/marketdata/power-plant-profile-hapcheon-dam-floating-solar-power-project-south-korea/?cf-view.

171. BP, L. *Queen Elizabeth II Reservoir solar*. 2016; Available from: https://lightsourcebp.com/uk/project/queen-elizabeth-ii-reservoir-solar/.

172. The_British_Hydropower_Association, *A guide to UK mini-hydro developments*. 2012.

173. Cink. *CINK Power Box*. 2023; Available from: https://www.cink-hydro-energy.com/cink-power-box.